
Characterization of the ubiquitin-like protein Hub1
and its role in pre-mRNA splicing in human cells



Dissertation der Fakultät für Biologie
der Ludwig-Maximilians-Universität München

vorgelegt von
Diplom Biologe
Tim Ammon

September 2013

Eidesstattliche Erklärung

Hiermit erkläre ich an Eides statt, dass ich die vorliegende Dissertation selbständig und ohne unerlaubte Hilfe angefertigt habe. Ich habe weder anderweitig versucht, eine Dissertation einzureichen oder eine Doktorprüfung durchzuführen, noch habe ich diese Dissertation oder Teile derselben einer anderen Prüfungskommission vorgelegt.

München, den 30.09.2013

(Unterschrift)

Die vorliegende Arbeit wurde zwischen Oktober 2005 und September 2013 unter Anleitung von Prof. Dr. Stefan Jentsch am Max-Planck-Institut für Biochemie in Martinsried durchgeführt.

Aus Teilen dieser Arbeit sind die folgenden Publikationen hervorgegangen:

Mishra, S.K., **Ammon, T.**, Popowicz, G.M., Krajewski, M., Nagel, R.J., Ares, M., Holak, T.A., and Jentsch, S. (2011). Role of the ubiquitin-like protein Hub1 in splice-site usage and alternative splicing. *Nature* 474, 173–178.

Bergink, S., **Ammon, T.**, Kern, M., Schermelleh, L., Leonhardt, H., and Jentsch, S. (2013). Role of Cdc48/p97 as a SUMO-targeted segregase curbing Rad51-Rad52 interaction. *Nat Cell Biol* 15, 526–532.

Ammon, T., Mishra, S.K., Kowalska, K., Popowicz, G.M., Holak, T.A., and Jentsch, S. (2013). The conserved ubiquitin-like protein Hub1 plays a critical role in splicing in human cells. *Submitted*

Promotionsgesuch eingereicht am: 30.09.2013

Datum der mündlichen Prüfung: 04.12.2013

Erster Gutachter: Prof. Dr. Stefan Jentsch

Zweiter Gutachter: Prof. Dr. Angelika Böttger

Table of contents

Eidesstattliche Erklärung	2
Table of contents	3
1 Summary	5
2 Introduction	6
2.1 Transcription and pre-mRNA processing	6
2.2 Introducing pre-mRNA splicing	9
2.3 Biochemistry of the splicing reaction	10
2.4 Constituents of the spliceosomal machinery	11
2.5 The splicing cycle	14
2.6 Alternative splicing	16
2.7 Posttranslational modification by ubiquitin	19
2.8 Ubiquitin and ubiquitin-like proteins	20
2.9 The ubiquitin-like protein Hub1	23
3 Aim of this study	26
4 Results	27
4.1 Identification of human Hub1 interactors by yeast two-hybrid screening	27
4.2 Hub1 binds the spliceosomal protein hSnu66 <i>in vivo</i>	28
4.3 A conserved motif in hSnu66 mediates Hub1 interaction	29
4.4 Mutations in the HIND abolish Hub1-hSnu66 interaction	32
4.5 Hub1 localizes to splicing-associated nuclear domains	34
4.6 hSnu66 actively recruits Hub1 to splicing speckles	37
4.7 Characterization of hSnu66's functional domains	39
4.8 Distinct and conserved protein properties of Hub1	43
4.9 Molecular tools for the characterization of Hub1 in human cells	45
4.10 <i>In vivo</i> depletion of Hub1 causes cell cycle defects and apoptotic cell death	46
4.11 Hub1 RNAi entails DNA damage, mitotic catastrophe, and apoptotic cell death	51
4.12 The functional C-terminal surface is crucial to mediate the vital activity of Hub1	55
4.13 Altered distribution of splicing factors and retention of mRNA upon Hub1 depletion <i>in vivo</i>	59
4.14 Identification of splicing defects upon Hub1 knockdown using splicing reporter systems	63
4.15 The splicing factor Hub1 is crucial for efficient and faithful pre-mRNA splicing in human cells	65
4.16 Identification of Hub1-dependent alternatively spliced transcripts by exon-specific microarray analysis	71
4.17 Antagonistic interactions between the transcription inhibitor actinomycin D and Hub1 RNAi	74
5 Discussion	78
5.1 Identification of binding factors by yeast two-hybrid link Hub1 to splicing-associated complexes	78
5.2 Hub1 binding is mediated via a conserved Hub1 interaction domain in hSnu66	80
5.3 Hub1 and hSnu66 reside in nuclear splicing speckles	86
5.4 Conserved and evolved protein features of Hub1	92
5.5 Different surfaces on Hub1 facilitate distinct interactions	94
5.6 <i>In vivo</i> depletion of Hub1 causes cell cycle defects and apoptotic cell death	96
5.7 Hub1 RNAi leads to aberrant splicing and mRNA retention	97
5.8 Human Hub1 is crucial for specific splicing events	98
5.9 Hub1 knockdown desensitizes cells to actinomycin D	101
5.10 The Hub1-dependent splicing model	103

6	Material and Methods	107
6.1	Cell biology	107
6.1.1	Human cell lines and transfections	107
6.1.2	Mammalian expression plasmids and siRNA	107
6.1.3	Flow cytometry	108
6.1.4	Immunofluorescence, FISH and live cell microscopy	108
6.1.5	Cell lysis and immunoprecipitation	109
6.1.6	Antibodies	110
6.1.7	Exon-specific alternative splicing microarray	110
6.1.8	Yeast strains and plasmids	111
6.2	Molecular biology	112
6.2.1	Preparation and transformation of chemically competent <i>E. coli</i>	112
6.2.2	Isolation of plasmid DNA	113
6.2.3	Polymerase chain reaction and site directed mutagenesis	113
6.2.4	DNA restriction, ligation and cloning	113
6.2.5	RNA-purification, RT-PCR and splicing gels	114
6.2.6	Gel electrophoresis of DNA and purification from agarose gels	114
6.2.7	DNA sequencing	114
6.2.8	Plasmids for recombinant protein expression in <i>E. coli</i>	114
6.2.9	Purification of recombinant proteins from <i>E. coli</i>	114
6.2.10	Determination of protein concentrations	116
6.2.11	CNBr coupling	116
6.2.12	Antibody purification	116
6.2.13	Polyacrylamide gel electrophoresis and immunoblotting	117
6.2.14	Structure determination of the human Hub1-HIND complex	117
6.2.15	Software	118
7	Figure Index	120
8	References	121
9	Abbreviations	142
10	Acknowledgement	143
11	Curriculum Vitae	144
12	Appendix	145
12.1	Affymetrix Human Exon 1.0 ST microarray data	145
12.2	Microarray mRNA expression analysis	146
12.3	Data collection and refinement statistics	147

1 Summary

For faithful gene expression eukaryotic transcripts are subjected to a series of processing steps in which the precursor messenger RNA (pre-mRNA) is matured and subsequently exported to the cytoplasm for translation and protein synthesis. Therefore, the excision of intervening, non-coding sequences from nascent pre-mRNAs is essential, which is catalyzed by a complex macromolecular machine, the spliceosome. In a highly regulated and dynamic process the spliceosomal subunits assemble in a stepwise manner and are subjected to major structural and compositional rearrangements in their RNA and protein interaction network in order to form the catalytically active spliceosome. The accurate recognition of splice sites and the coordinated assembly of spliceosomes are vital processes to ensure high splicing fidelity and efficiency in order to prevent aberrantly spliced transcripts that encode misfolded, non-functional, or toxic proteins in cells.

This study comprises the detailed characterization of the small, ubiquitin-like protein Hub1 in mammalian cells and reveals its crucial role in pre-mRNA splicing. *In vivo* depletion of Hub1 from human tissue culture cells leads to cell cycle arrest, mitotic defects and subsequent apoptotic cell death. Biochemical and cell biological analyses elucidated that Hub1 is essential for faithful pre-mRNA splicing of distinct introns and proper alternative splicing in human cells. Importantly, Hub1 does not influence general splicing, but facilitates processing of certain splicing events in particular pre-mRNAs. Moreover, the study demonstrates that knockdown of Hub1 causes an altered nuclear distribution of splicing factors and nuclear retention of mRNA species, further indicating defective mRNA splicing *in vivo*. In this study Hub1 was identified as a component of nuclear splicing speckles where it interacts with the conserved spliceosomal tri-snRNP protein hSnu66. Mapping and binding studies led to the characterization of the Hub1 interaction motif in hSnu66, which is sufficient and necessary to mediate binding of Hub1. The underlying molecular mechanism of this interaction between the non-canonical ubiquitin-like protein Hub1 and the splicing protein hSnu66 was resolved by determining the crystal structure of the complex. Additionally, mutational analysis elucidated that, although binding to hSnu66 facilitates the recruitment of Hub1 to nuclear speckles, the interaction is neither essential for viability nor Hub1's crucial function in pre-mRNA splicing. In contrast, it became apparent that another surface on Hub1 opposing the Hub1-hSnu66 interface conveys the pivotal activity of Hub1 in mRNA splicing.

Finally, the experimental data and derived conclusions are integrated into a revised pre-mRNA splicing model proposing a central function for Hub1 during spliceosomal complex formation. In summary, this study represents the first comprehensive characterization of the ubiquitin-like protein Hub1 in human cells and reveals the essential role of Hub1 as a non-covalent "modifier" of the splicing machinery.

2 Introduction

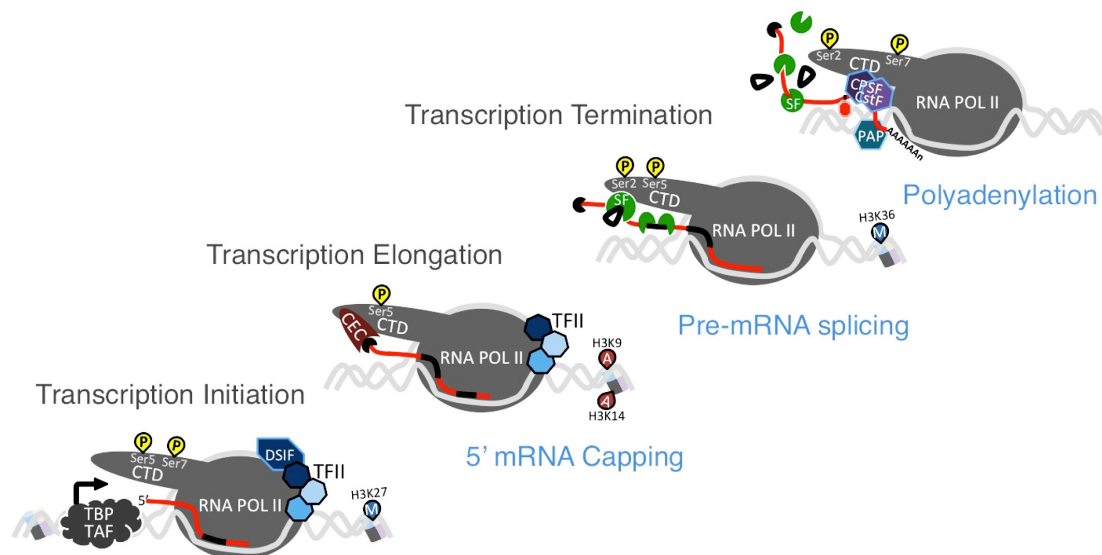
2.1 Transcription and pre-mRNA processing

Eukaryotic gene expression is a highly coordinated and dynamic process accomplished by an intricate network of macromolecular protein complexes, RNA-containing ribonucleoproteins (RNPs) and their regulatory circuits. During RNA synthesis by RNA polymerase II (RNA pol II), precursor messenger RNA (pre-mRNA) has to undergo several processing steps, namely 5'-capping, splicing and polyadenylation to give rise to the stable, mature gene product, which can be exported from the nucleus to the cytoplasm for later translation into proteins.

Upon transcription initiation TATA-box binding protein (TBP) and several associated factors (TAF) are recruited to the core promoter sequences, where general transcription factors TFIIA and TFIIB facilitate loading and engaging of the RNA pol II machinery onto DNA. This pre-initiation complex (PIC) is finally completed by the joining of multimeric mediator, TFIIH, and TFIIE complexes. In order to allow productive transcription, the densely packed chromatin has to be accessible and opened up by chromatin remodeling enzymes (Ho and Crabtree, 2010). Among this group of enzymes, acetyl- or methyltransferases are crucial to posttranslationally modify nucleosomal histones for subsequent reorganization of the chromatin structure. Upon histone acetylation (histone 3 at K9 and K14, histone 4 at K16) as well as methylation (histone 3 at K4), RNA pol II is released from its promoter to start productive mRNA synthesis.

The sequential steps of initiation, elongation, and termination during transcription are accompanied by different posttranslational modifications of a distinct C-terminal domain of the RNA pol II, the CTD. In humans the CTD, comprised of 52 heptad repeats of Y₁-S₂-P₃-T₄-S₅-P₆-S₇ residues, serves as a regulatory interaction platform for the various mRNA processing factors and thus directly couples transcription to subsequent mRNA maturation. Manipulation of the CTD by using mutant alleles or deletions directly impinges on splicing, capping and polyadenylation, respectively (McCracken et al., 1997). Site-specific phosphorylation of serines within the CTD controls and promotes distinct phases of RNA polymerase action, resembling the so-called serine code (Fong and Bentley, 2001). While RNA pol II is mainly phosphorylated at serine S₅ during transcription initiation, the serine S₂ phosphorylation serves as the predominant modification in the elongation phase and serine S₇ is found in paused or terminating RNA pol II complexes. This code is established by CTD-associated kinases like P-TEFb (positive transcription elongation factor) with Cyclin-dependent kinase CDK9 and TFIIH/CDK7, respectively, and subsequently read by RNA processing factors and elongation supporting co-factors (Dahmus, 1996). For productive transcription initiation the TFIIH/CDK7 complex acts

as the major S₅ kinase, while the P-TEFb/Cdk9 subunit inactivates the inhibitory DSIF and NELF complexes to stimulate RNA polymerase activity (Missra and Gilmour, 2010). Upon RNA synthesis the nascent chain and the CTD S₅ phosphorylation mark are recognized by the 5'-capping enzyme complex (CEC) to transfer a 7-methylguanosine (m7G) cap to the emerging 5' end of the mRNA. As the first mRNA processing step, 5'-capping is crucial for nuclear export, translation and stability as it prevents premature degradation by exonucleases (Anderson and Parker, 1998).

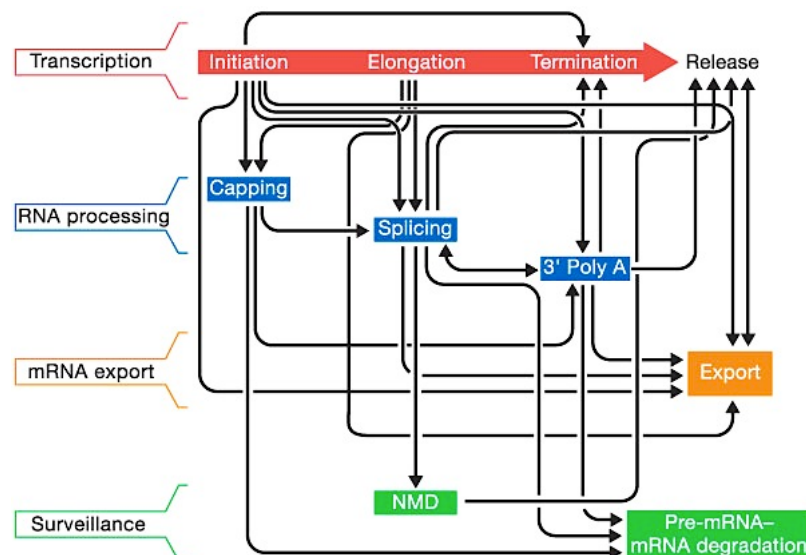


Introduction Figure I: Co-transcriptional mRNA processing

During distinct phases of the transcription cycle RNA polymerase II is phosphorylated at specific sites (yellow) in the C-terminal domain (CTD). The CTD serves as a platform to recruit specific mRNA processing complexes to the nascent pre-mRNA (red) in order to orchestrate 5' mRNA capping by the capping enzyme complex (CEC, dark red), pre-mRNA splicing with excision of introns (black) by the spliceosome (SF= splicing factors, green) and finally 3' cleavage with polyadenylation by cleavage stimulatory factor (CSF), polyadenylation specificity factor (CPSF) and the polyadenylate polymerase (PAP). (See text for more detail)

After co-transcriptional 5'-capping the RNA pol II machinery undergoes the transition to elongation phase with concomitant S₂ phosphorylation. As the majority of eukaryotic genes contain intervening non-coding sequences (so called introns) in their open reading frames (ORFs), these RNA segments have to be removed in a complex process called pre-mRNA splicing (Ruskin et al., 1984). The excision of intronic fragments with the concurrent ligation of coding sequences (exons) is catalyzed by an intricate macromolecular machinery of ribonucleoproteins, the spliceosome (detailed in chapter 2.3). The serine S₂ phosphorylated RNA pol II CTD serves as a platform to recruit auxiliary splicing factors like ASF/SF2 or SC35, which facilitate the recognition of exon-intron boundaries and *cis*-acting regulatory elements to promote the accurate and dynamic spliceosomal assembly on nascent mRNA (Millhouse and Manley, 2005; Morris and Greenleaf, 2000; Lin et al., 2008). Once a splice site is defined, subunits of the spliceosome, so called snRNPs (small nuclear ribonucleoproteins), bind specifically to crucial RNA sequences to assemble the

catalytically active spliceosome in a highly coordinated manner. The transesterification reaction, which excises the intron and ligates coding exons, involves global rearrangements of RNA-RNA, RNA-protein and protein-protein interaction networks mediated by powerful enzymes like GTPases and RNA-dependent helicases (Chang et al., 2013). After introns are removed and splicing reactions are completed, bound spliceosomes disassemble and the nascent mRNA undergoes its final co-transcriptional processing step, the polyadenylation. Downstream of the protein coding sequence most mRNAs contain a poly (A) signal sequence (5'AAUAAA-3') together with a GU-rich stretch at the 3' region, which is recognized by the polyadenylation machinery (Proudfoot, 2011). Again, RNA pol II CTD mediates the recruitment of RNA processing complexes and acts as a scaffold for the cleavage and polyadenylation specificity factor (CPSF) and the cleavage stimulatory factor (CSF). The emerging poly (A) signal sequence and the CTD S₂ phosphorylation recruit CPSF and CSF complexes, which induce polymerase pausing and cleavage of the transcript. After the mRNA is cleaved polyadenylate polymerase (PAP) supported by polyadenylated binding factor (PAB2) extends the free 3' end with a polyadenosine tail (250-300 adenines in human cells, 70-80 in yeast (Elkon et al., 2013)). As final step of co-transcriptional mRNA processing the attachment of a poly (A) tail is a prerequisite for efficient nuclear export, mRNA stability and productive translation.



Introduction Figure II: Interplay of the gene expression network

In order to ensure accurate gene expression mRNA maturation is highly regulated at several layers. The coordination of cellular processes including transcription, RNA processing, mRNA export and surveillance is accomplished by a complex interwoven network of direct physical and functional interactions between RNA-directed molecular machineries (indicated by black arrows). (Adapted from Maniatis, T., and Reed, R. (2002))

Taken together, the tight connection between transcription and RNA processing highlights the importance of the different pre-mRNA maturation steps as

regulatory elements of eukaryotic gene expression. Distinct RNA binding complexes like spliceosomal subunits are recruited to the nascent transcript and catalyze reactions in a highly coordinated and dynamic manner. Although the molecular capping, splicing and adenylation machineries perform discrete functions during pre-mRNA processing *in vivo*, their actions are interwoven and interdependent in an extensive RNA maturation network (Introduction Figure II) (Maniatis and Reed, 2002). Accurate and faithful mRNA processing is essential to ensure proper gene expression and synthesis of functional proteins. Defects in pre-mRNA maturation, like truncated polyadenylation or defective splicing, entail mRNA degradation, impaired nuclear export and aberrant transcripts that encode misfolded or non-functional proteins. Dysregulation of mRNA processing and particularly splicing has a strong implication in tumorigenesis as it substantially alters cellular homeostasis and biochemical pathways which affect proliferation, cell differentiation and cell viability resembling hallmarks of human cancer (Venables, 2004; Liu and Cheng, 2013).

2.2 Introducing pre-mRNA splicing

Based on early studies in prokaryotes, mRNA was considered as a complementary template copy of genomic information. In 1977 gene expression studies on adenoviral mRNAs revealed intriguing differences between the viral genome sequences and its transcripts at late stages of infection (Berk and Sharp, 1977; Chow et al., 1977). The discovery of those *sequence arrangements* in RNA:DNA hybridization assays together with subsequent advances in mRNA biology revolutionized the view on gene structure, transcription and mRNA maturation (Witkowski, 1988).

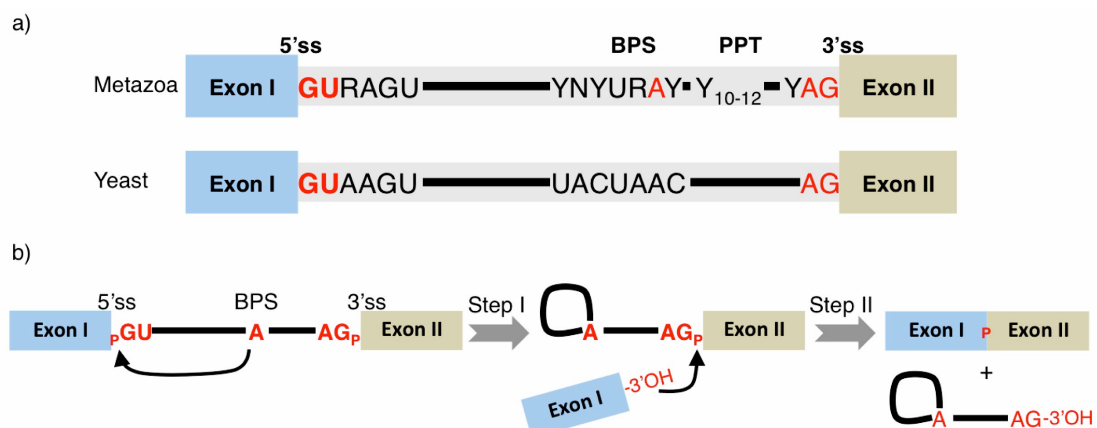
Most eukaryotic genes contain intervening non-coding sequences, so-called introns, which have to be removed after transcription by a process termed pre-mRNA splicing in order to obtain the mature and functional mRNA. Therefore, all eukaryotes evolved a highly conserved and sophisticated network of pre-mRNA splicing factors and enzymes to conduct this essential processing step (Ast, 2004).

In the human genome splicing is crucial for over 92-94% of transcripts, as they contain exons separated by at least one intron. The average human transcript comprises 8.8 relatively short exons (ca. 120 nt), while introns with an average size of >5400 nt are rather long (Sakharkar et al., 2004). In contrast, in *Saccharomyces cerevisiae* only three percent of the genes carry introns (ca. 253) with only six transcripts containing two introns (Barrass and Beggs, 2003). Although the fission yeast *Schizosaccharomyces pombe* represents the intermediate genomic state with 43% of intron-containing genes, both yeasts exhibit rather short introns with an average size of 40-75 nt (Ast, 2004). Despite the differences in splicing prevalence between lower eukaryotes like *S. cerevisiae* and mammals, which led to formulation of the exon- and intron-definition model (Robberson et al., 1990), the basic

biochemistry of pre-mRNA splicing is highly conserved. In a stepwise process the macromolecular spliceosome assembles on the pre-mRNA and recognizes crucial sequences within the pre-mRNA that determine the intron boundaries. The spliceosome machinery consists of an intricate network of distinct ribonucleoproteins (RNP) in complex with small nuclear RNA (snRNA), which guide and facilitate the transesterification reaction. Upon spliceosome activation in a cascade of major rearrangements, RNA-RNA, RNA-protein and protein-protein interactions are disrupted and re-assembled as novel intermediates to catalyze the intron excision with concomitant exon ligation. Based on the orchestrated activities of over 300 proteins including kinases, helicases and ATPases, intertwined with pre-mRNA bound ribonucleoprotein particles, the human spliceosome is considered to be among the *most complex macromolecular machines in the cell* (Nilsen, 2003).

2.3 Biochemistry of the splicing reaction

After transcription the splicing machinery assembles on the nascent pre-mRNA and recognizes crucial sequences within the pre-mRNA that define the exon-intron boundaries as 5' splice site (5'ss) and 3' splice site (3'ss). In addition, the intronic sequence harbors the crucial adenosine residue embedded in the branch point sequence (BPS), which serves as the acceptor site during the splicing reaction. In metazoans an additional element with 10-12 pyrimidine bases, the polypyrimidine track (PPT), is located in between the BPS and the 3'ss. In contrast, a minor fraction of introns (ca. 1% of all human introns) that are spliced via the minor U12-dependent spliceosome lack the polypyrimidine track, while PPTs are generally absent in *S. cerevisiae* (Burge et al., 1998; Will and Lührmann, 2005).



Introduction Figure III The pre-mRNA splicing reaction

a) Schematic representation of conserved sequence elements in metazoan and budding yeast pre-mRNAs, respectively. Consensus sequences of 5' splice sites (5'ss), 3' splice sites (3'ss), branch point sequences (BPS) and polypyrimidine track (PPT) are indicated. Bases abbreviations Y = pyrimidine, R = purine. b) The two transesterification steps of the splicing reaction. The branch point adenosine attacks the phosphodiester bond (p) at the 5'ss guanosine generating the lariat intermediate. Subsequently the liberated 3' hydroxyl group of the 5' exon reacts with the phosphodiester bond on the 3'ss resulting in the ligation of the two exons. (Adapted from Patel and Steitz (2003)).

The intron is excised in a two-step manner with two consecutive transesterification reactions (see Introduction Figure III). First, the 2' hydroxyl group of the branch point adenosine performs a nucleophilic attack on the phosphodiester bond at the guanosine of the 5'ss. This liberates a 3' hydroxyl group at the 5' exon, while the 5' end of the intron forms a lariat intermediate with the branch point. In the second step, the free 3' hydroxyl group of the 5' exon reacts with the phosphodiester bond on the 3'ss resulting in the ligation of the two exons, excision of the intron-lariat and completion of the splicing reaction.

2.4 Constituents of the spliceosomal machinery

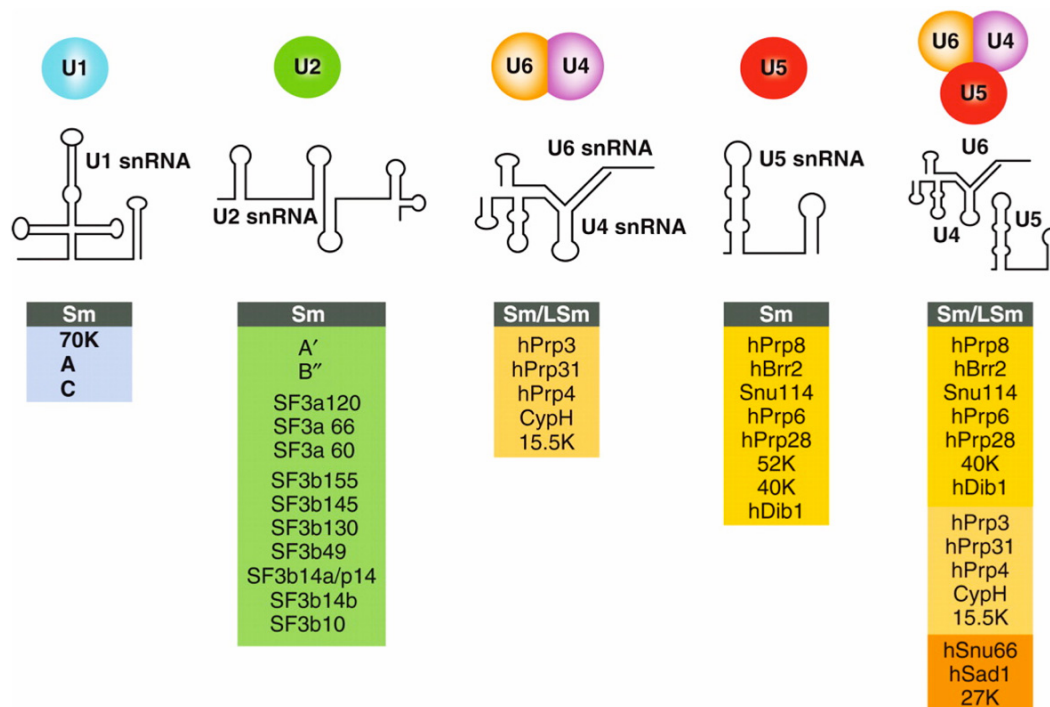
The enzymatic excision of non-coding introns from pre-mRNA is performed by the multi-subunit ribozyme complex, the spliceosome (Collins and Guthrie, 2000). The subunits can be categorized into snRNP and associated non-snRNP protein complexes.

The snRNPs are the major building blocks of the spliceosome and are characterized by the five uridine-rich small nuclear RNAs (U1, U2, U4, U5, U6) and their respective ribonucleoproteins. While each U1, U2 and U5 snRNA form distinct, solitary snRNPs, U4 and U6 snRNA share extensive base-pairing forming the dimeric U4/U6 snRNP complex (Bringmann et al., 1984; Nilsen, 1994). All non-U6 snRNAs are transcribed by RNA pol II and exported by the PHAX/CBC (phosphorylated adaptor of export protein / cap binding complex) to the cytoplasm. During cytoplasmic maturation snRNAs undergo modifications like 3' end processing and the addition of the characteristic 2,2,7-trimethylguanosine cap (3mG) at the 5' end. Each snRNA contains a conserved sequence motif, the Sm site, which is recognized and encompassed by the Sm proteins (SmE, SmG, SmD3, SmB, SmD1, SmD2, SmF) that form a heteroheptameric ring around the snRNA during biogenesis (Seraphin, 1995; Urlaub et al., 2001). Both the Sm ring assembly and 3mG capping are crucial for nuclear re-import and incorporation into functional snRNP in Cajal bodies (Will and Lührmann, 2001; Fischer et al., 2011). In contrast, U6 snRNA derives from RNA pol III transcription and matures entirely within the nucleus. Although the U6 snRNA lacks a canonical Sm-binding motif, Sm-like (Lsm2-8) proteins analogous to the Sm proteins are recruited to an uridine-rich sequence at the 3' end instead. Beside the Lsm ring the U6 snRNA carries an unique γ -monomethyl guanosine 5'-cap and undergoes extensive RNA modifications like 3' pseudouridylation and 2'-O-methylation (Karijolich and Yu, 2010). These maturation steps orchestrate the recruitment of snRNA-specific proteins, determine subnuclear localization to the nucleolus or Cajal bodies and mediate U6 snRNP recycling by SART3/p110 (Mroczek and Dziembowski, 2013).

During spliceosome assembly the 5'ss is recognized by the U1 snRNP which contains a rather small number of U1 specific proteins, namely U1-70K, U1-A and

U1-C in addition to the Sm ring. The auxiliary factors SF1/BBP in cooperation with U2AF65 and U2AF35 recruit the U2 snRNP to the branch point upstream of the 3'ss. The stable association to the BPS is supported by more than twelve U2 snRNP proteins including A', B'', as well as the SF3a and SF3b complexes. In particular, SF3b155 together with SF3b14/p14 play crucial roles as they physically interact with the BPS and ensure proper formation of the prespliceosomal complex A (see chapter 2.5).

The U5 snRNP comprises eight U5 proteins including pivotal enzymes like the DEAD box helicase hPrp28, the GTPase Snu114, the DExD/H-box protein hBRR2 and the multidomain protein hPRP8.



Introduction Figure IV: The human spliceosomal snRNPs

Composition of the major snRNP complexes depicting the uridine-rich snRNAs with respective secondary structures and the associated snRNP specific proteins. (Adapted from Will and Lührmann (2011)).

In contrast to the singular U1 and U2 snRNPs, complementary domains within the U4 and U6 snRNA allow RNA base-pairing which creates the platform for the dimeric U4/U6 snRNP complex associated with Sm, LSm, as well as snRNP specific proteins hPrp3, hPrp4, hPrp31, CypH and 15.5K (Schneider et al., 2002). The catalytic core subunit of the spliceosome is formed when the preassembled U5 snRNP joins the U4/U6 snRNP and thereby generates the U4/U6.U5 tri-snRNP complex. The tri-snRNP formation is accompanied by the recruitment of three additional complex-specific proteins 27K, hSad1 and hSnu66, while the U5 factor 52K dissociates during this transition (Gottschalk et al., 1999).

In addition to the different U1, U2, and U4/U6.U5 tri-snRNP complexes the spliceosomal activity is supported by a large number of non-snRNA containing RNPs.

The major non-snRNP complex which associates with the spliceosome during the formation of the precatalytic complex B is the PRP19/CDC5L or nineteen complex (NTC) in *S. cerevisiae* (Tarn and Steitz, 1994; Ajuh et al., 2000). The PRP19/CDC5L complex consists of at least seven proteins; while the central proteins hPRP19 (Prp19), CDC5L (Cef1), PRL1 (Prp46) and SPF27 (Snt309) are conserved, the subunits human AD002, CTNNBL1 (β -catenin-like 1) and HSP73 are not found in yeast. PRP19/CDC5L is crucial for pre-mRNA splicing in human cells and immunodepletion of this complex interferes with the first catalytic step in HeLa nuclear extracts (Makarova et al., 2004). After the U4/U5.U6 tri-snRNP joins the prespliceosomal complex A, PRP19/CDC5L mediates the dissociation of the U4 snRNP, which in turn allows the stable association of the U5 and U6 snRNPs with the spliceosome on the pre-mRNA during catalysis (Chan et al., 2003). Interestingly, the central Prp19 protein resembles an active ubiquitin E3 ligase comprising WD40 and U-box domains (Ohi et al., 2003; Vander Kooi et al., 2010), which mediates the ubiquitylation of hPrp3 and its association with hPrp8 to further stabilize the U4/U6.U5 tri-snRNP (Song et al., 2010). After precatalytic complex B formation, PRP19/CDC5L stays with the spliceosome until the splicing reaction is completed and the mRNA-bound post-spliceosomal complex disassembles with the release of the lariat intermediate.

In addition to the large PRP19/CDC5L complex, a large number of splicing factors associate only transiently with the spliceosome to precisely mediate rearrangements or support different steps during the transesterification reaction (Wahl et al., 2009). During spliceosomal activation RNA-RNA and RNA-protein interaction networks undergo extensive rearrangements that are facilitated by the coordinated action of various enzymes. The tri-snRNP itself contains the GTPase hSnu114, DExD/H-box helicases hBrr2 and hPrp28, and multi-domain protein hPrp8, which are considered to act as the “molecular motor” (Häcker et al., 2008) during U4/U6 unwinding for spliceosome activation. However, beside the activity of the tri-snRNP components, additional ATP-dependent helicases hPrp2, hPrp5, Sub2/UAP56, hPrp16, hPrp22, hPrp43 are crucial for individual steps during the splicing cycle (see Introduction Figure V). For example, the non-snRNP helicase, hPrp2, supports the U4/U6 unwinding activity of hBrr2 and, moreover, converts the precatalytic complex B to an activated spliceosome which then catalyzes the first splicing reaction step. On the other hand, other DExD/H-box proteins hPrp5 and Sub2/UAP56 mediate the stable association of the U2 snRNP at the BPS (Chang et al., 2013).

Another group of non-snRNP proteins, the serine/arginine (SR)-rich proteins and hnRNP (heterogeneous nuclear ribonucleoproteins), are RNA binding factors with regulatory functions. They are characterized by one to two RNA binding modules, RNA recognition motifs (RRMs) or hnRNP K-homology (KH) domains,

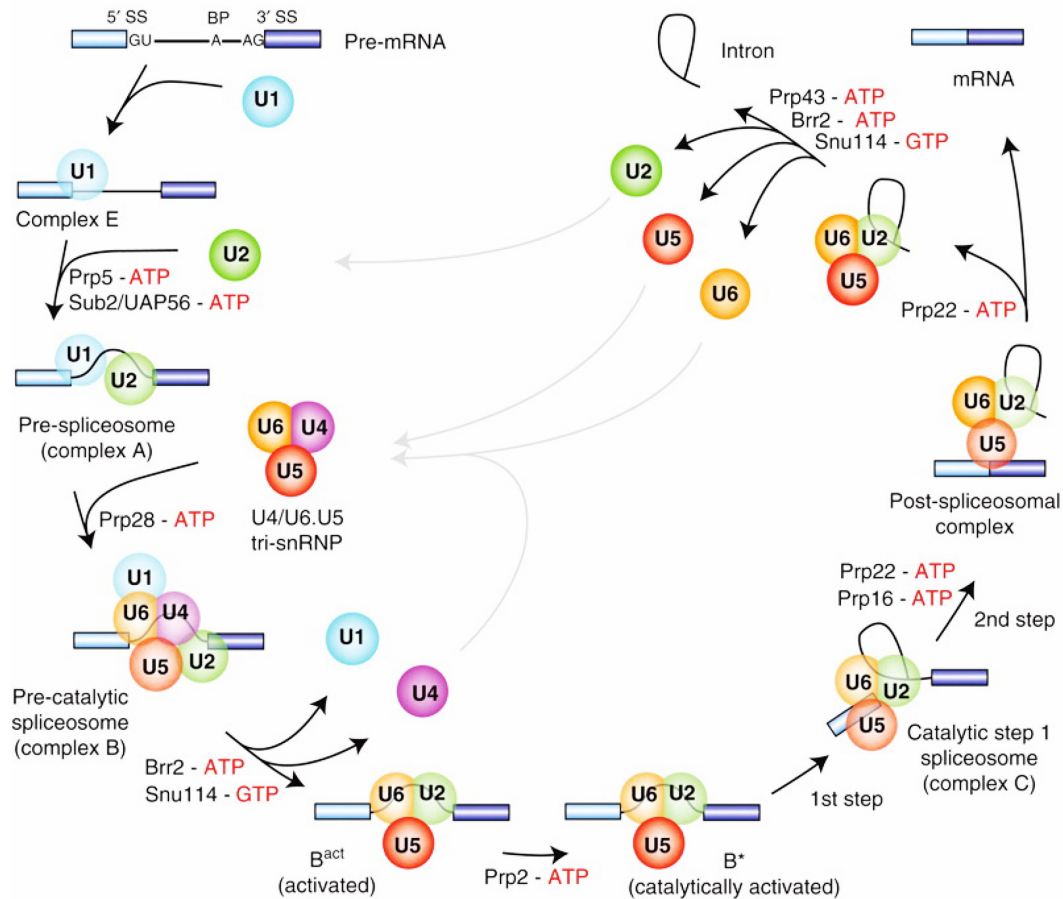
accompanied by their respective functional domains (Manley and Tacke, 1996; Krecic and Swanson, 1999); in case of SR proteins the RS-domain and in hnRNPs the more divergent RGG boxes, glycine-, acidic- or proline rich domains. Proteins of these two families are crucial regulators of alternative splicing, as they influence splice site recognition and usage by fostering the recruitment of the splicing machinery to the respective splice site or repress assembly, respectively (see chapter 2.6).

2.5 The splicing cycle

Due to the intricate and highly dynamic nature of the splicing cycle, the splicing machinery follows basic principles to allow profound structural and compositional rearrangements for accurate pre-mRNA processing. Firstly, in order to allow high flexibility of the snRNP complexes, the majority of interactions within the spliceosome network show rather low binding affinity, which is compensated by a strong avidity formed by the combination of multiple interaction surfaces. Secondly, the correct timing during the coordinated assembly and dissociation of spliceosomal complexes ensures high fidelity. Each crucial step during splicing activation is under the control of ATP-dependent DExD/H-box helicases like hPrp2 or hBrr2 to avoid pre-mature unwinding of snRNAs, misaligned base pairing or defective splicing reactions. Thirdly, the spliceosome ensures correct recognition of the reactive sites within the pre-mRNA like the BPS, and 5'ss and 3'ss at multiple check points. This is important, due to the highly divergent recognition sequences at the 5'ss in metazoan introns, while in yeast splice sites are almost invariant. Therefore, in addition to auxiliary splice site recognition factors like the SR protein family, the 5'ss is contacted by the U1 snRNA as well as the U6 and the U5 snRNP to ensure faithful and precise pre-mRNA splicing. However, the underlying biochemical principles of the splicing reaction are highly conserved from yeast to human and summarized in the following section (see Introduction Figure V).

In the initial step of the splicing cycle the U1 snRNP interacts with the 5' splice site forming the commitment complex (complex E) supported by RNA-binding serine-arginine-rich proteins. Here, short motifs in the U1 snRNA base pair with the splice donor site at the exon-intron boundary. Next, the branch point sequence is bound and marked by SF1/BBP accompanied by U2AF35 and U2AF65, which recognize the polypyrimidine track (PPT) and the AG motif of the 3'ss. The commitment complex is converted to prespliceosomal complex A by loading of the U2 snRNP. The DExD/H-box helicases UAP56 and hPrp5 mediate the stable interaction and snRNA-mRNA base pairing of the U2 snRNP with the BPS. Therefore, the SF1/BBP is replaced from the branch point adenosine by the p14 subunit of the SF3b complex. The following recruitment and incorporation of the U4/U6.U5 tri-snRNP gives rise to the pre-catalytic spliceosome (complex B). The U5

DExD/H-box helicase hPrp28 facilitates the displacement of the U1 snRNP allowing the later hybridization of the U6 snRNA with the intronic 5'ss. During this catalytic activation the activated spliceosome (complex B^{act}) undergoes profound conformational changes, in which the global RNA-RNA network is rearranged and protein interactions are disrupted and newly established. This conversion is triggered by hPrp8 and the DExD/H-box helicase hBrr2, which unwinds the tightly interconnected U4/U6 snRNA dimer.



Introduction Figure V: The stepwise assembly of the spliceosome during splicing cycles

The snRNPs (colored circles) recognize crucial sequences within the intron-containing pre-mRNA and mediate the assembly of the catalytically active spliceosome in a stepwise fashion. During spliceosome formation and activation major rearrangements of the RNA and protein interaction network are catalyzed by GTPases, DExD/H-box helicases and ATPases as indicated at different transition steps. For intelligibility, transient and auxiliary non-snRNP proteins like the Prp19 complex are not included. See text for more details. (Adapted from Will and Lührmann (2011)).

The free U6 snRNA is then able to form extensive base pairing with the U2 snRNA and the pre-mRNA's 5'ss at the same time, which arranges the BPS adenosine into close proximity with the splice site. The GTPase hSnu114 further supports the dissociation of the U1 snRNP and U4 snRNA from the spliceosome together with several tri-snRNP-associated proteins like hSnu66 and hPrp38. Another ATP-dependent DExD/H-box helicase hPrp2 (DHX16) is crucial for further activation

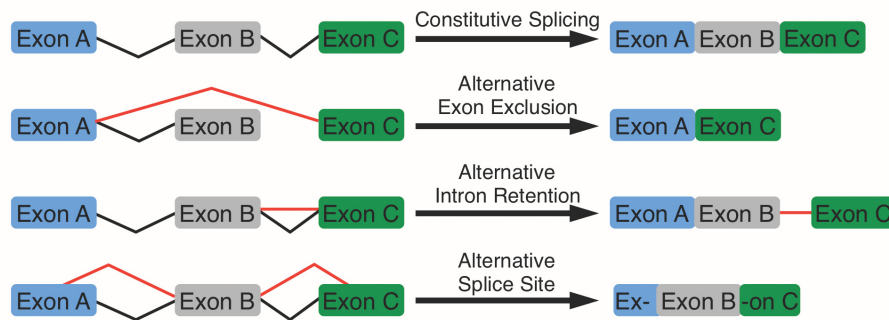
and transition from the B^{act} to the catalytically activated spliceosome (B* complex) by a yet unknown mechanism. Stabilized by the interplay of U6, U2, and U5 snRNAs, the catalytically activated spliceosome catalyzes the first transesterification reaction, in which the BPS adenosine attacks the 5'ss and forms the lariat intermediate. In the subsequent second reaction step the exon ligation and excision on the lariat by the catalytic complex C is fostered by complementary action of the hPrp16 and hPrp22 helicases. Finally, the spliced mRNA is released and the post-spliceosomal complex disassembles with the help of hPrp43 to allow recycling of the remaining U5, U6 and U2 snRNPs for another splicing cycle, while the intron-lariat is degraded.

The human transcriptome comprises many pre-mRNAs that are characterized by multiple long introns (with more than several hundreds of nt) separating rather short exons with 100-150 nt. As these distances challenge the coordinated spliceosomal assembly, mammalian cells have evolved an alternative process in addition to the linear 5' to 3' assembly (Robberson et al., 1990). During the so-called exon-definition, the early complex (ED-E complex) is formed by recruiting the U1 snRNP, which in turn facilitates the association of the U2 auxiliary factors U2AF with SF1/BBP to the 5' end of the same exon. In contrast to intron-definition here, the 3'ss U2AF/SF1 and the later U2 snRNP (ED-A complex), respectively, resemble a functional unit with the cross-exon downstream 5'ss U1 snRNP instead of the upstream cross-intron 5'ss (Schellenberg et al., 2008). The U4/U6.U5 tri-snRNP associates with the ED-A complex which then can convert into a B-like spliceosomal complex (Schneider et al., 2010). Thus, splicing via exon-definition uncouples the early spliceosome assembly from protracted intron transcription and allows shuffling of exons by mutual exclusion or inclusion in a process called alternative splicing (Bonnal et al., 2008; Sharma et al., 2005).

2.6 Alternative splicing

The initial recognition of the 5'ss and the BPS / 3'ss by the recruitment of the U1 and U2 snRNPs to form a pre-spliceosomal complex determines the efficiency of pre-mRNA splicing. In metazoans an additional layer of post-transcriptional expression regulation utilizes differential splice site recognition to extend the repertoire of the human genome by generating multiple mRNA isoforms from a single gene in a process called alternative splicing (AS). While alternative splicing is a rare event in lower eukaryotes like *S. cerevisiae* (three known AS genes), in humans over 95% of intron-containing transcripts undergo alternative splicing, giving rise to multiple mRNA isoforms (Pan et al., 2008). The prevalence of AS correlates with the high degree of degenerated splice site sequences found in metazoan genomes (Ast, 2004). Exons containing strong splice sites, which resemble the consensus sequence, stably base pair with the corresponding snRNA and are efficiently recognized by U1 snRNP and U2AF complexes. In contrast, divergent non-canonical

splice site sequences weaken exon recognition and subsequent spliceosomal assembly. In addition to the intrinsic splice site strength, metazoan pre-mRNAs contain *cis*-regulatory sequences, which can negatively or positively affect splice site recognition and usage. Dependent on their localization, these elements are termed exonic or intronic splicing enhancers and silencers, respectively.



Introduction Figure VI: Different types of alternative splicing

Basic types of alternative splicing can generate various mRNA isoforms including the sequential incorporation of constitutive exons, skipping or retention of individual exon cassettes (exon exclusion or inclusion), retention of distinct introns or usage of alternative 5' or 3' splice sites.

They serve as specific recognition motifs for RNA binding factors that either facilitate recruitment of snRNP subunits or repress spliceosomal assembly. Splicing enhancers attract positive regulators of the serine/arginine (SR)-rich protein family (SR protein) like SC35, ASF/SF2 or SRp20 (Shepard and Hertel, 2009). In the current model, the RS-domain mediates the direct physical interaction with spliceosomal subunits and binds other RS-domain containing factors (like U2AF35/U2AF65) to support splice site usage (Zhou and Fu, 2013). In contrast, the antagonistic group of heterogeneous nuclear ribonucleoproteins (hnRNP) associates with pre-mRNA via splicing silencer motifs where they interfere with the spliceosomal assembly at the respective splice site (Krecic and Swanson, 1999). Several members of this multifaceted family of RNA binding proteins including hnRNP A1 or PTBP1 (hnRNP1) can repress the engagement or progression of early prespliceosomal assemblies at respective exons and thereby avoid splice site usage.

Another layer of alternative splicing regulation modulates the activity of SR proteins and hnRNPs in human cells. Regulatory splicing factors are under tight control of SR-kinases, *e.g.* CLK1-4, SRPK1-2, AKT and counteracting phosphatases (PP1), which affect subnuclear distribution and recruitment to active splice sites (Ngo et al., 2005). Furthermore, many SR and hnRNP proteins are expressed in a tissue-specific manner (Ellis et al., 2012; Grosso et al., 2008) or upon certain stimuli (Paronetto et al., 2011; Li et al., 2006) and thereby switch between mRNA splice variants that express protein isoforms tailored to the individual needs of differentiated cell types. In the cellular context, alternative splicing regulation is an even more complex process. Considering the tight association between the transcription

machinery and pre-mRNA splicing, global alternative splicing patterns are significantly affected by parameters like promoter strength, RNA polymerase processivity and pausing as well as posttranslational histone modifications (Kornblihtt et al., 2013; Luco et al., 2011). In summary, alternative splicing is a complex and highly regulated process, in which the interplay between stimulatory splicing enhancers and negative silencers, spliceosomal activity and fidelity together with the intrinsic splice site strength determine the prevalent fate of each individual splicing event.

2.7 Posttranslational modification by ubiquitin

Posttranslational modifications serve as regulatory switches to alter the activity, stability, localization or function of proteins and constitute crucial control mechanisms in virtually all biochemical and cellular pathways. In addition to the attachment of small chemical substituents, *e.g.* during phosphorylation, acetylation, methylation or glycosylation, proteins can be modified by the covalent conjugation to another polypeptide.

Initially, a small, highly conserved protein called ubiquitin was identified serving as a molecular tag to target protein substrates for degradation via the 26S proteasome (Ciechanover et al., 1984; Hough et al., 1986; Wilkinson et al., 1980; Goldstein et al., 1975). Later, additional functions of ubiquitin were elucidated, showing that it is implicated in various cellular pathways including endocytosis, cell signaling, DNA replication, and repair (Strous et al., 1996; Hoege et al., 2002; Jentsch et al., 1987; Kölling and Hollenberg, 1994; Ea et al., 2006; Chen and Sun, 2009). The covalent attachment requires an enzymatic cascade to activate, transfer and conjugate ubiquitin specifically to a lysine residue of its substrate (Jentsch, 1992). Synthesized as an inactive precursor, ubiquitin has to be processed by ubiquitin C-terminal hydrolases (UCH) to liberate the free monomeric form (Pickart and Rose, 1985). In an ATP-dependent step, the E1 ubiquitin activating enzyme adenylates the C-terminus of ubiquitin in order to form a highly reactive E1~ubiquitin thioester bond in a subsequent reaction (Ciechanover et al., 1982). In the next step of the cascade, ubiquitin is transferred to a cysteine in the active center of the E2 conjugating enzyme. The loaded E2 enzyme associates and cooperates with E3 ubiquitin ligases, which convey substrate specificity. While RING E3 ligases mediate the direct ubiquitin transfer by spatially arranging the acceptor substrate in close proximity to the E2 enzyme, ligases of the HECT-family form an active intermediate complex in which the ubiquitin moiety is transiently forwarded to a reactive cysteine within the HECT domain before it is finally conjugated to the targeted protein (Hershko et al., 1983; Huibregtse et al., 1995). Here, the C-terminal carboxyl group at the double glycine motif of ubiquitin forms an isopeptide bond with an ϵ -amino group of a lysine residue on the substrate (Hershko et al., 1986). Through this enzymatic reaction, targeted proteins can be modified by a single ubiquitin moiety (monoubiquitylation) or via multiple separate ubiquitylation steps at different lysine positions (poly-monoubiquitylation). Furthermore, the conjugated ubiquitin molecule itself can serve as a platform for ubiquitylation forming an ubiquitin chain (polyubiquitylation). As ubiquitin contains several accessible lysine residues, they can be utilized by the conjugation machinery to attach multiple ubiquitin moieties via their respective C-terminal carboxyl group (Welchman et al., 2005). Dependent on the lysine position on the acceptor ubiquitin several types of linkages were identified and classified as K48, K63, K11, K33, K6, K27 and K29 polyubiquitylation chains while

mixed-chains were described *in vivo* as well (Nakasone et al., 2013; Xu and Peng, 2006; Crosas et al., 2006). Upon ubiquitin attachment to the targeted protein the *ubiquitylation code* is read by ubiquitin binding factors, which harbor ubiquitin binding domains (UBD) and recognize the unique chain topology, binding affinity or avidity in order to determine the fate of the substrate. In contrast to proteins decorated with K48-linked chains that are subjected to rapid protein degradation via the ubiquitin proteasome system (UPS), monoubiquitylation or K63-linked ubiquitin chains are implicated in regulatory functions during protein sorting, cell cycle control, endocytosis, signaling transduction, transcription, replication and DNA repair (Komander and Rape, 2012). The UBDs can be grouped according to their structural binding properties and come in different flavors, *e.g.* UBA (ubiquitin associated domain), ubiquitin interaction motifs (UIM), or Cue domains (named after Cue2). The vast majority of UBDs associate with ubiquitin via the hydrophobic area around I44 supported by L8 and V70 on sheets $\beta 3\beta 4$ (Dikic et al., 2009). In addition to canonical UBDs, other variously shaped domains have evolved like the Jab/MPN domain found in the U5 snRNP protein hPrp8 (Husnjak and Dikic, 2012). Thus, the ubiquitin system represents a versatile regulatory machinery that controls protein activity at various stages and, with its reversibility due to the action of de-ubiquitylating enzymes (DUB) (Clague et al., 2012), it enables cells to adapt to various stimuli, stresses and to maintain cellular homeostasis.

2.8 Ubiquitin and ubiquitin-like proteins

Ubiquitin is a small globular protein of 76 AA that is highly conserved from yeast to human. In recent years, additional so called ubiquitin-like proteins (UBL) were identified, which share the characteristic β -grasp fold, but show only low amino acid identity with ubiquitin (see Introduction Table). Most members of this UBL family contain a C-terminal double glycine motif and utilize an analogous conjugation machinery to covalently attach to their respective substrates like ubiquitin (Jentsch and Pyrowolakis, 2000). Similar to the ubiquitylation system, the small ubiquitin related modifier SUMO (Smt3 in *S. cerevisiae*) is conjugated to targeted lysines via an enzymatic cascade consisting of the SUMO E1 SAE1/SAE2 (AOS1/Uba2) and the E2 Ubc9 supported by various SUMO E3 ligases like PIAS or RanBP2 (Flotho and Melchior, 2013). SUMOylation can be reverted by the action of SUMO-specific proteases (SEN1-7 in humans, Ulp1-2 in yeast) that cleave SUMO moieties from the substrate (Mukhopadhyay and Dasso, 2007). Posttranslational modification with SUMO has been implicated in various cellular pathways including transcription, chromatin remodeling, DNA repair, nucleo-cytoplasmic transport, mitosis, and stress response (Müller et al., 2001). Similar to the non-covalent interaction between ubiquitin and UBDs, conjugated SUMO can mediate physical interactions by binding to linear SUMO interaction motifs (SIM) (Hay, 2013). Interestingly, beside the direct

competition for critical lysines on a substrate to modulate its activity, like in the case of PCNA (K164) (Hoegel et al., 2002), ubiquitylation and SUMOylation can also act synergistically (Bergink and Jentsch, 2009). SUMO-targeted ubiquitin ligases (STUbLs) like the Ubiquitin E3 ligase RNF4 (Slx5/Slx8 in yeast) harbor several SIMs, which are essential for the recognition and subsequent ubiquitylation and degradation of SUMOylated substrates, *e.g.* PML or PARP-1 (Tatham et al., 2008). Thus, the SUMOylation and ubiquitylation systems do not represent two separate branches, but rather a tightly interconnected network for protein regulation with large functional overlaps (Denuc and Marfany, 2010).

Ubiquitin-like protein		Identity to ubiquitin (%)	Substrate(s)	Attributed functions
<i>H. sapiens</i>	<i>S. cerevisiae</i>			
UBL5 / mHub1	Hub1	22	Unknown	Pre-mRNA splicing DNA damage repair,
SUMO1	Smt3	18	Many (<i>e.g.</i> PCNA, STAF65γ, TFII-I, PML, XRCC1, hSnu66)	transcriptional regulation, protein targeting, stress response
SUMO2/3 #	-	16	Many (<i>e.g.</i> Aurora-B, PML, Topoisomerase II, C/EBPβ1)	Mitosis, protein targeting, transcriptional regulation, stress response
URM1	URM1	12	Ahp1, tRNA	Oxidative stress response, tRNA modification
NEDD8	Rub1	58	Cullins, p53, MDM2	Regulation of Cullin-E3s
ISG15 / UCRP *	-	29 / 37	JAK1, STAT1, ERK1/2, PLCγ1, serpin 2a	Immune response, signal transduction
FAT10 *	-	29 / 36	p62/SQSTM1, p53	Immune response, cell cycle, protein degradation
FUB1	-	37	Bcl-G, TCR-α-like protein	T-cell activation
LC3	Atg8	10	Membrane lipids (Phosphatidylethanolamine)	Autophagy
ATG12	Atg12	17	Atg5	Autophagy

Introduction Table: Ubiquitin-like proteins

* ISG15 and FAT10 comprise two interconnected ubiquitin-like domains. # SUMO 2 and SUMO 3 share 95% identity. (Modified from Welchman et al., (2005)).

Another ubiquitin-like protein, Rub1 (NEDD8 in metazoans, Neural precursor cell expressed, developmentally down-regulated 8), shows the highest sequence similarity with ubiquitin and neddylation requires the action of specific E1, E2 and E3 enzymes (Liakopoulos et al., 1998). After C-terminal processing of the NEDD8 precursor by NEDP1 or UCHL3 its activation is catalyzed by the heterodimeric E1 enzyme APPBP1 (NAE1) / UBA3. The E2 conjugating enzyme Ubc12 and Ube2F in concert with several E3 ligases like Rbx1 / Dcn1, Mdm2 or c-Cbl then transfer NEDD8 moieties to lysine residues of specific substrates (Rabut and Peter, 2008). The covalent conjugation can be reversed by NEDD8 isopeptidases in a process termed deneddylation, which is catalyzed by the CSN5 subunit of the COP9 signalosome (CSN) (Cope and Deshaies, 2003). In contrast to ubiquitin and SUMO the diversity of NEDD8 substrates is rather limited. Rub1 / NEDD8 was shown to have regulatory functions by modifying the different cullin subunits of Skp1/Cullin/F-box (SCF) E3 ligases (Liakopoulos et al., 1998). Repetitive cycles of neddylation and

deneddylation are crucial for the stability and activity of cullin-based ubiquitin ligases (Bosu and Kipreos, 2008).

Ubiquitin-like proteins of the ATG family, Atg8 (alias MAP1LC3A-C in humans) and Atg12, play pivotal roles in the autophagy pathway. During this catabolic process, eukaryotic cells induce the formation of autophagosomal vesicles, which engulf proteins, aggregates or damaged organelles, and subject them to lysosomal degradation (Eskelinen, 2005). Interestingly, Atg8 and Atg12 share the same E1 activating enzyme Atg7, but in subsequent reactions Atg12 is conjugated to Atg5 via the E2 Atg10 in order to be incorporated in the multimeric Atg12-Atg5-Atg16 complex that is crucial for autophagosomal membrane formation (Geng and Klionsky, 2008). The other autophagy-related UBL, Atg8, undergoes a particularly interesting conjugation pathway, as it is covalently attached to the autophagosomal membrane lipid phosphatidylethanolamine, catalyzed by the E2 Atg3 and Atg12-Atg5-Atg16 serving as the Atg8 E3 ligase (Shpilka et al., 2011). Lipidated Atg8 plays a dual role in autophagy; firstly, it stimulates autophagosomal membrane formation and expansion and secondly, Atg8 attracts and tethers adaptor proteins like p62/SQSTM1 or NBR1 with their respective cargo to the inner leaflet of the autophagosomal vesicle for subsequent degradation (Waters et al., 2009; Pankiv et al., 2007). While there is only a single Atg8 variant in *S. cerevisiae*, the human genome encodes seven Atg8 paralogs including ubiquitin-like proteins of the LC3 group (microtubule-associated protein 1 light chain 3, MAP1LC3A-C), the GABARAP and GABARAPL1 proteins (γ -amino-butyric acid receptor-associated proteins) and GATE-16 (Golgi-associated ATPase enhancer of 16 kDa or GABARAPL2). Due to structural similarities, members of the human Atg8 family share multiple interaction partners with overlapping functions and thus are functionally closely interconnected within the autophagy network (Behrends et al., 2010).

In contrast to the abovementioned UBLs, the molecular conjugation machinery and cellular function of other ubiquitin-like proteins remains poorly understood. Although the enzymatic cascade for ISG15 (Interferon stimulated gene 15) with UbeL1 (E1), UbcH8 (E2), and Herc5 or EFP as E3 ligases is identified, the exact molecular mechanism of its action is still unclear (Sgorbissa and Brancolini, 2012). Upon immunostimulatory endotoxins or interferons, ISG15 is highly induced in human cells, which triggers antiviral signaling events like JAK-STAT activation and ISGylation of viral and host cell proteins (Malakhov et al., 2003; Durfee et al., 2010). Among the ISG15 substrates, several enzymes of the ubiquitin conjugation machinery like Ubc13, EFP and UbcH6 were identified for which ISGylation is thought to negatively regulate their activity in order to modulate ubiquitin-dependent pathways during infection (Zhang and Zhang, 2011).

Like ISG15 another UBL, FAT10, consists of two ubiquitin-like domains with a short linker region and is involved in the human immune defense system as well (Dye

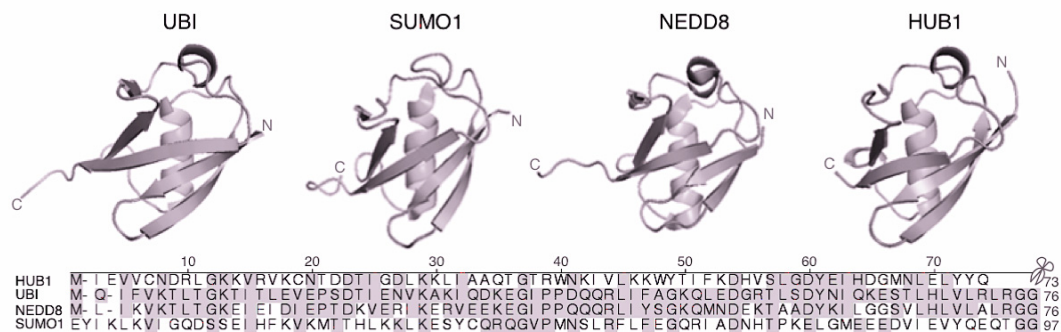
and Schulman, 2007). Cells treated with interferon γ or tumor necrosis factor α activate FAT10 expression and its conjugation machinery with the E1 enzyme Uba6 and the E2 USE1. During the immune response FAT10 has been implicated in transcriptional regulation via p53, NF κ B signaling and the degradation of viral substrates serving as an alternative molecular tag for proteasomal degradation (Aichem et al., 2012).

Based on *in silico* analysis, structural and sequencing data elucidated a close relationship between the prokaryotic sulfur transfer system and the eukaryotic ubiquitin/ubiquitin-like conjugation machinery. In bacteria, MoaD and ThiS proteins are crucial factors for the thiamine and molybdopterin synthesis (Chowdhury et al., 2012) and share the characteristic ubiquitin-like β -grasp fold and C-terminal activation step (Pedrioli et al., 2008). Here, the ubiquitin related modifier 1 (Urm1) might represent the evolutionary link between the sulfur carrier function and ubiquitin-like protein modification (Petroski et al., 2011). In eukaryotes Urm1 is adenylated by its E1 enzyme Uba4, which subsequently catalyzes the sulfur transfer to Urm1's C-terminus via its rhodanese-like domain with Nfs1 serving as a sulfur donor (Petroski et al., 2011). After the formation of this thiocarboxylate linkage with Uba4, Urm1 plays a crucial role in the thiolation of several tRNAs at the wobble position U₃₄ (Leidel et al., 2009). In addition to its function in tRNA modification, Urm1 can utilize an alternative conjugation pathway in order to be conjugated to proteins (Furukawa et al., 2000; Wang et al., 2011). Oxidative cellular stress up-regulates the Urm1 conjugation machinery including peroxiredoxin Ahp1, MOCS3 (Uba4 in yeast), the thiouridylases CTU1 and CTU2 (Ncs6 and Ncs2 in *S. cerevisiae*) and specifically induces additional urmylation substrates like the DUBs USP15, USP47, and the nucleo-cytoplasmic shuttling factor CAS (van der Veen et al., 2011). As oxidative stress affects both thiolation of tRNAs and protein urmylation, further investigation will be necessary to elucidate the interplay of Urm1-dependent pathways and the cellular function of the Urm1 modification.

2.9 The ubiquitin-like protein Hub1

Among the ubiquitin-like protein family Hub1 (homologous to ubiquitin 1, alias UBL5 or Beacon in metazoans) represents a special member, as it shares common features of UBLs, but it is not conjugated like canonical modifiers. Covalent conjugation of an UBL to a substrate's target residue is ATP-dependent, involves an enzyme cascade, and usually requires a free di-glycine motif at the C-terminus. Hub1 shares only 22% sequence identity with ubiquitin, but is highly conserved from yeast to human (64.4%, 80.8% from *C. elegans* to *H. sapiens*) (Friedmann et al., 2001). Although structurally very similar to ubiquitin (Ramelot et al., 2003; McNally et al., 2003), Hub1 does not function as a covalent modifier as it lacks the protruding C-terminal tail as well as the characteristic double glycine motif (Jentsch and

Pyrowolakis, 2000). Comprehensive studies affirmed that Hub1 is not conjugated, but binds proteins only non-covalently, and independently of ATP or the double tyrosine motif (Luders et al., 2003; Yashiroda and Tanaka, 2004).



Introduction Figure VII: Human Hub1 among other ubiquitin-like proteins

Structural ribbon representations of Hub1 (this study, (McNally et al., 2003)), human ubiquitin (1UBQ), SUMO1 (2ASQ) and NEDD8 (2KO3) (upper panel, respective PDB codes in brackets). Protein sequence alignment of HUB1 with ubiquitin, SUMO1 (AA21-97) and NEDD8 from *H. sapiens*. The scissors symbol indicates the processing site after the di-glycine motif in ubiquitin, NEDD8 and SUMO1. Hub1 shares the compact ubiquitin-like fold, but lacks the typical C-terminal extension and the di-glycine motif of conventional ubiquitin-like proteins.

Recently, yeast Hub1 was shown to interact with the spliceosomal protein Snu66, a protein of the U4/U6.U5 tri-snRNP complex (Mishra et al., 2011; Wilkinson et al., 2004). In *S. cerevisiae*, Hub1 is not essential for viability and is apparently also not required for general splicing as judged by splicing-sensitive microarray assays (Mishra et al., 2011). Intriguingly, Hub1 affects splicing directly through non-covalent interactions and *hub1Δ* cells fail to promote alternative splicing of *SRC1*, which is one of the rare cases of *S. cerevisiae* genes for which alternative splicing has been reported (Mishra et al., 2011). Abolishing Hub1-Snu66 interaction by mutation affects *SRC1* alternative splicing as well, suggesting that binding of Hub1 to Snu66 is critical for Hub1 function in *S. cerevisiae*. Since *SRC1* is also not essential for viability, it seems possible that the function of Hub1 in *S. cerevisiae* is restricted to *SRC1*. By contrast, in *S. pombe*, in which splicing is much more prevalent than in *S. cerevisiae*, Hub1 affects splicing of several pre-mRNAs and is essential for viability.

In spite of these detailed findings, much less is known about Hub1 from higher eukaryotes. Human Hub1 appears to be exported from the nucleus upon hypo-osmotic shock (Hatanaka et al., 2006), and is known to bind certain protein kinases (Kantham et al., 2003). Genetic analyses have correlated *HUB1* gene expression and single nucleotide polymorphisms with predisposition to obesity, diabetes and other factors of the metabolic syndrome (Bozaoglu et al., 2006; Jowett et al., 2004). Other studies postulate a regulatory role in the hypothalamus and in the secretion of corticosterone and cortisol from cultured *zona fasciculata/reticularis* cells, respectively (Ziolkowska et al., 2004; Brailoiu et al., 2003). In proteomic approaches using high-throughput mass spectrometry, Hub1 has been detected in purified, *in vitro* assembled human spliceosomes (Deckert et al., 2006) and reported to meet Cajal bodies as well (Švéda

et al., 2013), but Hub1's function remained unexplored. In the nematode *C. elegans*, Hub1 was identified in a genetic screen for genes implicated in the unfolded protein response in mitochondria (UPR^{mt}) (Benedetti et al., 2006). Moreover, co-immunoprecipitation experiments from cell extracts suggested that *C. elegans* and mammalian Hub1 associate with the DVE-1 transcription factor responsible for the UPR^{mt} pathway (Haynes et al., 2007). However, neither of these studies have addressed the molecular function of Hub1 directly, thus its implication in cellular pathways or the relevance of Hub1 for human cells remained obscure.

3 Aim of this study

Ubiquitin and ubiquitin-like proteins play pivotal roles in a multitude of cellular pathways, including signal transduction, protein sorting, DNA repair, and cell cycle regulation. Canonical members of this protein family are enzymatically conjugated to other proteins, thereby functioning as covalent protein modifiers affecting the stability, localization or function of their substrates.

Although the highly conserved protein Hub1 shares the characteristic ubiquitin-like fold, it does not function as a covalent modifier but binds proteins only non-covalently. Thus far, little is known about the molecular function as well as the cellular pathways in which the ubiquitin-like protein Hub1 is implicated particularly in mammalian cells.

The aim of this study was to investigate the function of human Hub1 in mammalian tissue culture cells. The unique feature of Hub1 lacking a C-terminal extension and thus solely resembling the ubiquitin-like fold raised the question of how Hub1 associates with other proteins. Therefore, various protein interaction assays were conducted in order to identify potential binding partners and to characterize the minimal Hub1 interaction domain. Additionally, Hub1 localization was studied in human cell lines by microscopy to shed light onto the cellular pathways and the functional context Hub1 is implicated in. Moreover, RNA interference techniques were applied to deplete Hub1 from human cells providing further insights into the relevance and function of the ubiquitin-like protein *in vivo*. Phenotypical characterization of Hub1-depleted cells by microscopy and flow cytometry was combined with a comprehensive biochemical analysis to identify Hub1-dependent pathways. Subsequently, the cellular responses to Hub1 inactivation were described and the detailed examination of altered biochemical processes elucidated the underlying molecular basis. Furthermore, complementation assays, in which mutant variants of Hub1 were reintroduced into Hub1-depleted cells, were conducted in order to functionally characterize crucial sites on the ubiquitin-like protein.

4 Results

4.1 Identification of human Hub1 interactors by yeast two-hybrid screening

As little was known about Hub1 and its cellular function, an unbiased approach to identify novel interaction partners of Hub1 was conducted. The yeast two-hybrid (Y2H) technique allows screening of protein-protein interactions based on human cDNA libraries from different tissues. A previous report indicated that Hub1, though ubiquitously expressed in human tissue, is highly up-regulated in brain, heart, skeletal muscle, kidney, and liver (Friedmann et al., 2001). Thus, libraries of fetal brain tissue and HeLa cell cDNAs with high transcript coverage were expressed as AD-fusions, whereas the Hub1 BD-fusion protein served as bait for screening. After optimization of transformation efficiency to ensure maximum cDNA library coverage, 332 positive candidate clones were obtained from the initial screening step.

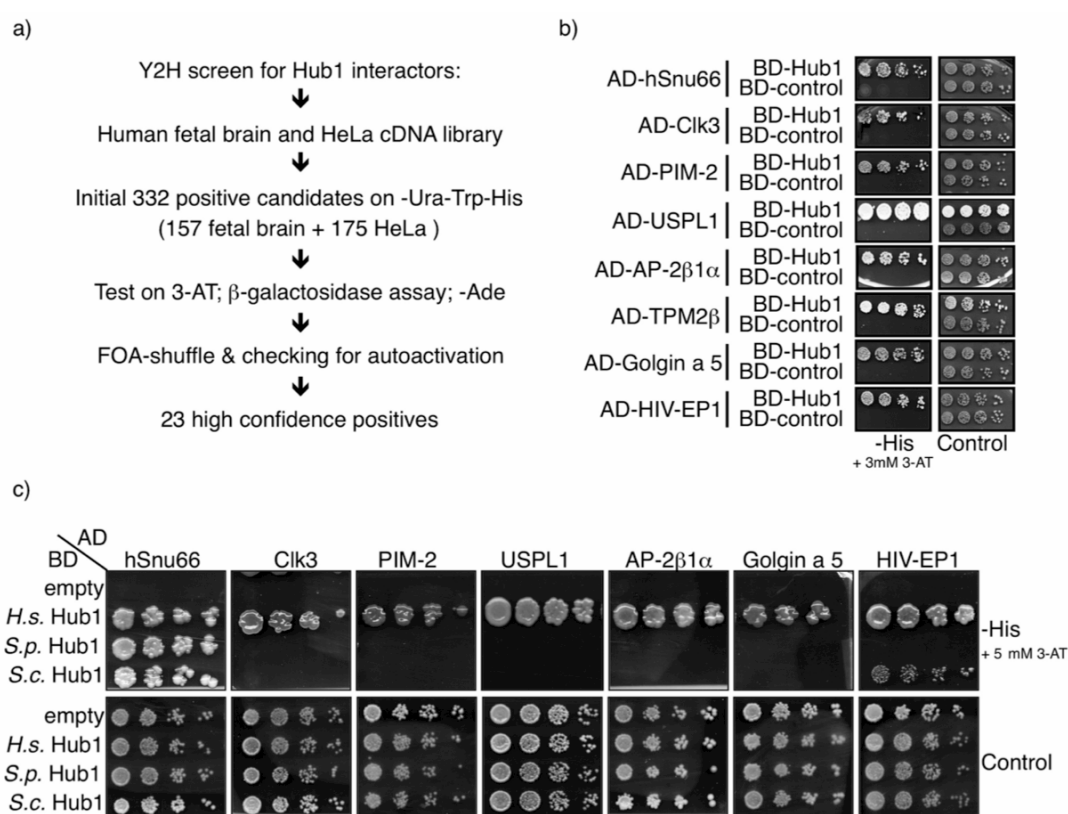


Figure 1: Identification of Hub1 interactors by mammalian yeast two-hybrid screen

a) Schematic overview of the yeast two-hybrid screen for human Hub1 interactors. BD-Hub1 was used as bait for screening mammalian cDNA libraries from human fetal brain and HeLa cells. b) Confirmation and identification of high confidence candidates. AD-Plasmids of candidate cDNAs fulfilling stringent criteria were isolated, sequenced and co-transformed with BD-Hub1 for re-confirmation. c) Yeast two-hybrid interaction studies of identified AD-candidates with different *HUB1* orthologs. BD-fusions of Hub1 from *S. cerevisiae* (*S.c.*), *S. pombe* (*S.p.*) and *H. sapiens* (*H.s.*) were co-transformed with AD-constructs identified in the cDNA library screen expressing hSnu66, Clk3, PIM2, USPL1, AP2 β , Golgin a 5, or HIV-EBP, respectively. Serial dilutions of cells were spotted on control or selective plates.

High confidence candidates which fulfilled the stringent criteria including 3-AT resistance (at 3 mM, 5 mM or 10 mM), β -galactosidase activity or growth on adenine-lacking (-Ade) plates were revalidated and tested for auto-activation after FOA-shuffle (Figure 1a). Subsequent DNA sequencing of the AD constructs revealed the identity of Hub1's Y2H interactors, namely spliceosomal tri-snRNP protein hSnu66, Cdc2/Cdc28-like dual specificity protein kinase Clk3, proto-oncogenic serine/threonine-protein kinase PIM-2, SUMO/ubiquitin-specific peptidase-like 1 USPL1, endocytosis receptor adapter protein complex AP-2 β subunit 1 α (AP-2 β 1 α), actin-binding cytoskeleton protein tropomyosin 2 β (TPM2 β), Golgi-associated protein Golgin a 5, and human zinc-finger transcription factor HIV-EP1 (Figure 1b).

Further interaction studies, in which the newly identified candidates were tested with *HUB1* orthologs from *S. cerevisiae*, *S. pombe* and *H. sapiens*, showed that the spliceosomal protein hSnu66 is the only common binding partner of all Hub1 variants despite Hub1's high conservation from yeast to human (Figure 1c). This finding indicates an important and conserved link between Snu66 is of Hub1 with a strong implication in pre-mRNA splicing.

4.2 Hub1 binds the spliceosomal protein hSnu66 *in vivo*

In order to validate the interaction between Hub1 and hSnu66 *in vivo*, co-immunoprecipitation experiments with tissue culture cells were conducted. For this, mammalian expression constructs encoding tagged Hub1 and hSnu66 proteins were transfected into human cells.

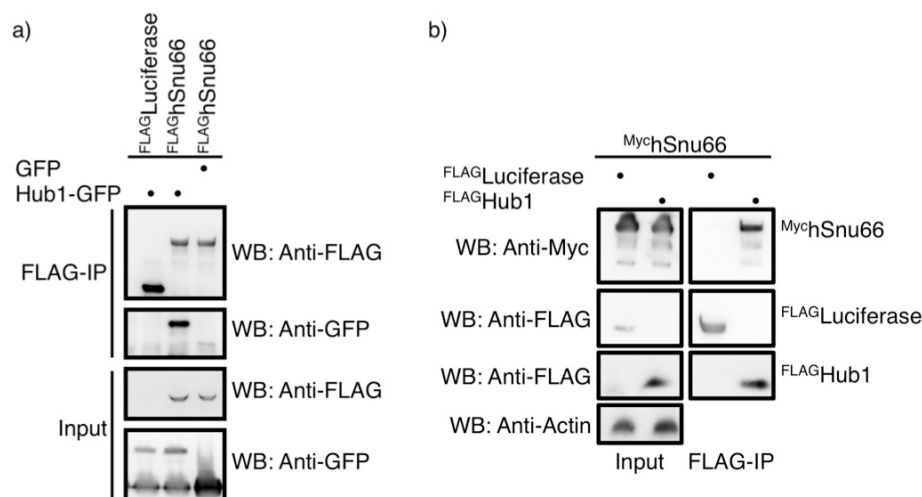


Figure 2: Hub1 and the tri-snRNP protein hSnu66 interact *in vivo*

a) hSnu66 co-precipitates with Hub1. HEK 293T cells were co-transfected with GFP-tagged Hub1 or free GFP and FLAG-tagged hSnu66 or ^{FLAG}luciferase. Cells were harvested, lysed and proteins were immunoprecipitated using anti-FLAG M2 IgGs coupled to agarose. Inputs and FLAG-precipitates were analyzed by immunoblotting using anti-GFP and anti-FLAG antibodies. b) Hub1 co-precipitates with hSnu66. HEK 293T cells were co-transfected with Myc-tagged Snu66 and FLAG-tagged Hub1 or ^{FLAG}luciferase. Cells were harvested, lysed and proteins were immunoprecipitated using anti-FLAG IgGs coupled to agarose. Inputs and FLAG-precipitates were analyzed by immunoblotting using anti-Myc and anti-FLAG antibodies. Actin served as a loading control.

24-48 h post transfection cells were harvested, lysed and the epitope tagged proteins were purified with tag-specific antibodies immobilized on beads. The immunoprecipitation of ^{FLAG}hSnu66 co-purified GFP-labeled Hub1, whereas the control using ^{FLAG}luciferase or free GFP remained negative (Figure 2a). *Vice versa*, ^{FLAG}Hub1 immunoprecipitated Myc-tagged hSnu66 and verified the binding, while luciferase served as negative control (Figure 2b). Consistent with the identification of Hub1-hSnu66 interaction in unbiased yeast two-hybrid screens these co-purification experiments indicate a tight association between the ubiquitin-like protein and the spliceosome-associated factor.

4.3 A conserved motif in hSnu66 mediates Hub1 interaction

After the initial findings of Hub1's conserved interaction with hSnu66 *in vivo*, the question of how the Hub1-hSnu66 interaction is mediated arose. Bioinformatics analyses indicated that hSnu66 is an intrinsically unstructured protein with low complexity regions, which has been proposed to be characteristic for a large fraction of spliceosome-associated factors, as this allows structural flexibility and different conformational stages (Korneta and Bujnicki, 2012). However, a previous report described a putative leucine zipper domain, which might mediate direct binding of Snu66 to DNA (Makarova et al., 2001). Moreover, protein sequence alignments of Snu66 from different species elucidated two highly conserved domains located at the amino- and carboxy-terminus, with no obvious homology to known protein domains. Compared to yeast, the human homolog hSnu66 gained additional domains (Figure 3a) like its amino-terminal arginine-serine rich domain (RS-domain, AA41-108) (Makarova et al., 2001), which can serve as a protein-protein interaction motif (Kohtz et al., 1994; Wu and Maniatis, 1993) or mediate binding to mRNA directly *e.g.* at regulatory exonic enhancer sequences (Shen and Green, 2006; Shen et al., 2004; Rudner et al., 1998). Besides the leucine zipper and nuclear localization signals, hSnu66 encodes another DNA directed domain, namely a putative transcription factor engrailed homology domain 1 (EH1). Interestingly, although Snu66 in yeast lacks the RS-domain, a short stretch of 18 AA within the N-terminal domain is highly conserved among species.

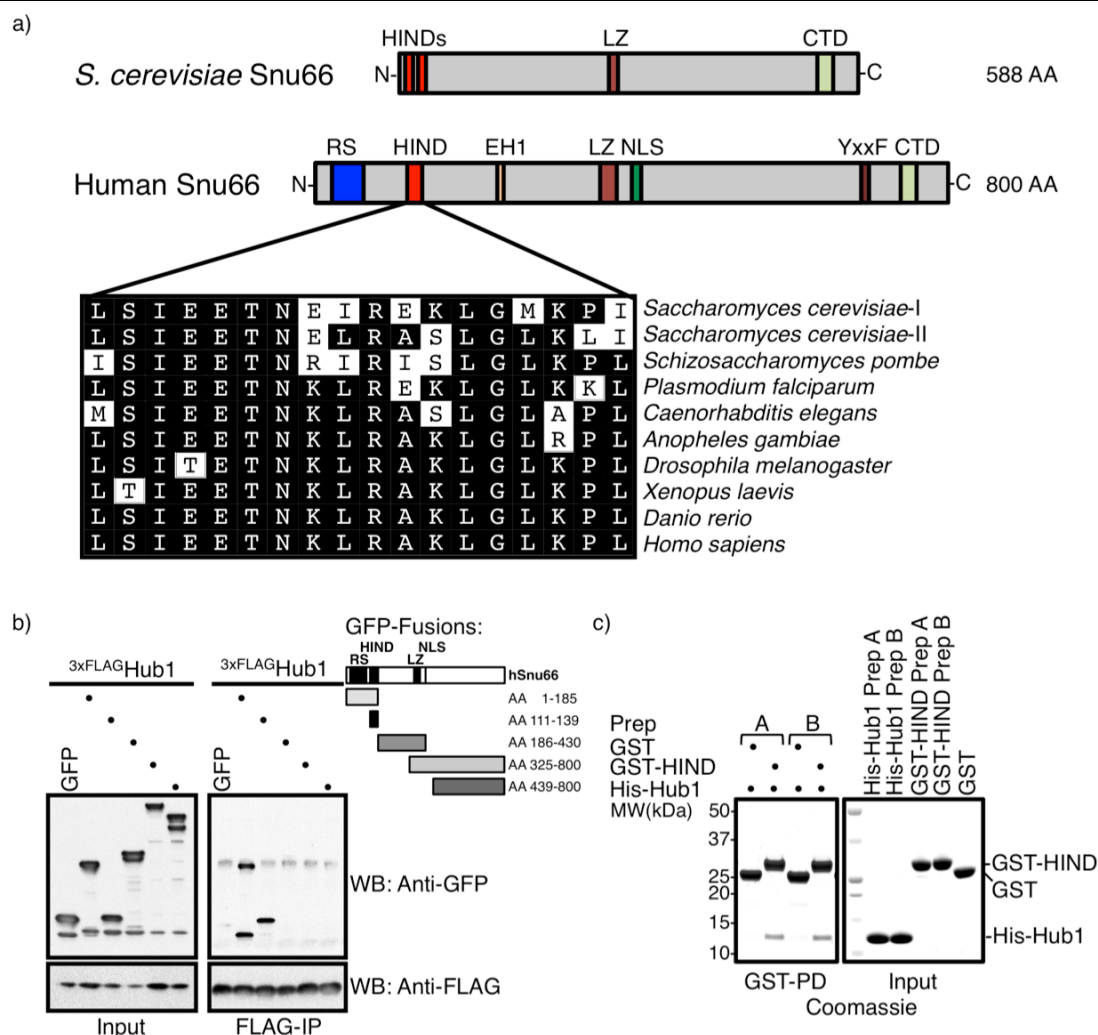


Figure 3: Mapping of the Hub1 interaction domain in hSnu66

a) The Hub1 Interaction Domain (HIND) is conserved from yeast to human. Schematic representation of ScSnu66 and hSnu66 and their putative domains. HIND: Hub1-interaction domain, LZ: leucine zipper, CTD: Carboxy-terminal domain, RS: arginine-serine rich domain, EH1: engrailed homology domain 1, NLS: nuclear localization signal, YxxF: AP-dependent endocytosis motif. Below: Alignment of putative HIND sequences in Snu66 orthologs as indicated aside. Amino acids which are identical with human HIND are shaded in black to highlight conservation. b) Binding of Hub1 is mediated via a N-terminal domain in hSnu66. Mapping of the Hub1 interaction domain in hSnu66 using FLAG-immunoprecipitation of ^{3xFLAG}HisHub1 after co-expression of GFP-tagged hSnu66 truncations (as indicated) or GFP as control in HEK 293T cells. Immunoprecipitates were immunoblotted with anti-FLAG and anti-GFP antibody. c) A short conserved N-terminal motif in hSnu66 (HIND) is sufficient for direct interaction with Hub1. GST pull-down assay with recombinant GST-HIND fusion protein and 6xHis-tagged Hub1. Free GST served as a control. Two different buffer conditions (Prep A: Tris-based B: HEPES based) were used. Coomassie blue staining is shown.

In order to identify the domain or motif mediating Hub1-hSnu66 direct interaction, several truncations of hSnu66 were generated comprising the N-terminus (AA1-185) with its arginine-serine rich domain (RS-domain) and the highly conserved stretch of 18 AA (AA111-139), the central region (AA 186-430, encoding for a putative leucine zipper (LZ) and nuclear localization sequences (NLS)) or C-terminal fragments, which overlap with the LZ and NLS (AA 325-800) or cover domains from AA439 to the end of the protein (AA439-800). These GFP-tagged truncations were co-expressed with ^{3xFLAG}HisHub1 to map down the binding motif by FLAG-

immunoprecipitation. The hSnu66 N-terminal fragment (AA1-185) was able to bind and co-purify with Hub1, but, notably, the short highly conserved stretch within hSnu66's N-terminus (AA111-139) was already sufficient for the interaction with Hub1 (Figure 3b). Like the negative control, free GFP, neither the central region of hSnu66 nor C-terminal fragments were able to co-purify with Hub1.

Importantly, the interaction between Hub1 and the short highly conserved stretch, which was termed HIND (for Hub1 interaction domain), was verified with purified recombinant proteins to exclude any bridging factor, thereby proving direct binding. After 6xHis-tagged Hub1, GST-HIND and free GST were isolated from *E. coli* by affinity-chromatography, Hub1 was incubated with either GST-HIND or GST as control and pull-down assays were conducted. Indeed, the isolated HIND was proficient in direct Hub1 binding and clearly precipitated Hub1 in GST-pull-down studies (Figure 3c).

This data indicated an intriguing mode of non-covalent interaction between a ubiquitin-like protein (Hub1) and a spliceosomal core component (Snu66). In order to obtain molecular insights, the crystal structure of human Hub1 in complex with hSnu66's HIND was solved. For this, HIND peptides, comprising AA 117-135 of hSnu66, were chemically synthesized (by MPIBC core facility) and incubated with recombinant 6xHis-tagged Hub1 for crystallization. In close collaboration with the NMR department at the MPIBC the crystallization and structure determination was conducted by K. Kowalska.

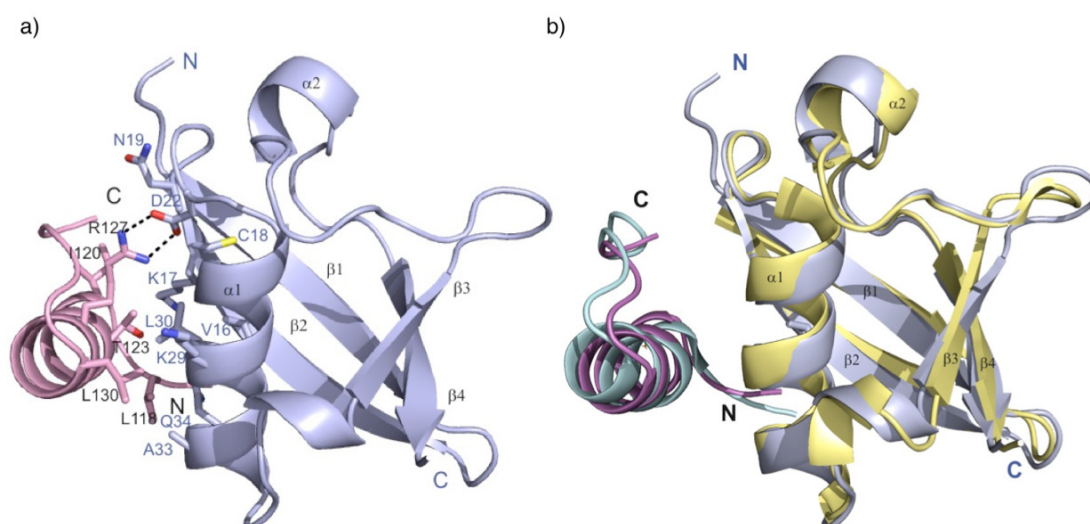


Figure 4: The crystal structure of the Hub1-HIND complex

a) Crystal structure of the human Hub1 in complex with the hSnu66 HIND peptide at 2 Å resolution shown as a ribbon plot. The human HIND - Hub1 interaction is mediated by a salt bridge between R11 of HIND (R127 in hSnu66) and D22 of HsHub1 accompanied by several hydrophobic contacts formed by aliphatic residues of HIND and Hub1. b) Overlay of crystal structures comparing human Hub1-HIND (blue, purple) interaction superimposed with yeast ScHub1-ScHIND II (yellow, cyan) complex shows high conservation on molecular level. NMR data was obtained in collaboration with K. Kowalska.

As described previously (McNally et al., 2003), Hub1 shares the β -grasp fold of ubiquitin and ubiquitin-like proteins with their typical $\beta\beta\alpha\beta\alpha\beta$ secondary structure pattern (Figure 4a). This new structure with a resolution of 2 Å clearly explains the nature of the human HIND - Hub1 interaction that is mediated via a salt bridge between R11 of HIND (R127 in hSnu66) and D22 of Hub1 accompanied by several hydrophobic contacts formed by aliphatic residues of the HIND (L2, I4, T7, L10, R11 (C β and C γ), L14, L16, L19) and Hub1 (M1, V16, K17 (C β , C γ , C δ), C18, N19 (C β , C γ), K29 (C β , C γ , C δ), V30, L33). Upon HIND binding the main-chain fold of Hub1 does not change significantly, but several side chains change their orientation representing an induced-fit conformation.

The direct comparison of human and yeast Hub1-HIND complexes (HsHub1-HsHIND (blue, purple), ScHub1-ScHIND II (yellow, cyan, PDB: 3PLV (Mishra et al., 2011)) emphasizes the similarity of the two structures with a root mean squared deviation of 0.716 Å for the main chain heavy atoms (Figure 4b). The interaction interface, formed by the salt bridge (R127-D22) among hydrophobic contacts between hSnu66 and Hub1, is almost identical and illustrates the high conservation of this interaction module at molecular level. Despite the high conservation and structural similarities between yeast and human Hub1, a unique patch appears to be particularly interesting. The loop formed by α 2- β 3 in human Hub1 contains two hydrophobic residues, W47 and Y48, which are strikingly exposed to the solvent. Moreover, although this unusual aromatic patch is highly conserved in all metazoan orthologs, it is not present in *S. cerevisiae* Hub1.

4.4 Mutations in the HIND abolish Hub1-hSnu66 interaction

The structural data gives detailed information about crucial amino acid residues that are important for the interaction surface between Hub1 and hSnu66. Beside the contributing hydrophobic contacts formed by aliphatic residues, the central interaction bond is created via the salt bridge between R127 of HIND in hSnu66 and D22 of Hub1. In order to validate this finding, co-immunoprecipitation experiments were performed, in which mutant alleles of hSnu66 and Hub1 leading to interaction-deficient variants were ectopically expressed. For this, human tissue culture cells were transfected with either ^{FLAG}hSnu66 WT or R127A mutant form together with GFP-labeled Hub1 WT or D22A point mutant (Figure 5a). When both wild type proteins were expressed and FLAG-immunoprecipitation was performed, binding of Hub1 to hSnu66 was evident. However, mutant alleles with point mutations at interaction surface residues abrogated binding of Hub1 WT in ^{FLAG}hSnu66 R127A immunoprecipitations. *Vice versa*, the interaction with hSnu66 WT was also disrupted when the crucial residue in Hub1 was mutated (D22A).

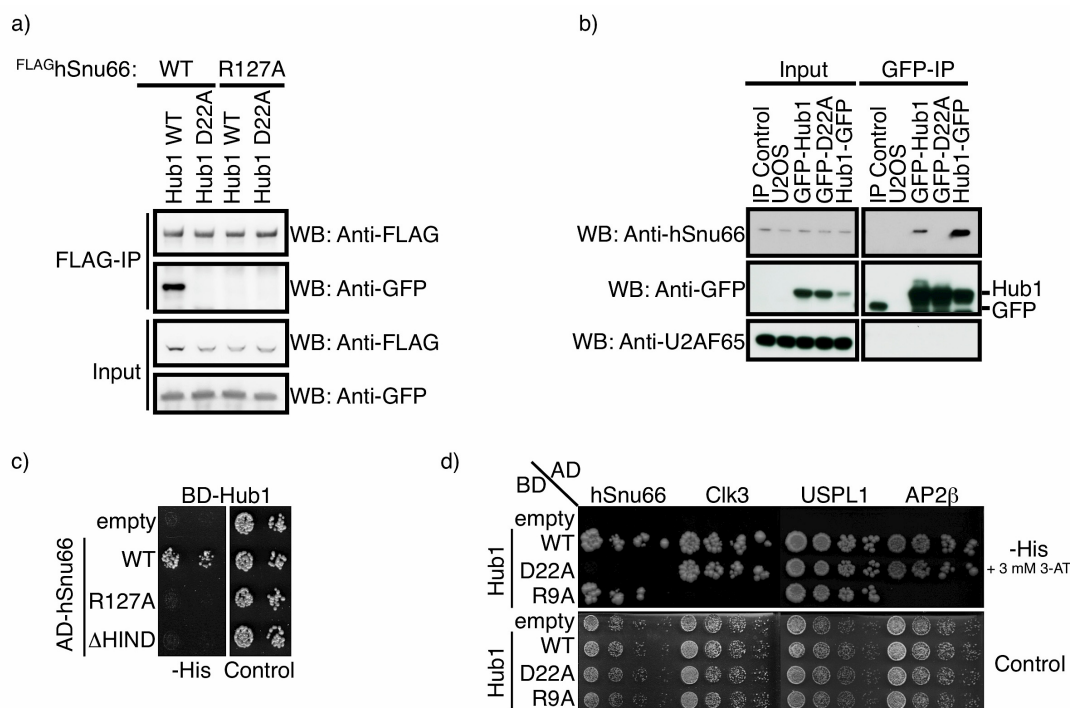


Figure 5: Single point mutations in the HIND interface disrupt Hub1 - hSnu66 interaction

a) Single point mutations in Hub1 (D22A) or hSnu66 (R127A) abolish interaction *in vivo*. GFP-tagged WT or D22A mutant Hub1 was co-transfected with FLAG-tagged hSnu66 WT or R127A mutant into HEK 293T cells. Cells were harvested, lysed and proteins were immunoprecipitated using anti-FLAG M2 IgGs. Inputs and FLAG-precipitates were analyzed by immunoblotting using anti-GFP and anti-FLAG antibodies. b) Hub1 interacts with endogenous hSnu66 *in vivo* depending on the D22 surface. U2OS WT or cells stably expressing N-terminally GFP-tagged Hub1 WT, Hub1 D22A, C-terminally GFP-tagged Hub1 or a GFP-control were harvested, lysed and proteins were immunoprecipitated using anti-GFP antibodies. Inputs and GFP-precipitates were analyzed by immunoblotting using anti-GFP and anti-hSnu66 antibodies. Untreated U2OS and anti-U2AF65 served as controls. c) Point mutations in the HIND disrupt yeast two-hybrid interaction. Cells expressing human Hub1 (N-terminal BD-fusion) with either hSnu66 WT or mutant hSnu66 R127A or Δ HIND as an AD-fusion. Whereas all strains grew on control plates, growth was restricted to cells co-expressing BD-Hub1 and AD-hSnu66 WT confirming the HIND-dependent interaction between Hub1 and hSnu66. d) Yeast two-hybrid interaction studies with Hub1 mutants and candidates from the mammalian cDNA library screen. BD-Hub1 WT, D22A or R9A were co-transformed with AD-constructs expressing hSnu66, Clk3, USPL1 or AP2 β , respectively. Cells were spotted on control plates or selective plates.

Considering the fact that conventional transient transfection techniques lead to high protein expression due to strong promoters and high copy numbers, it was important to characterize the interaction *in vivo* under more physiological conditions. In order to address this point, several U2OS cell lines stably expressing GFP-Hub1 WT, the binding-deficient mutant GFP-Hub1 D22A, C-terminally tagged Hub1-GFP and GFP-control, respectively, were generated. After testing the moderate expression of the GFP-fusion proteins, these cell lines were used for further interaction studies. Indeed, wild type Hub1 clearly co-purified with endogenous hSnu66 in GFP-immunoprecipitation assays, whereas the D22A mutation in Hub1 abolished the interaction. Notably, either of the amino- or carboxy-terminally GFP-tagged versions of Hub1 were able to precipitate hSnu66 under physiological conditions, indicating that both versions are properly folded proteins and their GFP-tag does not abrogate hSnu66 binding via the Hub1-HIND interaction surface.

As the initial findings had been obtained from the mammalian Y2H screen, another line of evidence came from yeast two-hybrid interactions studies. For this experiment, BD-Hub1 was co-transformed with AD-constructs encoding for hSnu66 WT, hSnu66 R127A mutant or a variant in which the whole HIND is deleted (hSnu66 Δ HIND), respectively. Yeast spottings on selective plates confirmed previous results, as only wild type Hub1 and hSnu66 showed an interaction, whereas both mutations in hSnu66 (R127A and Δ HIND) were negative (Figure 5c). Interestingly, interfering with the HIND interaction surface on Hub1 by mutating D22 to alanine disrupted hSnu66 binding specifically. Other candidates identified in the two-hybrid screen like Clk3, USPL1 or AP2 β , did not show any alterations in Hub1 binding when Hub1 WT and Hub1 D22A were compared. Furthermore, all two-hybrid interactions were reconfirmed in a *snu66 Δ* yeast strain to rule out any bridging effects of endogenous Snu66 (data not shown). In contrast, introducing an alanine substitution of R9 into Hub1 (Hub1 R9A) did not negatively affect hSnu66 binding, but the interaction with Clk3 and AP2 β was absent (Figure 5d). These data suggest that, besides the HIND-associated surfaces other motifs on Hub1 serve as additional interaction domains to mediate binding to alternative protein complexes.

4.5 Hub1 localizes to splicing-associated nuclear domains

The physical interaction of Hub1 with spliceosomal components like hSnu66 and SR protein kinase Clk3 (present study and Kantham et al., 2003) links Hub1 to the pre-mRNA splicing machinery, which is mainly located in the nucleus. Exploiting the stable U2OS cell lines, which stably express GFP-Hub1, the localization of Hub1 in human cells was determined. When standard immunofluorescence protocols were applied, GFP-tagged Hub1 showed a plain cellular distribution in the cytoplasm as well as in the nucleus without a distinct localization, which resembles the pattern of free GFP (Figure 7b). Nevertheless, introducing a pre-extraction step before fixation, the newly established immunofluorescence staining revealed a distinct, speckle-like localization of Hub1 within the nucleus. Immunofluorescence co-stainings elucidated that Hub1 is found in so-called *nuclear speckles* (also named SC35-domains or interchromatin granule clusters). Here, it co-localizes with nuclear speckle marker SR protein SC35 (Spector, 2003; Spector and Lamond, 2011), small nuclear ribonucleoparticle (snRNP) component U1A (Saitoh et al., 2004) or Sm proteins of snRNPs, which are recognized by Smith-antigen antibody Y12 (Boerbooms et al., 1985) (Figure 6a), but not with other nuclear domains like PML bodies or the nucleolus using PML, fibrillarin or UBF (data not shown). Nuclear speckles are highly dynamic structures from where splicing factors shuttle to active site of transcription (and concomitantly pre-mRNA splicing) (Spector et al., 1991; Ferreira et al., 1994; Wei et al., 1999). This nuclear compartment is thought to be important for splicing

factor maturation and modification as well as formation and storage of sub-complexes.

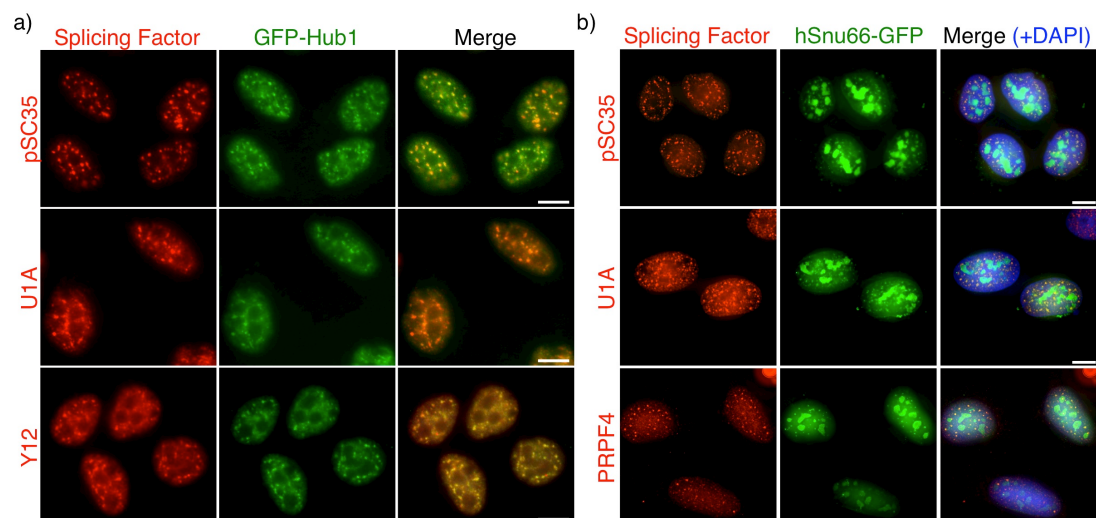


Figure 6: Co-localization of Hub1 and hSnu66 with nuclear speckle proteins

a) Hub1 localization in U2OS cells stably expressing GFP-Hub1 (green). Cells were pre-extracted, fixed and stained for splicing proteins (red) using antibodies against nuclear speckle marker phospho-SC35, snRNP protein U1A and SR proteins using Y12, respectively. Scale bar represents 10 μ M. b) Co-localization studies with U2OS cells stably expressing hSnu66-GFP (green). Cells were pre-extracted, fixed and stained for splicing proteins (red) using anti-phospho-SC35, anti-U1A and anti-PRPF4 antibodies, respectively. Images show z-stack projections of seven optical sections and are merged with DAPI as nuclear counterstain. Scale bar represents 10 μ M.

In addition, another U2OS cell line stably expressing C-terminally GFP-tagged hSnu66 was generated and used for localization studies. In these cells hSnu66 is efficiently imported into the nucleus where it is recruited to the same nuclear speckle compartment as observed in previous experiments with Hub1. Immunofluorescence studies with antibodies recognizing SR protein SC35, U1 snRNP factor U1A or tri-snRNP protein PRPF4 revealed co-localization with hSnu66-GFP (Figure 6b). In addition, hSnu66 is also found in the nucleolus, which was confirmed by co-stainings with nucleolar protein fibrillarin and upstream-binding factor 1 (UBF1) (data not shown). Hence, the co-localization data further support a close link of Hub1 and hSnu66 to pre-mRNA processing and splicing.

To further address Hub1 function and the interplay between Hub1 and hSnu66 in living cells, stable U2OS cell lines expressing the hSnu66-binding mutant GFP-Hub1 D22A or C-terminally GFP-tagged Hub1 (Hub1-GFP) were examined (Figure 7a). As shown before, GFP-Hub1 WT localization resembles the nuclear speckle pattern and co-localizes with the marker protein SC35. Interestingly, when the hSnu66-binding mutant was tested in immunofluorescence co-stainings, it became evident that GFP-Hub1 D22A still localizes to splicing speckles and overlaps with SC35-positive domains and thereby does not show significant differences to Hub1 WT. On the contrary, C-terminally GFP tagged Hub1 WT (Hub1-GFP), which was fully functional in hSnu66 binding (see Figure 5b), was not retained in nuclear substructures (Figure 7a). Thus, without proper incorporation into structural protein

complexes Hub1-GFP (like GFP serving as control) was washed out from the nucleus and staining was negative, while SC35 immunostaining was not altered and identical to previous samples.

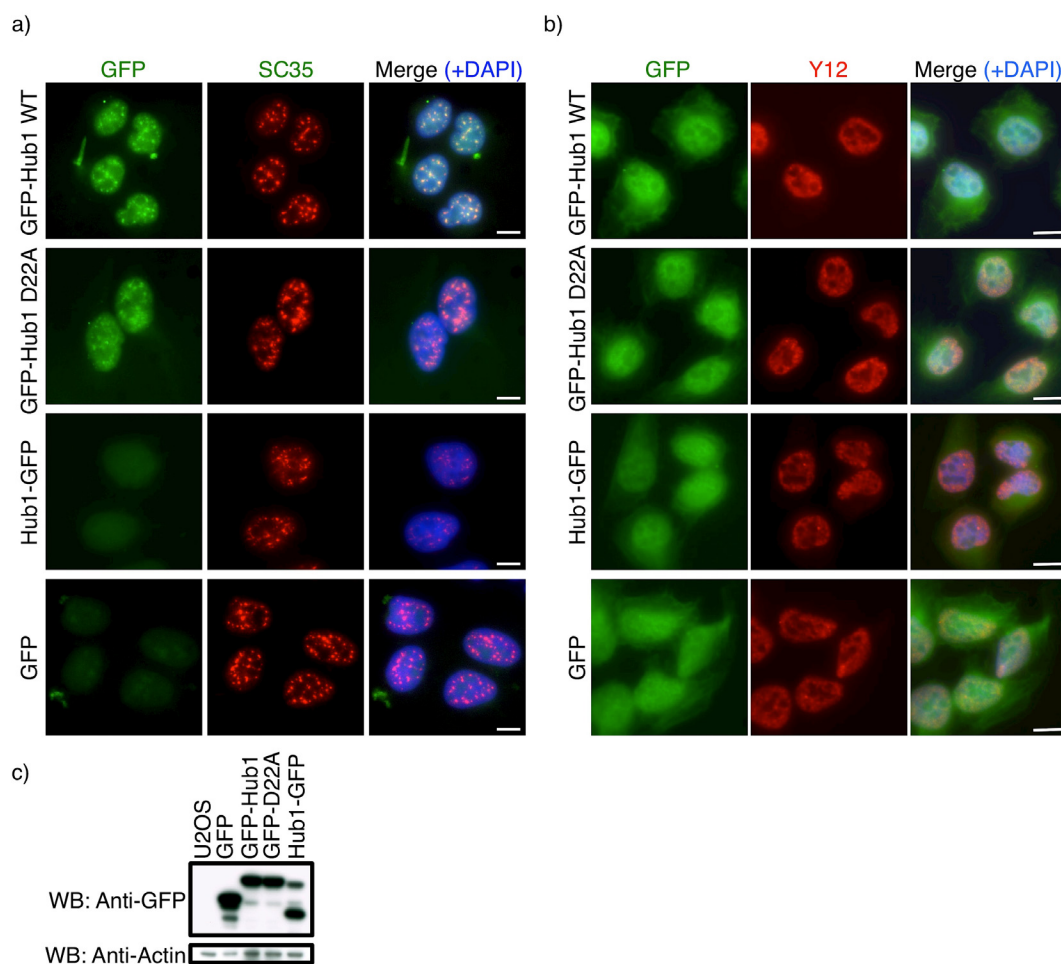


Figure 7: Hub1 recruitment to nuclear speckles depends on C-terminal surface

a) Co-localization studies in U2OS cells stably expressing GFP-Hub1, GFP-Hub1 D22A, Hub1-GFP or free GFP (all green). Cells were pre-extracted, fixed and stained for nuclear speckle marker phospho-SC35 (red). Note that Hub1-GFP and free GFP are washed out, whereas GFP-Hub1 and GFP-D22A are retained in nuclear speckles. DAPI (blue) was used as nuclear counterstain. Scale bar represents 10 μ M. b) Co-localization studies with stable cell lines similar to a). Cells were permeabilized after fixation (no pre-extraction) and stained for Sm-proteins using Y12 antibody (red). DAPI (blue) was used as nuclear counterstain. Scale bar represents 10 μ M. c) Protein expression levels of GFP-fusion proteins (GFP-Hub1, GFP-Hub1 D22A, Hub1-GFP or free GFP) stably expressed in U2OS cells (as shown in a and b) were analyzed by immunoblotting using anti-GFP antibodies. Actin served as loading control.

Moreover, besides the nuclear fraction a significant pool of Hub1 is found in the cytoplasm as well, as shown by immunofluorescence staining following the conventional fixation method with membrane permeabilisation after fixation and no pre-extraction. Despite the differences in nuclear localization after pre-extraction, here the different Hub1 fusion proteins show a similar diffuse distribution throughout the cell with no particular localization (Figure 7b). The protein levels of all fusion proteins were measured to ensure similar expression (Figure 7c).

4.6 hSnu66 actively recruits Hub1 to splicing speckles

After the detailed molecular characterization of the Hub1-hSnu66 interaction and the observation that both Hub1 and hSnu66 are found in nuclear splicing speckles, co-localization studies were conducted to determine the interdependency of the ubiquitin-like protein Hub1 and the splicing factor hSnu66 *in vivo*. Thus, after transient co-expression of tagged Hub1 WT or the binding mutant Hub1 D22A together with either hSnu66 WT or hSnu66 Δ HIND fused to GFP cells were analyzed by immunofluorescence. Interestingly, although a minor fraction of Hub1 WT was detected in the cytoplasm, the majority was recruited to nuclear splicing speckles where it co-localized with hSnu66 WT (Figure 8a, upper panel).

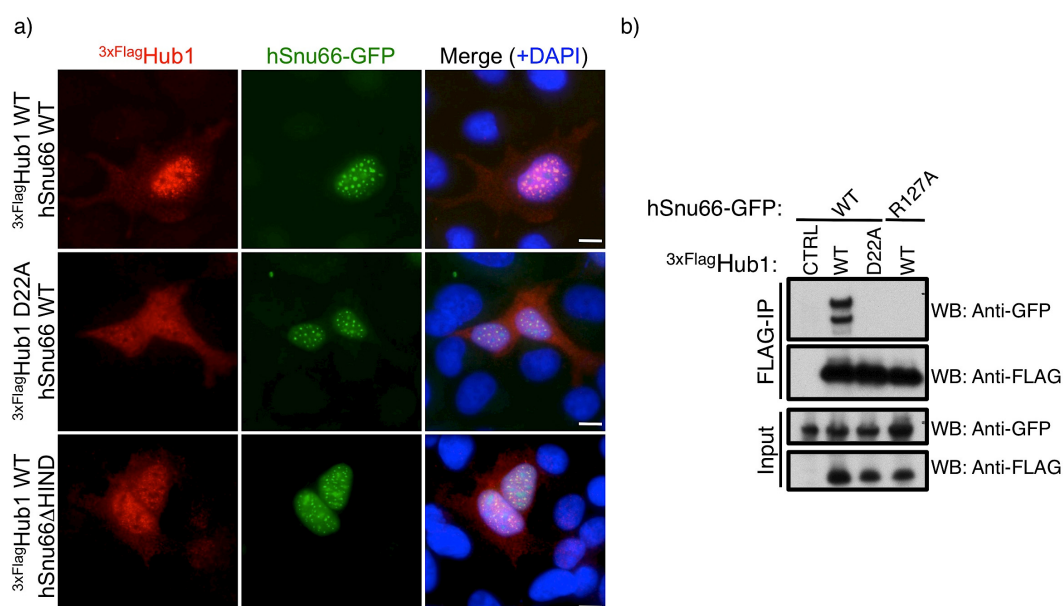


Figure 8: hSnu66 actively recruits Hub1 to nuclear speckles in a HIND-dependent manner

a) hSnu66 attracts Hub1 to co-localize in nuclear splicing speckles and recruitment is HIND-dependent. Immunofluorescence of U2OS transiently co-expressing 3^{\times} FLAG Hub1 WT or D22A mutant (red) with GFP-tagged hSnu66 WT or hSnu66 Δ HIND (green). Cells were fixed, permeabilized and stained with FLAG M2 antibody and DAPI as nuclear counterstain. Scale bar represents 10 μ M. b) hSnu66-GFP interacts with 3^{\times} FLAG Hub1 *in vivo* shown by immunofluorescence and precipitations. Constructs used for immunofluorescence (as in a) are also functional in binding assays. HEK 293T cells were co-transfected with constructs expressing either GFP-tagged hSnu66 WT or hSnu66 R127A in combination with 3^{\times} FLAG Hub1 WT or D22A mutant. Cells were harvested, lysed and proteins were immunoprecipitated using anti-FLAG M2 antibodies. Inputs and precipitates were analyzed by immunoblotting using antibodies against GFP and FLAG.

In contrast, in cells expressing the binding-deficient mutant alleles Hub1 D22A or hSnu66 Δ HIND, where Hub1-hSnu66 interaction is disrupted, the accumulation of Hub1 in nuclear speckles was largely diminished, whereas hSnu66 localization in splicing speckles was unaltered (Figure 8a, lower two panels). Immunofluorescence co-stainings of Hub1 D22A with hSnu66 WT showed that while hSnu66 was found in nuclear speckles, Hub1 D22A was widely and equally distributed throughout the cytoplasm and nucleus with no distinct accumulation in nuclear subcompartments like splicing speckles. In line with these data, co-

expression of Hub1-binding deficient hSnu66 Δ HIND with Hub1 WT showed similar results. hSnu66 Δ HIND efficiently localized to nuclear speckles, while Hub1 WT was not specifically enriched in SC35 domains, when compared to cells which co-expressed WT hSnu66. These data indicate that hSnu66 is targeted to the nuclear speckles in a Hub1-independent manner. Furthermore, hSnu66 itself can actively recruit Hub1 to nuclear speckles via its Hub1-interaction domain, as this accumulation of Hub1 in nuclear speckles depends on the HIND interface.

The finding that Hub1-binding is not crucial for hSnu66's nuclear localization raised the question, if Hub1 might modulate the protein interaction network of hSnu66. To address this point, co-immunoprecipitation studies with GFP-tagged hSnu66 WT or the Hub1 binding-deficient mutant version (hSnu66 Δ HIND) were conducted and compared by immunoblotting and mass spectrometry (Figure 9).

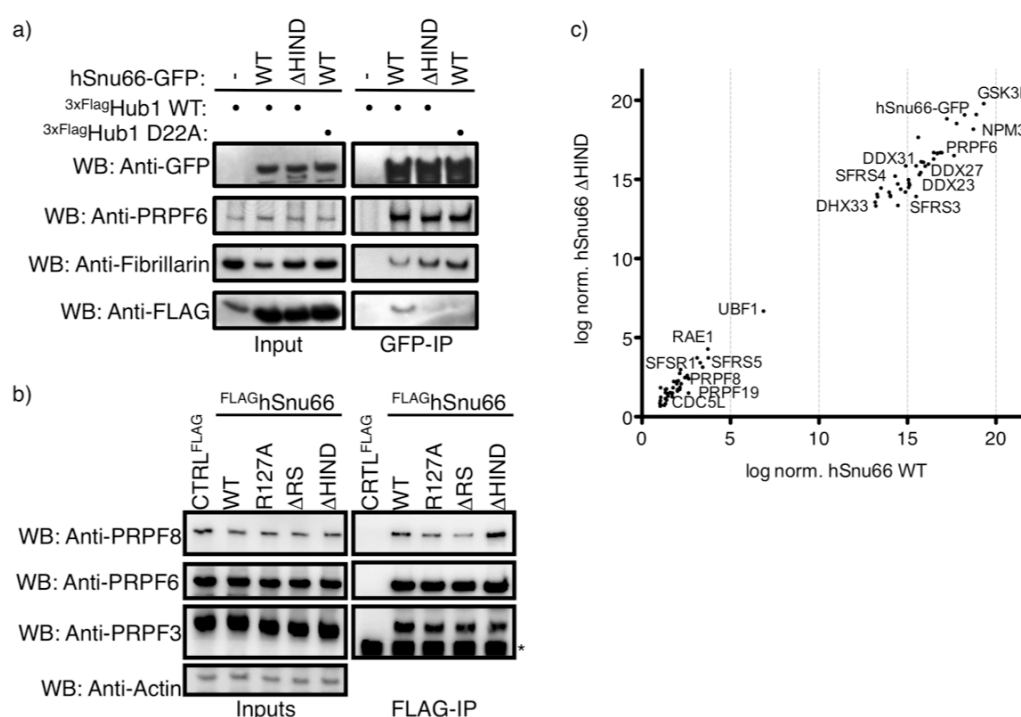


Figure 9: hSnu66 is incorporated into the tri-snRNP complex in a Hub1-independent manner

a) Interaction with tri-snRNP or nucleolar proteins is not altered in the Hub1 binding-deficient mutant hSnu66 Δ HIND. HEK 293T cells were co-transfected with constructs expressing either GFP-tagged hSnu66 WT or hSnu66 Δ HIND in combination with ^{3xFLAG}Hub1 WT or D22A mutant. Cells were harvested, lysed and proteins were immunoprecipitated using anti-GFP antibodies. Inputs and GFP-precipitates were analyzed by SDS-PAGE and subsequent immunoblotting using antibodies against GFP, FLAG, PRPF6 and fibrillarin. b) FLAG-tagged variants of hSnu66 (WT, R127A, Δ RS (deletion of AA1-78) or Δ HIND) or ^{FLAG}luciferase as control were expressed in HeLa cells. After harvesting cells were lysed and FLAG M2 immunoprecipitation was performed. Inputs and immunoprecipitates were analyzed by immunoblotting using antibodies against spliceosomal tri-snRNP proteins PRPF8, PRPF6 and PRPF3. Actin served as loading control. Asterisk indicates antibody heavy chain. c) Qualitative analysis of hSnu66 or hSnu66 Δ HIND immunoprecipitates via mass spectrometry. GFP-tagged hSnu66, hSnu66 Δ HIND or free GFP were immunoprecipitated from transfected HeLa lysates using GFP-trap affinity matrix. GFP-precipitates were analyzed by mass-spectrometry and hSnu66 WT interacting proteins were compared to hSnu66 Δ HIND after normalization and filtering of unspecific binding factors (free GFP sample) were subtracted. Identified RNA processing associated proteins co-purifying with hSnu66 and hSnu66 Δ HIND and their signal intensities are plotted.

It became evident that the interaction with Hub1 is neither essential for hSnu66 binding to tri-snRNP components, nor for the association with nucleolar factors (Figure 9a), as both hSnu66 WT and hSnu66 Δ HIND were able to efficiently co-purify factors like PRPF6 and fibrillarin.

Additional experiments confirmed that incorporation of hSnu66 into the tri-snRNP complex is independent of Hub1-binding. The association of hSnu66 with core spliceosomal proteins of the tri-snRNP complex was tested by co-purification of different hSnu66 variants (WT, R127A, Δ RS (N-terminal Δ AA1-78) or Δ HIND) with U4 snRNP protein PRPF3 and the U5 snRNP proteins PRPF6, and PRPF8, respectively (Figure 9b). Other than the slight decrease of PRPF8 in hSnu66 Δ RS samples, no significant alteration in tri-snRNP binding could be identified. Furthermore, in an unbiased proteomic approach hSnu66 or hSnu66 Δ HIND immunoprecipitates were analyzed qualitatively via mass spectrometry. Indeed, this data set affirmed only marginal alterations between WT or Hub1-binding deficient hSnu66, when co-purifying factors were compared (Figure 9c). These findings suggest other domains within hSnu66 being important for proper incorporation into the tri-snRNP, while Hub1 binding might mediate another, yet unknown, regulatory mechanism.

4.7 Characterization of hSnu66's functional domains

In order to gain further insights into the function of the Hub1 interaction partner hSnu66, which is a spliceosomal protein with many low complexity regions and poorly characterized domain structure, several truncated hSnu66 GFP-fusion proteins were generated bearing the different putative motifs (Figure 10c). In line with the abovementioned data, microscopic analysis highlighted the dual localization of hSnu66 WT or hSnu66 Δ HIND in nucleoli and nuclear speckles, which was confirmed by co-staining with SC35 in HeLa cells (Figure 10a). Even the direct linear fusion of Hub1 to the hSnu66' N-terminus (Hub1~hSnu66) did not alter the localization and resembled hSnu66 WT nuclear staining. Interestingly, the N-terminus of hSnu66 alone (AA1-139), comprising the RS-domain and the Hub1-binding domain HIND, is sufficient to be efficiently recruited to nuclear speckles and nucleoli (Figure 10a).

Besides the nuclear import signals encoded by the N-terminus, an additional domain in hSnu66's central part is responsible for incorporation into nuclear speckles. N-terminal truncations lacking the first 325 amino acids (AA325-800) led to a slightly less efficient nuclear import, but still allowed recruitment to splicing speckles (Figure 10b). Further deletions within the central domain (AA375-800) destroying the leucine zipper (AA365-386) interfered with proper localization to splicing foci and resulted in a pan-nuclear and cytoplasmic staining (Figure 10b). Constructs expressing C-terminal hSnu66 fragments did not show an association with any particular nuclear nor cytoplasmic subcompartment and exhibit a diffuse cellular distribution similar to free GFP (Figure 10b: AA439-800, AA678-800, GFP). In

addition to immunofluorescence localization studies, the GFP-tagged hSnu66 truncations were utilized in co-immunoprecipitation assays to identify novel interaction domains within hSnu66. Indeed, a central domain in hSnu66 (AA325-439) comprising the LZ and NLS is crucial to associate and to co-purify with tri-snRNP proteins like PRPF6 (Figure 10d).

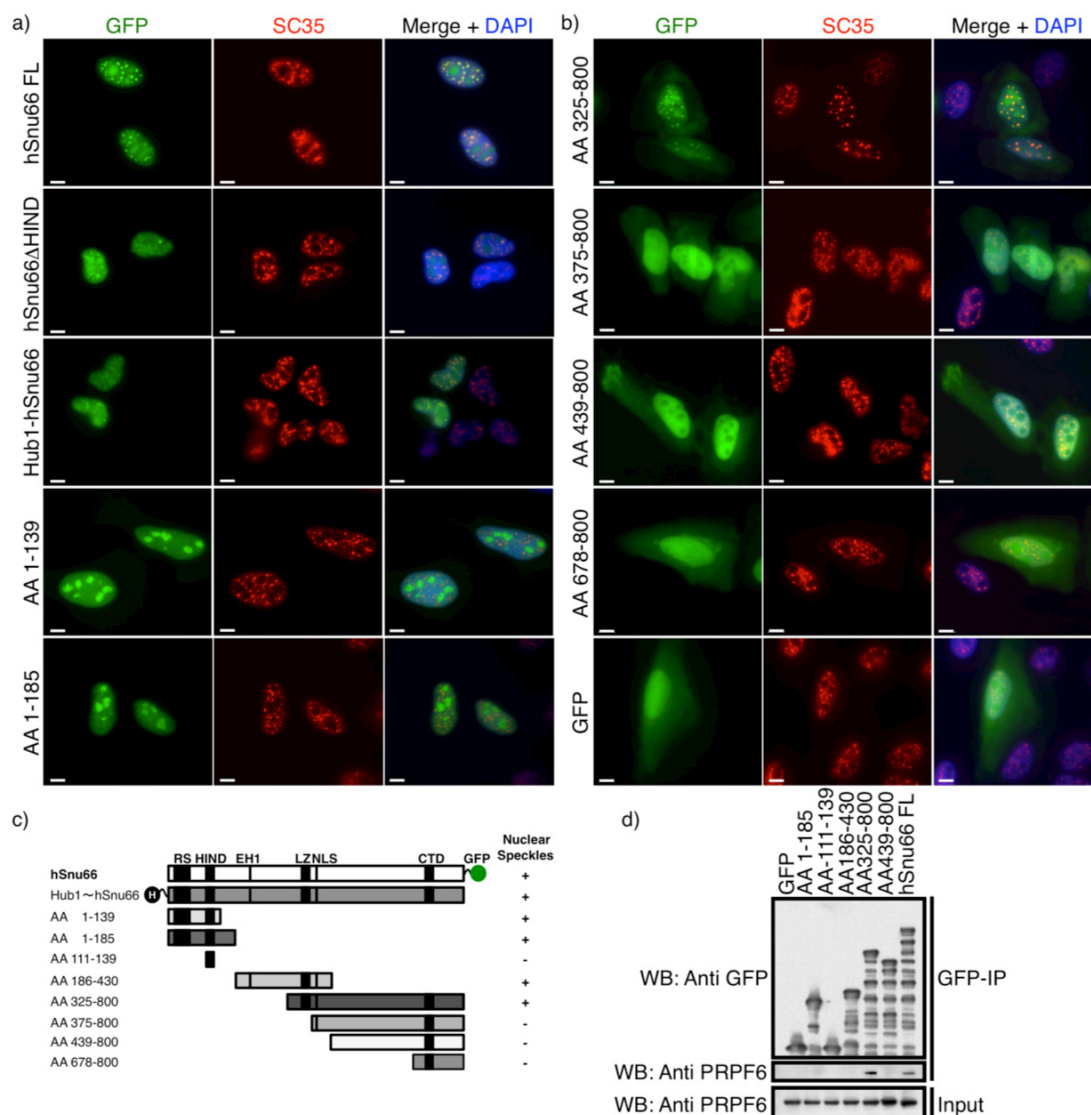


Figure 10: Mapping and characterization of hSnu66 domains

a-b) The N-terminus and the central leucine zipper in hSnu66 mediate recruitment to nuclear speckles. HeLa cells were transfected with constructs expressing hSnu66 truncations tagged with GFP (green). Cells were fixed, permeabilized and stained for nuclear speckle marker phospho-SC35 (red) and DAPI (blue). Scale bar represents 10 μ M. c) Schematic representation of GFP-tagged hSnu66 truncations and their putative domain structure used previous experiments. d) The central domain in hSnu66 (AA325-439) is crucial for binding to tri-snRNP protein PRPF6. HEK 293T cells were transfected with different hSnu66 truncations tagged with GFP as indicated (see c). Cells were harvested, lysed and proteins were immunoprecipitated using the GFPtrap matrix. Inputs and GFP-precipitates were analyzed by immunoblotting using antibodies against GFP and PRPF6.

Notably, although hSnu66's N-terminus (AA1-185) containing the RS- and HIND motifs is sufficient for recruitment to nuclear speckles, it does not co-precipitate with PRPF6. This data supports the model of hSnu66 acting as a platform with at least

two independent interaction modules; while its N-terminus binds Hub1 and contains the RS-domain, the central module mediates association with spliceosomal complexes like the tri-snRNP protein PRPF6.

As the abovementioned N-terminal fragments contain functional HINDs and are thereby potential Hub1 binders, a more detailed characterization was performed to determine whether Hub1-binding alters their nuclear import or localization (Figure 11a).

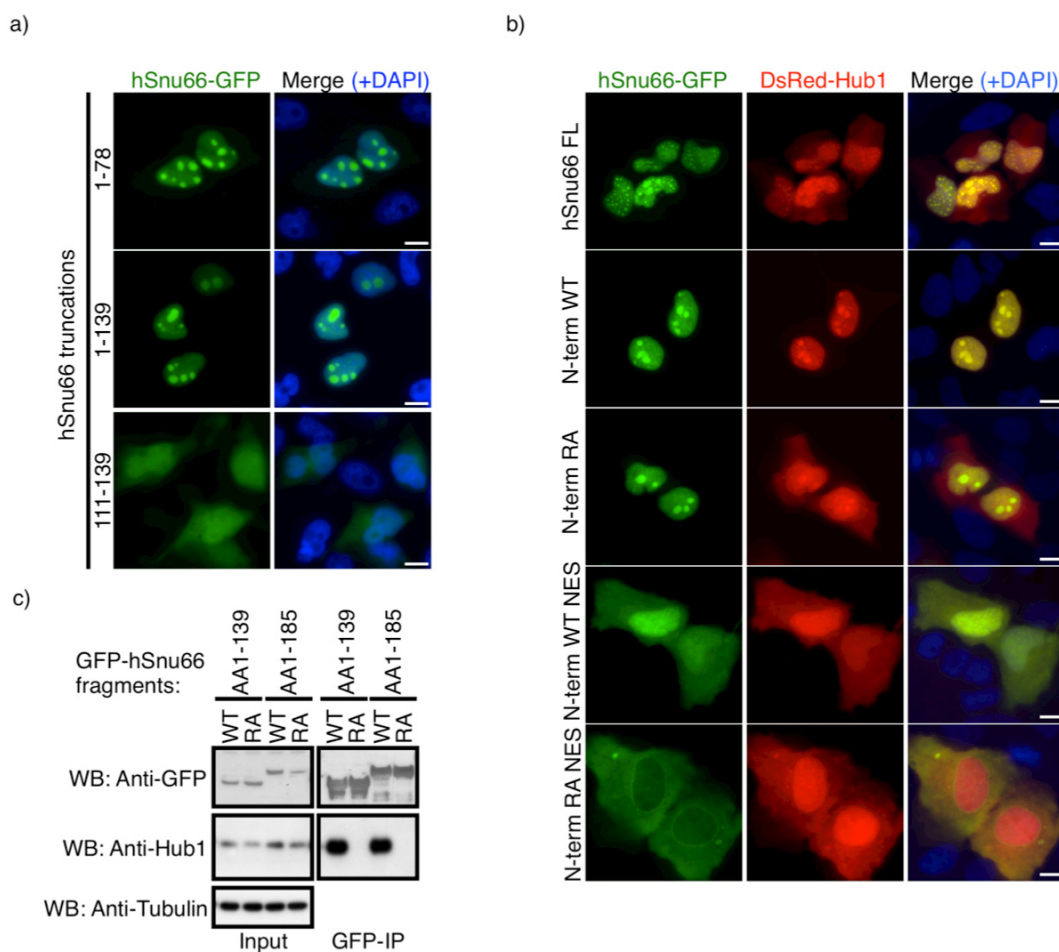


Figure 11: Hub1 binding retains N-terminus of hSnu66 in nuclear compartment

a) The N-terminal RS-domain of hSnu66 is sufficient to localize to nuclear speckles. HeLa cells were transfected with constructs expressing hSnu66 RS-domain (AA1-78), N-terminus containing the HIND (AA1-139) or the isolated HIND (AA111-139) as GFP-fusion proteins (green). Cells were fixed, permeabilized and nuclei were stained with DAPI (blue). Scale bar represents 10 μ M. b) Hub1 binding facilitates nuclear retention of hSnu66 N-terminus. DsRed-Hub1 (red) expressing HeLa cells were co-transfected with constructs encoding GFP-tagged hSnu66 N-termini (AA1-139) (green) with either WT HIND or bearing the Hub1-binding mutation R127A (R127A=RA). Cyto-nuclear shuttling of hSnu66 fragments was enforced by linear fusion with a nuclear export signal (NES) of export receptor CRM1 to GFP tagged hSnu66 constructs. Cells were fixed, permeabilized and nuclei were stained with DAPI (blue). Scale bar represents 10 μ M. c) The HIND-containing N-terminus of hSnu66 binds endogenous Hub1. GFP-tagged hSnu66 truncations (AA1-139 or AA1-185) were expressed as WT or Hub1 binding-deficient mutant version (RA) in HeLa cells. After transfection, cells were harvested, lysed and GFP-fusion proteins were immunoprecipitated using the GFPTrap matrix. Inputs and GFP-precipitates were analyzed by immunoblotting using antibodies against GFP and Hub1. Tubulin served as a loading control.

Further segmentation of hSnu66's N-terminus into RS-domain and HIND revealed that the RS-domain alone (AA1-78) is a potent nuclear import domain, which is efficiently recruited to nuclear speckles and nucleoli, similar to the extended fragment (AA1-139) comprising RS-domain and HIND. The HIND alone does not facilitate nuclear import by itself, as shown by the diffuse localization throughout the cyto- and nucleoplasm of the cell similar to free GFP.

Although Hub1 binding is not crucial for hSnu66 interaction with the tri-snRNP, full-length hSnu66 actively recruits Hub1 to nuclear speckles (Figure 8a and 10d). Furthermore, the HIND containing N-terminus is efficiently imported and associated with SC35 domains, but it remained unclear if Hub1 travels along. To address this point, hSnu66-GFP truncations were co-expressed with DsRed-tagged Hub1 and analyzed by microscopy (Figure 11b).

In line with the abovementioned data, full-length hSnu66 recruited and accumulated DsRed-Hub1 in nuclear speckles leading to almost cytoplasmic depletion of free Hub1 in HeLa cells. Co-expression of the hSnu66 N-terminal fragment clearly showed a similar effect by binding and importing Hub1 into the nucleus and speckles. When the Hub1-interaction domain was mutated (changing salt bridge residue R127 to alanine (RA)) abolishing Hub1 binding, the N-terminal fragment still localized to nuclear speckles and nucleoli, but DsRed-Hub1 was not recruited nor enriched in speckles (Figure 11b, upper and middle panel). In order to counterbalance the strong nuclear import of hSnu66 N-terminal fragment by the RS-domain the nuclear export sequence (NES) of the export receptor CRM1 (Engelsma et al., 2004) was linearly fused to hSnu66 truncations as GFP tagged protein. When the WT N-terminal fragment of hSnu66 with NES (N-term WT NES) was co-expressed with Hub1, it still localized to SC35 domains where it co-localizes with Hub1. As expected, due to the NES the cytoplasmic fraction also increased, but the major fraction resided in the nucleus. In contrast, when the Hub1-binding deficient N-terminus with NES (N-term RA NES) was examined, the equilibrium of nucleocytoplasm shuttling was shifted toward the cytoplasm and nuclear depletion of the fusion protein. Instead of splicing speckles the cytoplasm and nuclear rim were now stained, whereas the nucleoplasm was depleted of the hSnu66 N-terminal RA NES fragment. This had no effect on DsRed-Hub1 localization as it still remained nuclear and cytoplasmic.

Taken together, these data indicate that Hub1 supports the incorporation and retention of hSnu66 in nuclear speckles additionally to its RS-domain. While the RS-motif helps targeting hSnu66 to SC35 domains, the HIND creates an additional interaction surface with Hub1 that might contribute to a proper complex formation with other splicing-associated factors.

4.8 Distinct and conserved protein properties of Hub1

Recent work on Hub1 has focused on lower eukaryotes using model organisms like *S. cerevisiae* and *S. pombe* since its identification in the year 2000 (Jentsch and Pyrowolakis, 2000). Whereas knockout of *HUB1* in *S. cerevisiae* (*hub1Δ*) shows only minor phenotypes and cells are viable, its gene deletion in *S. pombe* is lethal (Luders et al., 2003; Yashiroda and Tanaka, 2004). Interestingly, rescue assays in which *hub1Δ S. pombe* strains were supplemented with constructs expressing *HUB1* orthologs from *S. cerevisiae* (*S.c.*), *S. pombe* (*S.p.*) and *H. sapiens* (*H.s.*), revealed significant differences between yeasts and human Hub1 in survival assays (Figure 12a). After FOA shuffling out the URA4-bearing plasmid, encoding the “back-up” copy of *SpHUB1*, the *HUB1* orthologs were the only remaining source of Hub1 in *hub1Δ S. pombe* cells.

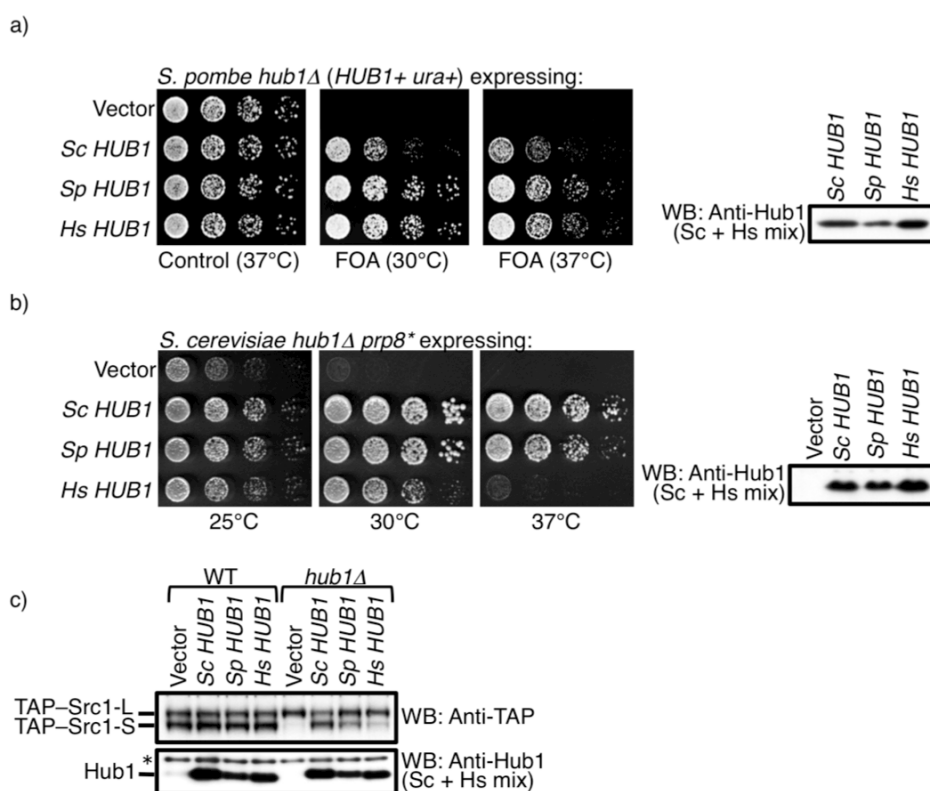


Figure 12: Functional complementarity of yeast and human *HUB1* orthologs

a) Rescue of *hub1Δ* in *S. pombe* by complementation with *HUB1* orthologs from *S. cerevisiae*, *S. pombe* and *H. sapiens*. Serial dilutions of *hub1Δ* cells expressing *HUB1* orthologs grown on control or FOA plates (*hub1Δ* with one copy of *spHUB1* encoded on an URA4-bearing plasmid for shuffle out). Protein expression of *HUB1* orthologs is shown in the right panel using anti-Hub1 antibodies. b) Rescue of synthetic sickness of *hub1Δprp8** in *S. cerevisiae* by expressing *HUB1* orthologs in cell growth assays at indicated temperatures. Protein expression of Hub1 orthologs is shown in the right panel using anti-Hub1 antibodies. c) Complementation of altered alternative splicing of SRC1 in *hub1Δprp8** cells by *HUB1* orthologs (according to b). Protein expression of TAP-tagged Src1-L and Src1-S isoforms as well as Hub1 versions were monitored by western blotting using anti-TAP and anti-Hub1 antibodies. Complementation experiments with *S. pombe* and *S. cerevisiae hub1Δ* cells were performed in collaboration with S.K. Mishra.

As shown previously (Yashiroda and Tanaka, 2004), the shuffle out resulted in Hub1 depletion and caused the lethal phenotype, when cells were supplemented with the empty vector control and no ectopically expressed Hub1 was present. Complementation with either *S. pombe* or *H. sapiens HUB1* fully rescued lethality and restored cell growth in spotting assays. In contrast, constructs expressing *S. cerevisiae HUB1* were not able to fully complement *S. pombe hub1Δ*, leading to growth defects at indicated temperatures. This effect was not attributable to reduced protein levels, as expression of the different *HUB1* orthologs was monitored by immunoblotting (Figure 12a, right panel).

Recent data described a strong genetic interaction between *hub1Δ* and a mutant allele of the tri-snRNP protein PRP8 (*point mutation P1384L* called *prp8**) in *S. cerevisiae* (Dahlmann, 2008; Mishra et al., 2011). Based on the *hub1Δprp8** genetic background, *HUB1* complementation experiments were conducted similar to previous assays in *S. pombe hub1Δ*. For this, *hub1Δ prp8** cells were transformed with constructs expressing yeast and human *HUB1* orthologs, and corresponding spottings were incubated at indicated temperatures (Figure 12b). While the empty vector control could not support growth of the *hub1Δ prp8** strain, *SchHUB1* and *SpHUB1* fully rescued the growth defect at restrictive temperatures. *HsHUB1*, on the other hand, partially complemented at lower temperatures (25°C and 30°C), but was not able to support growth at 37°C. Again, all *HUB1* orthologs were expressed at similar protein levels (Figure 12b, right panel).

In addition to survival assays, an additional complementation read-out was used in *S. cerevisiae*. Recent data elucidated an important role of Hub1 in splice site usage and alternative splicing in yeast (Mishra et al., 2011). In *S. cerevisiae* the *SRC1* gene gives rise to two mRNA isoforms due to alternatively splicing, termed SRC1-L (long isoform, larger protein) and SRC1-S (short isoform, smaller protein). The *SRC1* transcript contains crucial sequences directly at the two overlapping 5' splice sites, whose usage determines which isoform will be generated. It has been shown that Hub1 is important for proper splicing of certain 5' splice sites and thereby pivotal for alternative splicing *e.g.* of *SRC1* pre-mRNA (Mishra et al., 2011). WT cells generate both SRC1-L and SRC1-S isoforms and this equilibrium is not altered when different *HUB1* orthologs are expressed ectopically (Figure 12c). According to Hub1's role in 5' splice site usage, *hub1Δ* cells are defective in alternative splicing of *SRC1* and only the distal splice site is used which produces the SRC1-L isoform (Figure 12c). This splicing defect can be completely complemented by the ectopic expression of *SchHUB1*. Introducing the *HUB1* ortholog from *S. pombe* largely rescues the altered alternative splicing pattern and both isoforms are detectable as well. In line with the genetic interaction in *hub1Δ prp8** cells, the human *HsHUB1* was only able to partially complement the splicing defect, although its protein expression was similar to all other Hub1 orthologs tested (Figure 11c).

Based on the complementation data from *S. cerevisiae* and *S. pombe* it appears that, despite Hub1's high conservation, human and fission yeast Hub1 own a distinct protein property, which is absent in Hub1 of *S. cerevisiae*. This activity might have developed later in evolution, when Hub1 gained additional or more prevalent functions in eukaryotic cells.

4.9 Molecular tools for the characterization of Hub1 in human cells

Due to the recent research on Hub1, no molecular tools for further characterization of Hub1 were yet commercially available. To address the cellular function of Hub1 in human tissue culture cells it was necessary to establish a Hub1 depletion system by RNA-interference (RNAi) using short interfering RNAs. Furthermore, the knockdown efficiency and specificity needed to be validated by immunoblotting with Hub1-specific antibodies. In collaboration with the immunization service of the MPIBC, rabbits were injected with recombinant 6xHis-tagged human Hub1 and boosted twice to induce anti-Hub1 specific antibody synthesis. The isolated serum was incubated with a Hub1 matrix, where recombinant 6xHis-Hub1 was covalently tethered to activated CNBr-sepharose beads. After specific antibodies were isolated using the Hub1 affinity matrix, they were eluted and tested by immunoblotting. In a second purification step, the first round antibody eluate was incubated with another Hub1 matrix, where recombinant GST-Hub1 was covalently attached to a HiTrap NHS HP column. Like before, bound antibodies were eluted and Hub1-specificity tested (Figure 13a).

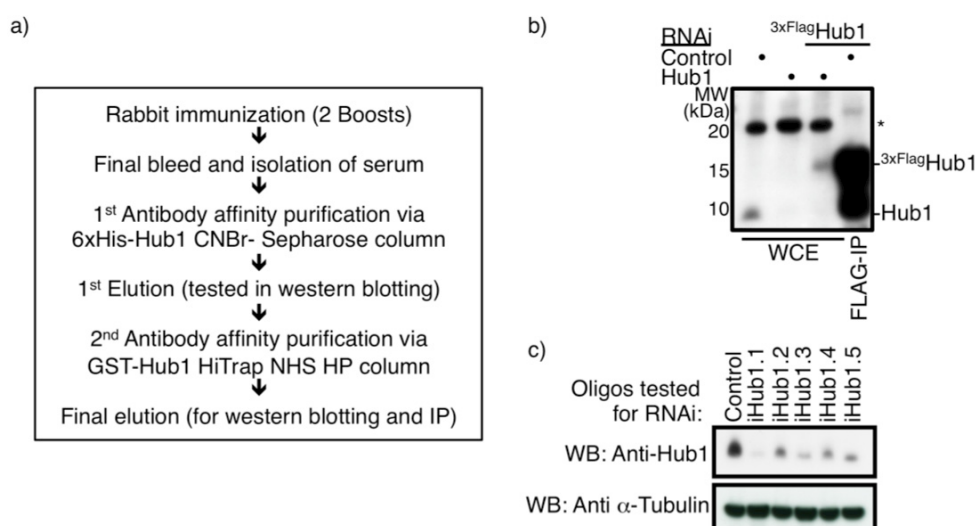


Figure 13: Generation of Hub1-specific antibodies and verification of Hub1 RNAi specificity.

a) Schematic overview of Hub1 antibody purification. b) Verification and specificity of the purified Hub1 antibody. For Hub1 detection, whole-cell extracts of WT or Hub1-RNAi treated HeLa cells as well as ectopically expressed 3xFLAG-tagged Hub1 in lysate and after FLAG-immunoprecipitation were analyzed by immunoblotting. c) Validation of Hub1 knockdown efficiency after RNAi using different siRNA oligonucleotides. 48 h after HeLa cells were transfected with siRNA, cells were harvested and lysed in denaturing RIPA buffer. Whole-cell lysates were analyzed by SDS-PAGE and immunoblotting using anti-Hub1 antibody. Tubulin served as a loading control.

Immunoblotting using the doubly affinity-purified anti-Hub1 antibody detected a specific band with a molecular weight of ca. 8 kDa, which corresponded to the size of endogenous Hub1 in whole-cell extracts (Figure 13b, first lane). Moreover, epitope-tagged and immunopurified ^{3xFLAG}Hub1 from transfected HeLa cells was detected as a supershifted protein band in immunoblotting as well (Figure 13b).

This newly generated antibody was used to validate and affirm *in vivo* depletion of Hub1 by RNAi. Several small interfering RNA oligonucleotides (siRNA oligos) were designed according to previously described criteria (Birmingham et al., 2007; Reynolds et al., 2004). Cells transfected with Hub1-targeting siRNA or control oligo were analyzed by immunoblotting. Five different RNAi sequences were tested for successful knockdown in various cell types and endogenous Hub1 protein levels were significantly decreased when siRNA oligo iHub1.1 and iHub1.3 were transfected (Figure 13c). Furthermore, whole-cell extracts of Hub1 RNAi treated cells were subjected to immunoblotting and served as ideal control for Hub1-antibody specificity. Extracts from HeLa cells co-transfected with Hub1 siRNA and constructs expressing RNAi-resistant 3xFLAG-tagged Hub1 clearly showed efficient depletion of endogenous Hub1, while ectopically expressed ^{3xFLAG}Hub1 was detectable (Figure 13b, third lane).

4.10 *In vivo* depletion of Hub1 causes cell cycle defects and apoptotic cell death

The aforementioned data indicate a special role of the ubiquitin-like protein Hub1 in human cells. Unlike other UBLs it is not conjugated to proteins but binds hSnu66 via a distinct unconventional interaction domain. In addition, Hub1 associates with nuclear speckles and splicing-related factors suggesting a role in pre-mRNA splicing in mammalian cells. After establishing the Hub1-targeted RNAi the key question of what might be the effect of Hub1-depletion in human cell lines was addressed.

Initially, Hub1 knockdown cells were phenotypically characterized. For this, HeLa cells stably expressing GFP-tagged histone 2B (H2B-GFP) were transfected with siRNAs against either Hub1 or non-targeting control and monitored using live cell fluorescence microscopy. Intriguingly, 48 h post transfection Hub1 knockdown cells started to exhibit delays in cell cycle progression with subsequent mitotic defects, whereas in knockdown control cells no alterations were detectable (Figure 14a). For example, while several control RNAi treated cells underwent cell divisions successfully in the depicted time-window of six hours, the Hub1-RNAi treated cells rarely divided, and, if they did, showed abnormal mitosis *e.g.* defects in metaphase plate formation or chromosome missegregation (Figure 14a). Live cell fluorescence microscopy with HeLa H2B-GFP demonstrated misaligned chromosomes during the arrangement of condensed chromosomes in metaphase and aberrant chromosome segregation during anaphase after Hub1 depletion.

This phenotype was affirmed when cell cycle progression was quantified by measuring the time from nuclear envelope breakdown until successful telophase (Figure 14b). Control H2B-GFP HeLa cells completed mitosis faithfully after approximately 1.6 hours (mean: 105.6 min), whereas it took Hub1-depleted cells around 4.3 hours (mean: 283.6 min) to undergo mitosis. Frequently, transfected cells, which exhibit a significant delay in cell cycle, induced and underwent apoptosis at later time points (in particular when associated with mitosis) after prolonged incubation of Hub1 RNAi (Figure 14c).

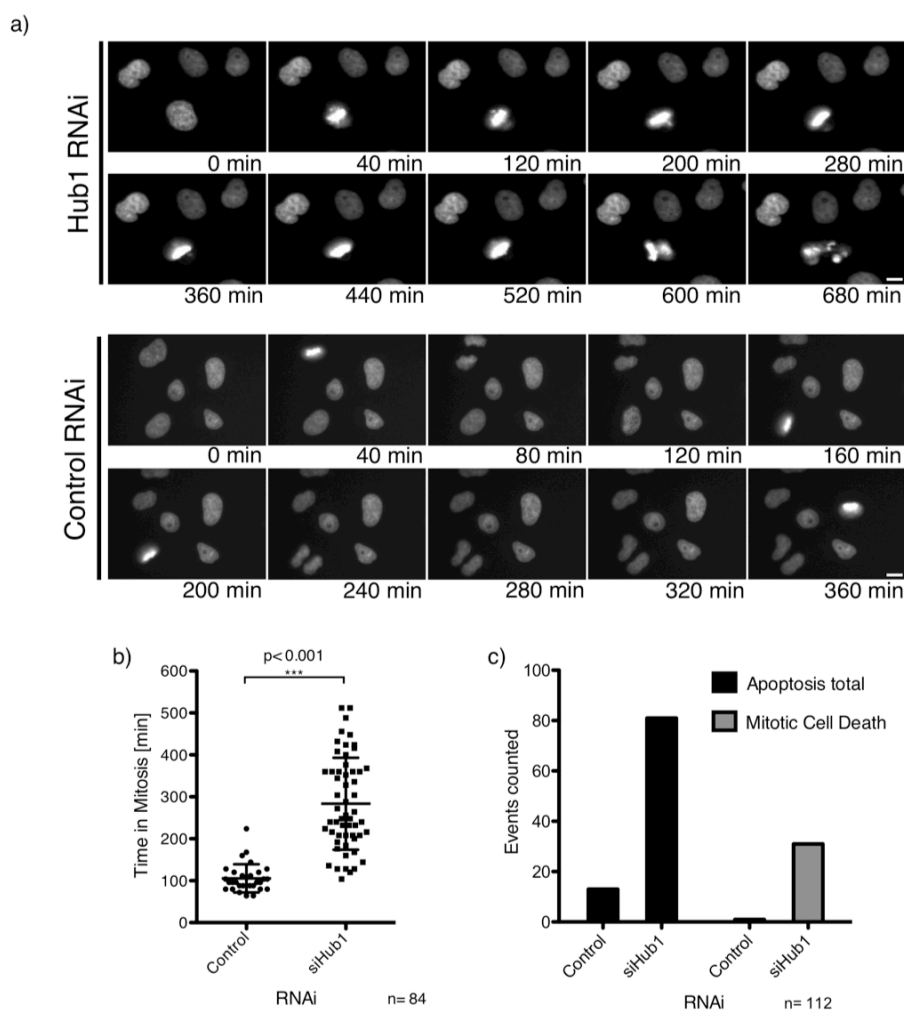


Figure 14: Knockdown of Hub1 causes cell cycle defects and mitotic catastrophe

a) Live cell microscopy of H2B-GFP HeLa cells after RNAi either against Hub1 or non-targeting control. The images represent stills of time-lapse video microscopy at representative time points. Scale bar represents 10 μ M. b) Quantification of cell cycle progression after Hub1 knockdown. Time in mitosis measured by live cell microscopy of H2B-GFP HeLa cells. Data represent mean and s.d. for control RNAi: mean 105.6 min (n=29) and Hub1 RNAi mean: 283.6 min (n=55). c) Quantification of cells undergoing apoptosis associated with mitosis. Counting of events during live cell imaging experiments with control of Hub1 RNAi H2B-GFP HeLa cells (n= 112).

A more precise way to characterize defects in cell cycle progression is to use cell cycle synchronization and release methods. Here, RNAi-transfected HeLa cells were arrested in S-phase by two cycles of thymidine blocks and subsequently

released to undergo cell cycle synchronously. At the indicated time points, cells were harvested, fixed and stained for flow cytometry analysis (Figure 15a). While cells treated with control RNAi exhibited a typical wild type cell cycle distribution in the asynchronous sample with a major fraction in G1 phase (2n DNA content) and minor S-phase and G2/M phase (>2n and 4n DNA content), respectively, thymidine treated cells showed a clear S-phase arrest indicated by an accumulation of cell counts at the corresponding DNA content (>2n S-phase <4n). During the following release, cells progressed through cell cycle after completing S-phase, entering G2 and mitotic phase after five hours. After nine hours, a large fraction of cells had successfully undergone mitosis and cytokinesis, thus a prominent population of cells in G1 phase became apparent.

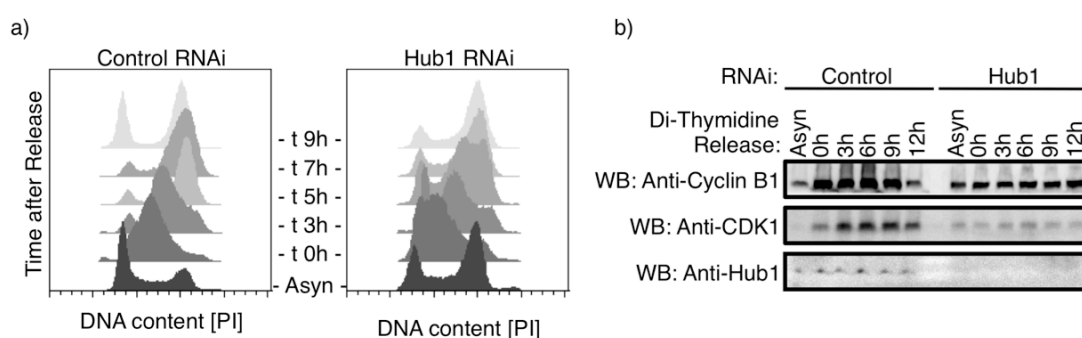


Figure 15: *In vivo* depletion of Hub1 causes G2/M arrest

a) Hub1 depletion leads to defects in cell cycle progression. HeLa cells were transfected with siRNA against Hub1 or control oligo and their cell cycles were synchronized by double thymidine block. After a second round of synchronization cells were released, harvested at indicated time-points, fixed and DNA content was stained for flow cytometry using propidium iodid. The overlay shows a time course of synchronized cell cycle progression after Hub1 or control knockdown. b) Cell cycle synchronization indicates deregulation of cell cycle proteins in Hub1 RNAi treated cells. After release from synchronization (as in (a)) HeLa cells were harvested and whole-cell lysates were analyzed by immunoblotting. Hub1 as well as cell cycle proteins Cyclin B1 and CDK1 as markers for G2 and M phase were detected by immunoblotting with their respective antibodies.

Although Hub1 knockdown cells were successfully synchronized in S-phase, their release showed significant differences when cells reached G2/M phase, compared to control siRNA treated cells. Even after nine hours of release Hub1 RNAi cells were largely restricted to G2/M and only a marginal G1 population was detectable (Figure 15a). This cell cycle arrest was verified when asynchronous Hub1-depleted HeLa cells were analyzed and a clear accumulation of cells in G2/M phase was detectable, confirming the cell cycle arrest observed in live cell microscopy (Figure 14).

The eukaryotic cell cycle is highly regulated by a complex network of protein kinases, phosphatases and proteolysis factors like the APC/C (Pesin and Orr-Weaver, 2008; Fisher et al., 2012). Cyclins and cyclin-dependent kinases (CDKs) are key players that coordinate temporal progression to ensure faithful DNA replication, segregation and cell division. As cyclin expression and CDK activity oscillate during the cell cycle (Hochegger et al., 2008), they are used as marker proteins to monitor

different cell cycle stages. Parallel to the flow cytometry assays, RNAi treated and synchronized cells were harvested at various time points and their extracts were analyzed by immunoblotting. Cyclin B1 protein levels started to rise in late S-phase and peaked in late G2 to early M phase, where CDK1 activity was highest as well, whereas both factors were expressed low in asynchronous and G1 cells (Porter, 2008), as reflected in control RNAi transfected cells (Figure 15b). Hub1 knockdown cells exhibited an altered protein expression profile of Cyclin B1 and CDK1 in synchronized cell extracts. Here, Cyclin B1 and CDK1 did not accumulate over time during S to G2/M transition and no climax was detectable. Apparently, these Hub1 depleted cells lacked the coordinated expression of cell cycle proteins, which is in line with the observed abnormal cell cycle progression after Hub1 RNAi.

For a more quantitative time-course, cells transfected with RNAi against Hub1 or non-targeting control oligo were analyzed by flow cytometry after 48 hours and 72 hours. The cell cycle profile of control cells remained unchanged over time and resembled the wild type profile with a large G1 fraction (> 40%) and minor mitotic populations in G2/M (around 15%). After 48 hours, Hub1-depleted cells displayed alterations in cell cycle progression and the G2/M arrest manifested with an increase of the G2/M population to over 35% (Figure 16a).

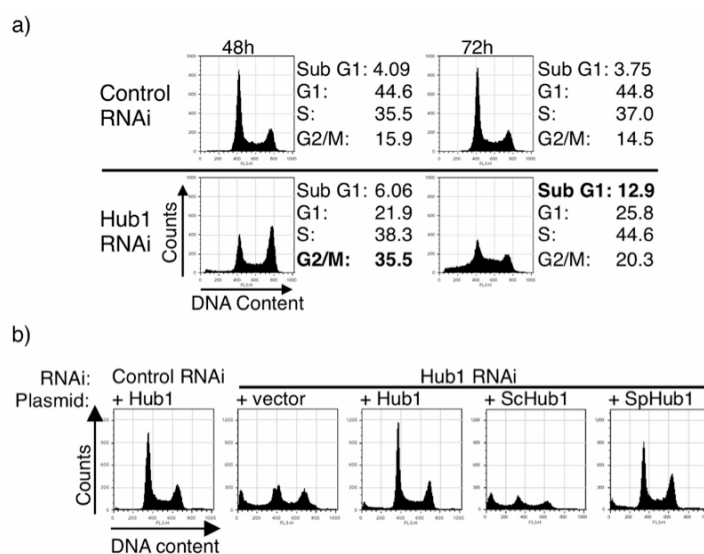


Figure 16: Rescue of Hub1 knockdown-mediated cell cycle defects affirm RNAi specificity

a) Time-course analysis of cell cycle distribution and induction of apoptosis after Hub1 depletion. 48 h and 72 h after Hub1 or control siRNA transfection HeLa cells were harvested, fixed, stained with propidium iodide and analyzed by flow cytometry. Cell cycle phases and apoptotic sub G1 fractions were quantified and are indicated next to the corresponding flow cytometry profile. b) Severe cell cycle phenotypes and apoptosis after RNAi are Hub1 knockdown specific. Complementation assays of Hub1 RNAi by either expression of siRNA-resistant human Hub1 cDNA encoding for WT or *HUB1* orthologs from *S. cerevisiae* (*ScHUB1*) or *S. pombe* (*SpHUB1*) were conducted. 24 h after transfection with siRNA targeting Hub1 or control, cells were co-transfected with respective constructs and incubated for 40 h. Cells were harvested, fixed and DNA content was stained for flow cytometry analysis.

Interestingly, after 60-72 h an additional fraction among Hub1 knockdown cells became more prominent. In contrast to cycling cells, this population contains damaged or aberrant cells, which have underwent apoptotic cell death (Lecoecur,

2002). Among others, one particular hallmark of this cellular process is the nuclear fragmentation and DNA cleavage executed by specific DNases like Caspase-activated DNase, CAD (Nagata, 2000). Apoptotic cells are detectable by flow cytometry as a population with DNA content size below that of intact G1 cells and are therefore termed “sub G1” fraction.

Whereas the sub G1 fraction was marginal in control cells, in Hub1 RNAi samples this cell population increased drastically ($\leq 4\%$ in WT, $> 12\%$ in Hub1 RNAi). Notably, the subpopulation of G2/M arrested cells after 48 hours (around 35%) corresponded to the now apoptotic sub G1 fraction (ca. 13%) and the remaining G2/M population (ca. 20%) at the 72 hours time point. This further indicates that cells facing defects after Hub1 depletion arrest in the mitotic phase and cannot faithfully progress through the cell cycle. As the Hub1 deficiency persists and defects are not corrected, arrested cells are subjected to cell death via apoptosis.

RNA interference is accomplished by the formation of a double-stranded RNA duplex between the transfected siRNA and the targeted mRNA, which is then recognized and degraded by the RNA-induced silencing complex (RISC) to achieve post-transcriptional gene silencing (Fire et al., 1998). To rule out any off-target effect of the designed siRNA oligo, complementation assays with expression constructs encoding siRNA-resistant cDNAs of Hub1 were conducted. Here, the complementary sequence within the Hub1 cDNA is changed by silent mutations, which makes it insusceptible to siRNA-mediated RISC-dependent, degradation while the endogenous Hub1 transcript is still efficiently knocked down.

First, a co-transfection protocol had to be established to achieve high knockdown efficiency with, at the same time, sufficient plasmid transfection coverage. In the following experiments, cells were co-transfected with control or Hub1 targeting siRNAs and expression constructs encoding siRNA-resistant Hub1 or empty vectors. The flow cytometry analysis highlighted that control knockdown with concomitant Hub1 overexpression did not alter the cell cycle profile (as depicted in Figure 16b, first panel). As expected, Hub1 depletion (with co-expression of a control vector) caused severe cell cycle defects and an increase of cell death, which was reflected by the strong induction of apoptosis (see sub G1 fraction) and collapsed G1 and G2 population peaks. Notably, this strong phenotype was rescued by complementation when siRNA-resistant human Hub1 had been co-transfected with Hub1 RNAi (Figure 16b). Here, the ectopically expressed Hub1 compensated the knockdown of endogenous Hub1 and the cell cycle profile was restored resembling cells with no G2 arrest nor major apoptosis events like control cells (protein levels of knockdown and ectopic expression shown in Figure 17c). The complementation of Hub1 RNAi by siRNA-resistant Hub1 cDNA confirmed the specificity of the siRNA oligo and proved that the observed cellular phenotypes were, indeed, related to the Hub1 depletion. Another interesting observation during the complementation

experiments was the rescuing capacity of different *HUB1* orthologs (Figure 16b, fourth and fifth panel). Instead of co-transfecting siRNA resistant human Hub1 cDNA, Hub1-RNAi was now combined with mammalian expression constructs encoding for *HUB1* from *S. cerevisiae* (ScHub1) or *S. pombe* (SpHub1). Interestingly, ScHub1 was not capable of complementing Hub1 knockdown, which led to severe cellular defects and induction of apoptosis as monitored by a drastic increase in the sub G1 fraction and reduced G1 and G2/M peaks. In contrast, *S. pombe* Hub1 efficiently rescued endogenous Hub1 depletion and fully restores cell cycle progression and Hub1-dependent activities. In line with the yeast complementation data, the RNAi rescue experiments underscore the finding that ScHub1 significantly differs from human and SpHub1 that own crucial protein properties that are essential for the vital functionality of Hub1 in higher eukaryotes.

4.11 Hub1 RNAi entails DNA damage, mitotic catastrophe, and apoptotic cell death

The morphological description by live cell imaging and flow cytometry analysis allowed the phenotypical characterization of cellular defects after Hub1 depletion by RNAi. An additional approach to identify Hub1 function and its pivotal role for cell viability is the molecular investigation of signaling cascades, which appear to be altered upon Hub1 knockdown. Thus, whole-cell extracts of RNAi treated cells were subjected to immunoblotting in order to monitor changes in key regulators levels and their activation.

A profound cell cycle arrest is a hallmark of the Hub1 depletion phenotype, therefore DNA surveillance and cell cycle checkpoint pathways were tested. Here, the tumor suppressor p53 plays a central role, as it is activated upon DNA damage, DNA replication stress or various cellular stresses, *e.g.* hypoxia (Reinhardt and Schumacher, 2012). The p53 protein is not only transcriptionally regulated, but also under tight control by the ubiquitin-proteasome system, which constantly degrades inactive p53 via the ubiquitin E3 ligase HMD2 (Mdm2 in mouse). After its activation, p53 is stabilized and acts as a transcriptional regulator for a whole network of genes including either “repair and survival” factors like negative regulators of cell cycle progression (*e.g.* 14-3-3 σ , p21^{WAF} and Growth Arrest and DNA Damage gene GADD45a) or “cell death execution” factors of the Bcl-2 antagonist family like BAX, BAK and p53 up-regulated modulator of apoptosis (PUMA) (Vogelstein et al., 2000). It has been shown that p53 does not only control G1 or S-phase progression (Bartek and Lukas, 2001; Agarwal et al., 1998), but can also induce and maintain G2/M arrests, senescence and apoptosis (Bunz, 1998; Taylor and Stark, 2001).

Proliferating, cycling U2OS cells transfected with non-targeting RNAi control do not face cellular stresses and thus exhibit low p53 and p21 protein levels, indicating inactive checkpoints (Figure 17).

In order to stimulate p53 activation, control cells were incubated with the transcriptional inhibitor actinomycin D (ActD), which binds DNA directly and abrogates transcription by blocking elongation of the emerging RNA strand during synthesis by RNA polymerase II (Bacchetti and Whitmore, 1969; Sobell, 1985). This triggers an increase in p53 stability and protein levels (Renton et al., 2003), but uncouples the transcriptional response targets like p21^{WAF} (Ljungman et al., 1999; Zhu et al., 2007). Indeed, control knockdown cells showed high levels of p53, but only moderate levels of p21 after ActD treatment (Figure 17a). In contrast, Hub1 depletion in U2OS cells alone already led to p53 stabilization and an increase of p21 levels, when compared to control cells. Furthermore, the transcriptional inhibition with actinomycin D in combination with Hub1 knockdown again reduced p21 expression, while p53 remained up-regulated (Figure 17a).

It appears that Hub1 is a crucial factor to ensure genome stability as indicated by microscopy and p53 data, thus, additional factors involved in DNA maintenance and repair were investigated. Beside exogenous factors like DNA attacking chemicals or UV- and gamma irradiation, defects in the DNA synthesis machinery, DNA replication stress or reactive oxygen species are intrinsic sources of DNA damage (Yi and He, 2013). After recognition of these damages by chromatin-associated enzymes, signaling cascades initiate the activation of repair processes in order to excise and replace defective nucleotides or repair even severe DNA double-strand breaks (DSBs) (Branzei and Foiani, 2008). The DSBs repair signal is transduced by the PI3 kinases DNA-dependent protein kinase (DNAPK), ataxia telangiectasia mutated (ATM) and its relative, ATR, which phosphorylate the histone variant H2AX at S139 (then termed γ H2AX) and thereby generate a platform for subsequent recruitment of the DNA repair machinery (Lavin, 2008). Another branch of DNA repair deals with base lesions after cyclobutane pyrimidine dimer (CPD) or pyrimidine-pyrimidone photoadduct (6-4PP) formation as well as chemically modified nucleotides *e.g.* after alkylation and intrastrand crosslinks (Naegeli and Sugawara, 2011). Moreover, these genomic insults constitute severe obstacles that can block the transcription machinery and lead to stalling of RNA polymerases on the DNA. Proteins of the xeroderma-pigmentosum-related gene family (XP) have been shown to be crucial for the detection and subsequent repair of abovementioned DNA damages (transcription-coupled nucleotide excision repair, TC-NER (Mellon, 2005; Nospikel, 2009)). While XPE (or DDB2) and DDB1 recognize lesions (Wittschieben et al., 2005), XPC in concert with hRad23B (Masutani et al., 1994) initiates local DNA unwinding by TFIIH (Sugawara et al., 2009) and excision via XPF-ERCC1 with XPG (Bessho et al., 1997; O'Donovan et al., 1994).

As depicted in Figure 17b, whole-cell extracts of RNAi treated cells were tested for changes in γ H2AX and XPC levels. Intriguingly, Hub1 depletion alone led to an activation of DNA damage signaling, as a strong induction of γ H2AX was

detectable, while control cells were unaffected and exhibited only low levels of the modified histone variant. The extent of H2AX phosphorylation in cells lacking Hub1 was similar to that of actinomycin D treated control cells, but additional Hub1 knockdown did not stimulate further phosphorylation of H2AX levels.

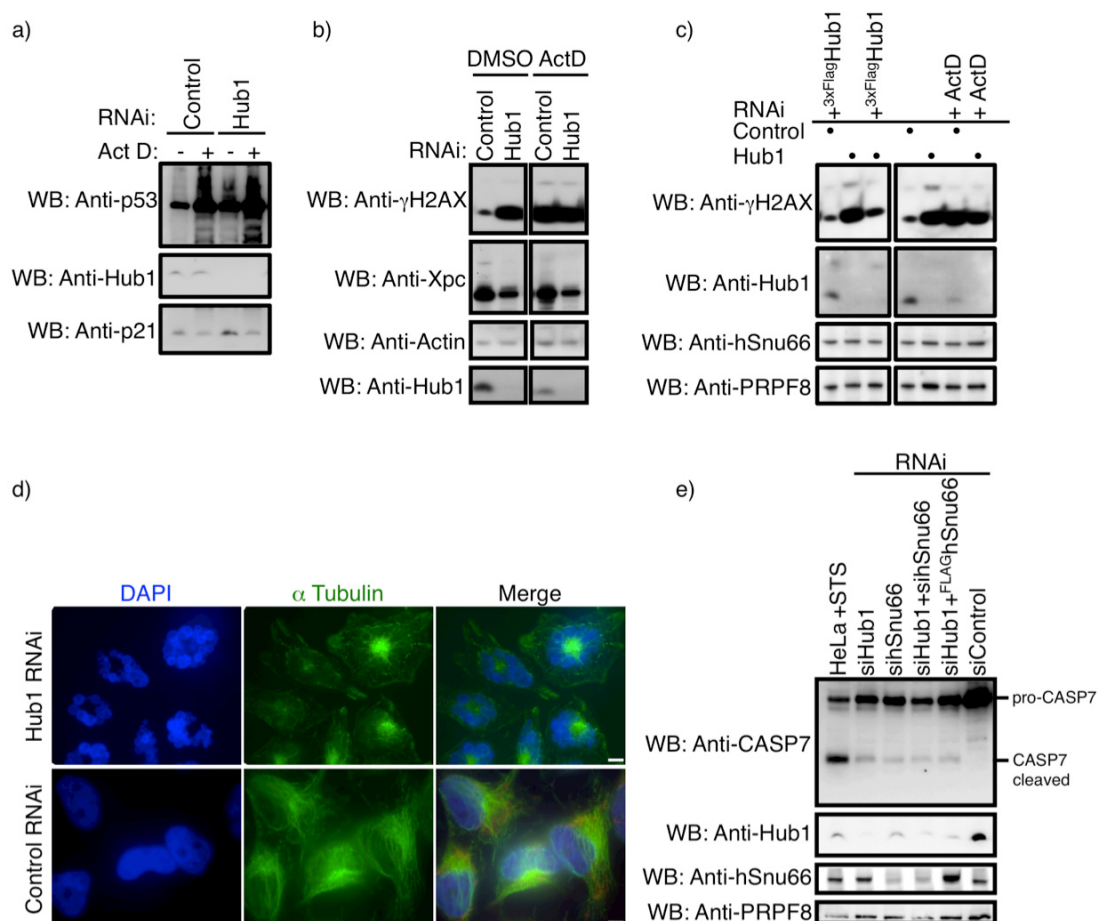


Figure 17: Nuclear disintegration and DNA damage are characteristics of Hub1 knockdown and entail apoptosis

a) Cell cycle regulator p53 is stabilized in Hub1-depleted cells. U2OS cells were transfected with RNAi targeting Hub1 or control and incubated for 60 h. After treatment with 5 μ M actinomycin D (ActD) or DMSO (vehicle) for 6 h cells were harvested and whole-cell lysates were analyzed by immunoblotting using antibodies against p53, p21 or Hub1. b) Hub1 knockdown induces DNA damage mark γ H2AX and abates nucleotide excision repair factor XPC. HeLa cells were transfected with Hub1 or control RNAi and incubated for 50 h. After treatment with 5 μ M ActD or DMSO for 6 h cells were harvested and whole-cell lysates were analyzed by immunoblotting using antibodies against γ H2AX, XPC or Hub1. Actin served as loading control. c) Hub1 RNAi induced DNA damage is rescued by siRNA-resistant Hub1 co-transfection. After RNAi targeting Hub1 or control HeLa cells were either co-transfected with siRNA-resistant 3xFLAG-Hub1 or treated with ActD (5 μ M) for 6 h. Cells were harvested and whole-cell lysates were analyzed by immunoblotting using antibodies against γ H2AX, Hub1, hSnu66 or PRPF8. d) Representative image of the abnormal (fragmented) nuclear morphology in human cells resulting from Hub1 depletion. 72 h after RNAi transfection HeLa cells were fixed and stained with α -Tubulin antibodies and DAPI. Scale bar represents 10 μ M. e) Activation of the apoptotic cascade monitored by caspase 7 cleavage after RNAi. HeLa cells were transfected with RNAi targeting Hub1, hSnu66 or control and co-transfected with a plasmid expressing hSnu66-GFP, respectively. Cells treated with kinase-inhibitor staurosporine (STS, 2 μ M for 6 h) served as positive control. Immunoblots using antibodies against caspase 7 (detecting pro-caspase 7 and its activated (cleaved) form), Hub1, hSnu66 and loading control PRPF8 are shown (similar results were obtained when assayed for caspase 3).

In addition, the nucleotide excision repair factor XPC, which facilitates recognition and repair of DNA lesions, was specifically down-regulated upon Hub1 RNAi, even when cells were challenged with the drug Act D (Figure 17b and c). The complementation of Hub1 knockdown by the co-expression of siRNA-resistant Hub1 cDNA prevented ATM/ATR activation and γ H2AX induction, again confirming the specificity of the knockdown and the cellular alterations caused by Hub1 depletion (Figure 17c).

The aforementioned role of Hub1 as crucial factor for genome stability became prominent after prolonged cultivation of Hub1-depleted cells (in U2OS cells >72 h, HeLa > 60 h). Although, initially arrested in G2/M phase, human cells depleted for Hub1 were able to overcome the cell cycle checkpoint and to exit from this blockage in cell cycle progression, which has been described as *mitotic slippage* (Di Leonardo et al., 1997; Riffell et al., 2009). Because of this unlicensed release with unsatisfied checkpoints these cells underwent aberrant mitosis, resulting in abnormal, fragmented nuclei and subsequent induction of apoptosis, as appreciated in live cell imaging as well as immunofluorescence staining (Figure 17d). In contrast to wild type or control RNAi cells, where nuclei were integer and regular in shape with a typical outspread α -tubulin network, Hub1 RNAi treated cells exhibited deformed and disintegrated nuclei, segmented and strangulated into multiple micronuclei, that were radially arranged around central dense α -tubulin material (Figure 17d, upper panel). The antibody staining of clustered α -tubulin emphasized structural abnormalities and nuclear rearrangements in Hub1-depleted cells.

Shortly after aberrant mitosis, Hub1-depleted cells are not able to recover and undergo apoptotic cell death concomitant with caspase cascade activation. Upon profound cellular damage (here: genomic instability upon Hub1 inactivation) the intrinsic pathway of apoptosis is triggered and “initiator caspases” (caspase 2, -8, -9 and -10) transduce the signal to “effector caspases” (caspase 3, -6 and -7) and activate them by proteolytic cleavage. These processed effector caspases act as highly active proteases that degrade the intracellular proteome and execute the cell death program (Riedl and Shi, 2004).

To address this point, HeLa cells were transfected with RNAi targeting Hub1 or hSnu66 and co-transfected with hSnu66-GFP expression constructs, respectively. 60-72 h post transfection, cells were harvested and lysed gently to avoid disruption of mitochondria (according to Deveraux et al., 1999) for caspase activation analysis. In cell lysates from control siRNA treated samples exclusively the uncleaved isoform of caspase 7, inactive pro-casp 7, was appreciated (Figure 17e). As a positive control, HeLa cells were treated with staurosporine (STS), which is a ATP-competitive kinase inhibitor and potent inducer of apoptosis (Okazaki et al., 1988). Indeed, STS treatment caused a massive activation of caspase 7 and thereby the appearance of the shorter isoform referring to proteolytically cleaved caspase 7. When Hub1 was

knocked-down, a similar activation was observed and pro-caspase was cleaved, indicating induction of apoptosis in these cells. Interestingly, hSnu66 knockdown also entailed severe defects in cell cycle progression and subsequent mitosis, leading to caspase-dependent apoptosis. Furthermore, neither Hub1 co-depletion with hSnu66 by RNAi nor overexpression of the tri-snRNP protein could suppress the Hub1 knockdown-dependent cell cycle defects and apoptosis (Figure 17e). Similar results were obtained when extracts were assayed for caspase 3 (data not shown) and in luminescence-coupled enzymatic cleavage experiments (see Figure 26c).

4.12 The functional C-terminal surface is crucial to mediate the vital activity of Hub1

After the phenotypical and molecular characterization of Hub1 knockdown it became evident that the Hub1-dependent activity is essential for human cells. Depletion of Hub1 leads to genomic instability and causes severe cell cycle defects, aberrant mitosis with subsequent nuclear segmentation and disintegration that finally entails apoptotic cell death.

Taking advantage of the established complementation assay, where siRNA-resistant Hub1 expression constructs were reintroduced into Hub1 knockdown cells, it was now possible to screen for loss-of-function mutations in Hub1, in order to address the question which surface on the protein is crucial to mediate its vital activity. Therefore, protein alignments of Hub1 orthologs were combined with the structural data obtained from the Hub1-HIND interaction studies. Residues D22 and K17 were particularly interesting, as they are involved in salt-bridge and interface formation between Hub1 and hSnu66 (Figure 18a). Moreover, the protruding R9 residue located in the turn between β -sheet β 1-2 was of interest, as it is important for yeast two-hybrid interaction with Clk3 (see Figure 5d). Besides the highly conserved residues (R9, K17 and D22) (see Figure 18b for alignment), another surface appears particularly interesting. On the opposing side of the Hub1-HIND interface, human Hub1 exposes three hydrophobic residues (W47, Y48, and F51) as a WYxxF motif on the “shoulder” formed by a loop between α 2 and β 3 to aqueous solvent (Figure 4a and 18a). As hydrophobic residues are usually buried inside the protein for stabilization or involved in the formation of hydrophobic interaction interfaces, this exposure of aromatic amino acids is thermodynamically unfavoured and unusual. While a motif, similar to the human WYxxF, is found in lower eukaryotes like *S. pombe* (comprising WHxxF) already, *S. cerevisiae* Hub1 does not contain the aromatic patch, but contains two glycines and leucine instead at these positions (*S.c.*: GGxxL).

Various amino acid substitutions were introduced into the Hub1 coding sequence by site-directed mutagenesis and multiple mammalian expression constructs were generated for Hub1 RNAi complementation studies. In order to

ensure proper folding and expression of the different Hub1 mutant variants, protein levels were examined (Figure 18c). After RNAi treatment, cells were co-transfected with tagged (3xFLAG or GFP) Hub1 WT or mutant versions (D22A, R9A, W47G Y48G (WY-GG), W47G Y48G F51L (WYF-GGL) or combinations R9A D22A (RD), D22A W47G Y48G (D22A WY-GG), R9A W47G Y48G (R9A WY-GG), D22A W47G Y48G F51L (D22A WYF-GGL) and C-terminally tagged Hub1 (Hub1-GFP), respectively (Figure 18c).

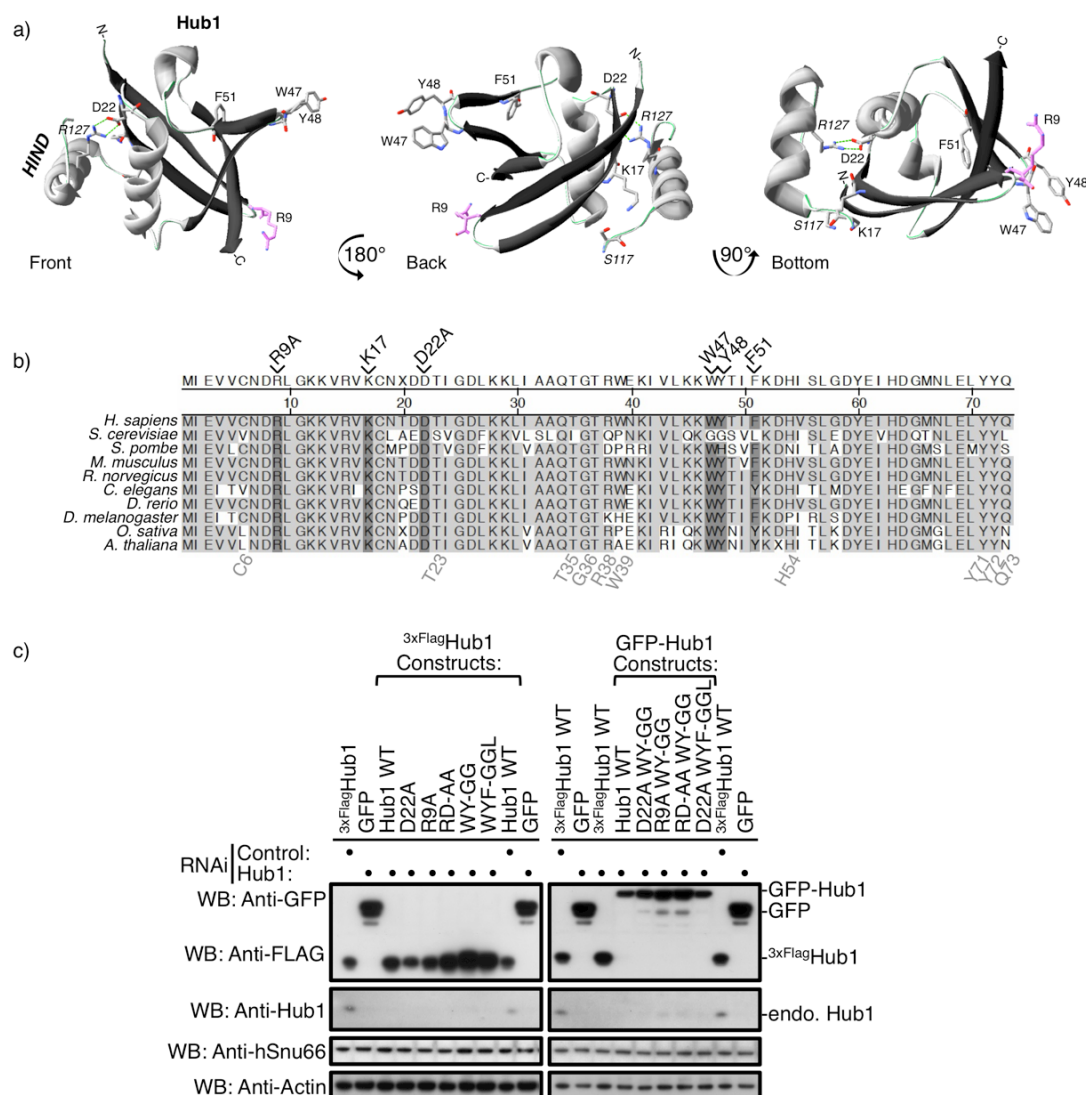


Figure 18: Characterization of crucial residues in Hub1 by mutational analysis

a) Position of crucial amino acid residues within the human Hub1-HIND complex. Three different perspectives of the Hub1-HIND crystal structure highlighting special amino acid side chains. Amino acids of HIND are labeled in italics. Three classes of residues are grouped: crucial for Hub1-HIND interaction (D22A, K17, R127A, S117), C-terminal surface (R9 and C-terminal tags), and hydrophobic patch (W47, Y48 and F51). b) Protein sequence alignment of Hub1 orthologs from yeast to human. Amino acids identical with human Hub1 are shaded in light grey. Residues mentioned in a) and c) are highlighted in dark grey and labeled above. Further mutational analysis was performed on residues depicted below in light grey, data not shown. c) Expression of Hub1 point mutants in RNAi complementation assays. HeLa cells were co-transfected with either Hub1 or control RNAi and constructs encoding siRNA-resistant Hub1 WT, point mutants (single or combined) or GFP vector control. All mutants were experimental tested as N-terminally 3xFLAG- and GFP-tagged versions of Hub1. 60 h post-transfection cells were harvested and whole-cell lysates were analyzed by

immunoblotting using anti-GFP, anti-FLAG M2 and anti-Hub1 antibodies. hSnu66 and actin served as loading controls.

In summary, none of the amino acid substitutions affected Hub1 protein stability negatively and mutant versions were expressed to similar extent, although, interestingly, alterations in the aromatic WY patch increased Hub1 protein levels. Beside the abovementioned mutations in Hub1, additional particularly interesting residues in putative motifs were tested (see Figure 18b, labeled grey below alignment), but will need further investigation (data not shown). For example, another central patch containing amino acids T35, G36, R38 and W39 play a potential role in human Hub1 oligomerization *in vitro*, whereas residues flanking T23 (DDTI) resemble an ideal polo-like kinase 1 (Plk1) phosphorylation consensus motif (D/E-x-S/T- ϕ , with ϕ being a hydrophobic residue) (Nakajima et al., 2003) implicated in cell cycle regulation and pro-apoptotic pathways.

In the following experiments, Hub1 mutant versions were screened for their complementation capacities in RNAi treated cells. Initially, the focus was set on mutant alleles which interfere with the interaction between the ubiquitin-like protein Hub1 and the tri-snRNP protein hSnu66 via a conserved domain termed HIND, which is mediated via a salt bridge formed by D22 of Hub1 and R127 of hSnu66 (Figure 4). Mutating these residues abrogates the physical interaction between Hub1 and hSnu66 (Figure 5), the hSnu66-dependent recruitment of Hub1 to nuclear speckles (Figure 8) and Hub1-dependent nuclear retention of the N-terminal RS-domain (Figure 11). Reintroducing Hub1 WT into RNAi treated cells was able to fully rescue the Hub1-depletion phenotype, restore cell cycle progression and suppress the induction of apoptosis (Figure 19a, first three panels). Notably, performing the same experiment with the Hub1 D22A mutant largely complemented cell cycle defects and cell death. However, the rescue efficiency is significantly lower than that of WT Hub1, as indicated by the reproducibly restrained flow cytometry profile and underscored by quantification (see graph in Figure 19a). In further experiments, 3xFlag-tagged Hub1 variants with additional single and double mutations (R9A, RDAA, D22AWYGG or D22AWYFGGL) were tested. None of the candidate Hub1 variants failed to rescue, but rather showed similar or even higher complementation capacity compared to the D22A single mutant (Figure 19b).

To rule out any tag-specific effects on the Hub1 fusion protein, the same experiments and read-out were performed with GFP-tagged Hub1 and corresponding mutations (Figure 19c). Again, similar results were obtained and tagged Hub1 mutants (D22AWYGG, D22AWYFGGL, R9AWYGG, R9AD22AWYFGGL) were able to complement to some extent. In fact, the complex *triple-surface mutation* R9AD22AWYFGGL, which interferes with the Clk3 association, hSnu66 binding and alters the hydrophobic patch, exhibited a more constricted flow cytometry profile than

single or double mutations, without affecting protein stability negatively (Figure 19c and 18c).

Interestingly, the most striking phenotype was observed when Hub1's C-terminus was decorated with bulky (GFP) or highly charged (FLAG) tags. Although these versions of Hub1 were expressed and folded properly (as shown by hSnu66 binding, Figure 5b) they were not capable of rescuing the Hub1 RNAi-mediated defects and subsequent apoptosis. In contrast to control transfected cells with few apoptotic cells (sub G1 fraction: 1.9%), cell death and apoptotic sub G1 fraction increased upon Hub1 knockdown (sub G1: 16.2%).

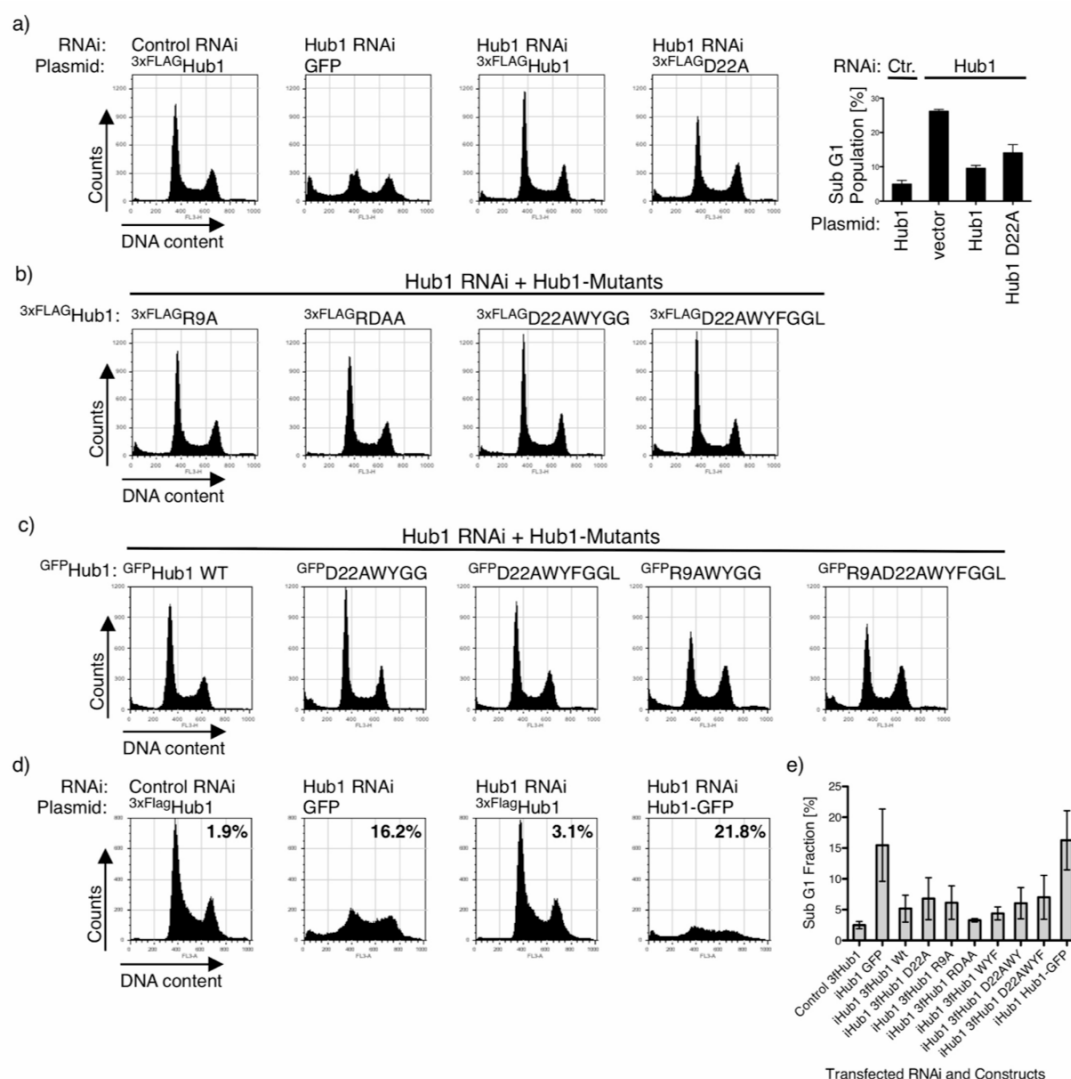


Figure 19: Complementation of Hub1 RNAi cytotoxicity by co-expression of Hub1-point mutants

a) hSnu66-binding mutant Hub1 (D22A) partially rescues Hub1 RNAi-mediated cell death. Complementation of Hub1 RNAi by either expression of siRNA-resistant human Hub1 cDNA encoding for WT or D22A mutant. 24 h after transfection with siRNA targeting Hub1 or control, cells were co-transfected with respective constructs and incubated for 40 h. Cells were harvested, fixed and DNA content was stained for flow cytometry analysis. Right panel: Quantification of apoptotic sub G1 fraction in Hub1 complementation assays. Mean and s.d. of at least three independent experiments are shown. b) Single or combined point mutations in Hub1 slightly reduce complementation capacity. HeLa cells were co-transfected with either Hub1 or control RNAi and constructs encoding siRNA-resistant Hub1 WT or point mutants (single or combined) or GFP vector control. 60 h post transfection cells were harvested, fixed

and DNA content was analyzed by flow cytometry. Three groups of Hub1 mutations: Hub1-HIND interaction (D22A), C-terminal surface (R9) and hydrophobic patch (W47, Y48 and F51) and their combinations are shown. Protein expression levels were tested as shown in Figure 18 c). d) The C-terminal surface is essential for Hub1 function. After Hub1 or control RNAi HeLa cells were transfected with siRNA-resistant Hub1 N- or C-terminally tagged with either FLAG or GFP, they were harvested, fixed and prepared for flow cytometry analysis. (*vice versa* experiments with exchanged tags *e.g.* using C-terminal FLAG resulted in the same deficiency). e) Quantification of apoptotic sub G1 fractions after RNAi in complementation assays with Hub1 mutants. Mean and SD of at least three independent experiments are shown.

While N-terminally tagged Hub1 was able to efficiently compensate the deleterious depletion of endogenous Hub1 (sub G1 dropped to 3.1%), the C-terminal fusion (here Hub1-GFP) failed to reconstitute the Hub1-dependent, vital activity (sub G1: 21.8%) (Figure 19d).

The same deficiencies in RNAi complementation were detected when Hub1 was C-terminally FLAG-tagged (data not shown). Importantly, overexpression of C-terminally tagged Hub1 (Hub1-GFP or Hub1^{FLAG}) in human cells alone (without RNAi pre-treatment) did not show a dominant negative phenotype in any assay tested (flow cytometry, apoptosis induction, morphological changes, immunofluorescence). Altogether, those data indicate that hSnu66 binding via HIND and D22 contributes to Hub1's activity, but its C-terminus appears to mediate the vital function of Hub1.

4.13 Altered distribution of splicing factors and retention of mRNA upon Hub1 depletion *in vivo*

In human cells Hub1 localizes to nuclear speckles and is tightly linked to central splicing-associated factors like tri-snRNP protein hSnu66 and SR-kinase Clk3. As shown by abovementioned RNAi experiments, depletion of Hub1 alters the intracellular homeostasis and thereby generates severe defects in cells, which lead to cellular responses like cell cycle arrest and subsequent cell death. As pre-mRNA processing and splicing are essential pathways in all eukaryotic cells, the fate of pre-mRNA maturation in Hub1 knockdown cells was investigated. For this, immunofluorescence staining of nuclear speckle marker protein SC35 was combined with the RNA fluorescence *in situ* hybridization (RNA FISH) technique targeting the poly (A) tail of mRNA after polyadenylation using fluorescently labeled oligo-dT probes (Tokunaga and Tani, 2008).

Already during RNA synthesis and co-transcriptional processing like capping, splicing and subsequent poly-adenylation, pre-mRNA is handed over to the nuclear export machinery and the mature transcript is released to the cytoplasm for translation into proteins where it is finally degraded (Maniatis and Reed, 2002). Thus, besides the cytoplasm and nucleoplasm polyadenylated mRNA has been found to pass nuclear speckles as well, as it was shown to co-localize with SC35-domains (Dias et al., 2010; Tokunaga et al., 2006).

In line with previous reports, normal SC35 domains with many small foci distributed within the interchromatin space were visualized in control RNAi cells

(Figure 6 and 20a). Furthermore, RNA FISH visualized the exported cytoplasmic pool of polyadenylated mRNA as well as its nuclear fraction partially co-localizing with SC35 (Figure 20a, left panel). In contrast, when Hub1 knockdown cells were examined, an aberrant SC35 pattern was apparent with high enrichment in nuclear speckles and small distinct foci collapsed into enlarged assemblies (Figure 20a). Additionally, not only SR proteins like SC35 were affected, but also polyadenylated mRNAs as shown by FISH. Hub1 RNAi caused strong nuclear retention of RNA species, while the cytoplasmic signal concomitantly decreased. Interestingly, polyadenylated mRNA accumulated in enlarged nuclear speckles as shown by co-localization in SC35 immunostaining (Figure 20a).

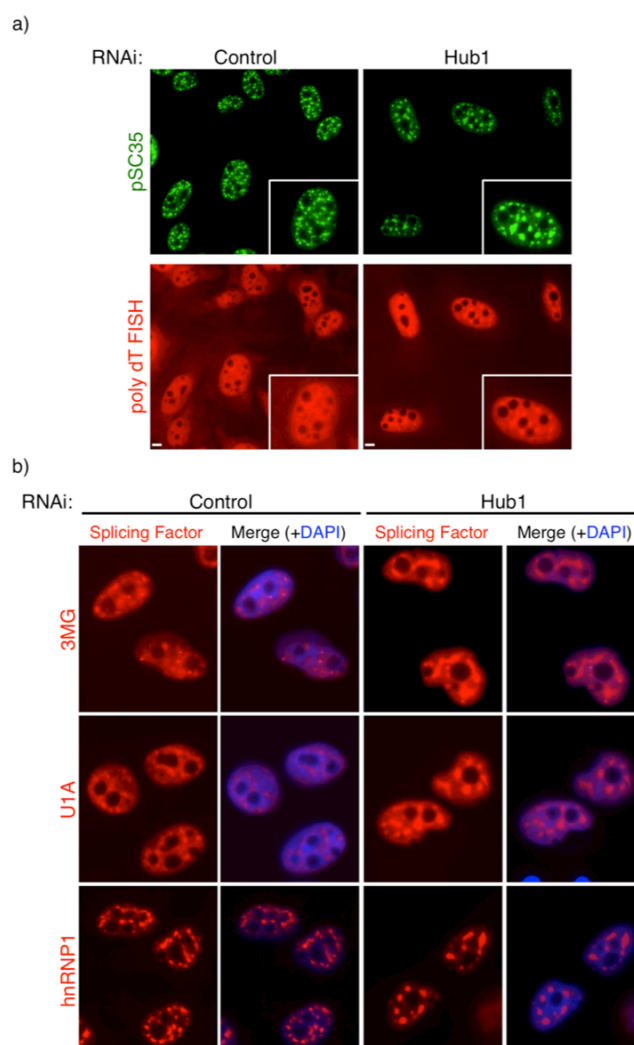


Figure 20: *In vivo* depletion of Hub1 causes an altered distribution of splicing factors and nuclear retention of polyadenylated mRNA

a) SR protein SC35 and mRNA exhibit an aberrant accumulation in nuclear speckles after Hub1 knockdown. After transfection of Hub1 siRNA or control oligos, cells were fixed, permeabilized and immunostained with phospho-SC35 antibodies (red) combined with poly-dT FISH targeting polyadenylated mRNA (green). b) Several splicing-associated factors show an altered nuclear distribution after Hub1 knockdown. RNAi treated cells were fixed, permeabilized and immunostained for 2,2,7-trimethylguanosine (3mG cap) of snRNAs, U1 snRNP protein U1A, or heterogeneous ribonucleo-protein particle hnRNP1 (all red). Nuclei were counterstained with DAPI (blue). Scale bars represent 10 μ M.

After focusing on splicing speckle marker proteins and to further prove that this nuclear retention and aberrant localization after Hub1 depletion is not restricted to SC35 or polyadenylated mRNA, additional factors of the splicing machinery were examined. As depicted in Figure 20b, several spliceosomal factors showed prominent changes in their localization and distribution. Immunostainings with 3mG-specific antibodies recognizing the hypermethylated cap of non-U6 snRNAs (U1, U2, U4, U5, see chapter 2.4), elucidated major rearrangements and altered nuclear distribution after Hub1 RNAi compared to control knockdown cells (Figure 20b, upper panel). Similar defects and altered nuclear localization were observed for the U1A protein, which binds to the U1 snRNA stem loop and thereby acts as a marker for U1 snRNPs localizing to Cajal bodies, nuclear speckles, and the nucleoplasm as well as for PTBP1 (alias pyrimidine track binding protein 1 or hnRNP1) that belongs to the hnRNP family of negative regulators for splice site selection.

Based on data showing that pre-mRNA splicing and nuclear export are tightly interconnected (Reed and Hurt, 2002) and unprocessed or improperly spliced transcripts are retained in nuclear speckles (Kaida et al., 2007; Dias et al., 2010) the hypothesis that Hub1 is a crucial factor for faithful splicing and mRNA processing in human cells was supported by the finding that Hub1 depletion causes an altered distribution of various splicing factors like SC35 and nuclear retention of polyadenylated mRNA in enlarged nuclear speckles.

As RNAi complementation experiments highlighted different functional surfaces on Hub1, stable cell lines expressing the corresponding, mutated versions of Hub1 were tested in SC35 localization assays. Therefore, U2OS cells stably expressing siRNA-resistant GFP-Hub1 WT, GFP-Hub1 D22A, Hub1-GFP or free GFP were transfected with control or Hub1 targeting RNAi. After incubation cells were pre-extracted, fixed and stained for nuclear speckle marker phospho-SC35 to examine its nuclear distribution. In control RNAi cells as well as Hub1 WT cells SC35 and GFP-Hub1 localization was not altered and small splicing foci were equally distributed throughout the interchromatin space (Figure 21a). Moreover, in complementation assays GFP-Hub1 D22A also co-localizes with SC35 like Hub1 WT in small discrete nuclear speckles (like in Figure 7a, without RNAi treatment). However, after Hub1 knockdown in GFP control cells or in U2OS expressing the functionally inactive version of Hub1 (Hub1-GFP), SC35 accumulates in enlarged splicing speckles and displays an aberrant nuclear distribution. Moreover, in contrast to GFP-Hub1 WT and D22A, C-terminally GFP-tagged Hub1 was washed out during the pre-extraction step thus nuclear staining was negative, indicating that Hub1-GFP was not incorporated into protein complexes within nuclear substructures similar to free GFP. Altogether, Hub1 conveys an important activity to maintain proper dynamics of SR protein shuttling and pre-mRNA processing.

Additionally, the impact of Hub1 on general mRNA export was compared to central components of the conserved TREX (TRanscription-EXport) complex and mRNA export machinery. In RNAi experiments two closely related major RNA helicases UAP56 and URH49 with redundant activities (Kapadia et al., 2006; Strasser et al., 2002) were co-depleted *in vivo* and polyadenylated mRNA was stained by poly-dT FISH (Figure 21b).

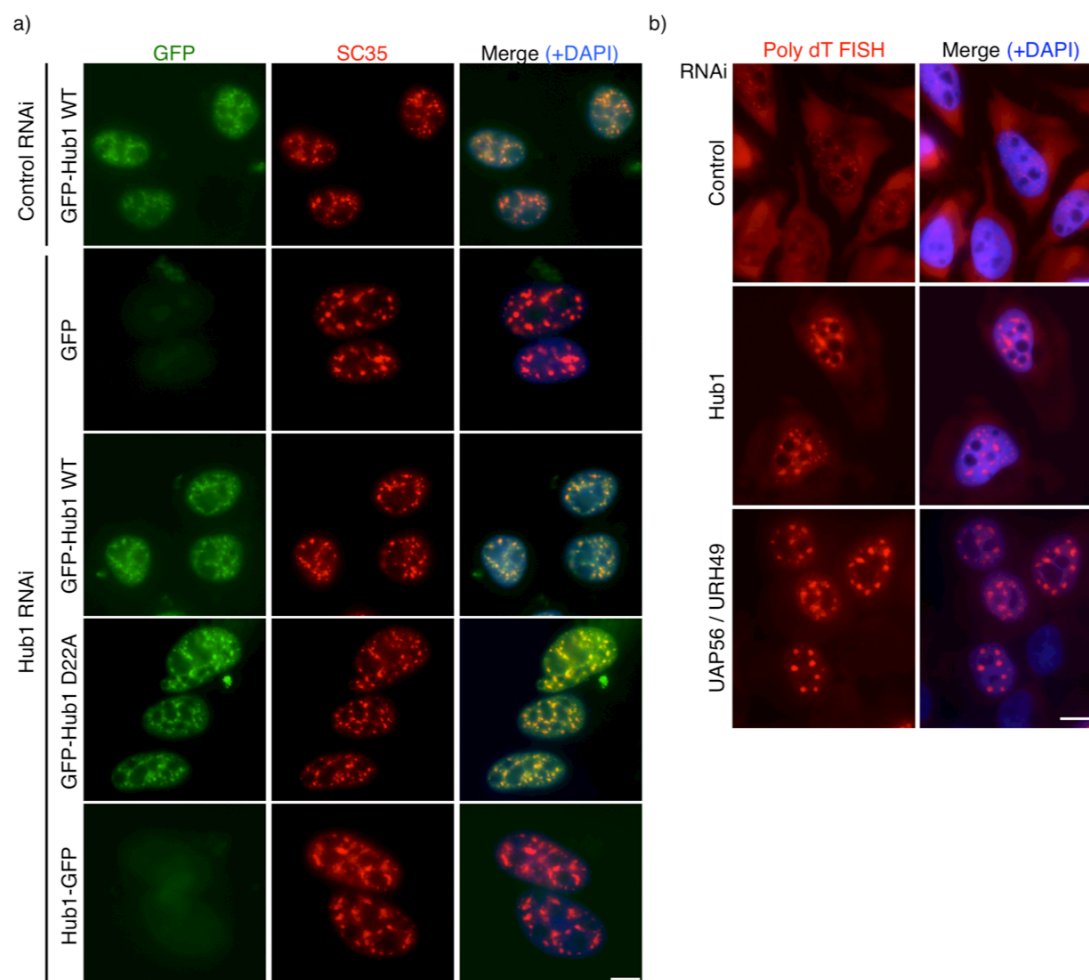


Figure 21: Hub1 RNAi complementation restores aberrant nuclear localization of splicing factors with Hub1 functioning upstream of mRNA export

a) Altered SC35 distribution is rescued in RNAi complementation assay. Hub1 or control RNAi transfected into U2OS cells stably expressing siRNA-resistant GFP-Hub1, GFP-Hub1 D22A, Hub1-GFP, or free GFP (all green). Cells were pre-extracted, fixed and stained for nuclear speckle marker phospho-SC35 (red). DAPI (blue) was used as nuclear counterstain. b) Nuclear mRNA retention after Hub1 RNAi is less profound than in mRNA export knockdown cells. Cells were transfected with RNAi against Hub1, mRNA export helicases UAP56/URH49 or control. Fixed, permeabilized and polyadenylated mRNA was stained by poly-dT FISH (red) and nuclear counterstain (DAPI, blue). Scale bars represent 10 μ M.

Control RNAi cells presented the normal cellular distribution of polyadenylated mRNA in the nucleus (found in nuclear speckles and the nucleoplasm) and diffusely in the cytoplasm. Simultaneous knockdown of UAP56/URH49 efficiently blocked mRNA export and led to a strong accumulation of polyadenylated mRNA in the nucleus and nuclear speckles, while the cytoplasmic fraction was virtually absent (Yamazaki et al.,

2010). In comparison cells depleted of Hub1 showed an intermediate phenotype with less profound mRNA export defect as polyadenylated mRNA was retained in the nucleus and accumulated in nuclear speckles, but reduced amounts of cytoplasmic transcripts were detectable.

In summary, although polyadenylated mRNA is retained in the nuclear compartments after Hub1 knockdown, Hub1 does not play a central role in mRNA transport, like the general mRNA export factors helicases UAP56/URH49, but its action appears to be important for crucial steps further upstream to ensure proper splicing and pre-mRNA processing.

4.14 Identification of splicing defects upon Hub1 knockdown using splicing reporter systems

The cell biological characterization of Hub1 depletion in human cells elucidated various alterations of cellular pathways involved in pre-mRNA processing. RNAi experiments showed that Hub1 is necessary for the proper localization of splicing factors and nuclear export of mRNA. If the pre-mRNA splicing machinery is impaired and aberrant transcripts accumulate, this interferes with downstream RNA processing and can lead to similar phenotypes (Girard et al., 2012; Kaida et al., 2007). In order to address the function of Hub1 in pre-mRNA splicing, an artificial minigene splicing reporter was used. Minigenes are helpful and commonly used tools to characterize various aspects of pre-mRNA splicing, for example recognition and usage of different 5'ss, 3'ss, or pyrimidine tract sequences (Singh and Cooper, 2006; Stoss et al., 1999; Shapiro and Senapathy, 1987). In addition, minigenes allow the characterization of *cis*-regulatory elements like splice site enhancers or silencers in alternatively spliced transcripts and identification of *trans*-acting splicing factors *e.g.* hnRNP and SR proteins (Wang and Burge, 2008; Lopez, 1998).

Here, the vector based fluorescent pGint / pRint reporter system was used (Bonano et al., 2007), in which the protein coding sequence for enhanced GFP (EGFP) was divided into two exons by a constitutively spliced intron (in the case of pGint). The same intron insertion was introduced into the open reading frame of RFP, generating the pRint constructs. The expression constructs carry an adenoviral intron of 125 nt in pGint and 122 nt in pRint, respectively, comprising consensus splice sites, strong branch point and polypyrimidine tract (Figure 22a). Based on the pGint reporter, various variants with different 5' splice sites were generated by site-directed mutagenesis in order to modulate splice site strength (see table in Figure 22a), while pRint's intron sequence remained unchanged, thereby serving as an internal control when co-transfected.

For mRNA splicing assays cells were treated with RNAi targeted against Hub1 or control, and abovementioned reporters, pGint or its 5' splice site variants, were co-transfected with pRint. After isolation of total RNA and cDNA synthesis via

reverse transcription, splicing reporter specific primers (located in flanking 5' and 3' exon of GFP and RFP, respectively) spanning the intron were used to detect spliced and unspliced transcripts. As expected, in RNA samples from control RNAi treated cells only the mature and properly spliced transcripts with a size of 320 nt for pGint and 375 nt for pRint were detectable (Figure 22b, upper right panel). In contrast, when pGint transcripts from Hub1 knockdown cells were analyzed, an additional RT-PCR product was detectable beside the mature transcript. This product with a total fragment length of ca. 445 nt comprised additional 120 nt, resembling the size of an unspliced transcript with retained intron (Figure 22b, upper left panel). This accumulation of an unspliced transcript product was also detected in pRint control samples albeit to a lesser extent. Notably, minor variations at the 5' splice site (pGint: GTGAGTA) generating strong, previously well characterized sequences (Burset et al., 2001; Roca et al., 2005), namely canonical human GTAAGTA, constitutive human GTATGTA or canonical *S. cerevisiae* GTATGTT, did not significantly affect splicing efficiency in this read-out (Figure 22).

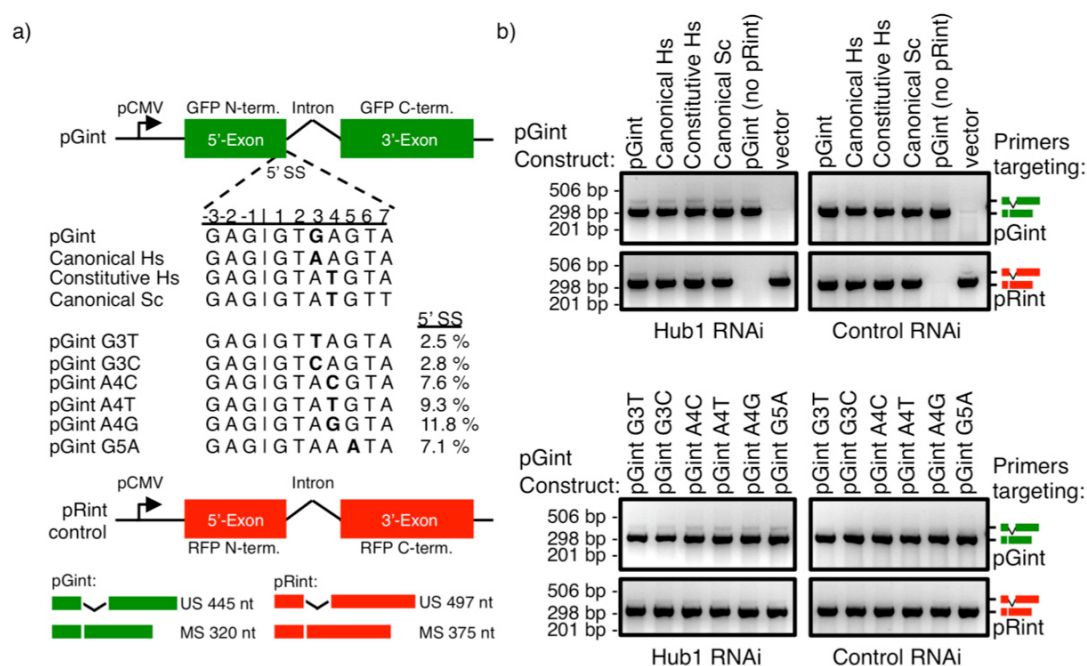


Figure 22: Splicing reporters indicate Hub1's crucial role for efficient pre-mRNA splicing

a) Schematic representation of splicing reporters (pGint/pRint) depicting exon-intron structure and 5' splice site (5'ss) variations tested. Intron-containing GFP-encoding reporter pGint with alternative 5'ss sequences for strong splice sites (upper part of table) or mutated weak splice sites (lower table, percentage shows splice site usage in human transcripts (Burset et al., 2001)) was co-transfected with RFP-expression construct pRint serving as constant internal control. Sizes of mRNA products are given below: unspliced (US) or spliced (MS, mature spliced transcript). b) Hub1 is important for proper splicing of reporter pre-mRNAs. Splicing reporter constructs pGint or its 5'ss variants were co-transfected with pRint into Hub1 RNAi treated cells and total RNA was isolated for RT-PCR analysis. Specific primers spanning the intron for detection of spliced and splicing-defective mRNAs.

Additional pGint constructs with mutated, weaker 5' splice sites (Table in Figure 22a (Buratti et al., 2007; Burset et al., 2001)) were tested, in order to determine

whether these substitutions would sensitize and further alter pre-mRNA splicing after Hub1 knockdown in human cells. While control RNAi treated cells did not show any alterations in splicing of these pGint variants, Hub1-depleted cells were not able to properly splice pGint transcripts, thus an additional, enlarged RT-PCR product was detectable besides the maturely spliced mRNA. However, weakening 5' splice sites by introducing changes at the exon-intron boundary artificially did not lead to a further increase of unspliced mRNA after Hub1 RNAi. These splicing reporter assays underscore Hub1's implication in the splicing machinery and further support its role as a crucial factor ensuring faithful pre-mRNA splicing in human cells.

4.15 The splicing factor Hub1 is crucial for efficient and faithful pre-mRNA splicing in human cells

Although minigenes are commonly used for the characterization of splice sites and exon usage in constitutive and alternative splicing (Cooper, 1999; Singh and Cooper, 2006; Cooper, 2005), endogenous transcripts are controlled by additional layers of regulation for example by histone modifications in the chromatin context or RNA Polymerase II CTD phosphorylation, transcription elongation speed and pausing (see (Cramer et al., 1999; la Mata et al., 2003; Luco et al., 2011; Moore and Proudfoot, 2009)). Based on the splicing reporter data, further experiments were carried out to characterize Hub1's impact on pre-mRNA splicing of endogenous transcripts.

First, transcripts were analyzed that are known to be under tight control of the splicing machinery, as they can be alternatively spliced upon stimuli or under certain cell growth conditions (developmental stages or metastasis) (Li et al., 2006; Lopez, 1998; Shkreta et al., 2011). For this, total RNA was isolated after cells had been transfected with control RNAi or siRNA-oligos targeted against Hub1, hSnu66 or the SR protein ASF/SF2 (alternative splicing factor/splicing factor 2; alias: SFRS1). After cDNA synthesis via reverse transcription gene-specific primers targeting flanking exons in Mcl-1 (myeloid cell leukemia sequence 1 (BCL2-related), exon 1-2), Casp2 (caspase 2, exon 6-7), ATG4 (autophagy related 4B, cysteine peptidase (exon 12a-13, UV treatment to induce alternative splicing) and beta-actin (exon 3-4) were used to detect alternatively spliced and unspliced transcripts (Figure 23a).

When control cells were analyzed by RT-PCR using transcripts specific primers, only one prominent band corresponding to the maturely spliced mRNA was apparent. Interestingly, in Hub1 RNAi samples, additional RT-PCR products of Mcl-1, Casp2 and ATG4 were detectable. The molecular sizes of these enlarged PCR bands were compared with intronic and exonic sequences of the targeted genes showing that the higher migrating band resembled the unspliced pre-mRNA of candidate transcripts. Another interesting finding based on the comparison of Hub1 RNAi-dependent splicing defects with RT-PCR results from hSnu66 or ASF/SF2 knockdown cells. Although the tri-snRNP protein hSnu66 interacts with Hub1 and

they co-localize in nuclear speckles, the impact on accurate pre-mRNA splicing diverges in splicing assays. While both, Hub1 and hSnu66 knockdown, affect Mcl-1 splicing and unspliced intermediates accumulate, defects in Hub1 samples appear more severe for Casp2 or ATG4 transcripts than in hSnu66 knockdown cells. Similar results were obtained for ASF/SF2, as similar mis-splicing was detected for ATG4 in Hub1 and ASF/SF2 samples, but not for Casp2 or Mcl-1. In addition to the splicing reporter data, this experiments support Hub1's role as a crucial factor for proper splicing of various endogenous transcripts.

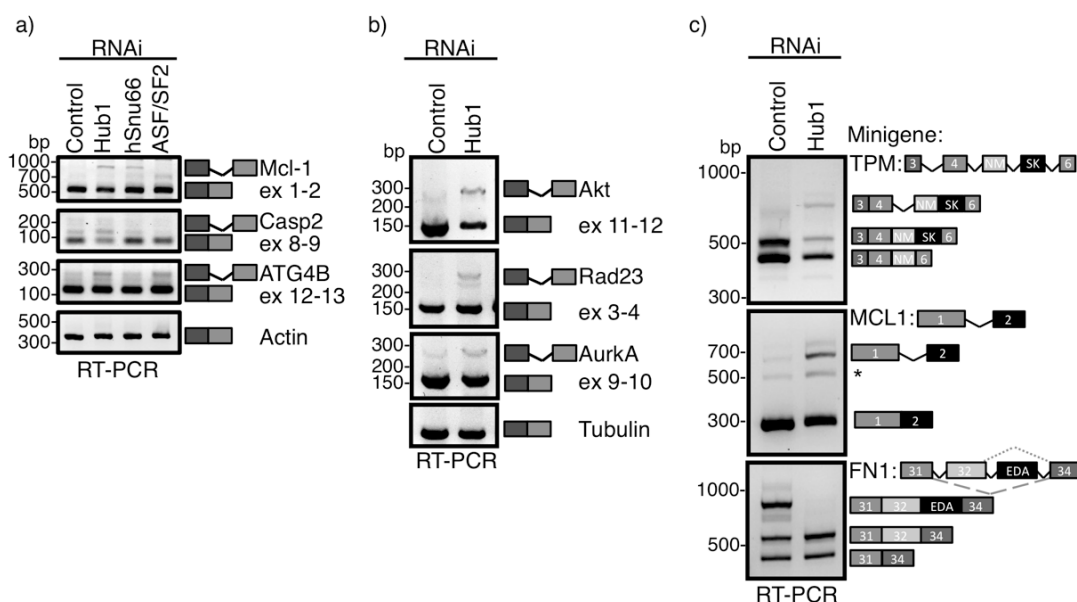


Figure 23: Depletion of Hub1 leads to aberrantly spliced mRNAs and altered splicing patterns

a) Depletion of Hub1 causes aberrant splicing of endogenous transcripts. After knock down of Hub1, hSnu66 or ASF/SF2 cells were harvested and total RNA was isolated. mRNAs of Mcl-1, Casp2 and ATG4 were subjected to intron-spanning RT-PCR. b) Detection of aberrant splicing of endogenous transcripts with putative weak 5' splice site after Hub1 knockdown. mRNAs of v-akt murine thymoma viral oncogene homolog 1 (Akt), RAD23 homolog A (Rad23A) and Aurora kinase A (Aurka) were subjected to intron-spanning RT-PCR (targeted exons indicated on the side). c) Hub1 knockdown influences alternative splicing of fibronectin mRNA and efficient splicing in minigene-assays. Genomic fragments containing alternatively spliced exons of fibronectin 1 (FN1, exon 31-34 incl. EDA), tropomyosin 1 α (TPM, exon 4-7) or Myeloid cell leukemia sequence 1 (BCL2-related) (Mcl-1, exon 1-2) expressed as minigenes in U2OS cells after Hub1 or control RNAi. After isolation of total RNA and reverse transcription, minigene-specific primers were used for PCR to detect altered splicing patterns (schematic exon-intron structure of minigenes depicted alongside).

Co-transcriptional recruitment of splicing factors to regulatory sequence elements within the nascent transcript and emerging exon-intron boundaries (splice sites) orchestrate the stepwise assembly of the spliceosome. Weak splice sites are considered to be recognized poorly by the splicing machinery and thereby require auxiliary factors (like SR proteins) to ensure proper and efficient splicing of intronic sequences. Thus, endogenous pre-mRNA transcripts with weak splice sites (Ahn et al., 2011) were investigated further in Hub1 knockdown experiments. Here, total RNA from Hub1 RNAi treated cells was tested for aberrant splicing of transcripts of v-akt murine thymoma viral oncogene homolog 1 (Akt), RAD23 homolog A (Rad23A) and

Aurora kinase A (AurKA) by intron-spanning RT-PCR (Figure 23b). Indeed, cells lacking Hub1 exhibited defective splicing and aberrantly spliced mRNA with retained introns accumulated. However, in control RNAi samples exclusively mature transcripts of Akt, Rad23A and AurKA were detectable in RT-PCR analysis.

In parallel to experiments focusing on endogenous transcripts, sophisticated minigene assays were established. Instead of artificial transcripts like the intron-containing GFP ORF in pGint, genomic fragments containing alternatively spliced exons of fibronectin 1 (FN1, exon 31-34 incl. EDA alias EIIIA), tropomyosin 1 α (TPM, exon 4-7, incl. NM and SK exons) or myeloid cell leukemia sequence 1 (BCL2-related) (Mcl-1, exon 1-2) were expressed as minigenes as described previously (Stoss et al., 1999; White and Muro, 2011; Gooding and Smith, 2008; Bae et al., 2000). These transcripts have been widely studied to address molecular processes like splice site usage, *cis*-acting regulatory elements and alternative splicing. After these genomic fragments were introduced into Hub1 or control RNAi treated U2OS cells as minigenes, total RNA was isolated, reversely transcribed and analyzed with PCR using minigene-specific primers to detect altered splicing patterns.

Gene products of fibronectin 1 (FN1) are well characterized and have been shown to give rise to various mRNA isoforms due to three alternatively spliced regions, namely extra domain A (EDA), extra domain B (EDB) and type III connecting segment (V region) (White and Muro, 2011). Alternative splicing of EDA, EDB or V region by exon retention or exclusion generates over 20 different isoforms of the extracellular matrix protein during developmental stages, tissue injuries or malignant transformation of human cells (Magnuson et al., 1991; Muro et al., 1998). Strikingly, when exons 31-34 of fibronectin 1 were examined, analysis of the splicing pattern elucidated that Hub1 depletion led to skipping of exon EDA and alternative splicing of FN1 (Figure 23c). In control cells the FN1 minigene expresses three isoforms to almost equal amounts including transcripts containing the EDA exon. The latter isoform is largely diminished in Hub1 knockdown cells while the smaller EDA negative transcripts appear more abundant, suggesting that Hub1 is necessary for correct exon usage and EDA exon retention during alternative splicing of fibronectin.

Similar defects could be identified in transcripts encoding for the actin filament binding protein tropomyosin 1 α . Here, alternative splicing is utilized to generate tissue-specific mRNA isoforms by preferentially retaining the NM (non-muscle) exon in non-muscle cells like fibroblasts, while the SK (skeletal) exon is preferred in skeletal muscle instead (Lin and Tarn, 2005; Xing and Lee, 2006). Analysis of tropomyosin transcripts in Hub1 knockdown cells revealed an aberrant splicing pattern compared to control cells (Figure 23c). From total RNA of control cells two transcripts were detected in RT-PCR assays, one corresponding to the long isoform, which comprises exons 4-5-NM-SK-7 and the other short isoform lacking the NM exon, which results in mRNAs containing exon 4-5-SK-7. Hub1-depleted cells

showed defective splicing of TPM, with reduced inclusion of the NM exon and retention of the intron between exon 5 and the NM exon.

Another gene tested for Hub1-dependent alternative splicing illustrates how switching between different transcript isoforms regulates cellular pathways and determines the fate of cells. The human Mcl-1 gene can give rise to three mRNAs termed Mcl-1L, Mcl-1S and Mcl-1ES (additional Mcl-1V variant in mouse) (Kim et al., 2009; Kojima et al., 2010), which are translated into protein isoforms with opposing functions. While the large transcript Mcl-1L encodes the anti-apoptotic variant comprising the transmembrane and all BCL2-homology (BH) domains 1-4, the shorter mRNA isoform Mcl-1S formed by alternative splicing of exon 2 produces the pro-apoptotic Mcl-1S protein variant lacking the crucial BH1, BH2 and TM domains. The other pro-apoptotic variant, Mcl-1ES, in which alternative splicing of exon 1 excludes the PEST sequence, encodes a hyperstable protein isoform and acts, like Mcl-1S, as a negative regulator of Mcl-1L to induce mitochondrial cell death (Bae et al., 2000; Bingle et al., 2000). The Mcl-1 minigene with genomic fragments containing alternatively spliced exons 1 and 2 was analyzed by RT-PCR after RNAi treatment. Upon Hub1 depletion, cells were defective in faithful splicing of the Mcl-1 transcript and mRNAs with retained intron 1-2 accumulated, in contrast to control cells, which showed proper splicing of Mcl-1 (Figure 23c).

In summary, the findings above consolidate and support Hub1 functioning in pre-mRNA splicing, as its depletion leads to altered splicing patterns and accumulation of aberrantly spliced transcripts from minigenes as well as on endogenous expression levels.

In order to further characterize Hub1-dependent splicing of Akt and Aurka mRNAs, the corresponding genomic sequences were introduced into minigene constructs and tested in RT-PCR assays after Hub1 knockdown (Figure 24a). The examination of critical exon-intron boundaries in Akt (exon 11-12) and Aurka (exon 9-10) transcripts from minigenes verified the aforementioned splicing defects with intron retention in Hub1-depleted cells, which was absent in control cells (Figure 24a, upper and middle panel). An additional gene was identified in an exon-specific microarray (see chapter 4.16) and characterized in analogous minigene assays: Laminin 5 alpha (Lama5). The transmembrane protein laminin 5 contacts integrins and components of the extracellular matrix, where it mediates attachment, migration, differentiation and organization of cells into tissues (Nguyen and Senior, 2006; Spenlé et al., 2013). In genome databases, more than 15 transcript isoforms for the Lama5 gene are documented, including an alternatively spliced variant of 5' exon 63 and exon 64 (mapped sequence Ensembl ID: AK074307).

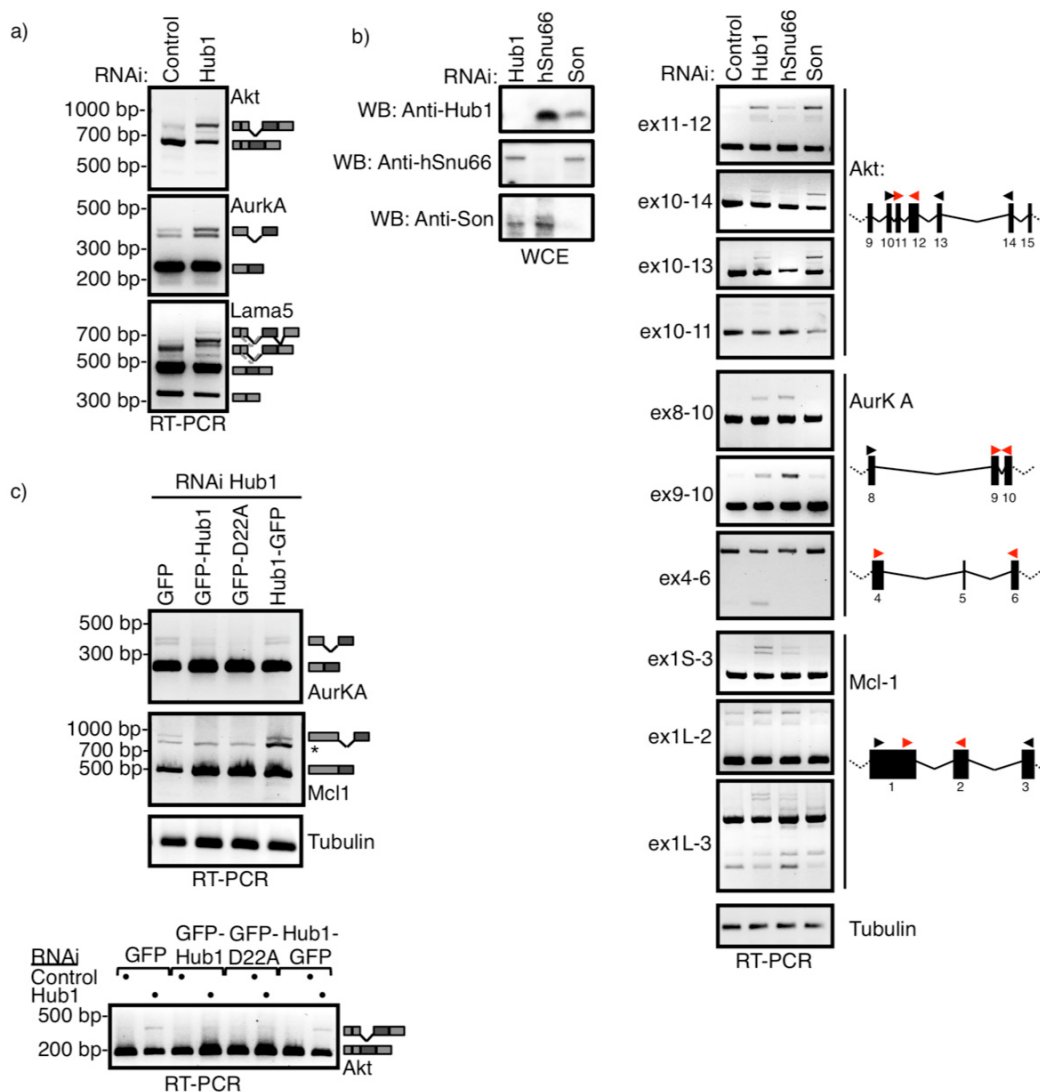


Figure 24: Hub1 is crucial for accurate splicing of specific splice events *in vivo*

a) Aberrant splicing of Akt, AurkA and Lama5 after Hub1 knockdown in RT-PCR based minigene assays. Minigenes were co-transfected with Hub1 or control RNAi and splicing patterns were analyzed by RT-PCR after total RNA extraction. b) Comparison of splicing specificities dependent on Hub1 and splicing factors hSnu66 and Son. Splicing of Hub1-dependent introns and flanking exons in Akt, Mcl-1 and AurkA mRNAs was analyzed by gene-specific RT-PCR after RNAi against Hub1, hSnu66 or Son in U2OS. Primer sets indicate Hub1-sensitive introns in the respective transcripts tested in RNAi experiments (red arrow heads), whereas mapping studies with PCR primers located in flanking sequences (black arrow head) detected no splicing alterations in neighboring exons/introns. c) Splicing proficiency in Hub1 RNAi complementation assays. Stable U2OS cells were transfected with Hub1 or control siRNA for subsequent isolation of total RNA. AurkA, Mcl-1, Akt and Tubulin as control were subjected to intron-spanning RT-PCR.

After minigene expression of Lama5 gene fragments (containing alternatively spliced exons 63 to 65), three transcripts were detectable, corresponding to constitutively spliced exons 63-64-65 (448 nt, all three exons), alternatively spliced exons 63+65 (310 nt, skipping exon 64) and an isoform with retained intron between exon 63-64 (620 nt, 63-intron-64-65, Figure 24a, lower panel). Lama5 pre-mRNA is spliced in a Hub1-dependent manner, as RNAi experiments demonstrated the accumulation of transcripts with intron retention when Hub1 was depleted. While the small alternatively spliced transcript variant with exons 63+65 was slightly reduced and

mRNAs with constitutively spliced exons 63-64-65 were equally expressed, one additional intron-containing mRNA became evident. Beside the intron-containing mRNA consisting of exon 63-intron-64-65, the unspliced transcript with exon 63-intron-64-intron-65 and both retained introns accumulated (Figure 24a).

Aberrant splicing upon Hub1 RNAi affects various transcripts and leads to alternatively spliced mRNA isoforms, proposing two possible models for Hub1 function. Hub1 could act as a constitutive spliceosomal factor, whose depletion could interfere unspecifically with general splicing of pre-mRNA. If this was the case, the catalytic activity of the spliceosomal machinery should be significantly reduced and any intron would be spliced with low efficiency in a sequence-independent manner. Alternatively, Hub1 could have a specific function by supporting spliceosomal activity and robustness at problematic splicing events to ensure accurate progression through the splicing cycle. Then, Hub1 would be crucial for splicing of a number of certain particularly sensitive pre-mRNAs or introns and functions in human cells.

Thus, the previously identified Hub1-dependent transcripts were re-examined and tested for intron-retention or mis-splicing, now including exon-intron boundaries of the flanking sequences. Several primer pairs were used in various combinations covering neighboring exons within the Akt, AurkA and Mcl-1 genes, respectively (Figure 24b, primer positions indicated as arrowheads in schematic representation of transcripts). If Hub1 depletion would lead to general splicing defects and insufficient removal of intronic sequences unspecifically, RT-PCR analysis would detect larger transcripts constantly, as additionally retained introns increase PCR product size. While in control samples exclusively maturely spliced products were detectable, in all cases Hub1 knockdown-induced altered splicing patterns were reproducibly intron-specific. With PCR primers located in neighboring exons spanning additional flanking exons and introns, no further size shift of mRNAs was identified in RT-PCR assays. For example, analysis of Akt transcripts confirmed the intron-retention between exon 11-12 upon Hub1 RNAi and an enlarged PCR product corresponding to the size of exon 11-intron-12 was detected. However, when primers were positioned in flanking exons like exon 10 and exon 13 spanning the critical exon-intron boundaries, transcripts show the same enlargement with no additional sequence elements retained in the transcript. This specificity for individual splice events was shown for AurkA (exon 9-10) and Mcl-1 (exon 1S-2) pre-mRNAs as well.

In subsequent RNAi experiments, the specificity of Hub1 for particular splicing events was compared to important splicing factors like the tri-snRNP hSnu66 or the SR protein Son (Figure 24b, upper left panel immunoblot for knockdown efficiency). Son has been reported to bind pre-mRNA directly via its RS- and RB (RNA binding) domains, but furthermore facilitates association of other SR proteins with weak splice sites (Ahn et al., 2011; Sharma et al., 2011). Interestingly, the aberrant splicing pattern in Hub1-depleted cells was not identical to that of hSnu66 or Son. On the one

hand, both knockdown of Hub1 and hSnu66 negatively affected splicing of particular introns in AurkA and Mcl-1 transcripts, which were not altered upon Son RNAi. On the other hand, hSnu66 RNAi affected Akt splicing marginally, while splicing defects were prominent after Son and Hub1 knockdown.

Moreover, characterization of several exons revealed a novel alternatively spliced isoform of AurkA, as exon 5 is excluded in the upstream 5' region when Hub1 is depleted, but not in hSnu66 or Son RNA samples (Figure 24b).

Finally, after the identification of aberrantly spliced transcripts and characterization of Hub1-specific splicing events, the question remained, which functional surface is necessary on Hub1 to mediate the crucial splicing activity. Thus, RNAi complementation in U2OS cells stably expressing siRNA-resistant GFP-Hub1, GFP-Hub1 D22A, Hub1-GFP or free GFP was combined with splicing assays, where AurkA, Mcl-1 and Akt mRNAs were subjected to intron-spanning RT-PCR (Figure 24c). When Hub1 was depleted by RNAi in GFP control cells, transcripts of AurkA, Mcl-1 and Akt with intron-retention and altered splicing patterns were detected. This splicing defect was fully rescued when GFP-Hub1 was expressed and pre-mRNAs were efficiently and faithfully processed. In addition, the hSnu66-binding mutant GFP-Hub1 D22A was also able to restore splicing activity, indicating that physical interaction of Hub1 with the tri-snRNP component might contribute, but is not essential for this process. In contrast, C-terminally tagged Hub1-GFP failed to complement the splicing defects and mis-spliced transcripts accumulated, comparable to Hub1 knockdown cells (GFP only).

4.16 Identification of Hub1-dependent alternatively spliced transcripts by exon-specific microarray analysis

During developmental stages and upon certain stimuli like growth factors or cellular stress human cells can react by various response pathways. In addition to transcriptional regulation, the mRNA repertoire is extended by alternative splicing in order to generate different isoforms from the same pre-mRNA. A widely used, sophisticated method to identify alternative splicing events is based on exon-specific microarray platforms (Cuperlovic-Culf et al., 2006). The *Affymetrix Human Exon 1.0 ST Array* combines validated cDNA-based sequences from various mRNA and EST databases with predicted gene structures from bioinformatics analyses in genome projects like Ensembl, Vega or GENSCAN, allowing the identification of previously unknown splice variants. In contrast to 3' expression analysis, here, probe sets target all exons along the entire length of the transcript with at least four probes per exon, probing more than one million exons (Gardina et al., 2006).

This microarray was utilized to unbiasedly characterize global changes in alternative splicing in human cells upon Hub1 depletion. Therefore, in three independent experiments total RNA was isolated from Hub1 or control RNAi treated

U2OS cells 60 h post transfection, when Hub1 depletion was accomplished, but cells did not exhibit any signs of cellular stress, nuclear degeneration or apoptosis as confirmed by microscopy and flow cytometry. After satisfying the quality control criteria, the isolated total RNA was reversely transcribed to synthesize cDNAs, which were then fragmented into hybridization-compatible samples and fluorescently labeled for hybridization with the microarray. Subsequently, exon-specific probes on the microarray chip specifically bound to complementary sequences within the cDNA samples and the fluorescent signal was detected and quantified. Sophisticated bioinformatics analysis based on the ARH entropy function (Rasche and Herwig, 2010) compared the individual exon expression levels and quantified the alternative splicing patterns in RNA samples from control RNAi treated cells versus Hub1 knockdown cells. RNA quality control, labeling, microarray hybridization and initial microarray analysis was conducted by Atlas Biolabs GmbH (Berlin).

In Figure 25a representative graphs of three candidate transcripts (Lama5, DPP10 and TCEA2) with high confidence hits for splicing alterations upon Hub1 depletion are depicted. The relative exon expression of each transcript-specific exon probe was calculated for control (red line) and Hub1 ("treatment", blue line) RNAi treated samples. The amplitude of difference between each exonic probe of control and Hub1 knockdown samples is represented as the splice index. Among the first 100 high confidence transcripts with altered exon expression the majority of transcripts (68%) showed a decrease of exon probe signal in Hub1 samples. In 25% of the cases exon probes detected increased levels of targeted RNA sequences in Hub1 knockdown cells in comparison to control cells. 3% of the probe set showed strong fluctuations or alterations in both directions (4%) within the same transcript. As shown previously in minigene assays, the laminin 5 alpha transcript is alternatively spliced upon Hub1 knockdown (see Figure 24a). In line with this finding, exon probes targeting Lama5 transcripts (probe ID: 987232-9872324; position in exon 63-65) reported a strong difference in relative exon expression resulting in high splice index values ($SI \geq 8$) due to low signals in Hub1 RNAi samples. Similar changes in relative exon expression patterns upon Hub1 depletion are exemplified for DPP10 and TCEA2 gene products (Figure 25a).

Based on bioinformatics analysis, genes listed in Figure 25b resemble the top 50 candidate transcripts exhibiting splicing alterations upon Hub1 depletion in U2OS cells, ranked according to their splice index and high confidence score. Interestingly, these Hub1-dependent genes appear to be not functionally linked, but rather implicated in diverse cellular pathways like G-protein signaling (RGS3), DNA damage repair (BRCA1), transcription elongation (TCEA2), cytoskeletal architecture (Lama5, Col3A1, EML1) and uncharacterized functions (DPP10, HPS1, HYSL1) (see appendix 12.1 for comprehensive microarray data).

In addition to the advanced, in-depth bioinformatics analysis mentioned above, the genome-wide exon expression and splice index analysis identified more than 3000 altered splice events in total after Hub1 RNAi (Figure 25c). This data further corroborated the global impact of Hub1 function on a broad spectrum of distinct splicing events and its pivotal role in pre-mRNA processing and alternative splicing in human cells.

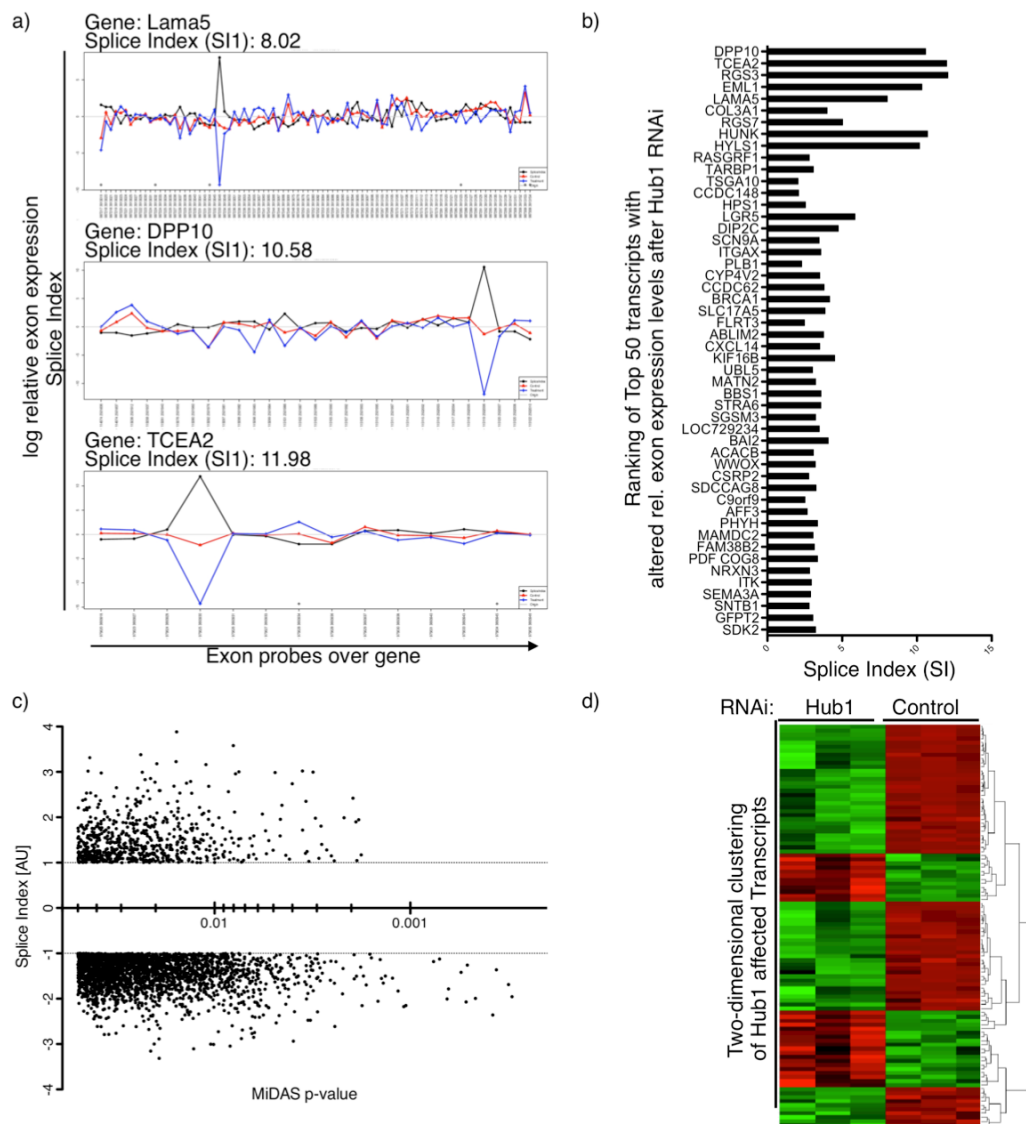


Figure 25: Exon-specific microarray revealed global alterations in alternative splicing and mRNA expression upon Hub1 depletion

a) Splice index profile of three candidate transcripts with high confidence hits for splicing alterations upon Hub1 depletion (Lama5, DPP10 and TCEA2). Exon-specific probe IDs and their relative positions on the targeted transcript are given on the X-axis. The relative exon expression for control samples (red line) and Hub1 RNAi samples (“treatment”, blue line) are plotted on the Y-axis (log). The amplitude of difference between each exonic probe of control and Hub1 knockdown samples is represented as the splice index graph (black line). b) Ranking of top 50 high confidence hits with significant splicing alterations upon Hub1 depletion. GeneID and splicing index values of affected transcripts are shown. c) Global exon expression and splice index analysis of the exon ST microarray (core) datasets using AltAnalyzer software. Basic exon expression profiling and signal processing of control and Hub1 RNAi sample datasets from three biological replicates using MiDAS and DABG detection parameters revealed over 3226 altered splice events in Hub1-knockdown cells (filtered for DABG and MiDAS $p > 0.05$ each).

d) Alteration in mRNA expression after depletion of Hub1. mRNA expression profiles of Hub1 and control RNAi U2OS cells were analyzed by exon-microarray. The heat map shows a two-dimensional clustering of top 100 genes with changes in mRNA expression represented by high (red) and low (green) intensities, where black indicate no changes in intensities, for 337 transcripts with increased levels (≥ 2 fold) and 1172 different mRNAs down-regulated (≤ -2 fold).

In addition to its primary quantification of probe-specific relative exon expression, the microarray yielded further information about global transcriptional alterations. When the abundance of gene products expressed in Hub1 knockdown cells were compared to control cells, 337 transcripts with increased levels (≥ 2 fold) were identified, whereas the majority of transcripts (1172 different mRNAs) was down-regulated (≤ -2 fold). Figure 25d summarizes the mRNA expression analysis graphically as a heat map showing the quantification of the 100 strongest induced and repressed genes, respectively.

The combination of splicing-specific microarray data and gene expression analysis strongly indicates global changes in mature mRNA synthesis upon *in vivo* depletion of Hub1. The decrease in mRNA levels and aberrant splicing of Hub1-dependent transcripts argue for a crucial role of Hub1 in faithful pre-mRNA processing.

4.17 Antagonistic interactions between the transcription inhibitor actinomycin D and Hub1 RNAi

Based on the molecular and cell biological characterization of Hub1 and its impact on cell viability in RNAi experiments, it was of interest to identify a chemical compound or regulatory proteins that modulate the Hub1-dependent cellular activity or pathway and can suppress the Hub1-depletion phenotypes. Two approaches were used to address this point: on the one hand, co-depletion of regulatory splicing-associated factors by RNAi, and, on the other hand, established inhibitory drugs targeting different cellular pathways were tested in Hub1 RNAi experiments. Among others, transcription inhibitors (actinomycin D, α -amanitin or DRB (5,6-dichloro-1-beta-D-ribofuranosylbenzimidazole), caspase inhibitors (Z-VAD-FMK), kinase inhibitors (Clk-inhibitor TG003, roscovitine, staurosporine, CHK2 inhibitor II) or cell cycle restrictive substances (thymidine, hydroxyurea, nocodazole, aphidicolin) were applied. From this list, two compounds gave particularly interesting results, the anti-apoptotic pan-caspase inhibitor Z-VAD-FMK and the transcription inhibitor actinomycin D.

Blocking the apoptotic cascade by the inhibition of caspases 1, 3, 6, 7, 8 and 9 (Wood and Shillitoe, 2011; Yang et al., 2003) using the tri-peptide Z-VAD-FMK (N-benzyloxy-carbonyl-Val-Ala-Asp-fluoromethylketone) suppressed the induction of cell death in Hub1 knockdown cells in caspase cleavage assays as well as microscopy and flow-cytometry analyses (data not shown). This further supports the model that at late stages of Hub1 knockdown, cells facing profound cellular and mitotic defects undergo caspase-dependent cell death (Castedo et al., 2004). Accordingly, when

untreated and Z-VAD-FMK-treated Hub1 RNAi cells were examined under the microscope, in both samples cells with segmented and disintegrated nuclei were detected (as described in section 4.11). However, after caspase inhibition a high number of cells exhibiting this fatal loss of genome integrity accumulated in Hub1 knockdown samples, as the terminal consequence with the induction of apoptotic cell death was suppressed by the pan-caspase inhibitor, although the cause of the cellular defects upon Hub1 depletion persisted. Thus, Hub1 depleted cells survived, despite their severe damage and genomic instability and were not eliminated from the population by apoptosis.

In contrast to Z-VAD-FMK, which acts on signaling events at late stages of Hub1 RNAi-mediated cellular defects, actinomycin D treatment alleviated those Hub1 depletion phenotypes at earlier stages. Actinomycin D has been described to bind DNA directly and thereby inhibit RNA-polymerase II-dependent RNA synthesis by blocking transcription elongation (Sobell, 1985; Hollstein, 1974). In the initial screening after 48 h of Hub1 knockdown cells were treated with ActD or the vehicle DMSO and their cell cycle profile as well as the apoptotic fraction were analyzed by flow cytometry (Figure 26a). While both control cell sample profiles with DMSO or ActD remained largely unaffected, the DMSO treated Hub1 RNAi sample reproduced the characteristic cell cycle arrest at G2/M phase. Surprisingly, the G2/M arrest was not triggered in Hub1 knockdown cells, when cells were treated with actinomycin D, resulting in a normal inconspicuous cell cycle profile with high G1 and low G2 populations in spite of Hub1 depletion (for quantification see graph in Figure 26a).

To further investigate this rescuing effect, later RNAi time points were examined after incubation with increasing concentrations of the drug. After prolonged incubation the inhibitory activity of actinomycin D showed cytotoxic effects in various mammalian cell lines (Bacchetti and Whitmore, 1969; Cassé et al., 1999), thus, a dose-dependent increase of the apoptotic sub G1 fraction was emerging in control RNAi cells, which was virtually absent in DMSO control samples (Figure 26b and quantification in lower panel).

In vivo depletion of Hub1 alone was sufficient to induce the apoptotic cascade after cellular defects and cell cycle arrest, thus the corresponding sub G1 fraction was evident after 60 h of Hub1 RNAi and DMSO treatment. Surprisingly, in contrast to control cells, where increasing concentrations of ActD were accompanied by an increase in apoptotic cell fraction, actinomycin D treatment resulted in a partial rescue of the cytotoxicity in Hub1 knockdown cells. Here, incubation with higher concentrations of the transcription inhibitor resulted in a decline of the apoptotic sub G1 fraction and improvement of G1 and G2 populations (Figure 26b). The quantification of the flow cytometry data (Figure 26b, lower panel) illustrates the opposing sensitivities of control and Hub1 RNAi cells to actinomycin D treatment

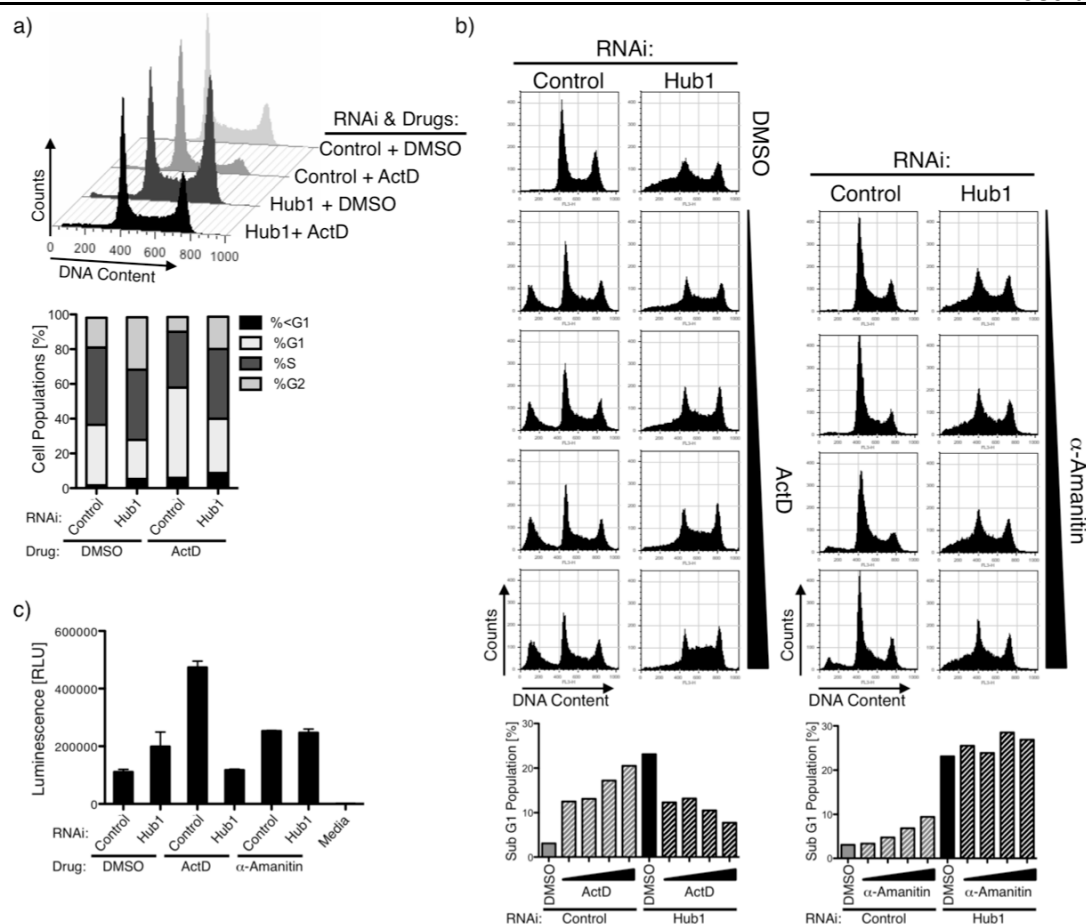


Figure 26: The transcription inhibitor actinomycin D alleviates fatal Hub1 depletion phenotypes

Cell cycle analysis of Hub1 knockdown cells after inhibition of transcription by actinomycin D. a) 48 h after Hub1 or control RNAi transfection HeLa cells were incubated with actinomycin D (ActD) or DMSO control for 6 h, then fixed and stained for FACS analysis. Cell cycle profiles and corresponding quantification graph (below) are shown. b) HeLa cells were transfected with Hub1 or control (lamin A/C) siRNA. After 60 h cells were incubated with DMSO, 1.25 μ M, 2.5 μ M, 5 μ M or 10 μ M actinomycin D (ActD) and 6.25 μ g/ml, 12.5 μ g/ml, 25 μ g/ml μ M or 50 μ g/ml α -amanitin, respectively, for 6 h, fixed and stained for flow cytometry analysis. Cell cycle profiles and corresponding quantifications are shown. c) Caspase activation after Hub1 RNAi and drug treatment. Control and Hub1 knockdown cells were treated (like in b) and subjected to luminescent reporter assays monitoring caspase cleavage activity.

Moreover, this rescuing property is specific for ActD in Hub1-knockdown cells and not a general feature to transcription inhibitors. In analogous experiments conducted with alternative compounds like α -Amanitin (Figure 26b, right panel), which interferes with RNA Pol II translocation during RNA synthesis (Bushnell et al., 2002; Gong et al., 2004) or DRB (data not shown), an inhibitor of the transcription associated kinases CDK9 and CDK7 (Yankulov et al., 1995; Zandomeni et al., 1982), neither of these drugs showed similar properties and even aggravated the Hub1 phenotype.

Using an alternative method to quantify the antagonistic effect of actinomycin D treatment, the caspase activity was measured in Hub1 knockdown or control cells after drug treatment. In a luminescent assay the proteolytic cleavage of a reporter substrate by activated caspases (effector caspase 3 and 7) was measured to monitor

the induction of the apoptotic cascade (Figure 26c). In DMSO treated control cells caspase cleavage was low, but ActD treatment strongly induced caspase activity, hence, apoptosis was induced upon transcription inhibition. Here, the Hub1 RNAi treated cells showed the contrary behavior. In line with aforementioned data, Hub1 depletion alone (DMSO treated sample) already caused a significant induction of caspase cleavage and apoptosis. Consistent with the flow cytometry data, actinomycin D treatment suppressed caspase activation in Hub1 knockdown cells and *vice versa*. The application of the alternative transcription inhibitor α -Amanitin, however, affected both control and Hub1 RNAi cells equally and gave similar results in caspase activation assays.

This data reveals that treatment with the drug actinomycin D can partially antagonize Hub1 depletion-mediated cell cycle and apoptosis phenotypes. At the same time, Hub1-depleted cells appear to be slightly desensitized to actinomycin D's cytotoxicity, as observed in flow cytometry and caspase cleavage assays.

5 Discussion

Previous work on the ubiquitin-like protein Hub1 has mainly focused on lower eukaryotes using model organisms like *S. cerevisiae* and *S. pombe* (Luders et al., 2003; Wilkinson et al., 2004; Yashiroda and Tanaka, 2004; Mishra et al., 2011). Now, over 10 years after its discovery, still little is known about Hub1, especially regarding higher eukaryotes and mammalian cells. Although Hub1 has been implicated in the signal transduction during mitochondrial unfolded protein response, metabolic regulatory circuits and lipid metabolism, the cellular and molecular functions of the unconventional ubiquitin-like protein Hub1 has remained obscure. This work presents the first direct and detailed characterization of Hub1 in human cell lines addressing various aspects of interaction studies, functional analysis and *in vivo* depletion experiments.

5.1 Identification of binding factors by yeast two-hybrid link Hub1 to splicing-associated complexes

An unbiased and comprehensive approach to identify protein interaction partners of Hub1 was based on the powerful yeast two-hybrid (Y2H) system combined with human cDNA libraries. After over 300 clones encoding potential interaction partners were isolated from the initial screen, stringent criteria and tests like auto-activation after FOA-shuffle, 3-AT resistance, or growth on adenine-lacking (-Ade) media were applied to define high confidence hits. Interestingly, the identified candidates resembled a heterogeneous group of proteins functioning in endocytosis (adapter protein complex AP-2 β subunit 1 α (AP-2 β 1 α), as actin-binding cytoskeleton proteins (tropomyosin 2 β (TPM2 β), SUMO/ubiquitin-specific peptidases (USPL1), serine/threonine-protein kinases (PIM-2), Golgi-associated proteins (Golgin a 5) and zinc-finger transcription factors (HIV-EP1) (Figure 1b). Despite extensive *in silico* analysis, a potential canonical Hub1 interaction motif common to all candidate proteins could not be recognized by sequence similarity or protein domain structure comparison.

Among these Hub1 binding factors, two splicing-associated factors, namely the spliceosomal tri-snRNP protein hSnu66 and the Cdc2/Cdc28-like dual specificity protein kinase Clk3, were of particular interest. On the one hand both factors have been implicated in pre-mRNA splicing in human cells (Makarova et al., 2001; Duncan et al., 1997), on the other hand, these factors have been reported to interact with human Hub1 in yeast two-hybrid previously (Wilkinson et al., 2004; Kantham et al., 2003), and thereby served as an internal positive control affirming validity of the screening results. Surprisingly, neither the mode of interaction nor the *in vivo*

relevance of binding to the ubiquitin-like protein was further investigated to elucidate the cellular function of Hub1 in these studies.

Due to the nature of Y2H cDNA libraries that base upon reverse transcription of tissue specific mRNAs, the spectrum of expressed transcripts is naturally limited to the selected cell types and thereby cannot comprise the whole human proteome. In consideration of this fact and the stringent screening criteria applied, it is likely that there are more Hub1 interaction partners remaining to be characterized by alternative techniques.

Although the yeast two-hybrid system has its disadvantages, as heterologous overexpression of human proteins in yeast does not ensure proper folding and functionality of all prey AD fusion proteins and auxiliary factors like required chaperones or posttranslational modifications can be missing, this unbiased approach provided an first important hint for the identification of interaction partners. Despite Hub1's high conservation from yeast to human, when the identified candidates were tested with *HUB1* orthologs from *S. cerevisiae*, *S. pombe* and *H. sapiens* in Y2H interaction studies, the spliceosomal tri-snRNP protein hSnu66 appeared to be the only common binding partner of all Hub1 variants (Figure 1c). This finding suggests that the association of Snu66 with Hub1 evolved early in eukaryotic evolution. Thus, Snu66 might be a primordial binding partner of Hub1 with strong implications in pre-mRNA processing.

In contrast, bioinformatics analysis could not clearly identify homologous proteins of the other novel Y2H binders in *S. cerevisiae*, which might explain why neither ScHub1 nor SpHub1 have acquired protein properties necessary for these interactions. However, in *S. pombe* pre-mRNA splicing is facilitated by auxiliary splicing factors like hnRNP-like proteins (Stutz et al., 2000), SR proteins (Srp2p (Webb et al., 2005)) and their respective kinases, Cdc2/Cdc28-like protein kinase Kic1 and SR protein kinase 1 homolog Dsk1 (Tang et al., 2003; 1998). Kic1 shows high similarity to the conserved class of LAMMER kinases Clk1-Clk4 of which human Clk3 was isolated as a Hub1 interactor in the Y2H screen. Despite the fact that fission yeast has developed regulatory RNA sequence elements for *trans*-acting factors like SR proteins that have not been identified in *S. cerevisiae*, both *HUB1* orthologs ScHub1 and, in particular, SpHub1 failed to bind the human Clk3 in yeast two-hybrid.

Like transcription, pre-mRNA splicing is an essential cellular process to ensure faithful processing, maturation and proper translation of the transcript to give rise to functional proteins. On the other side the ubiquitin-proteasome-system facilitates the efficient removal of abnormal, defective or undesired proteins by targeting doomed substrates for proteolysis. The covalent attachment of ubiquitin to proteins by an enzymatic cascade specifically marks proteins for degradation by the proteasome (Ciechanover, 2005; Peters, 1994). Besides serving as degradation

signals for proteolysis, ubiquitin and ubiquitin-like proteins were shown to play pivotal roles in virtually all cellular processes *e.g.* endosomal trafficking, autophagy, signal transduction, DNA replication and repair, transcription, cell cycle and cytokinesis (Grillari et al., 2010; van der Veen and Ploegh, 2012). Surprisingly, pre-mRNA splicing accomplished by its macromolecular machine, the spliceosome, has been widely excluded from this list.

Here, initial results demonstrating an interaction of the ubiquitin-like protein Hub1 with a core-spliceosomal protein hSnu66, raised several important questions. Firstly, does Hub1 bind hSnu66 directly and what is the molecular mode of interaction? Secondly, which cellular pathways is Hub1 implicated in and does this association with a spliceosomal factor accord with a potential function of Hub1 in human pre-mRNA splicing? And thirdly, the fundamental question, that had to be addressed, does Hub1 fulfill an essential role in human cells and how do cells respond to the inactivation of Hub1?

5.2 Hub1 binding is mediated via a conserved Hub1 interaction domain in hSnu66

Translating the findings from the heterologous yeast two-hybrid to the mammalian system, co-immunoprecipitation experiments with transiently transfected human cells validated the association of Hub1 with hSnu66 *in vivo*. The immunoprecipitation of epitope-tagged hSnu66 co-purified with Hub1 and *vice versa* (Figure 2).

In initial studies the Hub1 binding factor hSnu66 was characterized as a crucial constituent of the spliceosomal tri-snRNP complex (Makarova et al., 2001). Immunodepletion of hSnu66 from human nuclear extracts inhibited subsequent mRNA splicing reactions, and this activity could be re-established by supplementing the depleted extract with recombinant hSnu66 protein, which underscores its essential function in pre-mRNA splicing *in vitro*. Moreover, hSnu66 plays a particularly interesting role, as it is not part of pre-existing U5 or U4/U6 snRNP sub-complexes, but rather associates late during tri-snRNP assembly. These findings are supported by interaction and mapping studies analyzing the U4/U6.U5 tri-snRNP framework (Liu et al., 2006). Here, hSnu66 was shown to bind to the core components like the U4/U6 protein PRPF3, the U4/U6 and U5 bridging factor PRPF6, and central DExH/D-box helicase hBrr2, but not U5 key protein PRPF8. However, the important questions, how binding to these factors is mediated and which domains within hSnu66 are crucial for these interactions were not addressed. When biochemical analysis and purification of spliceosomal complexes at distinct stages of splicing catalysis were combined with sophisticated mass spectrometry approaches, hSnu66 was shown to be incorporated into the tri-snRNP, in pre-catalytic B complexes and activated spliceosomes (B^{act} complex) of human nuclear splicing extracts (Makarov et al., 2002; Bessonov et al., 2010; Agafonov et al., 2011). hSnu66

is thought to be an important factor mediating protein-protein interactions for the recruitment of the tri-snRNP to join the pre-spliceosomal complex A, when U1 and U2 snRNPs are already loaded on pre-mRNA, to stably form the pre-catalytic complex B. In addition to its splicing-associated function, hSnu66 has been discussed to act as a transcription activator of hypoxia-responsive genes, namely erythropoietin (*EPO*) and vascular endothelial growth factor (*VEGF*) (Gupta et al., 2000). In fact, hSnu66 might also function as a regulatory switch between hypoxia-induced factors (HIF1 α and HIF2 α) upon hypoxia (Koh et al., 2008; 2011), but the molecular mechanism of this regulatory circuit and if these effects are linked to mRNA splicing remains unclear. Notably, among other tri-snRNP factors like PRPF3, PRPF8 or PRPF31 hSnu66 is considered as a disease-relevant gene during hypoxia-induced retinal degeneration in autosomal dominant retinitis pigmentosa patients (Schmidt-Kastner et al., 2008). Furthermore, hSnu66 (alias SNRNP110 or SART1 (squamous cell carcinoma antigen recognized by T cells)) is implicated in various aspects of tumorigenesis as it is significantly up-regulated in various cancer tissues (Takaishi et al., 2008; Matsumoto et al., 1998; Kawamoto et al., 1999) and has been identified as an autoimmune epitope which is recognized by tumor-specific cytotoxic T lymphocytes (Kikuchi et al., 1999; Yoshida and Tanaka, 2004).

Structure prediction and bioinformatics analysis have elucidated that hSnu66 is an intrinsically unstructured protein with low complexity regions and belongs to the group of highly disordered proteins in the spliceosomal proteome (Korneta and Bujnicki, 2012). In fact, compared to other ribonucleoprotein-based “molecular machines” the spliceosomal complex is comprised of more intrinsically unstructured and disordered proteins than for example the ribosome. Due to complex RNA-RNA, protein-RNA and protein-protein interaction networks and major rearrangements during the transesterification steps, structural flexibility of spliceosomal factors for different conformational stages is necessary. Thus, SR-related proteins like hSnu66 involved in mRNA recognition, intron/exon definition and spliceosomal assembly tend to be more disordered than splicing factors that carry out the splicing catalysis (Korneta et al., 2012). Furthermore, the formation of intricate protein-RNA complexes like snRNPs is facilitated and coordinated by molecular chaperones to prevent premature assembly or aggregation. For example, the specialized chaperone pICln orchestrates the Sm ring formation on snRNA, while other auxiliary factors like Aar2 support correct incorporation of large multidomain proteins including PRPF8 into functional U5 and tri-snRNPs, respectively (Chari et al., 2008; Weber et al., 2011; Sahi et al., 2010).

However, hSnu66 contains several short motifs, which underscore its nucleic acid-directed function, as the putative leucine zipper, the engrailed homology domain 1 and the nuclear localization signal can mediate direct contact with DNA, whereas its N-terminal RS-domain is involved in RNA related processes. Both, LZ and EH1

domains, have been identified and characterized as DNA binding domains in transcriptional regulators where they can act alone or in concert with co-activators or repressors like the mammalian *Groucho* to control gene expression (Kutay and Güttinger, 2005; Struhl, 1989; Goldstein et al., 2005; Copley, 2005; Makarova et al., 2001). With respect to its aforementioned putative role in transcription of *e.g.* hypoxia-induced genes, an additional role for hSnu66 in transcriptional regulation cannot be ruled out, but both aspects require further investigation.

The N-terminus of hSnu66 reveals another interesting domain, the arginine-serine rich domain. In contrast to yeast ScSnu66, the human ortholog hSnu66 gained this additional domain that is widely distributed among splicing factors. The over 240 RS-domain-containing proteins are interwoven with diverse functions during mRNA processing like splicing, mRNA export, regulating kinase and phosphatase activity, translation, transcription, and RNA Polymerase CTD binding (Tarn and Steitz, 1994; Huang et al., 2004; Stojdl and Bell, 1999; Sanford et al., 2004; McCracken et al., 1997). Notably, arginine-serine rich domains can stimulate direct binding to mRNA, *e.g.* at regulatory exonic enhancer sequences (Hertel and Graveley, 2005; Shen et al., 2004), but can serve as platforms for protein-protein interactions as well (Graveley, 2004; Kohtz et al., 1994; Wu and Maniatis, 1993). Interestingly, several RS-domains do not only anchor the SR protein to certain RNA sequences or binding partners, they also appear to have intrinsic splicing-stimulatory activities. Isolated RS-domains are sufficient to activate splicing in HeLa cell nuclear extracts if they are artificially tethered to pre-mRNAs that contain splicing enhancer sequences (Shen and Green, 2006; Philipps et al., 2003). In fact, RS-domain proteins play important roles during early steps of spliceosome assembly and orchestrate the communication between 5' and 3' splice site during early spliceosome assembly (Fu, 1995; Ram and Ast, 2007). Although the snRNA of the U1 snRNP is able to base-pair with 5' splice sites of pre-mRNA exons, a stable association is only established by protein-protein and protein-RNA contacts between RS proteins like ASF/SF2 and the SR-related factor U1-70k (Kohtz et al., 1994). Furthermore, the inactivation of nuclear splicing extracts by depleting the U1 snRNP can be complemented by the addition of purified SR proteins that restore splicing activity (Stark et al., 1998; Crispino et al., 1994; Tarn and Steitz, 1994).

Surprisingly, although hSnu66 associates with central tri-snRNP proteins and is implicated in central steps of mRNA splicing, little is known about the molecular mechanism of hSnu66 and its function is poorly understood. The interaction with the ubiquitin-like protein Hub1 is an intriguing feature of hSnu66. In order to identify which domain or motif is crucial for Hub1-hSnu66 interaction, mapping studies with several hSnu66 truncations were performed. Surprisingly, not the central LZ or EH1 domains but the hSnu66 N-terminal fragment (AA1-185) comprising the RS-domain and the highly conserved stretch of 18 AA (AA111-139) was able to bind and co-

purify with Hub1. Although RS-domains are well-known protein interaction module, further dissection of the N-terminus revealed that a short, highly conserved stretch within hSnu66 was already sufficient and necessary for the interaction with Hub1 (Figure 3b). Despite the clean and precise mapping of this interaction interface, co-immunoprecipitations of overexpressed fusion proteins can be bridged by co-purifying factors or chaperones. Therefore, direct binding was further confirmed by GST pull down assays with recombinant Hub1 and the isolated binding motif, HIND, as a GST fusion (Figure 3c).

Interestingly, this HIND domain is highly conserved among hSnu66 orthologs from yeast to humans. In Snu66 of *S. cerevisiae* and some other Saccharomycotina, two HINDs are positioned in tandem at the very N-terminus, but they lack the RS-domain, which is a common domain among all vertebrate Snu66 orthologs (Mishra et al., 2011). The Hub1 interaction domain is an intriguing module; while Saccharomycotina have evolved the tandem HIND, higher eukaryotes up to vertebrates express single HIND versions of Snu66. However, plants like *Arabidopsis thaliana* lack the Hub1 interaction domain in AtSnu66, but this is compensated by the translocation of the HIND to another tri-snRNP protein, PRP38. Surprisingly, in the protozoan parasite *Plasmodium falciparum*, both tri-snRNP proteins Snu66 and PRP38 contain HIND sequences, which bind Hub1 (Mishra et al., 2011). This phenomenon might be due to the complex evolutionary origin of apicomplexa with characteristics of protists and features of photosynthetic algae (Gould, 2012).

The functionality of these “unusual” HINDs in AtPRP38, PfPrp38 and PfSnu66 was verified by GST pull down assays and yeast two-hybrid interaction studies (data not shown, (Mishra et al., 2011)). Even when Hub1 activity was constrained by linearly fusing it to various tri-snRNP proteins like PRP38, Snu66 or PRP8, artificial tethering of Hub1 to the now fully “Hub1-modified” spliceosome was able to complement the *SRC1* alternative splicing defect in *S. cerevisiae hub1Δ* strains. This phenomenon suggests that Hub1 binding is not crucial for its respective direct binding partner, but rather for the functional complex within the spliceosome.

Due to the unique features of Hub1 as an unusual ubiquitin-like protein implicated in interactions with spliceosomal core components, the crystal structure of human Hub1 in complex with the hSnu66 HIND was solved in order to obtain molecular insights into this mode of binding. During this project, the human Hub1-HIND complex structure was resolved in parallel with its yeast homolog (Mishra et al., 2011), which allowed a direct comparison of conserved but also unique features of this interaction interface. The obtained structure with a resolution of 2 Å highlights human Hub1 sharing the characteristic β -grasp fold similar to ubiquitin and ubiquitin-like proteins with their typical $\beta\beta\alpha\beta\alpha\beta$ secondary structure pattern, as described previously (McNally et al., 2003) (Figure 4a).

In addition, the HIND itself exhibits an interesting feature, as the short 18 AA peptide has the intrinsic ability to form an α -helical secondary structure in solution (Mishra et al., 2011). The interaction interface between the human HIND and Hub1 is mediated via a salt bridge between R127 of hSnu66 HIND and D22 of Hub1 accompanied by several hydrophobic contacts formed by aliphatic residues. This structure clearly reveals the nature of the non-covalent mode of binding and elucidates crucial residues responsible for a stable interaction between human Hub1 and Snu66. In both Snu66-Hub1 interfaces the binding is strengthened by the central salt bridge and supported by accompanying hydrophobic contacts. The structural comparison of human and yeast Hub1-HIND complexes emphasizes the similarity of the two superimposable structures indicating the high evolutionary conservation of the complex at molecular level (Figure 4b).

Compared to non-covalent binding interfaces of ubiquitin and ubiquitin-like proteins, the Hub1-HIND structure highlights an unique mode of interaction and a novel binding paradigm. Several ubiquitin binding domains (UBDs) have been identified and crystalized in complex with the ubiquitin protein (Dikic et al., 2009). The UBDs can be grouped according to their structural binding properties and come in different flavors; domains like the UBA (ubiquitin associated domain), Cue (named after Cue2) and various types of ubiquitin interaction motifs (UIMs like double sided UIM (DUIM) or inverted UIM ubiquitin interaction motifs MIU) utilize single or multiple α -helices to generate an interaction platform for ubiquitin binding. Another module for interaction is formed by zinc finger domains like the nuclear protein localization 4 zinc finger (NZF) or zinc finger ubiquitin binding protein A20 (ZnF A20). Furthermore, the pleckstrin-homology fold is a common feature of GLUE (GRAM-like ubiquitin binding) and PRU (pleckstrin-like receptor for ubiquitin) UBDs that are found in EAP45 and RPN13, respectively. Two other domains (UBC and UEV) mimic the ubiquitin interaction interface of E2 conjugating enzymes to mediate binding by but lacking catalytic activity of the respective enzymes. Finally, beside these classical UBDs further variously shaped ubiquitin-interaction modules like the Jab/MPN domain in PRPF8 were identified (Husnjak and Dikic, 2012). The vast majority of UBDs associate with ubiquitin via the hydrophobic area around I44 supported by L8 and V70 on sheets β 3 β 4 (Dikic et al., 2009). In contrast, the Hub1-HIND interaction surface is located on the opposing side to the canonical UBD patch formed by helix α 1 and sheets β 1 β 2 (Mishra et al., 2011). Both ubiquitin and Hub1 adapt their conformation and undergo an induced fit upon interaction with their respective interaction domains, but their main-chain fold remains unchanged (Lange et al., 2008; Wlodarski and Zagrovic, 2009). Moreover, the Hub1-HIND complex also clearly differs from the non-covalent interaction of other ubiquitin-like modifiers like SUMO with its SIM (SUMO interaction motif) (Song et al., 2005; Hecker et al., 2006) and the Atg8 homolog LC3 with its interaction region (LIR) (Noda et al., 2010).

Despite the detailed information obtained in binding studies and the crystal determination, the structure only includes the isolated HIND peptide while flexible flanking regions of hSnu66 are missing. Therefore, it remains unclear how Hub1 is imbedded into larger complexes *e.g.* with Snu66 in the spliceosomal context. Heteronuclear single quantum coherence (HSQC) data of recombinant yeast ScSnu66 affirmed the largely unstructured nature of the full-length protein. Remarkably, upon addition of its binding partner Hub1, the spectrum of the N-terminal region containing the two HINDs changes drastically, showing that Hub1 binding induces folding of the otherwise unstructured protein (Mishra et al., 2011). During the different steps of splicing the spliceosome undergoes extensive rearrangements, in which RNA and protein networks are disrupted, while new physical interactions are established leading to different conformations of the spliceosome. Considering the Hub1-HIND structure and folding experiments *in vitro*, it is likely that in distinct spliceosomal complexes Snu66 is engaged in different conformations converting between the Hub1-bound and -unbound state. It would be interesting to investigate at which stage and in which complex Hub1 interacts with Snu66 and if this binding might act as a molecular switch between two conformations.

Besides the highly conserved properties, human Hub1 exhibits an additional particularly interesting surface formed by the loop on $\alpha 2$ - $\beta 3$ with two unusually exposed hydrophobic residues, W47 and Y48. Although this aromatic patch is highly conserved in all metazoan orthologs, it is not present in yeast ScHub1. This particular patch is not common among ubiquitin or other ubiquitin-like proteins as judged from structure and sequence comparisons. Due to Hub1's unique properties as shown for Snu66 binding, this aromatic patch might be involved in the formation of an additional interaction interface with an hitherto unidentified factor, thereby underscoring the special position of Hub1 among ubiquitin-like proteins.

The data obtained from structural and interaction studies allowed molecular insights into the mode of interaction between Hub1 and hSnu66. After crucial amino acid residues important for the binding were identified, they were characterized by mutational analysis in further experiments.

As the salt bridge between R11 of HIND (R127 in hSnu66) and D22 of Hub1 strengthens and stabilizes the interaction, point mutations were inserted at these particular residues to abrogate the interaction. Indeed, single alanine substitutions in Hub1 or hSnu66 that interfered with the formation of the salt bridge abolished the formation of a stable Hub1-HIND complex as demonstrated in different co-immunoprecipitation and protein interaction experiments under various conditions. Furthermore, these point mutations including the hSnu66 mutant with deleted HIND (Δ HIND) were also tested in yeast two-hybrid studies as the initial findings had been obtained from the mammalian Y2H screen. Here, exclusively Hub1 WT and hSnu66

WT showed physical interaction, whereas both mutations in hSnu66 (R127A and Δ HIND) and Hub1 (D22A) abrogated binding, confirming the abovementioned results (Figure 5c). Given the fact that the Hub1-hSnu66 interaction is highly conserved and orthologs of different species cross-interact, endogenous ScSnu66, which is present in the Y2H parental strain, could have bridged interactions from the screen. To rule out this possibility the corresponding Y2H constructs were introduced into Δ snu66 knock-out strains and interaction studies were repeated. Also, in this Δ snu66 strain background all interactions of identified Y2H candidates with Hub1 were confirmed and supported the data. However, in addition to the D22 surface on Hub1 mediating the interaction with hSnu66, another region on Hub1, namely the C-terminal surface around R9, functions as a crucial interface for binding to the SR protein kinase Clk3 and endocytosis adapter AP2 β (Figure 5d). Interestingly, both residues (D22 and R9) are not critical for the Y2H interaction with USPL1 (SUMO/ubiquitin-specific peptidase-like 1), a factor which can bind and cleave SUMO species (SUMO1 and SUMO2/3) in human cells, but for its essential function the catalytic activity is dispensable (Schulz et al., 2012). The molecular function of USPL1 is yet unknown, but it is likely that it rather recognizes the compact ubiquitin-like fold of Hub1 than single specific residues in the heterologous system. Considering the aromatic patch formed by W47 and Y48, the HIND surface D22, and the exposed residue R9, Hub1 utilizes at least three different crucial surfaces located on opposing sides of the protein. This allows Hub1 to act as a multifaceted binding module with fundamentally different interaction properties, reflecting an intriguing feature of the small ubiquitin-like protein. Further investigation will be necessary to fully characterize potential interaction interfaces and their respective binding domains.

5.3 Hub1 and hSnu66 reside in nuclear splicing speckles

In order to allow metabolic and catabolic processes, expression and replication of genetic information, and complex biochemical reactions, eukaryotic cells are compartmentalized into specialized organelles and membrane-bound compartments. In particular, the nucleus is highly organized into chromosome territories, several nuclear bodies and subnuclear domains, which coordinate gene expression, RNA processing and export, signaling cascades and various cellular functions (Lanctôt et al., 2007). In addition to the genetic information densely packed as chromatin, the nuclear space is subdivided into so-called nuclear bodies like the nucleolus, promyelocytic leukemia nuclear bodies (PML bodies), Cajal bodies (or coiled bodies, nuclear splicing speckles (or interchromatin granule clusters or SC35 domains) and several other poorly characterized domains like perinucleolar caps, paraspeckles and clastosomes (Lamond and Earnshaw, 1998). Nuclear bodies can vary in shape and number depending on cell type, cell cycle stage and stimuli, as they fulfill diverse functions in the cell. For example, beside rDNA transcription, rRNA processing as

well as pre-assembly of ribosomal subunits the nucleolus plays an important role in cell cycle regulation by the sequestration of crucial key players like the Cdc14 phosphatase (Visintin and Amon, 2000). PML bodies respond to various stimuli including oxidative stress, viral infection and DNA damage and are implicated in transcriptional regulation and cell cycle control (Ruggero et al., 2000). Protein complexes containing small nuclear RNAs (snRNA) or small nucleolar RNAs (snoRNAs), are modified and assembled into snRNPs and snoRNPs, respectively, in Cajal bodies. After their maturation, snRNPs cycle from Cajal bodies to nuclear splicing speckles, where they are engaged in splicing-competent complexes and return after participating in splicing catalysis for reassembly into functional complexes (Fischer et al., 1997; Cioce and Lamond, 2005). Nuclear splicing speckles are believed to be important for pre-mRNA splicing factor maturation and modification, as well as for complex formation and storage (Lamond and Spector, 2003). They are highly dynamic structures from which snRNPs and splicing factors like SR proteins shuttle to active sites of splicing (Wei et al., 1999; Misteli et al., 1997). In the current model this shuttling of splicing proteins is orchestrated by kinases and phosphatases that regulate the phosphorylation status of their substrates. In particular, members of the SR protein family and their regulatory counterparts, hnRNPs, change their nuclear distribution and activity upon phosphorylation by Cdc2/Cdc28-like protein kinases CLK1-4, SR protein kinases SRPK1/SRPK2 and AKT kinase, respectively (Colwill et al., 1996; Stojdl and Bell, 1999; Blaustein et al., 2005). Splicing factors like ASF/SF2 (SRSF1) and SC35 (SRSF2) are established constituents of nuclear speckles, but also inactive RNA Pol II, poly-adenylated mRNA and long non-coding RNAs like MALAT1 have been identified in these structures (Tripathi et al., 2012; 2010; Caceres et al., 1998; Xie et al., 2006).

The physical interaction of Hub1 with spliceosomal components like hSnu66 and SR protein kinase Clk3 strongly indicated a conserved role of Hub1 in pre-mRNA splicing. Considering this link of Hub1 to pre-mRNA processing localization studies were performed to underscore its functional relationship to splicing-associated nuclear domains like Cajal bodies or nuclear speckles. Indeed, immunofluorescence staining elucidated a distinct speckle-like distribution of Hub1 within the nucleus (Figure 6). Here, it co-localizes with splicing factors SC35, U1A and Y12, which serve as well-established marker proteins for nuclear splicing speckles affirming Hub1's functional and spatial association with the splicing machinery. Furthermore, Hub1 has been recently described to associate with coilin in Cajal bodies, where spliceosomal subcomplexes assemble and mature into functional tri-snRNPs (Švéda et al., 2013). Importantly, Hub1's interaction partner hSnu66 is found in nuclear speckles as well, co-localizing with SC35 and other tri-snRNP factors like PRPF4, which supports the physical interaction data and indicates the functional link to pre-mRNA splicing (Figure 6b).

In co-expression experiments, hSnu66 actively recruited Hub1 to nuclear splicing speckles in an HIND dependent manner, which led to an accumulation of hSnu66 and Hub1 in these subnuclear domains (Figure 8a). While interfering with the Hub1-hSnu66 interaction by using Hub1 D22A or hSnu66 Δ HIND mutants had no negative impact on the nuclear distribution of the tri-snRNP protein, the accumulation of Hub1 in splicing speckles was diminished. Beside the Hub1 interaction domain, mapping studies with hSnu66 revealed additional domains involved in tri-snRNP binding, nuclear localization and nuclear speckle targeting (Figure 10). The central domain comprises the interaction interface for the association with PRPF6 and nuclear localization signals (Figure 10b-d). Notably, the N-terminus of hSnu66 containing the RS-domain and the HIND harbors an additional targeting signal and is proficient for nuclear speckle localization. This fragment efficiently binds Hub1 *in vivo* (Figure 11c) and is sufficient to recruit Hub1 to splicing speckles in a RS-domain-dependent manner (Figure 11a). RS-domains are widely common features of splicing-associated factors often combined with RNA recognition motifs to mediate protein–RNA and protein–protein interactions (Shen et al., 2004; Manley and Tacke, 1996; Graveley, 2004; Hertel and Graveley, 2005). Furthermore, nuclear import and targeting to nuclear splicing speckles can be enforced by RS-domains as they are recognized by specific nuclear import factors, so called SR transportins, in a phosphorylation-dependent manner (Allemand et al., 2001; Kataoka et al., 1999). Further experiments dissected the effect of Hub1 binding and the contribution of the RS-domain to the localization of the N-terminal fragment of hSnu66. While full-length hSnu66 and the isolated N-terminus are efficiently recruited to splicing speckles together with Hub1 (Figure 11b), the RS-domain is sufficient for targeting to nuclear speckles, as shown in experiments with the Hub1 binding-deficient mutant (N-terminal RA). Interestingly, the crucial role of Hub1 in nuclear retention of the hSnu66 fragment became evident, when the nuclear/cytoplasmic shuttling was enforced by the attachment of a nuclear export signal from the export receptor CRM1 (Figure 11b). Hub1 binding allows hSnu66's N-terminus to be incorporated into nuclear speckles and spliceosomal subcomplexes, while the NES-HIND RA mutant fragment lacking this Hub1-dependent integration is efficiently exported and depleted from the nuclear compartment. In summary, the data revealed an interesting interplay between Hub1 and hSnu66; hSnu66 actively recruits Hub1 to nuclear speckles, as it is efficiently imported into the nucleus via its RS-domain and NLS. As the central region in hSnu66 mediates the association with tri-snRNP factors, while the RS-domain likely serves as an additional interaction platform, the Hub1 interaction domain directly binds and directs Hub1 to splicing complexes piggy-back.

Interestingly, the interaction with hSnu66 contributes to Hub1 targeting to nuclear speckles, but is not essential as the binding mutant Hub1 D22A still localizes to splicing speckles and overlaps with SC35 pattern exhibiting no significant

difference to Hub1 WT (Figure 7a). Although both Hub1 WT and Hub1 D22A show a similar nuclear localization in fixed, pre-extracted immunofluorescence staining, the kinetics of targeting and shuttling between these structures might be significantly different for the two proteins. In order to address this point FRAP (fluorescence recovery after photobleaching) experiments would be an excellent method to gain further insights into Hub1 dynamics (Ishikawa-Ankerhold et al., 2012). Here, the GFP moiety of the respective Hub1 fusion protein is bleached *in vivo* by laser pulses around distinct nuclear speckle areas and the time for fluorescence recovery correlates with the mobility and dynamics of the Hub1 protein. In a similar approach, shuttling of WT hSnu66 and the Hub1 binding-deficient mutant hSnu66 Δ HIND between active sites and nuclear speckles could be compared to further examine the contribution of the Hub1–HIND interaction *in vivo*.

Another important issue deals with the interplay between Hub1 and its binding partner hSnu66. As ubiquitin-like proteins are known to modulate the activity, localization or physical interactions of their substrates, co-purification studies with hSnu66 WT and hSnu66 Δ HIND were conducted to determine Hub1-dependent changes in protein complex composition upon Hub1 binding (Figure 9). As a constituent of the tri-snRNP complex the association of hSnu66 with central components of the U4/U6 (PRPF3, PRPF4) and the U5 (PRPF8, PRPF6) was monitored. Hub1 binding is not essential for the incorporation of hSnu66 into the tri-snRNP, as no significant changes in co-purification experiments were observed for Hub1-deficient mutants (hSnu66 Δ HIND or hSnu66 R127A). In addition to the directed tri-snRNP complex analysis, mass spectrometry was used as a proteomic approach to identify alterations in co-purifying protein complexes with WT and Hub1-binding deficient hSnu66 (Figure 9). A broad spectrum of splicing factors as well as proteins involved in mRNA processing and export were detected specifically in samples with immunoprecipitated hSnu66 and hSnu66 Δ HIND. In addition to the already characterized hSnu66-associated tri-snRNP factors PRPF6 and PRPF8, spliceosomal proteins like CDC5L and PRP19 of the NTC (PRP19 complex), DEAD box helicases (DDX) and SR proteins like ASF/SF2, SFRS3 and SRSF5 as well as their respective kinases SRPK1 and GSK3 were significantly enriched in co-immunoprecipitation experiments. Moreover, as a substantial fraction of hSnu66 localizes to both nuclear speckles and the nucleolus (Figure 6b), nucleolar proteins including NPM3, UBF1 and NOP52 were identified in hSnu66 purifications. This dual localization has been reported for other splicing factors as well, *e.g.* the DEAH box ATPase Prp43 (Leeds et al., 2005; Van Koningsbruggen et al., 2004) and could reflect additional functions of RNA binding factors like hSnu66 in rRNA metabolism, as suggested previously (Li et al., 2009). Furthermore, it was shown that snRNPs and Sm proteins pass the nucleolus and Cajal bodies before reaching their destination, the nuclear speckles (Sleeman et al., 2001; Sleeman and Lamond,

1999). Thus, the dual localization might represent to snapshots during hSnu66 nuclear speckle targeting and incorporation into functional snRNP complexes.

The qualitative comparison of co-immunoprecipitation experiments with WT and Hub1 binding-deficient hSnu66 by mass spectrometry revealed only mild differences in the abundance of multiple co-purified and interacting proteins. This finding is in line with recent data in which the interactomes of yeast ScSnu66 in WT and *HUB1*-deletion strains (*hub1Δ*) were analyzed and compared by quantitative mass spectrometry (Mishra et al., 2011). Here, the composition of ScSnu66 interactors was largely unaltered, but components of the U2 snRNP and the SF3 complex were overrepresented in the absence of Hub1. As human hSnu66 provides multiple interaction interfaces (RS-domain, HIND and central PRPF6 association domain) it is possible that loss of Hub1 binding can be compensated via alternative modes of recruitment and binding modules (Figure 8,10,11). However, for quantitative analysis a more sophisticated approach like SILAC (stable isotope labeling by amino acids in cell culture) would be necessary, which would give a detailed and robust readout with high resolution and sensitivity compared to conventional mass spectrometry.

Although the data presented here allows a detailed characterization and molecular insights into a unique non-covalent mode of interaction between an ubiquitin-like protein and an important tri-snRNP splicing factor, the spatial and temporal framework for Hub1-HIND complex formation requires further investigation. Additional layers of regulation like posttranslational modification might influence the interaction network of Hub1 and hSnu66, as phosphorylation is the main regulatory element within the splicing machinery. While SR-kinases control the recruitment of RNA binding factors to pre-mRNA, phosphorylation is also essential for splicing catalysis itself, as PRP28 needs to be modified in order to allow the incorporation of the tri-snRNP and the formation of the pre-catalytic spliceosome (C complex) (Mathew et al., 2008). Recently, additional posttranslational modifications like acetylation and notably, ubiquitylation have come into focus (Kuhn et al., 2009; Bellare et al., 2006). The spliceosome core component PRPF8 was shown to be modified by ubiquitin, which is important for the regulation of the helicase activity of Brr2 unwinding the U4/U6 snRNAs *in vitro* (Bellare et al., 2008). Interestingly, when hSnu66 was tested for posttranslational modifications by denaturing immunoprecipitations and mass spectrometry, over 16 phosphorylation sites on serine and threonine residues in hSnu66 were identified (data not shown). Two of them are in close proximity of the Hub1 interaction domain at position S111 and S117 (HIND: AA 116-135). Furthermore, directed assays elucidated that hSnu66 is also multiply modified by the ubiquitin-like protein SUMO. This data was supported by large scale quantitative mass spectrometry analyses in which K94, K141, K709 were identified as SUMOylated lysines in hSnu66 (Vertegaal et al., 2006). Thus, the short

stretch in hSnu66 (AA 111-141) might constitute a regulatory hotspot that is modified by SUMO, phosphorylated and embeds the HIND for Hub1 binding. To address this point amino acid substitutions that mimic or abrogate posttranslational modifications of the targeted residues can be introduced in hSnu66 and the effect on Hub1-binding kinetics and affinities can be measured.

Considering phosphorylation and SUMOylation as quick and reversible posttranslational modifications involved in multifaceted regulatory cellular processes, covalent attachment of SUMO and phosphate moieties to crucial residues in flanking sequences of the HIND might modulate Hub1 binding to hSnu66. These data suggest a model, in which posttranslational modifications serve as a cellular control mechanism to prevent undesired Hub1-binding to hSnu66 in order to spatially or temporally restrict this interaction to a particular process. A plausible explanation would be that this regulation is necessary to ensure correct tri-snRNP formation and licensing as hSnu66 is recruited late during assembly. To avoid premature association of Hub1, hSnu66 is kept in a *HIND inactive state* by phosphorylation or SUMOylation and Hub1-binding is blocked until the U4/U6.U5 tri-snRNP is properly assembled. Only when hSnu66 is incorporated into a functional tri-snRNP complex, the HIND becomes accessible and Hub1 binding is permitted to facilitate progression in the splicing cycle.

In line with the immunofluorescence data showing that Hub1 and hSnu66 co-localize in nuclear speckles in the context of pre-mRNA splicing complexes, several proteomic studies dissecting the composition of spliceosomal subcomplexes at different steps during the splicing cycle independently identified hSnu66 and Hub1. While Hub1 was found in human B and B^{act} complexes, hSnu66 was detected in the isolated tri-snRNP as well as in B, B^{act} and C spliceosomal complexes (Herold et al., 2009; Bessonov et al., 2010; 2008; Deckert et al., 2006; Agafonov et al., 2011; Jurica et al., 2002).

Taking advantage of the different variants of Hub1 and hSnu66 characterized in this work, further experiments with *in vitro* splicing assays and interaction studies might elucidate the functional role of Hub1 and hSnu66 in splicing. For example, as the splicing reaction can be reconstituted *in vitro* the different functional spliceosomal complexes can be arrested at particular steps of the transesterification reaction. It would be interesting to isolate Hub1 or hSnu66 from spliceosomes at various stages, deplete these factors from splicing extracts and to perform complementation assays with the recombinant proteins and their mutant variants. Due to the multifaceted nature of protein-protein, RNA-protein and RNA-RNA interactions within splicing complexes, crosslinking and co-immunoprecipitation experiments with splicing extracts would be feasible approaches to further characterize the molecular function of Hub1.

While hSnu66 is efficiently imported into the nucleus and exclusively recruited to nuclear subdomains, additional functions of Hub1 outside the nuclear envelope can not be excluded as live cell imaging and cellular sub-fractionation experiments detected notable cytoplasmic pools of Hub1 (Figure 7b, 11b). In contrast to the hSnu66 binding-deficient mutant Hub1 D22A the C-terminally tagged variant of Hub1 (Hub1-GFP or Hub1^{FLAG}) was not retained in nuclear substructures after pre-extraction (Figure 7a), even though it was properly folded and functional in hSnu66 interaction (see Figure 5b). Thus, the C-terminal surface, which is compromised of bulky or charged extensions, appears to be a crucial interface on Hub1 important for proper recruitment and incorporation into splicing-associated protein complexes within nuclear speckles.

5.4 Conserved and evolved protein features of Hub1

Although Hub1 is highly conserved from yeast to human, little was known about its molecular function. Initial work in lower eukaryotes *S. cerevisiae* and *S. pombe* addressed the ubiquitin-like nature of Hub1 and its impact on cell growth. Interestingly, while *S. cerevisiae* cells with a deletion of *HUB1* (*hub1Δ*) are viable and exhibit no discernable growth defects (Mishra et al., 2011; Luders et al., 2003), *hub1Δ* in *S. pombe* is lethal (Yashiroda and Tanaka, 2004; Wilkinson et al., 2004). However, in *S. cerevisiae* *hub1Δ* shows negative genetic interactions with mutant alleles of several splicing factors like *prp17Δ*, *snu17Δ* and *prp8**, which expresses a partially defective variant of the core-spliceosomal protein Prp8 (Mishra et al., 2011). This provides further evidence for Hub1 functioning in pre-mRNA splicing. With these two strain backgrounds, *S. cerevisiae* and *S. pombe hub1Δ*, different variants of Hub1 were tested for functionality in complementation cell growth assays. Importantly, although each Hub1 variant could complement the growth defects in the respective yeast strain under normal conditions, rescue assays revealed significant differences between yeast and human Hub1 at restrictive temperatures (Figure 12). When *hub1Δ S. pombe* cells were supplemented with constructs expressing *HUB1* orthologs from *S. cerevisiae*, *S. pombe* and *H. sapiens*, only the human and fission yeast *HUB1* fully complemented the lethality at higher temperature, while *S. cerevisiae* Hub1 exhibited clear growth defects. *Vice versa*, the human Hub1-encoding gene could not fully rescue the synthetic lethality of the double mutant *hub1Δ prp8** in *S. cerevisiae*, while *SchUB1* and *SpHUB1* facilitated growth at restrictive temperatures.

Based on recent data elucidating an important role of Hub1 in splice-site usage and alternative splicing in yeast (Mishra et al., 2011), an alternative complementation readout highlights the functional differences between the different *HUB1* orthologs. Alternative splicing of the *SRC1* gene product in *S. cerevisiae* depends on Hub1 for proper splicing of the overlapping non-canonical 5' splice sites

giving rise to two mRNA isoforms, SRC1-L (long isoform) and SRC1-S (short isoform). While both yeast variants of Hub1 were able to rescue the splicing defect in *hub1Δ* strains, human Hub1 failed to fully restore alternative splicing of *SRC1*.

These distinct activities of Hub1 in complementation assays might be explained by the fundamental differences of pre-mRNA splicing in various species. Only three percent of the genes in the *S. cerevisiae* genome carry introns with only six ORFs containing two introns (Barrass and Beggs, 2003). In contrast, splicing of pre-mRNA with multiple introns is much more prevalent in fission yeast with 43 % of its genes comprising intronic sequences (Wood et al., 2002). These differences in splicing prevalence and regulation in splice site recognition and selection (as discussed in 5.1) might reflect the impact of *HUB1*-deletions in the respective yeast species and correlate with the implication of Hub1 in pre-mRNA splicing.

In *S. cerevisiae* Hub1 enables the spliceosome to process transcripts with non-canonical splice sites to ensure proper and faithful splicing even at suboptimal sequences like the overlapping splice sites in *SRC1*. As the number of critical Hub1-dependent splice sites is limited, deletion of the ubiquitin-like protein (*hub1Δ*) does not challenge cells under normal growth conditions, because difficult splice sites in non-essential transcripts might still be processed by the spliceosome even in the absence of Hub1, albeit with very low efficiency. If the spliceosome is compromised in activity (for example by mutations in core-splicing factors like Prp8) non-canonical splice sites constitute serious obstacles for the dynamic splicing machinery. Here, Hub1 might mediate conformational rearrangements, which allow higher flexibility of the spliceosome to tolerate and to process critical splice sites in order to ensure efficient and faithful pre-mRNA splicing. The accurate transition between the different spliceosomal complexes is under tight control of DExH/D-box helicase like hPrp28 and hBrr2. Moreover, as non-canonical splice sites are recognized poorly and challenge spliceosomal assembly, Hub1 might serve in spliceosomal quality control to facilitate the correct incorporation and activation of spliceosomal subcomplexes by DExH/D-box helicases.

Due to the low complexity of pre-mRNA splicing in *S. cerevisiae*, this model for the molecular function of Hub1 in the spliceosome might reflect the original activity of the ubiquitin-like protein in the spliceosome very early in evolution. In higher eukaryotes, where alternative splicing is utilized to expand the cellular repertoire of gene products, several additional surveillance mechanisms were established to facilitate correct pre-mRNA processing and high fidelity by the spliceosome. In order to cope with a higher complexity on sequence level and splice variants due to variations at splice sites, auxiliary RNA binding factors (SR proteins and hnRNPs) are recruited to cis-regulatory elements on pre-mRNAs to mediate loading of the splicing machinery at the correct splice site for efficient exon recognition and proper splicing. Although initial steps like splice site recognition and recruitment of the

prespliceosomal complex A with U1 and U2 snRNPs are more sophisticated in higher eukaryotes, the spliceosomal core machinery catalyzing the transesterification splicing reaction is largely identical from yeast to man. Thus, the function of Hub1 might have become particularly important at the interface between the “evolved” splice site recognition with prespliceosomal complex assembly and processing of suboptimal splice sites by the conserved core spliceosome. Despite the high conservation, in higher eukaryotes Hub1 might have gained an additional or more prevalent function in pre-mRNA splicing, which is conveyed by a distinct, intrinsic feature of the ubiquitin-like protein, but is absent in *S. cerevisiae*.

5.5 Different surfaces on Hub1 facilitate distinct interactions

Even though Hub1 is structurally very similar to ubiquitin, the mode of interaction is very different. Encompassing solely the ubiquitin-fold and lacking any N- or C-terminal extensions, Hub1 is only able to function through non-covalent interactions with other proteins.

Based on the structural data and hSnu66 interaction studies, the question of which surface on Hub1 is crucial for its essential activity, was addressed. For this approach, various Hub1 point mutations, changing conspicuous residues in different patches on the Hub1 protein were generated and tested in RNAi complementation and immunoprecipitation assays.

Firstly, the siRNA-resistant cDNA expressing a Hub1 variant deficient in Snu66 interaction (D22A) rescued viability only partially, indicating that specific binding of Hub1 to the spliceosomal protein hSnu66 contributes, but is not essential in human cells under standard growth conditions. These data were further supported by analogous complementation experiments in *S. pombe*, where Hub1 D22A restored viability in *hub1* Δ strains (Mishra et al., 2011). Notably, further analysis of mutations interfering with hSnu66 binding (Hub1 D22A) or Clk3 kinase interaction (Hub1 R9A) individually or in combination (Hub1 RDAA) did not further attenuate the rescue capacity. Thus, the interplay of Hub1 with tri-snRNP protein hSnu66 or SR-kinase Clk3 might contribute to the Hub1 mediated activity in pre-mRNA processing, but additional factors utilize alternative surfaces on Hub1 to execute its essential function.

Intriguingly, RNAi complementation experiments revealed the importance of Hub1’s C-terminus as variants carrying C-terminal extensions, like charged or bulky epitope tags, were not able to rescue the lethal depletion phenotype. These extensions did not negatively affect Hub1 hSnu66 interaction, protein stability or folding, but rather interfered with physical interactions, which might be mediated via this surface. Notably, introducing mutations into very C-terminal residues of Hub1 or truncating the terminal amino acids (Δ YYQ/YYL), did not significantly alter the activity of Hub1 (Luders et al., 2003; Mishra et al., 2011). In addition to the characterization

in RNAi complementation experiments, the relevance of this C-terminal interface became more evident in localization studies in human cells (Figure 21). While Hub1 WT and the Snu66 binding deficient mutant Hub1 D22A resided in nuclear speckles, the C-terminally tagged Hub1-GFP failed to be incorporated into respective nuclear substructures and was washed out of the nucleus. Due to the compact ubiquitin-fold of Hub1 with the typical protruding C-terminus of UBLs missing, this site might have gained particular importance for Hub1 as a non-conventional ubiquitin-like protein.

Analogous to the complementation experiments performed in yeast, RNAi rescue assays reintroducing different Hub1 orthologs into human tissue culture cells were conducted (Figure 16b). Here, human and fission yeast Hub1 were able to restore viability after Hub1 knockdown, while *S. cerevisiae* Hub1 failed to complement the lethal RNAi phenotype despite equal protein expression levels. This supports the model that Hub1 from mammals and *S. pombe* owns crucial protein properties that are missing in the ScHub1 variant.

This finding drew the attention to particular surfaces, which are conserved from fission yeast to mammalian Hub1, but differ from *S. cerevisiae* Hub1. The most significant structural difference was identified in the loop on $\alpha 2$ - $\beta 3$ in human Hub1, with exposed hydrophobic residues W47, Y48 and F51, which are conserved in all metazoan orthologs.

Due to the unusually exposed orientation of the tryptophan and tyrosine, these residues might create an additional binding site opposing the HIND surface. Initial experiments showed that single mutations in Hub1 (WYFGGL) did not significantly affect the rescue capacity, but in combination with mutations in the Clk3 of hSnu66 binding sites (Hub1 R9AWYGG and RDAAWYFGGL), these Hub1 variants were less potent in restoring viability after RNAi, despite similar expression levels.

Most hydrophobic amino acids are buried within the protein tertiary structure during protein folding for stabilization, while hydrophilic residues are oriented to the solvent (Dyson et al., 2006). Alternatively, exposed hydrophobic amino acids like tryptophan and tyrosine were reported to be crucial for the formation of various interaction interfaces for multimerization or ligand binding (Moreira et al., 2007). For example, RNA binding proteins harboring RNA recognition motifs (RRM) utilize tryptophan, phenylalanine and tyrosine residues in their four β -sheets to recruit and coordinate binding to RNA species (Cléry et al., 2008).

Hub1 exhibits remarkable features, as it utilizes several residues and surfaces for various interactions. Beside the Hub1-HIND surface mediated via D22 and the Clk3 interaction via R9, the C-terminal surface and the hydrophobic patch with W47, Y48 and F51 resemble binding sites, which might act synergistically to accomplish Hub1's essential function in human cells.

5.6 *In vivo* depletion of Hub1 causes cell cycle defects and apoptotic cell death

Human cells arrest in distinct cell cycle phases upon checkpoint activation as a cellular response to stress or toxic insults *e.g.* accumulation of aberrant synthesis products or DNA damage. After the transfection with Hub1 RNAi all tissue culture cell lines tested (U2OS, HCT116, HeLa) exhibited strong cell cycle progression delays, accompanied by defects in mitotic cell division, including aberrant metaphase plate formation and chromosome missegregation. Further cell cycle synchronization and release assays elucidated that Hub1 RNAi cells, but not cells treated with a control siRNA, exhibited G2/M cell cycle progression defects after S-phase release. Flow cytometry analysis revealed that Hub1 siRNA treatment initially (after 48 hours) caused defects in G2/M cell cycle progression, and later (72 hours) culminated in a rise of sub G1 fractions, indicative of cells undergoing apoptosis (Figure 14-16).

Cell lines with compromised checkpoints, for example HeLa, with inactive p53 pathway (Hoppe-Seyler and Butz, 1993) are prone to overcome G2/M arrests, a process called *mitotic slippage*, frequently observed in DNA replication checkpoint mutants (Di Leonardo et al., 1997; Riffell et al., 2009). Due to the checkpoint override, cells face unfaithful chromosome segregation and undergo aberrant mitosis, resulting in abnormally fragmented nuclei and subsequent induction of apoptosis reflecting hallmarks of mitotic catastrophe (Castedo et al., 2004), as observed in Hub1 RNAi treated cells. As the accumulation of aberrantly spliced transcripts causes multifaceted cellular stresses and misregulation of various cellular pathways (Venables, 2004), Hub1 appears to be a pivotal factor to facilitate efficient and faithful splicing which is crucial for maintaining cellular homeostasis.

In line with the obtained Hub1 RNAi data, recent high throughput siRNA screenings (Neumann et al., 2006) underscored the importance of core splicing components like tri-snRNP proteins PRPF8, hBrr2, PRPF6 and associated non-snRNP proteins like components of the PRP19 complex (NTC) for proper cell cycle progression and faithful mitosis. Interestingly, only one fifth of the 150 core spliceosomal factors analyzed exhibited mitotic defects in this RNAi based approach (Neumann et al., 2010; Hofmann et al., 2010), while Hub1 appears to be an additional potent candidate for this list.

Similar to Hub1, inactivation of important splicing factors like SR proteins SC35 and ASF/SF2 causes genome instability and cell cycle defects, which entail proto-oncogenic potential in vertebrate cells (Karni et al., 2007; Li and Manley, 2005; Xiao et al., 2007). Furthermore, it was shown that efficient splicing of pre-mRNA and its incorporation into mRNP complexes is important to maintain genome stability (Li and Manley, 2006). In eukaryotes, co-transcriptional processing couples mRNA synthesis directly to splicing and mRNA export. If mRNA processing is impaired during transcription by chemical inhibition (Gan et al., 2011), depletion of crucial

splicing factors by RNAi (Li et al., 2007; Li and Manley, 2005; Stirling et al., 2012) or mutant alleles of genes involved in mRNA export (THO/THREX (Huertas and Aguilera, 2003)), the nascent transcript stalls and accumulates at DNA. Similarly stalled RNA polymerase that faces obstacles blocking transcription elongation like DNA damage, replication forks or hypernegative supercoiled DNA can lead to free nascent pre-mRNA. As a result, the naked RNA strand emerging from RNA polymerase, which is not incorporated into functional mRNP, can form undesired RNA:DNA hybrid structures, so called R-loops (Aguilera and García-Muse, 2012). If the hybridizes stretches are not resolved by RNase H-like enzymes, these structures can cause substantial DNA damage and give rise to mutations, recombination or chromosomal rearrangements.

In addition to the cell cycle arrests and mitotic defects, *in vivo* depletion of Hub1 triggers the DNA damage response pathway and the activation of several key effector proteins (Figure 17). Hub1 knockdown leads to stabilization and activation of p53, transcriptional up-regulation of p21 and phosphorylation of histone 2A at S139 (γ H2AX). Interestingly, cells treated with Hub1 siRNA exhibit reduced proteins levels of the nucleotide excision repair factor xeroderma pigmentosum group C (XPC), whose activity is regulated via ubiquitylation and degradation upon UV-irradiation to facilitate efficient DNA repair in concert with hRad23B (Wang, 2005; Sugasawa et al., 2005). However, at the moment it is unclear what the cause and type of DNA damage is that accumulates in Hub1-depleted cells and how Hub1 might affect DNA damage signaling and stability of crucial factors. Whether Hub1 functions like RNA processing factors that play crucial roles during DNA damage repair directly, *e.g.* hnRNP-like proteins (hnRNPUL1/2) which contribute to DNA-end resection (Polo et al., 2012; Beli et al., 2012; Pont et al., 2012) will require further research. Altogether, this data clearly indicates that the ubiquitin-like protein Hub1 is a crucial factor to ensure genome integrity.

5.7 Hub1 RNAi leads to aberrant splicing and mRNA retention

Active splicing is a highly dynamic process in which spliceosomal subcomplexes are constantly recruited to regulatory sequences within the nascent pre-mRNA emerging from the RNA polymerase to perform the splice cycle (chapter 2.5). Furthermore, co-transcriptional recruitment of the splicing machinery and active splicing are required for efficient mRNA export (Riedl and Shi, 2004; Reed and Hurt, 2002). The phospho-protein SC35 is a well-established nuclear speckle marker that illustrates the shuttling of splicing factors between splicing foci and sites of active transcription. SC35 was shown to associate with pre-mRNA sequences as well as to directly contact RNA Pol II's CTD (Riffell et al., 2009; Lin et al., 2008; Di Leonardo et al., 1997).

To address the effect of Hub1 knockdown on pre-mRNA splicing, central splicing and RNA processing factors were investigated in a time window, in which

Hub1 protein levels were already significantly reduced, but cells did not show any signs of severe stress nor degeneration like nuclear disintegration. Whereas control cells showed normal distinct SC35 domains with many small foci distributed within the interchromatin space, Hub1 knockdown cells exhibited an aberrant SC35 pattern with high enrichment in enlarged nuclear speckles, while small foci diminished. These changes in nuclear distribution were not restricted to SC35, as this effect of Hub1 depletion was also observed for various other splicing-associated factors like U1A, hnRNP1 or trimethylguanosine-capped snRNPs (Figure 20).

Direct evidence of Hub1 RNAi-dependent defects in pre-mRNA processing was obtained when endogenous poly-adenylated mRNA was visualized by FISH. In line with aberrant splicing factor distribution, depletion of Hub1 caused nuclear retention of polyadenylated mRNA in enlarged speckles, while the cytoplasmic fraction was significantly reduced, indicating impaired processing and nuclear shuttling as described previously (Kaida et al., 2007; Dias et al., 2010). The observed RNA accumulation was weaker compared to cells in which crucial mRNA export factors had been depleted (Yamazaki et al., 2010), indicating that Hub1 activity is crucial for early mRNA processing steps rather than facilitating mRNA export further downstream.

However, the characterized Hub1 knockdown phenotypes were highly similar to those observed in cells in which splicing was repressed by the splicing inhibitor Spliceostatin A, repressing oligonucleotides, or RNAi (Kaida et al., 2007; O'Keefe et al., 1994; Tanackovic and Krämer, 2005). These data further underscore that Hub1 is a crucial factor for pre-mRNA splicing and processing *in vivo*.

5.8 Human Hub1 is crucial for specific splicing events

The strong phenotypes associated with Hub1 depletion in human cells suggest that human Hub1 plays a much more fundamental cellular role than its *S. cerevisiae* counterpart. Reasonable models are that Hub1 is crucial in human cells either for general splicing, or for splicing of a number of certain, particularly sensitive pre-mRNAs or introns.

To address splicing competence of Hub1-depleted human cells, firstly splicing of artificial splicing reporters was analyzed. Minigenes are frequently used tools to characterize and manipulate various aspects of pre-mRNA splicing *e.g.* strength of particular splice sites, branch point or pyrimidine tract sequences (Gaildrat et al., 2010; Cooper, 2005; Stoss et al., 1999; Singh and Cooper, 2006). Furthermore, transcript specific *cis*- and *trans*- active regulatory elements like splice site enhancer or silencer sequences and their respective RNA binding proteins can be examined in detail (Wang and Burge, 2008; Lopez, 1998). Notably, specifically in Hub1 siRNA treated cells, splicing of the GFP minigene pre-mRNA was defective and unspliced transcripts accumulated, proving that Hub1 indeed is crucial for pre-mRNA splicing in

human cells (Figure 22). However, in this setup variations at the 5' splice sites did not significantly affect Hub1-dependent splicing defects even when highly divergent sequences were introduced into the respective gene products. This might be explained by the fact that the artificial pGint / pRint minigene transcripts are constitutively highly expressed and comprised of a single, relatively short intron lacking *cis*-regulatory elements. Thus, to address the physiological role of Hub1 in pre-mRNA splicing, endogenous transcripts and alternative splicing model substrates were examined.

Several layers of regulation have been identified to affect splicing efficiency and alternative splicing in human cells. Chromatin structure, histone modification and promoter strength modulate recruitment of splicing factors and RNA pol II associated factors which can then lead to significant changes in splice site recognition and usage (Luco et al., 2010; Cramer et al., 1999; Luco et al., 2011). By transplanting genomic fragments containing alternatively spliced exons into mammalian expression plasmids, some of these regulatory effects can be omitted to address Hub1's splicing specificity. For this, gene products were examined that are known to be regulated by alternative splicing at different developmental stages, tissue-specific programs or upon exogenous stimuli. Fibronectin 1 (*FN1*, (Muro et al., 1998)), tropomyosin 1 α (*TPM*, (Graham et al., 1992)) or myeloid cell leukemia sequence 1 (*MCL1*, (Bae et al., 2000)) served as model transcripts in U2OS cells after RNAi treatment (Figure 23c). The RT-PCR analyses elucidated that Hub1 is crucial for correct splice site usage and faithful pre-mRNA splicing of distinct splice sites as Hub1 depletion resulted in different forms of alternative and constitutive splicing defects in various transcripts. In case of *FN1*, Hub1 knockdown caused exon (ED-A) skipping, whereas intron retention coupled to moderately lower steady-state mRNA levels was observed for *TPM* and *Mcl-1*. Furthermore, these data demonstrate that individual sequences like ED-A, *TPM* intron 4-5 and *Mcl-1* intron 1-2 are particularly sensitive to Hub1 depletion, while other flanking sequences within the same transcript show no alterations, indicating that Hub1 is not a general splicing factor, but promotes specific splice events.

The model that Hub1 enables the spliceosome to process certain unprivileged transcripts to ensure efficient and faithful splicing was further strengthened, when endogenous Hub1-dependent transcripts were identified. Splicing of various endogenous pre-mRNAs (*Mcl-1*, *Akt*, *Casp2*, *AurkA* etc.) was affected in Hub1-depleted cells, as shown in a candidate-based RT-PCR screen. Apparently, Hub1 activity owns sequence specificity, as splicing defects were restricted to distinct splice sites in certain transcripts, while other gene-products tested simultaneously were processed normally, arguing that Hub1 is not essential for splicing *per se*, but needed for efficient splicing events via specific splice sites.

In addition to direct candidate approaches comprehensive exon-specific RNA microarray profiling was performed to detect global changes in alternative splicing in human cells upon Hub1 depletion (Figure 25). The unbiased microarray analysis elucidated broad alterations in mRNA exon patterns for multiple transcripts with a majority (ca. 68%) exhibiting exon exclusion specifically in Hub1 knockdown cells. Furthermore, the splicing array data clearly demonstrates, with single exon resolution, that Hub1 depletion affects alternative splicing of individual exons, while flanking sequences within the same transcript show no alterations. This might be explained by splice site usage defects in cells with spliceosomes lacking Hub1. Here, the Hub1-deprived splicing machinery fails to efficiently recognize and define the exon boundaries, which hinders spliceosomal assembly. As co-transcriptional splicing is a highly dynamic process, neighboring flanking exons with strong splice sites and/or splicing enhancer sequences could be favored over Hub1 sensitive exons, which are subsequently excluded from the transcript. Splice site usage and thus alternative splicing is determined by the interplay of multiple factors including SR, hnRNP and other spliceosomal proteins as well as RNA pol II activity and histone modifications (Mabon and Misteli, 2005; la Mata et al., 2003). However, this data demonstrates that Hub1 is an additional determining factor for alternative pre-mRNA splicing in human cells.

Although these data further extend the view on transcripts, which are spliced in a Hub1-dependent manner, the growing list of Hub1 substrates is most likely not complete due to several technical challenges. Although the Affymetrix human exon array comprises specific probes for validated cDNA-based sequences as well as predicted and previously unknown splice variants, alternative splicing events like intron-retention and proximal cryptic splice site recognition cannot be resolved by this technique. To address this question, comparative RNA sequencing would be a powerful method and might give in depth insights into Hub1-dependent splicing reactions. Additionally, in Hub1 knockdown cells a certain fraction of aberrantly and alternatively spliced transcripts are subjected to rapid mRNA decay, as Hub1-dependent splicing defects most likely interfere with mRNA maturation and give rise to pre-mature stop codons, the *bona fide* nonsense-mediated decay (NMD) substrates (Kervestin and Jacobson, 2012). This is supported by the observed substantial down regulation of mRNAs upon Hub1 knockdown on transcription level detected in microarray expression data sets.

Interestingly, a considerable number of Hub1-dependent splice substrates were previously characterized as transcripts containing weak splice sites (Akt, FANCG, Rad23) (Ahn et al., 2011). While strong splice sites are efficiently recognized and spliced by the spliceosome, proper splicing of pre-mRNAs with weak splice sites challenge the spliceosomal assembly and require auxiliary factors like the RS-domain protein Son. Son was reported to facilitate recruitment and stable

association of U1-70K, U2AF65 and SC35 at weak splice sites and is thereby crucial for accurate and efficient splicing of certain pre-mRNAs (Ahn et al., 2011; Sharma et al., 2011). To further dissect if Hub1 affects splicing of weak splice sites similar to Son or the spliceosomal core with hSnu66, Hub1 RNAi induced aberrant splicing was compared to splicing defects in cells in which the tri-snRNP protein hSnu66 or the SR protein Son were knocked down. Whereas Hub1 and Son are important factors for efficient Akt pre-mRNA splicing, Hub1 and hSnu66 (but apparently not Son) facilitated splicing of Mcl-1 and Aurka. These data suggest that Hub1 might act at the crossroads between the early steps during spliceosome assembly and spliceosomal core, as Hub1 knockdown phenotypes combine characteristics of both crucial branches for splicing activity. In line with the hSnu66-independent activities of Hub1 identified in knockdown complementation assays, RNAi rescue experiments showed that the hSnu66 binding-deficient Hub1 D22A variant was able to complemented the splicing defects, while the C-terminally extended version of Hub1 failed to support splicing. This finding reinforces the model in which direct binding of Hub1 to hSnu66 via the HIND element is not essential for Hub1-dependent splicing, even though, the additional surface opposing the Hub-HIND interface on Hub1 mediates its crucial activity in human cells.

Since the splice sites of the investigated introns that are sensitive to Hub1 show no obvious sequence similarity, Hub1 may act as a splicing qualifying factor for splicing events that are unprivileged for different reasons. Further studies will be necessary to characterize, which crucial sequence features mediate Hub1-dependent splicing *e.g.* pre-mRNA folding constrains (secondary structures), *cis*-acting splicing enhancers or silencers, or presence of RNA binding proteins (Matlin et al., 2005; Wang and Burge, 2008; Hiller et al., 2007). However, in striking contrast to canonical regulators of alternative splicing that directly target pre-mRNAs by binding to regulatory sites using their sequence-specific RNA recognition motifs, Hub1 appears to stimulate unprivileged splicing events through modifying the splicing machinery rather than targeting specific RNA substrates.

5.9 Hub1 knockdown desensitizes cells to actinomycin D

Aberrant mRNA splicing is a common characteristic of many cancers (Fackenthal and Godley, 2008; Venables, 2004), as it causes cellular stresses and mis-regulation of various cellular pathways underlining that efficient and faithful splicing is crucial for cellular homeostasis. In eukaryotic cells, Hub1 plays a central role to ensure efficient and faithful splicing of suboptimal splice substrates, as its inactivation leads to extensive splicing defects entailing abnormal mitosis and, finally, apoptosis. Several RNAis and chemical compounds were tested to identify growth conditions under which the Hub1-dependent cellular activity becomes particularly important or to find drugs that modulate cellular pathways to suppress the Hub1 depletion phenotypes.

To this end, transcription inhibitors like actinomycin D (ActD), α amanitin and 5,6-dichloro-1-beta-D-ribofuranosylbenzimidazole (DRB), were included in this study, which affect RNA polymerase activity and reduce mRNA synthesis by different modes of action (Bensaude, 2011).

Intriguingly, actinomycin D was able to partially rescue the Hub1 RNAi phenotype (Figure 26). At early time points after siRNA transfection, ActD treatment affected control RNAi cells only marginally, while the observed G2/M arrest in Hub1 knockdown cells was already significantly decreased after incubation with ActD. At later stages of knockdown, when control cells were treated with increasing drug concentrations, the fraction of apoptotic cells increased accordingly due to the cytotoxic effect of transcription inhibition by ActD. Notably, although Hub1 knockdown is fatal for human cells, after incubation with actinomycin D HeLa cells did not show a synergistic effect at increasing drug concentrations, but rather exhibited an improved cell cycle distribution ratio for G1 and G2/M populations, while the apoptotic fraction decreased.

As alternative transcription inhibitors like α amanitin or DRB, did not show similar antagonistic effects with Hub1 knockdown, this effect was specific for Hub1-depletion combined with ActD. This might be explained by the different modes of action of these drugs on RNA Pol II during RNA synthesis.

Actinomycin D belongs to the family of natural polypeptide antibiotics produced by *Actinobacteria* of the genus *Streptomyces*. It binds ssDNA with high affinity and intercalates preferentially into GC rich regions (Hollstein, 1974; Sobell, 1985). Thereby, ActD specifically inhibits transcription elongation by RNA pol II (but also RNA Pol I and III) and most significantly affects synthesis of long mRNAs and rRNAs (Perry and Kelley, 1970). At high cellular concentrations actinomycin D can interfere with DNA synthesis and cause DNA double strand breaks (Mischo et al., 2005).

In contrast, the cyclic peptide mushroom toxin, α -Amanitin, specifically binds to the catalytic center of RNA pol II where it blocks the incorporation of NTPs and RNA synthesis as an irreversible inhibitor (Bushnell et al., 2002; Lindell et al., 1970). The nucleoside analog DRB interferes with RNA pol II elongation by inhibiting its transcription promoting kinase complexes CDK9 / cyclin T of pTEFb and CDK7 of TFIIH (Yankulov et al., 1995; Zandomeni et al., 1982; Marshall et al., 1996). The CDK9/7 activities are crucial to overcome repression of transcription by negative transcription elongation factors (N-TEFs) in order to allow the transition to productive mRNA synthesis (Price, 2000).

While transcriptional inhibition by ActD in combination with Hub1 knockdown mitigated Hub1 depletion-dependent apoptosis and, in turn, drug-dependent toxicity, neither α -Amanitin nor DRB treatment exhibited similar properties, but rather aggravated the Hub1 phenotype. Considering the crucial role of Hub1 in pre-mRNA

splicing, reducing the transcription rate and thereby splicing dynamics by actinomycin D could be beneficial for human cells when the splicing machinery lacks Hub1 as in RNAi experiments. In addition to the inhibition of transcription, actinomycin D affects pre-mRNA processing and increases mRNA stability (Clement et al., 1999). Furthermore, actinomycin D treatment has been shown to alter alternative splicing patterns for example of Mdm2 (Lents et al., 2008).

While under standard growth conditions with high transcription rates and spliceosomal dynamics Hub1 depletion results in extensive splicing defects, nuclear RNA retention and aberrant gene-products, additive actinomycin D treatment might positively affect RNA metabolism. As long transcripts are particularly sensitive to ActD and might contain multiple Hub1-dependent splice events, slowed down transcription elongation rates might allow the spliceosome to process and splice nascent pre-mRNA correctly even under Hub1-deprived conditions upon actinomycin D treatment. Although additional functions of Hub1 that affect transcription directly cannot be ruled out at the moment, this phenomenon might be valuable to gain further insights into the close link between chromatin, transcription and mRNA splicing and their regulatory feedback loops.

5.10 The Hub1-dependent splicing model

The efficient and correct splicing of nascent transcripts is an essential regulatory element of posttranscriptional eukaryotic gene expression. This intricate process is accomplished by the coordinated assembly and orchestrated transition of multifarious RNA-protein complexes, which constitute the catalytically active spliceosome. Based on the characterization of human Hub1 presented in this thesis and considering respective work in yeast, a comprehensive model for the molecular function of the ubiquitin-like protein Hub1 in pre-mRNA splicing is proposed (Figure 27).

The splicing pathway includes several control mechanisms to verify spliceosomal complex formation at distinct transition steps to either promote correctly assembled spliceosomes or reject aberrantly composed complexes from further progression (Koodathingal and Staley, 2013). In order to guarantee the low error rate in pre-mRNA splicing (Fox-Walsh and Hertel, 2009), a group of DEXD/ H-box ATPases including Prp5, Prp16, Prp22, and Prp43 serve as proofreading enzymes, which discard splicing intermediates after spliceosomal stalling as a result of aberrant spliceosome assembly and suboptimal splice substrates, respectively (Egecioglu and Chanfreau, 2011). At early stages the correct engagement of the U2 snRNP at the branch point sequence is inspected by Prp5 (Xu and Query, 2007). In later steps, after the formation of the catalytically active B* complex, suboptimal splice substrates are detected and rejected by the DEXD/H-box ATPase Prp16 before 5'ss cleavage (Mayas et al., 2006). The second transesterification step is monitored by Prp22, which certifies the proper complex formation at the 3'ss for correct exon ligation

(Koodathingal et al., 2010). While proofreading enzymes promote the splice cycle progression of accurate splicing intermediates, defective spliceosomes and suboptimal splice substrates are finally discarded and disassembled by DEAH-box proteins like Prp43 (Mayas et al., 2010).

Importantly, the fundamental concept of spliceosomal quality control is based on the highly dynamic nature of global RNA/protein network rearrangement during spliceosomal complex assembly and is manifested in the “kinetic proofreading model” (Hopfield, 1974). In this model, two antagonistic activities or pathways compete for directionality, in which the equilibrium shifts depending on biochemical reaction kinetics (Semlow and Staley, 2012). In the case of pre-mRNA splicing and its quality control mechanisms, these antagonistic activities are reflected by the anterograde reactions during splice cycle progression with complex assembly, snRNA unwinding, and snRNP rearrangements, while retrograde directionality is represented by the disassembly kinetics of DEXD/H-box ATPases, which enforce the rejection of spliceosomal transitions and complex conversions.

Ideally, optimal splice substrates are continuously processed, as the accurate spliceosomal assembly and immediate complex conversions support highly dynamic splicing kinetics promoting productive splice cycle progression. In contrast to the ideal splicing cycle, spliceosomes are challenged at suboptimal splice substrates, e.g. by poor recognition of weak splice sites, pre-mRNA folding constrains, or presence of faulty RNA binding proteins, which compromise splicing dynamics. Here, due to impaired transition between different spliceosomal conformations and slow conversion reaction kinetics the equilibrium shifts towards the retrograde rejection pathway, which entails the disengagement and discarding of the splice substrate mediated via the proofreading DEXD/H-box ATPase enzymes.

In this context, the ubiquitin-like protein Hub1 might constitute an additional layer of quality control at an early stage of the splicing pathway. For this, Hub1 appears to associate with the spliceosome in order to facilitate the correct assembly and proper engagement of spliceosomal subcomplexes on suboptimal splice substrates. Extending the kinetic proofreading model presented earlier, Hub1 could mediate two non-mutually exclusive activities.

On the one hand, Hub1 might induce conformational changes and thereby convey spliceosomal flexibility and robustness to tolerate minor deficiencies in suboptimal substrates. In this case, inhibition of Hub1 activity by *in vivo* depletion or mutation would not affect constitutive splicing of ideal splice substrates, but defective splicing factors or aberrant RNA would cause spontaneous stalling of active spliceosomes. As Hub1 binding might induce global conformational changes in spliceosomal proteins, as shown for Snu66, it is likely that Hub1-deprived spliceosomes are structurally restricted.

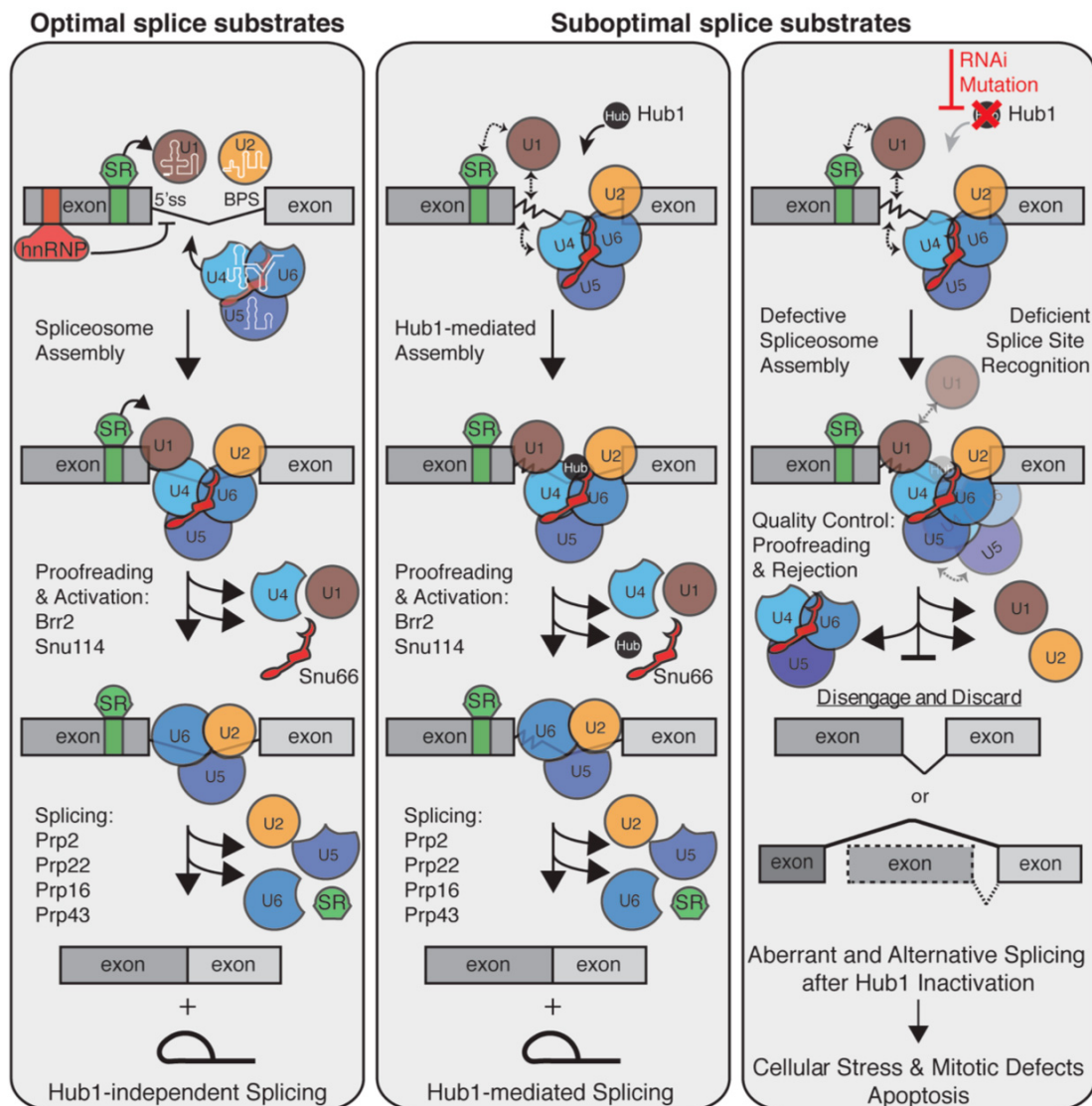


Figure 27: Proposed model for Hub1's crucial role in pre-mRNA splicing

Optimal splice substrates (left panel) are efficiently recognized by the spliceosomal snRNPs (colored circles), as crucial RNA sequences within the intron-containing transcript (grey boxes) mediate the accurate assembly by snRNA/mRNA base pairing. The initial step of exon definition and splice site recognition is regulated by auxiliary SR proteins (green) and repressive hnRNP factors (red). After U4/U6.U5 tri-snRNP incorporation the spliceosome formation and activation is scrutinized by proofreading enzymes. After satisfying the quality control, RNA helicases and ATPases promote the spliceosome activation and splicing reaction with subsequent dissociation of the spliced mRNA and late snRNP complexes. In contrast, suboptimal splice substrates (serrated lines) interfere with proper spliceosomal complex formation and efficient recognition by the snRNPs (dotted line), thus requiring the qualifying factor Hub1 (middle panel). Hub1 facilitates the correct assembly and enables compromised spliceosomes to process suboptimal splice substrates by conveying structural flexibility (e.g. by binding to tri-snRNP protein Snu66 (red)) and modulating the enzymatic activities of promoting enzymes, respectively. Thus, the ubiquitin-like protein Hub1 is a crucial factor for faithful pre-mRNA splicing of distinct splice sites. Accordingly, inactivation of Hub1 (by RNAi or mutant alleles of Hub1) leads to stalling of spliceosomal complexes on suboptimal splice substrates as the Hub1-assisted assembly is abrogated (right panel). Hub1-deficient spliceosomes fail to properly engage in the correct conformation in order to initiate global RNA/protein rearrangements for the splice cycle progression and transition to spliceosomal activation. Defective and stalled splicing intermediates are detected by proofreading DExD/H-box ATPases and subjected to spliceosomal disengagement and release of the misspliced mRNA. Hence, Hub1 inactivation causes continuous splicing defects and the accumulation of aberrantly spliced transcripts leading to cellular stress, cell cycle defects and subsequent apoptosis.

This rigidity would impinge on the splicing processivity of suboptimal substrates and thereby entail the rejection of splicing intermediates by the proofreading surveillance enzymes.

On the other hand, Hub1 could act directly on the quality control factors for pre-mRNA splicing by modulating the activity and stringency of the proofreading enzymes in order to adjust the accuracy and tolerance by which spliceosomal intermediates are scrutinized. Here, Hub1 inactivation and subsequent alterations in proofreading factors would result in the premature disengagement of suboptimal complexes or random stalling of defective spliceosomes.

Several lines of evidence support a crucial role of Hub1 at the crossroads between the early steps of spliceosome assembly and the formation of the activated complex B^{act}. After the early spliceosomal subunits U1 and U2 snRNP have defined the exon-intron boundaries, the U4/U6.U5 tri-snRNP and the PRP19/NTC are recruited to form the pre-catalytic spliceosomal complex B. For further activation the RNA/protein networks has to undergo major rearrangements including snRNA unwinding and re-establishing of new base pairing. In the proposed model Hub1 facilitates the correct spliceosomal assembly and engagement of snRNAs on suboptimal splice substrates during this complex conversion. This is accomplished by the interaction of Hub1 with the tri-snRNP factor hSnu66, which presumably initiates conformational changes and structural rearrangements. In addition to the Hub1-Snu66 interaction via the HIND, the opposing surface on Hub1 is recognized by a pivotal, yet unidentified, component of the spliceosome to further promote processing of suboptimal splice substrates. Here, the association with Hub1 could stimulate the enzymatic activity of an ATP-driven helicase to catalyze splice cycle progression.

Intriguingly, the ubiquitin-like fold might serve as a general binding module in the spliceosomal protein network. Recent structural bioinformatics analyses have identified several ubiquitin-like domains in different spliceosomal proteins including SF3A120, SAP18 and XAP-5, which function at late stages of the splicing cycle, where proofreading surveillance is most prevalent (Korneta et al., 2012). This indicates that the transient association with ubiquitin-like domain proteins represents a fundamental principle during spliceosomal complex formation and conversion. Here, the ubiquitin-like protein Hub1 appears to play a unique role as it facilitates the correct assembly and engagement of spliceosomal subcomplexes and ensures proper proofreading at early stages of the splicing process.

Taken together, the splicing data, the tight association with central splicing components, and the detrimental phenotypes of Hub1 depletion in eukaryotic cells suggest a conserved, pivotal function of Hub1 in the context of pre-mRNA splicing quality control to ensure high fidelity and faithful splice cycle progression on suboptimal splice substrates.

6 Material and Methods

Basic molecular biological and biochemical methods were performed according to standard techniques (Maniatis et al., 1989; Ausubel et al., 1988) or based on the manufacturers' instructions. Newly established and modified techniques are described below in more detail. Unless otherwise mentioned, chemicals and reagents were purchased from Amersham-Pharmacia, Applied Biosystems, Biomol, Biorad, Fluka, Invitrogen, Jackson and Jackson, Kodak, Merck, New England Biolabs, Promega, Roth, Roche, Serva or Sigma Aldrich.

6.1 Cell biology

6.1.1 Human cell lines and transfections

The established human cell lines HeLa, U2OS and HEK293T were cultured at 37°C, 6% CO₂ in Dulbecco's Modified Eagle Medium (DMEM) high glucose with GlutaMAX (Invitrogen), supplemented with 10% fetal calf serum (Biochrom). HEK 293T and HeLa cells were transfected using the calcium phosphate precipitation technique with HBS buffer and BES buffer, respectively, as described previously (Bartke et al., 2004). Lipofectamine 2000 (Invitrogen) or Fugene HD (Roche) was used to transfect U2OS and HeLa cells. For RNAi experiments, cells were transfected with siRNA duplexes by RNAiMax (Invitrogen) or via electroporation with the Amaxa Nucleofector II system (Lonza) according to the manufacturer's protocol. U2OS cells stably expressing GFP-Hub1 WT, GFP-Hub1 D22A, hSnu66 WT-GFP, hSnu66 Δ HIND-GFP and free GFP were generated by selecting cells under 750 -1000 μ g/ml G418 (Sigma Aldrich) after lipofection for 3-4 weeks. Single G418-resistant colonies were isolated using cloning discs and expanded for later analysis. To further enrich and purify GFP-positive cells fluorescence-activated cell sorting was performed using the FACSaria cell sorter system (Becton Dickinson).

In experiments with RNA Polymerase inhibition, cells were treated with actinomycin D (5 μ M), α -Amanitin (25 μ g/ml) or 5,6-dichloro-1-beta-D-ribofuranosyl-benzimidazole (DRB, 25 μ g/ml) (all Sigma-Aldrich) for indicated time intervals.

6.1.2 Mammalian expression plasmids and siRNA

Standard cloning techniques were used to generate mammalian expression constructs with vectors of the pCMV-Tag2/3/4 (Stratagene), pcDNA3.1 and pUB6 (both Invitrogen) series as well as pCI/pCI-Neo (Promega), pEGFP and pDsRed (Clontech) and p3xFlag-CMV-10 (Sigma-Aldrich) vectors. Plasmids with point mutations were constructed by site-directed mutagenesis using target specific primers in PCR reactions. Genomic fragments of fibronectin 1 (*FN1*), tropomyosin 1

a (*TPM*), myeloid cell leukemia sequence 1 (*MCL1*), v-akt murine thymoma viral oncogene homolog 1 (*AKT*) and aurora kinase A (*AURKA*) for minigene constructs were amplified from genomic human DNA (U2OS) by PCR and subcloned into modified pUB6/V5 vectors (Invitrogen). For RNAi siRNA sequences were designed as 19- or 21-mer duplexes with 3' TT-overhangs according to stringent criteria previously described (Jagla et al., 2005) and purchased from MWG. siRNA duplexes targeting Hub1 in human cells were iHub1_1 GGA AGA AGG UCC GCG UUAA, iHub1_2 CAA GAU UGU CCU GAA GAA G, iHub1_3 AUA GAU GAG AAU CCU CAUC, iHub1_4 UGC AAC ACG GAU GAU ACCA, iHub1_5 GGG AAG AAG GUC CGC GUUA. For knockdown of hSnu66 siRNA sihSnu66_1 CUA ACA AAC UCC GGG CAAA or sihSnu66_3 GUA UGA CGA AGA GCU UGA ATT, for ASF/SF2 siSRSF1_5 GGA CUG CCU CCA AGU GGA ATT or siSRSF1_6 GGC AGG AUU UAA AGG AUC ATT for URH49 AAA GGC CUA GCC AUC ACU UUU and for UAP56 AAG GGC UUG GCU AUC ACA UUU (both described in Kapadia et al., 2006) were used. The GL2 siRNA targeting luciferase (Elbashir et al., 2001) CGU ACG CGG AAU ACU UCGA was used as knockdown control. RNAi of Son was performed with Silencer pre-designed siRNA (ID# 143161) from Applied Biosystems / Ambion.

6.1.3 Flow cytometry

DNA histograms were obtained by flow cytometry of propidium iodide (PI)-stained ethanol-fixed cells using standard protocols. Briefly, cells were harvested by trypsinization and washed with ice-cold PBS. For fixation, cells were resuspended in 300 μ l PBS and 700 μ l cold EtOH (-20°C) and incubated on ice. Afterwards fixed cells were washed twice with PBS and subsequently stained in PI-buffer (PBS, 100 μ g/ml propidium iodide (Sigma Aldrich), 200 μ g/ml RNase A (Roche)) for one hour. Data was acquired on a FACSCalibur system with CELLQuest software (Becton Dickinson) and further analyzed with FlowJo software (Tree Star). HeLa cells were synchronized following standard double-thymidine block protocols using 2 mM thymidine.

6.1.4 Immunofluorescence, FISH and live cell microscopy

For standard immunofluorescence microscopy, cells were seeded and transfected on glass coverslips (Roth). Cells were washed twice with PBS and fixed in 3.7% fresh paraformaldehyde (PFA) / PBS for 18 min at room temperature. After fixation, residual formaldehyde was inactivated by quenching with PBS-glycine (30 mM) and cells were washed three times in PBS. Permeabilisation of cells was performed using PBS-Triton X-100 0.4% (6 min), followed by three PBS-Tween (Tween 0.05%; PBS-T) washing steps and blocking in PBS-T with 2% BSA for 1 h at room temperature.

Coverslips were incubated with primary antibody for 3 h (appropriate dilutions in blocking buffer) and then washed three times in PBS-T. After incubation with secondary antibody, cover slips were mounted using DAPI-containing mounting medium (Vectashield, Vector Labs). For pre-extraction experiments cells were permeabilized in CSK buffer (100 mM NaCl, 300 mM sucrose, 10 mM PIPES pH 6.8) supplemented with 0.4% Triton X-100 and complete protease inhibitors (Roche) for 8 min at 4°C. After two gentle wash-out steps with detergent free CSK buffer, cells were fixed with 3.7% formaldehyde. The subsequent antibody staining was performed according to the abovementioned standard protocol.

The RNA FISH method to visualize poly-adenylated mRNA using fluorescently labeled poly-(dT)₇₀-TRITC probes was adapted from previous protocols (Tokunaga and Tani, 2008). HeLa or U2OS cells grown on glass slides were fixed in 3.7% fresh paraformaldehyde / PBS for 15 min at room temperature. After PFA quenching and permeabilisation with 0.5% PBS-Triton X-100 (5 min at 4°C) cells were washed with 2xSSC (300 mM NaCl, 30 mM Na₃Citrate·2H₂O pH 7.0). Poly-adenylated mRNA was stained with the hybridization solution (2xSSC, 20 % formamide, 1 mg/ml tRNA, 10 % dextran sulfate and 2 µg TRITC labeled poly-(dT)₇₀ probe) in a sealed humid chamber at 37°C overnight. After three 2xSSC washing steps with DAPI as nuclear counterstain slides were mounted and sealed for microscopy analysis.

Images were acquired on a Zeiss AxioImager Z1 microscope equipped with an AxioCam MRm Rev.3 camera. Image acquisition was carried out using AxioVision Rel. 4.7 software (Zeiss).

For fluorescence time-lapse microscopy, HeLa H2B-GFP cells were seeded into 4 well µ-dishes (ibidi) after RNAi transfection and transferred into the live cell imaging system, BioStation IM (Nikon). Images were acquired every 8 min over a time frame of 24–48 h with BioStation IM software and further processed by ImageJ and Photoshop (Adobe).

6.1.5 Cell lysis and immunoprecipitation

For immunoprecipitation, cells were harvested, washed in ice-cold PBS and cell pellets were lysed in 5x pellet volumes of immunoprecipitation buffer (50 mM HEPES pH 7.2, 150 mM NaCl, 2 mM EDTA, 0.5% Triton X-100, 1 mM PMSF, and complete protease inhibitors (Roche)) at 4°C for 30 min with several passages through a 25 gauge needle attached to a syringe. After removal of cell debris by centrifugation (10 min, 16000xg, 4°C), cleared lysates were incubated with anti-FLAG M2 affinity gel (Sigma-Aldrich), anti-c-Myc-agarose (Sigma-Aldrich) or GFP trap (Chromotek) for 2 h at 4°C. The affinity matrix was washed four times with immunoprecipitation buffer and eluted in Laemmli SDS buffer for later analysis by SDS-PAGE and immunoblotting.

For caspase activation assay, cytosolic extracts were prepared as described previously (Deveraux et al., 1999). In immunoprecipitation experiments with hSnu66 WT or Δ HIND co-purifying protein interactors were identified by mass spectrometry using LTQ-Orbitrap mass spectrometers as a service of the MPI core facility.

6.1.6 Antibodies

Antibodies used in this study were anti- α -tubulin (DM1A, Sigma Aldrich), anti-caspase-7 (C7, Cell Signaling), anti-caspase-3 (8G10, Cell Signaling), anti-GFP (clone B-2, Santa Cruz and ab1218, Abcam), hnRNP I (Z-22, Santa Cruz), anti-lamin A/C (clone 636, Santa Cruz), anti-c-Myc (clone 9E10, Sigma Aldrich), anti-p21 (clone 187, Santa Cruz), anti-p53 (clone DO-1, Santa Cruz), anti-PRPF8 (ab87433, Abcam), anti-TAP/PAP (Sigma Aldrich), anti-hSnu66 (A301-423A, Bethyl), anti-SC35 (ab11826, Abcam), anti-Son (HPA023535, Sigma Aldrich), anti-2,2,7-trimethylguanosine (K121, Calbiochem), anti-U1A (ab55751, Abcam), anti-U2AF65 (ab37483, Abcam), anti-Sm antigen Y12 (ab3138, Abcam).

For immunofluorescence, Alexa Fluor 488- and Alexa Fluor 555-labeled secondary goat anti-mouse and donkey anti-rabbit / anti-mouse antibodies from Invitrogen were applied. Hub1-specific antibodies against recombinant *S. cerevisiae* Hub1 and human Hub1, respectively, were affinity-purified from serum of immunized rabbits (see chapter 6.2.12). For standard applications antibodies were diluted 1:1000 to 1:5000 for immunoblot analysis and 1:200 to 1:2000 for immunofluorescence detection.

6.1.7 Exon-specific alternative splicing microarray

For genome-wide analysis of altered splicing patterns in Hub1-depleted U2OS cells, total RNA was isolated from Hub1 or control RNAi treated cells (see section 6.2.4) 50-60 h after transfection. Experiments were performed in biological triplicates with each sample tested for cell viability and fitness to avoid indirect effects by cell degeneration or apoptosis as observed at late stages of Hub1 knockdown. Further processing of the RNA samples including quality control of total RNA, reduction of ribosomal RNA, cDNA synthesis and purification, fragmentation and labeling were conducted by Atlas Biolabs GmbH (Berlin). Finally, the labeled cDNA probes were hybridized against an Affymetrix GeneChip Human Exon 1.0 ST, which utilizes 1.4 million probe sets to target over 1 million exon for genome-wide exon-level expression profiling. The microarray is designed to provide a comprehensive coverage of the transcriptome comprising of validated, annotated sequences from various transcript and EST databases as well as predicted mRNA sequences based on bioinformatics analyses of genome projects allowing the identification of previously unidentified splice variants. The exon-specific microarray combines mRNA

expression profiling with quantitative exon-specific probes and allows quantification of alternatively spliced transcripts and the identification of newly generated isoforms as multiple probes per exon are targeted to sequences along the entire length of the respective transcript (≥ 4 probes per probe selection region *e.g.* individual exons). The following computational analysis includes data normalization, quality control measures and algorithms for alternative splicing detection. Here, the entropy-based ARH prediction method was applied to identify probe sets which exhibit significant alterations in individual exonic sequences (relative exon expression) without changes in overall transcript expression levels (Rasche and Herwig, 2010). After this process, high confidence hits are translated into the splicing index (SI), statistically tested and ranked. The final data set gives strong indications which transcripts undergo alternative splicing and changes in splicing patterns upon a certain stimulus or treatment, here, after Hub1 depletion.

6.1.8 Yeast strains and plasmids

Complementation assays with *S. cerevisiae* and *S. pombe* strains, western blot analysis and *SRC1* alternative splicing assays used in this study were described in detail previously (Mishra et al., 2011). p415 *ADH* plasmid harboring coding sequences of *S. cerevisiae*, *S. pombe* and human *HUB1* were used for complementation of *S. cerevisiae hub1* Δ mutants. pREP81 plasmid harboring coding sequences for *HUB1* orthologs were used for complementation of the *S. pombe* mutant. Complementation experiments with *S. pombe* and *S. cerevisiae hub1* Δ cells were performed in collaboration with S.K. Mishra.

For yeast two-hybrid screening of whole cDNA libraries, potential binding factors were expressed as Gal4 activation domain fusion proteins (AD-fusion), whereas the bait protein carries the Gal4 DNA binding domain. In case of physical interaction between the two fusion proteins reporter gene expression (*HIS3* and *ADE2*) was induced which allows growth on selective media of the otherwise auxotrophic cells (SC-Ura-Trp-His: 3.5 % bacto-yeast nitrogen base, 2 % glucose, 0.2 % amino acid mix). Here, Hub1 served as the BD-fusion bait protein for screening of human cDNA libraries from different tissues with high transcript coverage (average insert size ≥ 2.1 kb). Based on data showing that Hub1 is ubiquitously expressed in human cells, but particularly up-regulated in brain tissue (Friedmann et al., 2001), libraries of fetal brain tissue and HeLa cells cDNAs were selected (Invitrogen). After the optimization of transformation efficiency the two-hybrid yeast strain PJ69-7A harboring the Hub1-pGBDU construct was used to screen the human cDNA libraries. Intriguingly, human BD-Hub1 exhibited auto-activation activity of the *HIS3* reporter gene, thus the addition of 3-amino-1,2,4-triazole (3-AT) to the growth media (2 - 5 mM) was required to ensure restrictive screening conditions. After the candidates were tested for auto-activation after FOA-shuffle, the -Ura-Trp-His positive clones

were subjected to further interaction validation using standard assays like X-Gal overlay or growth on -Ade plates.

6.2 Molecular biology

6.2.1 Preparation and transformation of chemically competent *E. coli*

E. coli strains used for cloning or protein expression:

XL1-Blue MR	$\Delta(mcrA)183$ $\Delta(mcrCB-hsdSMR-mrr)173$ <i>endA1</i> <i>supE44 thi-1 recA1 gyrA96 relA1 lac</i>
BL21 Codon Plus (DE3)-RIL	B ⁻ F ⁻ <i>ompT</i> <i>hsdS</i> (r _B - m _B -) <i>dcm</i> ⁺ Tet ^r gal λ (DE3) <i>endA Hte</i> [<i>argU ileY leuW Cam</i> ^r]
BL21 Rosetta 2 Φ DE3	F ⁻ <i>ompT</i> <i>hsdS</i> _B (r _B ⁻ m _B ⁻) <i>gal dcm</i> pRARE2 Cam ^R

When culturing *E. coli* strains under standard conditions, e.g. for plasmid DNA preparation, LB media (1 % bacto-tryptone, 0.5 % yeast extract, 1 % NaCl) or LB 1.5 % agarose plates were used. Plasmid-containing bacteria were selected by their antibiotic resistance under 50 μ g/ml Ampicillin or 30 μ g/ml Kanamycin at 37 °C. The absorption of liquid cultures was measured with a standard spectrophotometer at a wavelength of 600 nm to determine optical density (OD_{600nm}).

To obtain highly competent *E. coli* cells were prepared according to the Inoue protocol (Inoue et al., 1990). Briefly, the pre-culture grown 4-5 h at 37 °C in SOB (2 % bacto-tryptone, 0.5 % yeast extract, 10 mM NaCl, 2.5 mM KCl, pH 7.0 NaOH) served as inoculant for the main culture (\geq 500 ml) which was incubated at lower temperature (18 °C) overnight. Next day, when the cell suspension had reached OD_{600nm} 0.5 - 0.6, the main cultures were cooled down in flasks for 10 min in an ice bath. After centrifugation, cells were resuspended and washed in pre-chilled Inoue transformation buffer (55 mM MnCl₂, 250 mM KCl, 15 mM CaCl₂, 10 mM PIPES pH 6.7). Cells were collected by centrifugation and resuspended again in Inoue buffer. DMSO was added slowly to the cell suspension to a final concentration of 7.5 % and further incubated in an ice bath for 10 min. Finally, competent cells were aliquoted, snap frozen in liquid nitrogen and stored in PCR tubes at -80 °C until use.

For transformation, competent cells were thawed on ice and incubated with 1-4 μ l of plasmid DNA suspension in TE. After 10 - 30 min *E. coli* cells were heat-shocked for 1 min at 42 °C in a water bath and immediately chilled on ice for recovery. Next, growth media was added to the suspension for further cell proliferation and incubated at 37 °C on a shaking device. Finally, cells were streaked on LB plates containing the appropriate selection antibiotics and grown overnight at 37 °C. To enforce high transformation efficiency, 0.2 % β -mercaptoethanol was added to *E. coli* cells prior the addition of DNA.

6.2.2 Isolation of plasmid DNA

Small-scale (mini) preparations of plasmid DNA were performed using kits from Qiagen or Bioneer according to the manufacturers' protocols. For mammalian cell culture large quantities of highly pure DNA were necessary in order to prevent cytotoxic effects during transfection caused by residual endotoxins. For this, Qiagen or Sigma-Aldrich maxi kits with optimized protocol were used for plasmid DNA purification after alkaline lysis from *E. coli* overnight cultures (250 - 400 ml). The isolated DNA was further concentrated by an isopropanol precipitation step mixing eluate TE buffer with isopropanol and 3 M Na-Acetate pH 5.2 in a ratio of 10:7:1. After centrifugation at 5000xg for 30-60 min at 4°C the resulting DNA pellet was washed with 70 % EtOH and finally resuspended in TE buffer. DNA concentration and purity was measured using the Nanodrop (Thermo Scientific).

6.2.3 Polymerase chain reaction and site directed mutagenesis

Polymerase chain reaction was conducted according to the manufacturer's protocols. For DNA amplification, DNA polymerases Phusion (NEB) and Pfu Turbo (Aligent) were used with dNTPs solution mix (NEB) and the respective buffers. Point mutants were introduced by site-directed mutagenesis using primers carrying the modified sequence flanked by 10-15 nt overhangs for correct targeting to the designated DNA site. PCR products were subsequently digested with DpnI restriction enzyme (NEB) for 1-2 h, heat inactivated and transformed into *E. coli*.

6.2.4 DNA restriction, ligation and cloning

In order to introduce specific PCR fragments into expression vectors, 1-5 µg of DNA were incubated with 5-10 U of appropriate DNA restriction enzymes (NEB) in the corresponding buffer systems following standard cloning techniques. While plasmids and plasmid-derived inserts were digested by endonucleases for 1 - 2 h, PCR products were digested overnight. Cut vectors were subjected to calf intestinal phosphatase (CIP, NEB) treatment for 1 h to avoid re-ligation of linear DNA. After restriction, digested DNA fragments were analyzed by agarose gel electrophoresis and subsequently re-isolated using gel extraction kits (see chapter 6.2.6). Finally, DNA fragments (in 3-5 fold excess) were ligated into vectors via complementary cohesive ends using standard T4 ligase or the derived Quick T4 ligase (both NEB) in their respective buffers. The Quick T4 ligation reaction was performed for 5-30 min at RT while standard T4 reactions were incubated at 16°C overnight until transformation into chemically competent bacteria.

6.2.5 RNA-purification, RT-PCR and splicing gels

Total RNA was isolated from control or Hub1 RNAi-transfected cells using the RNeasy kit (Qiagen) or the High Pure RNA Isolation kit (Roche) according to the manufacturer protocols. Reverse transcription was performed using the Transcriptor First Strand cDNA Synthesis Kit (Roche) with random hexamer or poly-(dT) primers. Transcript specific PCR was performed using PfuTurbo polymerase (Aligent) and subsequently analyzed on 2-2.5% ethidium bromide containing TBE agarose gels.

6.2.6 Gel electrophoresis of DNA and purification from agarose gels

For the separation of PCR fragments, cloning intermediates or RT-PCR products, DNA samples were loaded with orange G sample dye (5 % glycerol, 0.05 % SDS, 5 mM EDTA pH 8.0) on 1-2 % TBE (90 mM Tris-borate, 2 mM EDTA pH 8.0) agarose gels containing 0.005% ethidium bromide. Depending on DNA fragment size and agarose concentration gel electrophoresis was performed in Tris-borate buffered chambers for 30-90 min at 10-15 V/cm and analyzed in GenoSmart UV transillumination documentation system. For subsequent cloning steps, PCR or restriction DNA fragments were isolated following gel electrophoresis. The corresponding bands were excised from the gel on an UV transilluminator screen, DNA was solubilized and subsequently purified using standard DNA gel extraction kits (Bioneer, Macherey&Nagel).

6.2.7 DNA sequencing

DNA sequencing of cloning constructs and PCR products was performed by the core facility service of the MPIBC using the Sanger dideoxy terminator cycle sequencing chemistry with the ABI BigDye kit on an ABI 3730 48-capillary sequencer and 36 cm capillaries.

6.2.8 Plasmids for recombinant protein expression in *E. coli*

For recombinant protein expression in *E. coli* following plasmids were used: pET (pET24b(+)) and pET28a/b/c(+) (Novagen) for 6xHis-tagged proteins and GST-tagged proteins were expressed using the pGEX vector series (pGEX4T1/2/3 and pGEX5X1) (Amersham).

6.2.9 Purification of recombinant proteins from *E. coli*

E. coli BL21(DE3)/RIL and BL21 Rosetta cell pre-cultures were inoculated in 50 ml antibiotic-containing LB or TB (Terrific Broth, 1.2 % bacto-tryptone, 2.4 % yeast extract, 0.4 % glycerol NaCl, 10 % TB salt (170 mM KH₂PO₄, 720 mM K₂HPO₄ in

H₂O) media and cultured at 25°C overnight. For recombinant protein expression these cultures served as inoculants for larger volumina starting OD_{600 nm} at 0.2. Then *E. coli* were shifted to 37°C until OD_{600 nm} of 0.4-0.7 was reached, and protein expression was induced by the addition of 1 mM IPTG for 2-5 h at RT.

In the case of GST-fusion proteins, after cells were pelleted (6000xg, 10 min, 4°C) and resuspended in lysis buffer (10 mM Na₂HPO₄, 1.8 mM KH₂PO₄, 400 mM NaCl, 2.7 mM KCl, pH of 7.4, 1 mM DTT), enzymatic cell wall digestion by lysozyme on ice for 30 min preceded mechanical lysis with EmulsiFlex-C3 cell disruptor (Avestin). After 3-5 shearing cycles, lysates were supplemented with 2 mM PMSF and detergent (0.5 % Triton-X-100 or NP40) and transferred to polypropylene tubes for removal of remaining intact cells and debris by centrifugation (30 min, 20000xg, 4°C). For affinity-purification of the recombinant GST-fusion protein the cleared supernatants were loaded onto ethanol-free Glutathione Sepharose 4Fast Flow columns (GE healthcare) and incubated for 2 h at 4°C on a rotation wheel. Subsequently, columns were extensively washed with ca. 300 column volumes GST washing buffer (10 mM Na₂HPO₄, 1.8 mM KH₂PO₄, 400 mM NaCl, 2.7 mM KCl, pH of 7.4, 1 mM DTT, 2 mM PMSF, 0.5 % Triton-X-100). Finally, affinity matrix bound proteins were eluted with 6 column volumes GST elution buffer (PBS, 50 mM glutathione, pH 7.5) in several aliquots, which were analyzed by protein concentration measurements and SDS PAGE, to ensure successful and efficient purification. The eluate was dialyzed against glycerol-containing buffers of choice prior to freezing in liquid nitrogen.

Similarly, 6xHis-tagged fusion proteins were purified from *E. coli* lysates after induction, expression and harvest. Here, cell pellets were resuspended in Ni-NTA buffer (50 mM NaH₂PO₄ pH 8.0, 300 mM NaCl, 20 mM imidazole) before lysis via lysozyme digestion and mechanical cell disruption (see above). After centrifugation cleared lysates were applied onto Ni-NTA agarose columns (Qiagen) and incubated for 2 h at 4°C in order to couple 6xHis-tagged proteins to the affinity matrix. Extensive washing removed unspecific protein binding factors, followed by elution with Ni-NTA elution buffer (50 mM NaH₂PO₄ pH 8.0, 150 mM NaCl, 250 mM imidazole). The eluates were analyzed by protein concentration measurements and SDS PAGE and dialyzed against glycerol-containing buffers of choice prior to freezing in liquid nitrogen.

To obtain highly pure recombinant proteins, *e.g.* for crystal structure determination additional biophysical methods like gel filtration were applied in collaboration with groups of the NMR department and the MPIBC core facility using Äkta avant systems (GE).

6.2.10 Determination of protein concentrations

Protein concentrations of lysates and purified proteins were measured using a modified Bradford method, the Bio-Rad Protein assay, combined with standard spectrophotometers (Eppendorf) or alternatively, with NanoDrop (Thermo).

6.2.11 CNBr coupling

For antibody purification from serum the epitope containing peptide or its respective recombinant full-length protein was covalently coupled to a CNBr sepharose matrix. For this, the pre-activated CNBr sepharose 4 fast flow (GE Healthcare) was first resuspended in 1 mM HCl for 30 min and then transferred to a Buchner funnel where the matrix was washed with 15 gel volumes of cold 1 mM HCl and subsequently with coupling buffer (0.5 M NaCl, 0.1 M NaHCO₃ pH 8.3). The coupling was performed by incubating the unloaded matrix with the protein or peptide of interest overnight at 4°C or for 3-4 h at RT. Coupling efficiency was tested by taking samples before and after coupling and during washing steps. In order to avoid precipitation, the protein was dialyzed against the coupling buffer prior to coupling. After covalent attachment of the protein to the matrix, the remaining supernatant was removed, the column was washed before uncoupled sites were blocked by ethanolamine (1 M at pH 9.0) for 2 h at RT. Finally, free ethanolamine was removed by several washing steps with PBS and the affinity matrix was used for antibody purification. The columns were stored in PBS / 0.1 % azide at 4°C.

6.2.12 Antibody purification

For generation of Hub1 specific antibodies rabbits were immunized with recombinant Hub1 supported by TiterMax Gold adjuvant (Sigma). The immunization injection, boosting and bleeding was conducted by the animal facilities of the MPIBC. A crude serum was obtained after the final bleed had been incubated for initial agglutination at 37 °C for 30-60 min. After removal of clogged material an additional incubation at 4°C overnight allowed contraction of residual material. The serum was recovered as the supernatant of the blood sample after centrifugation (10000xg, 10 min, 4°C) and stored in aliquots at -20°C.

In an additional step, the Hub1 specific antibodies were further purified and enriched. Therefore, the CNBr coupled Hub1 column served as an affinity matrix and was incubated with a fraction of the crude serum at 4°C using a circulation pump. The matrix was washed several times with PBS to remove unspecific serum proteins and bound Hub1-specific antibodies were subsequently eluted by pH shift (100 mM glycine, 100 mM NaCl pH 2.5). The eluate's pH was immediately neutralized by the addition of 100 mM Tris (pH 9.0) buffer. Finally, the antibody concentration of the

collected fractions was measured with the NanoDrop spectrometer (Thermo) and fractions were stored at -20°C after the addition of glycerol.

6.2.13 Polyacrylamide gel electrophoresis and immunoblotting

Protein samples were denatured in Laemmli sample buffer and separated by sodium dodecyl sulfate polyacrylamide gel electrophoresis using 4-12% NuPAGE Bis-Tris gradient gels in combination with MES and MOPS buffer (Invitrogen). This system provides a wide range of molecular weight separation that allows high resolution of small sized proteins like Hub1 (< 10 kDa) as well as large proteins like PRPF8 (220 kDa) in the same gel. After SDS PAGE proteins were transferred to methanol-activated PVDF membranes (Millipore) using a semi-dry blotting device (MPI engineering) for 90 min with a constant current of 0.8 mA/cm². The transfer was supported by NuPAGE transfer buffer (25 mM Bicine, 25 mM Bis-Tris, 1 % EDTA and 20% methanol). Subsequently, PVDF membranes were blocked using 5% w/v skim milk powder in PBS-T and incubated with primary antibody (5% w/v skim milk powder in PBS-T) for 1-3 h or overnight at 4°C. After extensive washing with PBS-T the membranes were incubated with species-specific secondary antibodies coupled to HRP for chemiluminescence detection (ECL – Western blot Detection Kit, Amersham) on conventional films (Kodak) or CCD cameras (Fuji).

6.2.14 Structure determination of the human Hub1-HIND complex

The crystal structure of human Hub1 in complex with hSnu66's HIND was solved in close collaboration with Kaja Kowalska of the NMR department at the MPIBC (Kowalska, 2012).

For crystallization 6xHis-tagged human Hub1 was expressed in BL21-CodonPlus (DE3)-RIL cells (Stratagene) and the recombinant protein was purified via Ni-NTA agarose beads, followed by gel filtration on Superdex 75 (GE Healthcare) in PBS buffer. Proper folding of the protein was analyzed by 1D NMR spectrum recorded by a 600-MHz Bruker NMR spectrometer. The hSnu66 HIND peptide, comprising residues 117 - 135 of hSnu66, containing the sequence SLSIEETNKLRAKLGKPL, was chemically synthesized in the core facility of the MPIBC.

For crystallization, purified Hub1 was mixed with the HIND peptide at a molar ratio of 1:3 and the complex was separated by gel filtration on Superdex 75 (GE Healthcare) in 10 mM Tris/HCl pH 8.0, 100 mM NaCl, and 5 mM β-mercaptoethanol. The complex was concentrated to 10-13 mg/mL and crystallized at 20 °C, using the sitting drop vapor diffusion method. The 2 - 3 μl drops consisted of a 1:1 (vol/vol) mixture of protein solution and well solution. Crystals appeared after 3 days and grew to final size after 2 weeks of incubation. The best diffracting crystals of the human

Hub1/HIND complex grew in 0.1 M Tris/HCl pH 9.0, 0.15 M sodium acetate, 20% (w/v) PEG 4000. Crystals were soaked in cryoprotection solution containing mother liquor supplemented with 30% glycerol and were snap frozen in liquid nitrogen.

For data collection and structure determination a high quality X-ray dataset up to 2.0 Å was collected at the Swiss Light Source beamline PXII at Paul Scherrer Institute (Villigen, Switzerland). The collected data was integrated, scaled and merged by XDS and XSCALE programs (Kabsch, 1993) in space group P21212. The structure was determined by molecular replacement using the Molrep program from the CCP4 suite ccp (Collaborative Computational Project, Number 4, 1994) and the structure of the SchHub1/HINDII complex as a search model (PDB entry 3PLV). Refinement and model building were carried out with the REFMAC5 (Collaborative Computational Project, Number 4, 1994) and XtalView/Xfit (McRee, 1999). The Arp/Warp program (Lamzin and Wilson, 1993) was used to add water molecules. Certain solvent-exposed side-chains without clear electron density were removed from the model. Detailed data collection and refinement statistics are shown in the appendix 12.3. Residues W47 and Y48 of human Hub1 were found to lie in prohibited regions of the Ramachandran plot. These disallowed conformations are forced by crystal contacts with symmetry related molecules. The Ramachandran plot distribution for residues in the structure was 95.4% in most favored regions, 3.4% in allowed regions, 1.2% in disallowed regions. All structural-model figures were generated by Pymol.

6.2.15 Software

For bioinformatics analysis, DNA and protein sequences were obtained from resources of the National Center for Biotechnology Information (NCBI) and the Ensembl project (<http://www.ensembl.org/>). Sequence characterization, alignments and processing was carried out using Lasergene software Vers .9 (DNA Star) combined with Basic Local Alignment Search Tools (BLAST). Data mining was conducted using various data-base platforms including Universal Protein Resource (UniProt), Simple Modular Architecture Research Tool (SMART), Eukaryotic linear motif resource (ELM), *Saccharomyces* Genome Database (SGD), *Schizosaccharomyces pombe* Database (PomBase). Protein structures were visualized with Pymol and Swiss-PDB viewer (SIB) and external NMR structures were obtained from the protein data bank (PDB) and Research Collaboratory for Structural Bioinformatics (RCSB). Flow cytometry data was analyzed using FlowJo (TreeStar) and CellQuestPro (BD).

The exon-specific microarray datasets as well as EST and sequencing data on alternative splicing and mRNA isoforms were retrieved from Ensembl and the Alternative Splicing Database project (ASD) and analyzed using AltAnalyze (version 2.0.8), Affymetrix Power Tools software together with the Integrated Genome

Browser (IGB; version 7.0.1). Texts, graphs and tables were prepared using Excel, Word (both Microsoft) and Prism (GraphPad), images were prepared using Powerpoint (Microsoft), Photoshop and Illustrator (both Adobe).

7 Figure Index

Introduction Figure I: Co-transcriptional mRNA processing	7
Introduction Figure II: Interplay of the gene expression network	8
Introduction Figure III The pre-mRNA splicing reaction	10
Introduction Figure IV: The human spliceosomal snRNPs.....	12
Introduction Figure V: The stepwise assembly of the spliceosome during splicing cycles.....	15
Introduction Figure VI: Different types of alternative splicing	17
Introduction Table: Ubiquitin-like proteins	21
Introduction Figure VII: Human Hub1 among other ubiquitin-like proteins.....	24
Figure 1: Identification of Hub1 interactors by mammalian yeast two-hybrid screen.....	27
Figure 2: Hub1 and the tri-snRNP protein hSnu66 interact <i>in vivo</i>	28
Figure 3: Mapping of the Hub1 interaction domain in hSnu66.....	30
Figure 4: The crystal structure of the Hub1-HIND complex.....	31
Figure 5: Single point mutations in the HIND interface disrupt Hub1 - hSnu66 interaction.....	33
Figure 6: Co-localization of Hub1 and hSnu66 with nuclear speckle proteins.....	35
Figure 7: Hub1 recruitment to nuclear speckles depends on C-terminal surface	36
Figure 8: hSnu66 actively recruits Hub1 to nuclear speckles in a HIND-dependent manner.....	37
Figure 9: hSnu66 is incorporated into the tri-snRNP complex in a Hub1-independent manner... ..	38
Figure 10: Mapping and characterization of hSnu66 domains	40
Figure 11: Hub1 binding retains N-terminus of hSnu66 in nuclear compartment.....	41
Figure 12: Functional complementarity of yeast and human <i>HUB1</i> orthologs.....	43
Figure 13: Generation of Hub1-specific antibodies and verification of Hub1 RNAi specificity. ...	45
Figure 14: Knockdown of Hub1 causes cell cycle defects and mitotic catastrophe	47
Figure 15: <i>In vivo</i> depletion of Hub1 causes G2/M arrest.....	48
Figure 16: Rescue of Hub1 knockdown-mediated cell cycle defects affirm RNAi specificity	49
Figure 17: Nuclear disintegration and DNA damage are characteristics of Hub1 knockdown and entail apoptosis.....	53
Figure 18: Characterization of crucial residues in Hub1 by mutational analysis	56
Figure 19: Complementation of Hub1 RNAi cytotoxicity by co-expression of Hub1-point mutants	58
Figure 20: <i>In vivo</i> depletion of Hub1 causes an altered distribution of splicing factors and nuclear retention of polyadenylated mRNA	60
Figure 21: Hub1 RNAi complementation restores aberrant nuclear localization of splicing factors with Hub1 functioning upstream of mRNA export.....	62
Figure 22: Splicing reporters indicate Hub1's crucial role for efficient pre-mRNA splicing.....	64
Figure 23: Depletion of Hub1 leads to aberrantly spliced mRNAs and altered splicing patterns	66
Figure 24: Hub1 is crucial for accurate splicing of specific splice events <i>in vivo</i>	69
Figure 25: Exon-specific microarray revealed global alterations in alternative splicing and mRNA expression upon Hub1 depletion	73
Figure 26: The transcription inhibitor actinomycin D alleviates fatal Hub1 depletion phenotypes	76
Figure 27: Proposed model for Hub1's crucial role in pre-mRNA splicing.....	105

8 References

- Agafonov, D. E., Deckert, J., Wolf, E., Odenwaelder, P., Bessonov, S., Will, C. L., Urlaub, H., and Luehrmann, R. (2011). Semiquantitative Proteomic Analysis of the Human Spliceosome via a Novel Two-Dimensional Gel Electrophoresis Method. *Molecular and Cellular Biology* 31, 2667–2682.
- Agarwal, M. L., Agarwal, A., Taylor, W. R., Chernova, O., Sharma, Y., and Stark, G. R. (1998). A p53-dependent S-phase checkpoint helps to protect cells from DNA damage in response to starvation for pyrimidine nucleotides. *Proc. Natl. Acad. Sci. U.S.A.* 95, 14775–14780.
- Aguilera, A., and García-Muse, T. (2012). R loops: from transcription byproducts to threats to genome stability. *Molecular Cell* 46, 115–124.
- Ahn, E.-Y., DeKolver, R. C., Lo, M.-C., Nguyen, T. A., Matsuura, S., Boyapati, A., Pandit, S., Fu, X.-D., and Zhang, D.-E. (2011). SON Controls Cell-Cycle Progression by Coordinated Regulation of RNA Splicing. *Molecular Cell* 42, 185–198.
- Aichem, A., Kalveram, B., Spinnenhirn, V., Kluge, K., Catone, N., Johansen, T., and Groettrup, M. (2012). The proteomic analysis of endogenous FAT10 substrates identifies p62/SQSTM1 as a substrate of FAT10ylation. *Journal of Cell Science* 125, 4576–4585.
- Ajuh, P., Kuster, B., Panov, K., Zomerdijk, J. C., Mann, M., and Lamond, A. I. (2000). Functional analysis of the human CDC5L complex and identification of its components by mass spectrometry. *EMBO J.* 19, 6569–6581.
- Allemand, E., Gattoni, R., Bourbon, H. M., Stevenin, J., Caceres, J. F., Soret, J., and Tazi, J. (2001). Distinctive features of Drosophila alternative splicing factor RS domain: implication for specific phosphorylation, shuttling, and splicing activation. *Molecular and Cellular Biology* 21, 1345–1359.
- Anderson, J. S., and Parker, R. P. (1998). The 3' to 5' degradation of yeast mRNAs is a general mechanism for mRNA turnover that requires the SKI2 DEVH box protein and 3' to 5' exonucleases of the exosome complex. *EMBO J.* 17, 1497–1506.
- Ast, G. (2004). How did alternative splicing evolve? *Nat. Rev. Genet.* 5, 773–782.
- Ausubel, F. M., Brent, R., Kingston, R. E., Moore, D. D., Seidman, J. G., and Struhl, K. (1988). *Current Protocols in Molecular Biology*. Current Protocols.
- Bacchetti, S., and Whitmore, G. F. (1969). Actinomycin D: effects on mouse L-cells. *Biophys. J.* 9, 1427–1445.
- Bae, J., Leo, C. P., Hsu, S. Y., and Hsueh, A. J. (2000). MCL-1S, a splicing variant of the antiapoptotic BCL-2 family member MCL-1, encodes a proapoptotic protein possessing only the BH3 domain. *J. Biol. Chem.* 275, 25255–25261.
- Barrass, J., and Beggs, J. (2003). Splicing goes global. *Trends Genet.* 19, 295–298.
- Bartek, J., and Lukas, J. (2001). Mammalian G1- and S-phase checkpoints in response to DNA damage. *Curr. Opin. Cell Biol.* 13, 738–747.
- Bartke, T., Pohl, C., Pyrowolakis, G., and Jentsch, S. (2004). Dual role of BRUCE as an antiapoptotic IAP and a chimeric E2/E3 ubiquitin ligase. *Molecular Cell* 14, 801–811.
- Behrends, C., Sowa, M. E., Gygi, S. P., and Harper, J. W. (2010). Network organization of the human autophagy system. *Nature*, 1–10.
- Beli, P., Lukashchuk, N., Wagner, S. A., Weinert, B. T., Olsen, J. V., Baskcomb, L., Mann, M., Jackson, S. P., and Choudhary, C. (2012). Proteomic Investigations Reveal a Role for RNA Processing Factor THRAP3 in the DNA Damage Response. *Molecular Cell* 46, 212–225.
-

References

- Bellare, P., Kutach, A. K., Rines, A. K., Guthrie, C., and Sontheimer, E. J. (2006). Ubiquitin binding by a variant Jab1/MPN domain in the essential pre-mRNA splicing factor Prp8p. *RNA* 12, 292–302.
- Bellare, P., Small, E. C., Huang, X., Wohlschlegel, J. A., Staley, J. P., and Sontheimer, E. J. (2008). A role for ubiquitin in the spliceosome assembly pathway. *Nat Struct Mol Biol* 15, 444–451.
- Benedetti, C., Haynes, C. M., Yang, Y., Harding, H. P., and Ron, D. (2006). Ubiquitin-Like Protein 5 Positively Regulates Chaperone Gene Expression in the Mitochondrial Unfolded Protein Response. *Genetics* 174, 229–239.
- Bensaude, O. (2011). Inhibiting eukaryotic transcription: Which compound to choose? How to evaluate its activity? *Transcription* 2, 103–108.
- Bergink, S., and Jentsch, S. (2009). Principles of ubiquitin and SUMO modifications in DNA repair. *Nature* 458, 461–467.
- Berk, A. J., and Sharp, P. A. (1977). Sizing and mapping of early adenovirus mRNAs by gel electrophoresis of S1 endonuclease-digested hybrids. *Cell* 12, 721–732.
- Bessho, T., Sancar, A., Thompson, L. H., and Thelen, M. P. (1997). Reconstitution of human excision nuclease with recombinant XPF-ERCC1 complex. *J. Biol. Chem.* 272, 3833–3837.
- Bessonov, S., Anokhina, M., Krasauskas, A., Golas, M. M., Sander, B., Will, C. L., Urlaub, H., Stark, H., and Lührmann, R. (2010). Characterization of purified human Bact spliceosomal complexes reveals compositional and morphological changes during spliceosome activation and first step catalysis. *RNA* 16, 2384–2403.
- Bessonov, S., Anokhina, M., Will, C. L., Urlaub, H., and Lührmann, R. (2008). Isolation of an active step I spliceosome and composition of its RNP core. *Nature* 452, 846–850.
- Bingle, C. D., Craig, R. W., Swales, B. M., Singleton, V., Zhou, P., and Whyte, M. K. (2000). Exon skipping in Mcl-1 results in a bcl-2 homology domain 3 only gene product that promotes cell death. *J. Biol. Chem.* 275, 22136–22146.
- Birmingham, A., Anderson, E., Sullivan, K., Reynolds, A., Boese, Q., Leake, D., Karpilow, J., and Khvorova, A. (2007). A protocol for designing siRNAs with high functionality and specificity. *Nature Protocols* 2, 2068–2078.
- Blaustein, M., Pelisch, F., Tanos, T., MuNoz, M. J., Wengier, D., Quadrana, L., Sanford, J. R., Muschietti, J. P., Kornblihtt, A. R., Cáceres, J. F., et al. (2005). Concerted regulation of nuclear and cytoplasmic activities of SR proteins by AKT. *Nat Struct Mol Biol* 12, 1037–1044.
- Boerbooms, A., Mattioli, M., Reichlin, M., and Smith, P. R. (1985). Characterization of the Sm antigen by using monoclonal antibodies. *Biochem. Soc. Trans.*
- Bonano, V. I., Oltean, S., and Garcia-Blanco, M. A. (2007). A protocol for imaging alternative splicing regulation in vivo using fluorescence reporters in transgenic mice. *Nature Protocols* 2, 2166–2181.
- Bonnal, S., Martínez, C., Förch, P., Bachi, A., Wilm, M., and Valcárcel, J. (2008). RBM5/Luca-15/H37 regulates Fas alternative splice site pairing after exon definition. *Molecular Cell* 32, 81–95.
- Bosu, D. R., and Kipreos, E. T. (2008). Cullin-RING ubiquitin ligases: global regulation and activation cycles. *Cell Div* 3, 7.
- Bozaoglu, K., Curran, J. E., Elliott, K. S., Walder, K. R., Dyer, T. D., Rainwater, D. L., Vandeberg, J. L., Comuzzie, A. G., Collier, G. R., Zimmet, P., et al. (2006). Association of genetic variation within UBL5 with phenotypes of metabolic syndrome. *Hum Biol* 78, 147–159.
- Brailoiu, G. C., Dun, S. L., Chi, M., Ohsawa, M., Chang, J. K., Yang, J., and Dun, N. J. (2003). Beacon/ubiquitin-like 5-immunoreactivity in the hypothalamus and pituitary of the mouse. *Brain Res.* 984, 215–223.
-

References

- Branzei, D., and Foiani, M. (2008). Regulation of DNA repair throughout the cell cycle. *Nat. Rev. Mol. Cell Biol.* 9, 297–308.
- Bringmann, P., Appel, B., Rinke, J., Reuter, R., Theissen, H., and Lührmann, R. (1984). Evidence for the existence of snRNAs U4 and U6 in a single ribonucleoprotein complex and for their association by intermolecular base pairing. *EMBO J.* 3, 1357–1363.
- Bunz, F. (1998). Requirement for p53 and p21 to Sustain G2 Arrest After DNA Damage. *Science* 282, 1497–1501.
- Buratti, E., Chivers, M., Kralovicova, J., Romano, M., Baralle, M., Krainer, A. R., and Vorechovsky, I. (2007). Aberrant 5' splice sites in human disease genes: mutation pattern, nucleotide structure and comparison of computational tools that predict their utilization. *Nucleic Acids Research* 35, 4250–4263.
- Burge, C. B., Padgett, R. A., and Sharp, P. A. (1998). Evolutionary fates and origins of U12-type introns. *Molecular Cell* 2, 773–785.
- Burset, M., Seledtsov, I., and Solovyev, V. (2001). SpliceDB: database of canonical and non-canonical mammalian splice sites. *Nucleic Acids Research* 29, 255–259.
- Bushnell, D. A., Cramer, P., and Kornberg, R. D. (2002). Structural basis of transcription: α -Amanitin–RNA polymerase II cocrystal at 2.8 Å resolution. *Proc. Natl. Acad. Sci. U.S.A.* 99, 1218–1222.
- Caceres, J. F., Sreaton, G. R., and Krainer, A. R. (1998). A specific subset of SR proteins shuttles continuously between the nucleus and the cytoplasm. *Genes & Development* 12, 55–66.
- Cassé, C., Giannoni, F., Nguyen, V. T., Dubois, M. F., and Bensaude, O. (1999). The transcriptional inhibitors, actinomycin D and alpha-amanitin, activate the HIV-1 promoter and favor phosphorylation of the RNA polymerase II C-terminal domain. *J. Biol. Chem.* 274, 16097–16106.
- Castedo, M., Perfettini, J.-L., Roumier, T., Andreau, K., Medema, R., and Kroemer, G. (2004). Cell death by mitotic catastrophe: a molecular definition. *Oncogene* 23, 2825–2837.
- Chan, S.-P., Kao, D.-I., Tsai, W.-Y., and Cheng, S.-C. (2003). The Prp19p-associated complex in spliceosome activation. *Science* 302, 279–282.
- Chang, T.-H., Tung, L., Yeh, F.-L., Chen, J.-H., and Chang, S.-L. (2013). Functions of the DExD/H-box proteins in nuclear pre-mRNA splicing. *Biochim. Biophys. Acta* 1829, 764–774.
- Chari, A., Golas, M. M., Klingenhäger, M., Neuenkirchen, N., Sander, B., Englbrecht, C., Sickmann, A., Stark, H., and Fischer, U. (2008). An assembly chaperone collaborates with the SMN complex to generate spliceosomal SnRNPs. *Cell* 135, 497–509.
- Chen, Z. J., and Sun, L. J. (2009). Nonproteolytic Functions of Ubiquitin in Cell Signaling. *Molecular Cell* 33, 275–286.
- Chow, L. T., Gelinis, R. E., Broker, T. R., and Roberts, R. J. (1977). An amazing sequence arrangement at the 5' ends of adenovirus 2 messenger RNA. *Cell* 12, 1–8.
- Chowdhury, M. M., Dosche, C., Lohmannsroben, H.-G., and Leimkuhler, S. (2012). Dual role of the molybdenum cofactor biosynthesis protein MOCS3 in tRNA thiolation and molybdenum cofactor biosynthesis in humans. *J. Biol. Chem.* 287, 17297–17307.
- Ciechanover, A. (2005). Proteolysis: from the lysosome to ubiquitin and the proteasome. *Nat. Rev. Mol. Cell Biol.* 6, 79–87.
- Ciechanover, A., Elias, S., Heller, H., and Hershko, A. (1982). “Covalent affinity” purification of ubiquitin-activating enzyme. *Journal of Biological Chemistry* 257, 2537–2542.
- Ciechanover, A., Finley, D., and Varshavsky, A. (1984). Ubiquitin dependence of selective protein degradation demonstrated in the mammalian cell cycle mutant ts85. *Cell* 37, 57–66.

-
- Cioce, M., and Lamond, A. I. (2005). CAJAL BODIES: A Long History of Discovery. *Annu. Rev. Cell Dev. Biol.* 21, 105–131.
- Clague, M. J., Coulson, J. M., and Urbe, S. (2012). Cellular functions of the DUBs. *Journal of Cell Science* 125, 277–286.
- Clement, J. Q., Qian, L., Kaplinsky, N., and Wilkinson, M. F. (1999). The stability and fate of a spliced intron from vertebrate cells. *RNA* 5, 206–220.
- Cléry, A., Blatter, M., and Allain, F. H. T. (2008). RNA recognition motifs: boring? Not quite. *Curr Opin Struct Biol* 18, 290–298.
- Collaborative Computational Project, Number 4 (1994). The CCP4 suite: programs for protein crystallography. *Acta Crystallogr. D Biol. Crystallogr.* 50, 760–763.
- Collins, C. A., and Guthrie, C. (2000). The question remains: is the spliceosome a ribozyme? *Nat Struct Biol* 7, 850–854.
- Colwill, K., Feng, L., Yeakley, J., Gish, G., Caceres, J., Pawson, T., and Fu, X. (1996). SRPK1 and Clk/Sty protein kinases show distinct substrate specificities for serine/arginine-rich splicing factors. *J. Biol. Chem.* 271, 24569–24575.
- Cooper, T. A. (1999). Defining pre-mRNA cis elements that regulate cell-specific splicing. *Methods Mol. Biol.* 118, 391–403.
- Cooper, T. A. (2005). Use of minigene systems to dissect alternative splicing elements. *Methods* 37, 331–340.
- Cope, G. A., and Deshaies, R. J. (2003). COP9 signalosome: a multifunctional regulator of SCF and other cullin-based ubiquitin ligases. *Cell* 114, 663–671.
- Copley, R. R. (2005). The EH1 motif in metazoan transcription factors. *BMC Genomics* 6, 169.
- Cramer, P., Caceres, J. F., Cazalla, D., Kadener, S., Muro, A. F., Baralle, F. E., and Kornblihtt, A. R. (1999). Coupling of transcription with alternative splicing: RNA pol II promoters modulate SF2/ASF and 9G8 effects on an exonic splicing enhancer. *Molecular Cell* 4, 251–258.
- Crispino, J. D., Blencowe, B. J., and Sharp, P. A. (1994). Complementation by SR proteins of pre-mRNA splicing reactions depleted of U1 snRNP. *Science* 265, 1866–1869.
- Crosas, B., Hanna, J., Kirkpatrick, D. S., Zhang, D. P., Tone, Y., Hathaway, N. A., Buecker, C., Leggett, D. S., Schmidt, M., King, R. W., et al. (2006). Ubiquitin chains are remodeled at the proteasome by opposing ubiquitin ligase and deubiquitinating activities. *Cell* 127, 1401–1413.
- Cuperlovic-Culf, M., Belacel, N., Culf, A. S., and Ouellette, R. J. (2006). Microarray analysis of alternative splicing. *Omic* 10, 344–357.
- Dahlmann, M. (2008). Die Funktion des Ubiquitin-ähnlichen Proteins Hub1 in *S. cerevisiae*.
- Dahmus, M. E. (1996). Reversible phosphorylation of the C-terminal domain of RNA polymerase II. *Journal of Biological Chemistry* 271, 19009–19012.
- Deckert, J., Hartmuth, K., Boehringer, D., Behzadnia, N., Will, C. L., Kastner, B., Stark, H., Urlaub, H., and Lührmann, R. (2006). Protein Composition and Electron Microscopy Structure of Affinity-Purified Human Spliceosomal B Complexes Isolated under Physiological Conditions. *Molecular and Cellular Biology* 26, 5528–5543.
- Denuc, A., and Marfany, G. (2010). SUMO and ubiquitin paths converge. *Biochem. Soc. Trans* 38, 34–39.
-

References

- Deveraux, Q. L., Leo, E., Stennicke, H. R., Welsh, K., Salvesen, G. S., and Reed, J. C. (1999). Cleavage of human inhibitor of apoptosis protein XIAP results in fragments with distinct specificities for caspases. *EMBO J.* 18, 5242–5251.
- Di Leonardo, A., Khan, S. H., Linke, S. P., Greco, V., Seidita, G., and Wahl, G. M. (1997). DNA rereplication in the presence of mitotic spindle inhibitors in human and mouse fibroblasts lacking either p53 or pRb function. *Cancer Research* 57, 1013–1019.
- Dias, A. P., Dufu, K., Lei, H., and Reed, R. (2010). A role for TREX components in the release of spliced mRNA from nuclear speckle domains. *Nature Communications* 1, 1–10.
- Dikic, I., Wakatsuki, S., and Walters, K. J. (2009). Ubiquitin-binding domains - from structures to functions. *Nat. Rev. Mol. Cell Biol.* 10, 659–671.
- Duncan, P. I., Stojdl, D. F., Marius, R. M., and Bell, J. C. (1997). In vivo regulation of alternative pre-mRNA splicing by the Clk1 protein kinase. *Molecular and Cellular Biology* 17, 5996–6001.
- Durfee, L. A., Lyon, N., Seo, K., and Huibregtse, J. M. (2010). The ISG15 conjugation system broadly targets newly synthesized proteins: implications for the antiviral function of ISG15. *Molecular Cell* 38, 722–732.
- Dye, B. T., and Schulman, B. A. (2007). Structural Mechanisms Underlying Posttranslational Modification by Ubiquitin-Like Proteins. *Annu. Rev. Biophys. Biomol. Struct.* 36, 131–150.
- Dyson, H. J., Wright, P. E., and Scheraga, H. A. (2006). The role of hydrophobic interactions in initiation and propagation of protein folding. *Proc. Natl. Acad. Sci. U.S.A.* 103, 13057–13061.
- Ea, C.-K., Deng, L., Xia, Z.-P., Pineda, G., and Chen, Z. J. (2006). Activation of IKK by TNF α requires site-specific ubiquitination of RIP1 and polyubiquitin binding by NEMO. *Molecular Cell* 22, 245–257.
- Egecioglu, D. E., and Chanfreau, G. (2011). Proofreading and spellchecking: A two-tier strategy for pre-mRNA splicing quality control. *RNA* 17, 383–389.
- Elbashir, S. M., Harborth, J., Lendeckel, W., Yalcin, A., Weber, K., and Tuschl, T. (2001). Duplexes of 21-nucleotide RNAs mediate RNA interference in cultured mammalian cells. *Nature* 411, 494–498.
- Elkon, R., Ugalde, A. P., and Agami, R. (2013). Alternative cleavage and polyadenylation: extent, regulation and function. *Nat. Rev. Genet.* 14, 496–506.
- Ellis, J. D., Barrios-Rodiles, M., Çolak, R., Irimia, M., Kim, T., Calarco, J. A., Wang, X., Pan, Q., O'Hanlon, D., Kim, P. M., et al. (2012). Tissue-Specific Alternative Splicing Remodels Protein-Protein Interaction Networks. *Molecular Cell* 46, 884–892.
- Engelsma, D., Bernad, R., Calafat, J., and Fornerod, M. (2004). Supraphysiological nuclear export signals bind CRM1 independently of RanGTP and arrest at Nup358. *EMBO J.* 23, 3643–3652.
- Eskelinen, E.-L. (2005). Maturation of autophagic vacuoles in Mammalian cells. *autophagy* 1, 1–10.
- Fackenthal, J. D., and Godley, L. A. (2008). Aberrant RNA splicing and its functional consequences in cancer cells. *Dis Model Mech* 1, 37–42.
- Ferreira, J. A., Carmo-Fonseca, M., and Lamond, A. I. (1994). Differential interaction of splicing snRNPs with coiled bodies and interchromatin granules during mitosis and assembly of daughter cell nuclei. *J Cell Biol* 126, 11–23.
- Fire, A., Xu, S., Montgomery, M. K., Kostas, S. A., Driver, S. E., and Mello, C. C. (1998). Potent and specific genetic interference by double-stranded RNA in *Caenorhabditis elegans*. *Nature* 391, 806–811.
- Fischer, U. U., Liu, Q. Q., and Dreyfuss, G. G. (1997). The SMN-SIP1 Complex Has an Essential Role in Spliceosomal snRNP Biogenesis. *Cell* 90, 7–7.

-
- Fischer, U., Englbrecht, C., and Chari, A. (2011). Biogenesis of spliceosomal small nuclear ribonucleoproteins. *WIREs RNA* 2, 718–731.
- Fisher, D., Krasinska, L., Coudreuse, D., and Novák, B. (2012). Phosphorylation network dynamics in the control of cell cycle transitions. *Journal of Cell Science* 125, 4703–4711.
- Flotho, A., and Melchior, F. (2013). Sumoylation: a regulatory protein modification in health and disease. *Annu. Rev. Biochem.* 82, 357–385.
- Fong, N., and Bentley, D. L. (2001). Capping, splicing, and 3' processing are independently stimulated by RNA polymerase II: different functions for different segments of the CTD. *Genes & Development* 15, 1783–1795.
- Fox-Walsh, K. L., and Hertel, K. J. (2009). Splice-site pairing is an intrinsically high fidelity process. *PNAS* 106, 1766–1771.
- Friedmann, J., Koop, B., Raymond, V., and Walter, M. (2001). Isolation of a ubiquitin-like (UBL5) gene from a screen identifying highly expressed and conserved iris genes. *Genomics* 71, 252–255.
- Fu, X. D. (1995). The superfamily of arginine/serine-rich splicing factors. *RNA* 1, 663.
- Furukawa, K., Mizushima, N., Noda, T., and Ohsumi, Y. (2000). A protein conjugation system in yeast with homology to biosynthetic enzyme reaction of prokaryotes. *J. Biol. Chem.* 275, 7462–7465.
- Gaildrat, P., Killian, A., Martins, A., Tournier, I., Frébourg, T., and Tosi, M. (2010). Use of splicing reporter minigene assay to evaluate the effect on splicing of unclassified genetic variants. *Methods Mol. Biol.* 653, 249–257.
- Gan, W., Guan, Z., Liu, J., Gui, T., Shen, K., Manley, J. L., and Li, X. (2011). R-loop-mediated genomic instability is caused by impairment of replication fork progression. *Genes & Development* 25, 2041–2056.
- Gardina, P. J., Clark, T. A., Shimada, B., Staples, M. K., Yang, Q., Veitch, J., Schweitzer, A., Awad, T., Sugnet, C., Dee, S., et al. (2006). Alternative splicing and differential gene expression in colon cancer detected by a whole genome exon array. *BMC Genomics* 7, 325.
- Geng, J., and Klionsky, D. J. (2008). The Atg8 and Atg12 ubiquitin-like conjugation systems in macroautophagy. “Protein modifications: beyond the usual suspects” review series. *EMBO reports* 9, 859–864.
- Girard, C., Will, C. L., Peng, J., Makarov, E. M., Kastner, B., Lemm, I., Urlaub, H., Hartmuth, K., and Lührmann, R. (2012). Post-transcriptional spliceosomes are retained in nuclear speckles until splicing completion. *Nature Communications* 3, 994.
- Goldstein, G., Scheid, M., Hammerling, U., Schlesinger, D. H., Niall, H. D., and Boyse, E. A. (1975). Isolation of a polypeptide that has lymphocyte-differentiating properties and is probably represented universally in living cells. *Proc. Natl. Acad. Sci. U.S.A.* 72, 11–15.
- Goldstein, R. E., Cook, O., Dinur, T., Pisanté, A., Karandikar, U. C., Bidwai, A., and Paroush, Z. (2005). An eh1-like motif in odd-skipped mediates recruitment of Groucho and repression in vivo. *Molecular and Cellular Biology* 25, 10711–10720.
- Gong, X. Q., Nedialkov, Y. A., and Burton, Z. F. (2004). Alpha-amanitin blocks translocation by human RNA polymerase II. *J. Biol. Chem.* 279, 27422–27427.
- Gooding, C., and Smith, C. W. J. (2008). Tropomyosin exons as models for alternative splicing. *Adv. Exp. Med. Biol.* 644, 27–42.
- Gottschalk, A., Neubauer, G., Banroques, J., Mann, M., Lührmann, R., and Fabrizio, P. (1999). Identification by mass spectrometry and functional analysis of novel proteins of the yeast [U4/U6.U5] tri-snRNP. *EMBO J.* 18, 4535–4548.
-

-
- Gould, S. B. (2012). Evolutionary genomics: Algae's complex origins. *Nature* 492, 46–48.
- Graham, I. R., Hamshere, M., and Eperon, I. C. (1992). Alternative splicing of a human alpha-tropomyosin muscle-specific exon: identification of determining sequences. *Molecular and Cellular Biology* 12, 3872–3882.
- Graveley, B. R. (2004). A protein interaction domain contacts RNA in the prespliceosome. *Molecular Cell* 13, 302–304.
- Grillari, J., Grillari-Voglauer, R., and Jansen-Duerr, P. (2010). Post-Translational Modification of Cellular Proteins by Ubiquitin and Ubiquitin-Like Molecules: Role in Cellular Senescence and Aging. *Adv. Exp. Med. Biol.* 694, 172–196.
- Grosso, A. R., Gomes, A. Q., Barbosa-Morais, N. L., Caldeira, S., Thorne, N. P., Grech, G., Lindern, von, M., and Carmo-Fonseca, M. (2008). Tissue-specific splicing factor gene expression signatures. *Nucleic Acids Research* 36, 4823–4832.
- Gupta, M., Mungai, P. T., and Goldwasser, E. (2000). A new transacting factor that modulates hypoxia-induced expression of the erythropoietin gene. *Blood* 96, 491–497.
- Hatanaka, K., Ikegami, K., Takagi, H., and Setou, M. (2006). Hypo-osmotic shock induces nuclear export and proteasome-dependent decrease of UBL5. *Biochemical and Biophysical Research Communications* 350, 610–615.
- Hay, R. T. R. (2013). Decoding the SUMO signal. *Biochem. Soc. Trans* 41, 463–473.
- Haynes, C. M. C., Petrova, K. K., Benedetti, C. C., Yang, Y. Y., and Ron, D. D. (2007). ClpP mediates activation of a mitochondrial unfolded protein response in *C. elegans*. *Developmental Cell* 13, 467–480.
- Häcker, I., Sander, B., Golas, M. M., Wolf, E., Karagöz, E., Kastner, B., Stark, H., Fabrizio, P., and Lührmann, R. (2008). Localization of Prp8, Brr2, Snu114 and U4/U6 proteins in the yeast tri-snRNP by electron microscopy. *Nat Struct Mol Biol* 15, 1206–1212.
- Hecker, C.-M., Rabiller, M., Haglund, K., Bayer, P., and Dikic, I. (2006). Specification of SUMO1- and SUMO2-interacting motifs. *J. Biol. Chem.* 281, 16117–16127.
- Herold, N., Will, C. L., Wolf, E., Kastner, B., Urlaub, H., and Lührmann, R. (2009). Conservation of the protein composition and electron microscopy structure of *Drosophila melanogaster* and human spliceosomal complexes. *Molecular and Cellular Biology* 29, 281–301.
- Hershko, A., Heller, H., Elias, S., and Ciechanover, A. (1983). Components of Ubiquitin-Protein Ligase System - Resolution, Affinity Purification, and Role in Protein Breakdown. *J. Biol. Chem.* 258, 8206–8214.
- Hershko, A., Heller, H., Eytan, E., and Reiss, Y. (1986). The protein substrate binding site of the ubiquitin-protein ligase system. *J. Biol. Chem.* 261, 11992–11999.
- Hertel, K. J., and Graveley, B. R. (2005). RS domains contact the pre-mRNA throughout spliceosome assembly. *Trends in Biochemical Sciences* 30, 115–118.
- Hiller, M., Zhang, Z., Backofen, R., and Stamm, S. (2007). Pre-mRNA secondary structures influence exon recognition. *PLoS Genet* 3, 2147–2155.
- Ho, L., and Crabtree, G. R. (2010). Chromatin remodelling during development. *Nature* 463, 474–484.
- Hochegger, H., Takeda, S., and Hunt, T. (2008). Cyclin-dependent kinases and cell-cycle transitions: does one fit all? *Nat. Rev. Mol. Cell Biol.* 9, 910–916.
- Hoege, C., Pfander, B., Moldovan, G.-L., Pyrowolakis, G., and Jentsch, S. (2002). RAD6-dependent DNA repair is linked to modification of PCNA by ubiquitin and SUMO. *Nature* 419, 135–141.
-

-
- Hofmann, J. C., Husedzinovic, A., and Gruss, O. J. (2010). The function of spliceosome components in open mitosis. *Nucleus* 1, 447–459.
- Hollstein, U. (1974). Actinomycin - Chemistry and Mechanism of Action. *Chem. Rev.* 74, 625–652.
- Hopfield, J. J. (1974). Kinetic proofreading: a new mechanism for reducing errors in biosynthetic processes requiring high specificity. *Proc. Natl. Acad. Sci. U.S.A.* 71, 4135–4139.
- Hoppe-Seyler, F., and Butz, K. (1993). Repression of endogenous p53 transactivation function in HeLa cervical carcinoma cells by human papillomavirus type 16 E6, human mdm-2, and mutant p53. *J Virol* 67, 3111–3117.
- Hough, R., Pratt, G., and Rechsteiner, M. (1986). Ubiquitin-lysosome conjugates. Identification and characterization of an ATP-dependent protease from rabbit reticulocyte lysates. *Journal of Biological Chemistry* 261, 2400–2408.
- Huang, Y., Yario, T. A., and Steitz, J. A. (2004). A molecular link between SR protein dephosphorylation and mRNA export. *Proc. Natl. Acad. Sci. U.S.A.* 101, 9666–9670.
- Huertas, P., and Aguilera, A. (2003). Cotranscriptionally formed DNA : RNA hybrids mediate transcription elongation impairment and transcription-associated recombination. *Molecular Cell* 12, 711–721.
- Huibregtse, J. M., Scheffner, M., Beaudenon, S., and Howley, P. M. (1995). A Family of Proteins Structurally and Functionally Related to the E6-Ap Ubiquitin Protein Ligase. *Proc. Natl. Acad. Sci. U.S.A.* 92, 2563–2567.
- Husnjak, K., and Dikic, I. (2012). Ubiquitin-binding proteins: decoders of ubiquitin-mediated cellular functions. *Annu. Rev. Biochem.* 81, 291–322.
- Inoue, H., Nojima, H., and Okayama, H. (1990). High efficiency transformation of *Escherichia coli* with plasmids. *Gene* 96, 23–28.
- Ishikawa-Ankerhold, H. C., Ankerhold, R., and Drummen, G. P. C. (2012). Advanced fluorescence microscopy techniques--FRAP, FLIP, FLAP, FRET and FLIM. *Molecules* 17, 4047–4132.
- Jagla, B., Aulner, N., Kelly, P. D., Song, D., Volchuk, A., Zatorski, A., Shum, D., Mayer, T., De Angelis, D. A., Ouerfelli, O., et al. (2005). Sequence characteristics of functional siRNAs. *RNA* 11, 864–872.
- Jentsch, S. (1992). Ubiquitin-dependent protein degradation: a cellular perspective. *Trends in Cell Biology* 2, 98–103.
- Jentsch, S., and Pyrowolakis, G. (2000). Ubiquitin and its kin: how close are the family ties? *Trends in Cell Biology* 10, 335–342.
- Jentsch, S., McGrath, J. P., and Varshavsky, A. (1987). The yeast DNA repair gene RAD6 encodes a ubiquitin-conjugating enzyme. *Nature* 329, 131–134.
- Jowett, J., Elliott, K., Curran, J., Hunt, N., Walder, K., Collier, G., Zimmet, P., and Blangero, J. (2004). Genetic variation in BEACON influences quantitative variation in metabolic syndrome-related phenotypes. *Diabetes* 53, 2467–2472.
- Jurica, M. S., Licklider, L. J., Gygi, S. R., Grigorieff, N., and Moore, M. J. (2002). Purification and characterization of native spliceosomes suitable for three-dimensional structural analysis. *RNA* 8, 426–439.
- Kabsch, W. (1993). Automatic processing of rotation diffraction data from crystals of initially unknown symmetry and cell constants. *J Appl Crystallogr* 26, 795–800.
- Kaida, D., Motoyoshi, H., Tashiro, E., Nojima, T., Hagiwara, M., Ishigami, K., Watanabe, H., Kitahara, T., Yoshida, T., Nakajima, H., et al. (2007). Spliceostatin A targets SF3b and inhibits both splicing and nuclear retention of pre-mRNA. *Nature Chemical Biology* 3, 576–583.
-

- Kantham, L., Kerr-Bayles, L., Godde, N., Quick, M., Webb, R., Sunderland, T., Bond, J., Walder, K., Augert, G., and Collier, G. (2003). Beacon interacts with cdc2/cdc28-like kinases. *Biochemical and Biophysical Research Communications* 304, 125–129.
- Kapadia, F., Pryor, A., Chang, T.-H., and Johnson, L. F. (2006). Nuclear localization of poly(A)⁺ mRNA following siRNA reduction of expression of the mammalian RNA helicases UAP56 and URH49. *Gene* 384, 37–44.
- Karijolic, J., and Yu, Y.-T. (2010). Spliceosomal snRNA modifications and their function. *RNA Biol* 7, 192–204.
- Karni, R., de Stanchina, E., Lowe, S. W., Sinha, R., Mu, D., and Krainer, A. R. (2007). The gene encoding the splicing factor SF2/ASF is a proto-oncogene. *Nat Struct Mol Biol* 14, 185–193.
- Kataoka, N., Bachorik, J. L., and Dreyfuss, G. (1999). Transportin-SR, a nuclear import receptor for SR proteins. *J Cell Biol* 145, 1145–1152.
- Kawamoto, M., Shichijo, S., Imai, Y., Imaizumi, T., Koga, T., Yanaga, H., and Itoh, K. (1999). Expression of the SART-1 tumor rejection antigen in breast cancer. *Int. J. Cancer* 80, 64–67.
- Kervestin, S., and Jacobson, A. (2012). NMD: a multifaceted response to premature translational termination. *Nat. Rev. Mol. Cell Biol.* 13, 700–712.
- Kikuchi, M., Nakao, M., Inoue, Y., Matsunaga, K., Shichijo, S., Yamana, H., and Itoh, K. (1999). Identification of a SART-1-derived peptide capable of inducing HLA-A24-restricted and tumor-specific cytotoxic T lymphocytes. *Int. J. Cancer* 81, 459–466.
- Kim, J.-H., Sim, S.-H., Ha, H.-J., Ko, J.-J., Lee, K., and Bae, J. (2009). MCL-1ES, a novel variant of MCL-1, associates with MCL-1L and induces mitochondrial cell death. *FEBS Lett.* 583, 2758–2764.
- Koh, M. Y., Darnay, B. G., and Powis, G. (2008). Hypoxia-Associated Factor, a Novel E3-Ubiquitin Ligase, Binds and Ubiquitinates Hypoxia-Inducible Factor 1, Leading to Its Oxygen-Independent Degradation. *Molecular and Cellular Biology* 28, 7081–7095.
- Koh, M. Y., Lemos, R., Liu, X., and Powis, G. (2011). The hypoxia-associated factor switches cells from HIF-1 α - to HIF-2 α -dependent signaling promoting stem cell characteristics, aggressive tumor growth and invasion. *Cancer Research* 71, 4015–4027.
- Kohtz, J. D., Jamison, S. F., Will, C. L., Zuo, P., Lüthmann, R., Garcia-Blanco, M. A., and Manley, J. L. (1994). Protein-protein interactions and 5'-splice-site recognition in mammalian mRNA precursors. *Nature* 368, 119–124.
- Kojima, S., Hyakutake, A., Koshikawa, N., Nakagawara, A., and Takenaga, K. (2010). MCL-1V, a novel mouse antiapoptotic MCL-1 variant, generated by RNA splicing at a non-canonical splicing pair. *Biochemical and Biophysical Research Communications* 391, 492–497.
- Komander, D., and Rape, M. (2012). The Ubiquitin Code. *Annu. Rev. Biochem.* 81, 203–229.
- Koodathingal, P., and Staley, J. P. (2013). Splicing fidelity: DEAD/H-box ATPases as molecular clocks. *RNA Biol* 10.
- Koodathingal, P., Novak, T., Piccirilli, J. A., and Staley, J. P. (2010). The DEAH box ATPases Prp16 and Prp43 cooperate to proofread 5' splice site cleavage during pre-mRNA splicing. *Molecular Cell* 39, 385–395.
- Kornblihtt, A. R., Schor, I. E., Allo, M., Dujardin, G., Petrillo, E., and MuNoz, M. J. (2013). Alternative splicing: a pivotal step between eukaryotic transcription and translation. *Nat. Rev. Mol. Cell Biol.* 14, 153–165.
- Korneta, I., and Bujnicki, J. M. (2012). Intrinsic Disorder in the Human Spliceosomal Proteome. *PLoS Comp Biol* 8.

-
- Korneta, I., Magnus, M., and Bujnicki, J. M. (2012). Structural bioinformatics of the human spliceosomal proteome. *Nucleic Acids Research* 40, 7046–7065.
- Kowalska, K. M. (2012). Biochemical and biophysical characterization of CD44 and its binding partner, hyaluronic acid and structural investigations of the ubiquitin-like protein 5.
- Kölling, R., and Hollenberg, C. P. (1994). The ABC-transporter Ste6 accumulates in the plasma membrane in a ubiquitinated form in endocytosis mutants. *EMBO J.* 13, 3261–3271.
- Krecic, A., and Swanson, M. (1999). hnRNP complexes: composition, structure, and function. *Curr. Opin. Cell Biol.* 11, 363–371.
- Kuhn, A. N., van Santen, M. A., Schwienhorst, A., Urlaub, H., and Lührmann, R. (2009). Stalling of spliceosome assembly at distinct stages by small-molecule inhibitors of protein acetylation and deacetylation. *RNA* 15, 153–175.
- Kutay, U., and Güttinger, S. (2005). Leucine-rich nuclear-export signals: born to be weak. *Trends in Cell Biology* 15, 121–124.
- la Mata, de, M., Alonso, C. R., Kadener, S., Fededa, J. P., Blaustein, M., Pelisch, F., Cramer, P., Bentley, D., and Kornblihtt, A. R. (2003). A Slow RNA Polymerase II Affects Alternative Splicing In Vivo. *Molecular Cell* 12, 525–532.
- Lamond, A. I., and Earnshaw, W. C. (1998). Structure and function in the nucleus. *Science* 280, 547–553.
- Lamond, A. I., and Spector, D. L. (2003). Nuclear speckles: a model for nuclear organelles. *Nat. Rev. Mol. Cell Biol.* 4, 605–612.
- Lamzin, V. S., and Wilson, K. S. (1993). Automated refinement of protein models. *Acta Crystallogr. D Biol. Crystallogr.* 49, 129–147.
- Lancôt, C., Cheutin, T., Cremer, M., Cavalli, G., and Cremer, T. (2007). Dynamic genome architecture in the nuclear space: regulation of gene expression in three dimensions. *Nat. Rev. Genet.* 8, 104–115.
- Lange, O. F., Lakomek, N.-A., Farès, C., Schröder, G. F., Walter, K. F. A., Becker, S., Meiler, J., Grubmüller, H., Griesinger, C., and de Groot, B. L. (2008). Recognition dynamics up to microseconds revealed from an RDC-derived ubiquitin ensemble in solution. *Science* 320, 1471–1475.
- Lavin, M. F. (2008). Ataxia-telangiectasia: from a rare disorder to a paradigm for cell signalling and cancer. *Nat. Rev. Mol. Cell Biol.* 9, 759–769.
- Lecoeur, H. (2002). Nuclear Apoptosis Detection by Flow Cytometry: Influence of Endogenous Endonucleases. *Experimental Cell Research* 277, 1–14.
- Leeds, N. B., Small, E. C., Hiley, S. L., Hughes, T. R., and Staley, J. P. (2005). The Splicing Factor Prp43p, a DEAH Box ATPase, Functions in Ribosome Biogenesis. *Molecular and Cellular Biology* 26, 513–522.
- Leidel, S., Pedrioli, P. G. A., Bucher, T., Brost, R., Costanzo, M., Schmidt, A., Aebersold, R., Boone, C., Hofmann, K., and Peter, M. (2009). Ubiquitin-related modifier Urm1 acts as a sulphur carrier in thiolation of eukaryotic transfer RNA. *Nature* 458, 228–232.
- Lents, N. H., Wheeler, L. W., Baldassare, J. J., and Dynlacht, B. D. (2008). Identification and characterization of a novel Mdm2 splice variant acutely induced by the chemotherapeutic agents adriamycin and actinomycin D. *Cell Cycle* 7, 1580–1586.
- Li, C., Kato, M., Shiue, L., Shively, J. E., Ares, M., and Lin, R.-J. (2006). Cell type and culture condition-dependent alternative splicing in human breast cancer cells revealed by splicing-sensitive microarrays. *Cancer Research* 66, 1990–1999.
-

References

- Li, X., and Manley, J. L. (2006). Cotranscriptional processes and their influence on genome stability. *Genes & Development* 20, 1838–1847.
- Li, X., and Manley, J. L. (2005). Inactivation of the SR Protein Splicing Factor ASF/SF2 Results in Genomic Instability. *Cell* 122, 365–378.
- Li, X., Niu, T., and Manley, J. L. (2007). The RNA binding protein RNPS1 alleviates ASF/SF2 depletion-induced genomic instability. *RNA* 13, 2108–2115.
- Li, Z., Lee, I., Moradi, E., Hung, N.-J., Johnson, A. W., and Marcotte, E. M. (2009). Rational extension of the ribosome biogenesis pathway using network-guided genetics. *Plos Biol* 7, e1000213.
- Liakopoulos, D., Doenges, G., Matuschewski, K., and Jentsch, S. (1998). A novel protein modification pathway related to the ubiquitin system. *EMBO J.* 17, 2208–2214.
- Lin, J.-C., and Tarn, W.-Y. (2005). Exon selection in alpha-tropomyosin mRNA is regulated by the antagonistic action of RBM4 and PTB. *Molecular and Cellular Biology* 25, 10111–10121.
- Lin, S., Coutinho-Mansfield, G., Wang, D., Pandit, S., and Fu, X.-D. (2008). The splicing factor SC35 has an active role in transcriptional elongation. *Nat Struct Mol Biol* 15, 819–826.
- Lindell, T. J., WEINBERG, F., Morris, P. W., Roeder, R. G., and Rutter, W. J. (1970). Specific inhibition of nuclear RNA polymerase II by alpha-amanitin. *Science* 170, 447–449.
- Liu, S., and Cheng, C. (2013). Alternative RNA splicing and cancer. *WIREs RNA* 4, 547–566.
- Liu, S., Rauhut, R., Vornlocher, H.-P., and Lührmann, R. (2006). The network of protein-protein interactions within the human U4/U6.U5 tri-snRNP. *RNA* 12, 1418–1430.
- Ljungman, M., Zhang, F., Chen, F., Rainbow, A. J., and McKay, B. C. (1999). Inhibition of RNA polymerase II as a trigger for the p53 response. *Oncogene* 18, 583–592.
- Lopez, A. J. (1998). Alternative splicing of pre-mRNA: developmental consequences and mechanisms of regulation. *Annu. Rev. Genet.* 32, 279–305.
- Luco, R. F., Allo, M., Schor, I. E., Kornblihtt, A. R., and Misteli, T. (2011). Epigenetics in Alternative Pre-mRNA Splicing. *Cell* 144, 16–26.
- Luco, R. F., Pan, Q., Tominaga, K., Blencowe, B. J., Pereira-Smith, O. M., and Misteli, T. (2010). Regulation of alternative splicing by histone modifications. *Science* 327, 996–1000.
- Luders, J., Pyrowolakis, G., and Jentsch, S. (2003). The ubiquitin-like protein HUB1 forms SDS-resistant complexes with cellular proteins in the absence of ATP. *EMBO reports* 4, 1169–1174.
- Mabon, S. A., and Misteli, T. (2005). Differential recruitment of pre-mRNA splicing factors to alternatively spliced transcripts in vivo. *Plos Biol* 3, e374.
- Magnuson, V. L., Young, M., Schattenberg, D. G., Mancini, M. A., Chen, D. L., Steffensen, B., and Klebe, R. J. (1991). The alternative splicing of fibronectin pre-mRNA is altered during aging and in response to growth factors. *J. Biol. Chem.* 266, 14654–14662.
- Makarov, E. M., Makarova, O. V., Urlaub, H., Gentzel, M., Will, C. L., Wilm, M., and Lührmann, R. (2002). Small nuclear ribonucleoprotein remodeling during catalytic activation of the spliceosome. *Science* 298, 2205–2208.
- Makarova, O. V., Makarov, E. M., and Lührmann, R. (2001). The 65 and 110 kDa SR-related proteins of the U4/U6.U5 tri-snRNP are essential for the assembly of mature spliceosomes. *EMBO J.* 20, 2553–2563.
- Makarova, O. V., Makarov, E. M., Urlaub, H., Will, C. L., Gentzel, M., Wilm, M., and Lührmann, R. (2004). A subset of human 35S U5 proteins, including Prp19, function prior to catalytic step 1 of splicing. *EMBO J.* 23, 2381–2391.

- Malakhov, M. P., Kim, K. I., Malakhova, O. A., Jacobs, B. S., Borden, E. C., and Zhang, D.-E. (2003). High-throughput immunoblotting. Ubiquitin-like protein ISG15 modifies key regulators of signal transduction. *Journal of Biological Chemistry* 278, 16608–16613.
- Maniatis, T., and Reed, R. (2002). An extensive network of coupling among gene expression machines. *Nature* 416, 499–506.
- Maniatis, T., Sambrook, J., Fritsch, E. F., and Maniatis, T. (1989). *Molecular cloning : a laboratory manual*.
- Manley, J. L., and Tacke, R. (1996). SR proteins and splicing control. *Genes & Development* 10, 1569–1579.
- Marshall, N. F., Peng, J., Xie, Z., and Price, D. H. (1996). Control of RNA polymerase II elongation potential by a novel carboxyl-terminal domain kinase. *J. Biol. Chem.* 271, 27176–27183.
- Masutani, C., Sugasawa, K., Yanagisawa, J., Sonoyama, T., Ui, M., Enomoto, T., Takio, K., Tanaka, K., van der Spek, P. J., and Bootsma, D. (1994). Purification and cloning of a nucleotide excision repair complex involving the xeroderma pigmentosum group C protein and a human homologue of yeast RAD23. *EMBO J.* 13, 1831–1843.
- Mathew, R., Hartmuth, K., Möhlmann, S., Urlaub, H., Ficner, R., and Lührmann, R. (2008). Phosphorylation of human PRP28 by SRPK2 is required for integration of the U4/U6-U5 tri-snRNP into the spliceosome. *Nat Struct Mol Biol* 15, 435–443.
- Matlin, A. J. A., Clark, F. F., and Smith, C. W. J. C. (2005). Understanding alternative splicing: towards a cellular code. *Nat. Rev. Mol. Cell Biol.* 6, 386–398.
- Matsumoto, H., Shichijo, S., Kawano, K., Nishida, T., Sakamoto, M., and Itoh, K. (1998). Expression of the SART-1 Antigens in Uterine Cancers. *Cancer Science* 89, 1292–1295.
- Mayas, R. M., Maita, H., and Staley, J. P. (2006). Exon ligation is proofread by the DExD/H-box ATPase Prp22p. *Nat Struct Mol Biol* 13, 482–490.
- Mayas, R. M., Maita, H., Semlow, D. R., and Staley, J. P. (2010). Spliceosome discards intermediates via the DEAH box ATPase Prp43p. *PNAS* 107, 10020–10025.
- McCracken, S., Fong, N., Yankulov, K., Ballantyne, S., Pan, G., Greenblatt, J., Patterson, S. D., Wickens, M., and Bentley, D. L. (1997). The C-terminal domain of RNA polymerase II couples mRNA processing to transcription. *Nature* 385, 357–361.
- McNally, T., Huang, Q., Janis, R., Liu, Z., Olejniczak, E., and Reilly, R. (2003). Structural analysis of UBL5, a novel ubiquitin-like modifier. *Protein Sci.* 12, 1562–1566.
- McRee, D. E. (1999). XtalView/Xfit--A versatile program for manipulating atomic coordinates and electron density. *Journal of Structural Biology* 125, 156–165.
- Mellon, I. (2005). Transcription-coupled repair: a complex affair. *Mutat. Res.* 577, 155–161.
- Millhouse, S., and Manley, J. L. (2005). The C-Terminal Domain of RNA Polymerase II Functions as a Phosphorylation-Dependent Splicing Activator in a Heterologous Protein. *Molecular and Cellular Biology* 25, 533–544.
- Mischo, H. E., Hemmerich, P., Grosse, F., and Zhang, S. (2005). Actinomycin D induces histone gamma-H2AX foci and complex formation of gamma-H2AX with Ku70 and nuclear DNA helicase II. *J. Biol. Chem.* 280, 9586–9594.
- Mishra, S. K., Ammon, T., Popowicz, G. M., Krajewski, M., Nagel, R. J., Ares, M., Holak, T. A., and Jentsch, S. (2011). Role of the ubiquitin-like protein Hub1 in splice-site usage and alternative splicing. *Nature* 474, 173–178.

- Missra, A., and Gilmour, D. S. (2010). Interactions between DSIF (DRB sensitivity inducing factor), NELF (negative elongation factor), and the Drosophila RNA polymerase II transcription elongation complex. *PNAS* 107, 11301–11306.
- Misteli, T., Caceres, J. F., and Spector, D. L. (1997). The dynamics of a pre-mRNA splicing factor in living cells. *Nature* 387, 523–527.
- Moore, M. J., and Proudfoot, N. J. (2009). Pre-mRNA processing reaches back to transcription and ahead to translation. *Cell* 136, 688–700.
- Moreira, I. S., Fernandes, P. A., and Ramos, M. J. (2007). Hot spots-A review of the protein-protein interface determinant amino-acid residues. *Proteins* 68, 803–812.
- Morris, D. P., and Greenleaf, A. L. (2000). The splicing factor, Prp40, binds the phosphorylated carboxyl-terminal domain of RNA polymerase II. *J. Biol. Chem.* 275, 39935–39943.
- Mroczek, S., and Dziembowski, A. (2013). U6 RNA biogenesis and disease association. *WIREs RNA* 4, 581–592.
- Mukhopadhyay, D., and Dasso, M. (2007). Modification in reverse: the SUMO proteases. *Trends in Biochemical Sciences* 32, 286–295.
- Muro, A., Iaconig, A., and Baralle, F. (1998). Regulation of the fibronectin EDA exon alternative splicing. Cooperative role of the exonic enhancer element and the 5' splicing site. *FEBS Lett.* 437, 137–141.
- Müller, S., Hoegel, C., Pyrowolakis, G., and Jentsch, S. (2001). SUMO, ubiquitin's mysterious cousin. *Nat. Rev. Mol. Cell Biol.* 2, 202–210.
- Naegeli, H., and Sugawara, K. (2011). The xeroderma pigmentosum pathway: Decision tree analysis of DNA quality. *DNA Repair* 10, 673–683.
- Nagata, S. (2000). Apoptotic DNA fragmentation. *Experimental Cell Research* 256, 12–18.
- Nakajima, H., Toyoshima-Morimoto, F., Taniguchi, E., and Nishida, E. (2003). Identification of a consensus motif for Plk (Polo-like kinase) phosphorylation reveals Myt1 as a Plk1 substrate. *J. Biol. Chem.* 278, 25277–25280.
- Nakasone, M. A., Livnat-Levanon, N., Glickman, M. H., Cohen, R. E., and Fushman, D. (2013). Mixed-Linkage Ubiquitin Chains Send Mixed Messages. *Structure/Folding and Design* 21, 727–740.
- Neumann, B., Held, M., Liebel, U., Erfle, H., Rogers, P., Pepperkok, R., and Ellenberg, J. (2006). High-throughput RNAi screening by time-lapse imaging of live human cells. *Nat. Methods* 3, 385–390.
- Neumann, B., Walter, T., Hériché, J.-K., Bulkescher, J., Erfle, H., Conrad, C., Rogers, P., Poser, I., Held, M., Liebel, U., et al. (2010). Phenotypic profiling of the human genome by time-lapse microscopy reveals cell division genes. *Nature* 464, 721–727.
- Ngo, J. C. K., Chakrabarti, S., Ding, J.-H., Velazquez-Dones, A., Nolen, B., Aubol, B. E., Adams, J. A., Fu, X.-D., and Ghosh, G. (2005). Interplay between SRPK and Clk/Sty kinases in phosphorylation of the splicing factor ASF/SF2 is regulated by a docking motif in ASF/SF2. *Molecular Cell* 20, 77–89.
- Nguyen, N. M., and Senior, R. M. (2006). Laminin isoforms and lung development: all isoforms are not equal. *Developmental Biology* 294, 271–279.
- Nilsen, T. W. (1994). RNA-RNA interactions in the spliceosome: unraveling the ties that bind. *Cell* 78, 1–4.
- Nilsen, T. W. (2003). The spliceosome: the most complex macromolecular machine in the cell? *Bioessays* 25, 1147–1149.

- Noda, N. N., Ohsumi, Y., and Inagaki, F. (2010). Atg8-family interacting motif crucial for selective autophagy. *FEBS Lett.* 584, 1379–1385.
- Nouspikel, T. (2009). DNA repair in mammalian cells : Nucleotide excision repair: variations on versatility. *Cell. Mol. Life Sci.* 66, 994–1009.
- O'Donovan, A., Davies, A. A., Moggs, J. G., West, S. C., and Wood, R. D. (1994). XPG endonuclease makes the 3' incision in human DNA nucleotide excision repair. *Nature* 371, 432–435.
- O'Keefe, R. T., Mayeda, A., Sadowski, C. L., Krainer, A. R., and Spector, D. L. (1994). Disruption of pre-mRNA splicing in vivo results in reorganization of splicing factors. *J Cell Biol* 124, 249–260.
- Ohi, M. D., Vander Kooi, C. W., Rosenberg, J. A., Chazin, W. J., and Gould, K. L. (2003). Structural insights into the U-box, a domain associated with multi-ubiquitination. *Nat Struct Biol* 10, 250–255.
- Okazaki, T., Kato, Y., Mochizuki, T., Tashima, M., Sawada, H., and Uchino, H. (1988). Staurosporine, a novel protein kinase inhibitor, enhances HL-60-cell differentiation induced by various compounds. *Exp. Hematol.* 16, 42–48.
- Pan, Q., Shai, O., Lee, L. J., Frey, B. J., and Blencowe, B. J. (2008). Deep surveying of alternative splicing complexity in the human transcriptome by high-throughput sequencing. *Nat. Genet.* 40, 1413–1415.
- Pankiv, S., Clausen, T. H., Lamark, T., Brech, A., Bruun, J.-A., Outzen, H., Overvatn, A., Bjorkoy, G., and Johansen, T. (2007). p62/SQSTM1 binds directly to Atg8/LC3 to facilitate degradation of ubiquitinated protein aggregates by autophagy. *Journal of Biological Chemistry* 282, 24131–24145.
- Paronetto, M. P., Miñana, B., and Valcárcel, J. (2011). The Ewing Sarcoma Protein Regulates DNA Damage-Induced Alternative Splicing. *Molecular Cell* 43, 353–368.
- Pedrioli, P. G. A., Leidel, S., and Hofmann, K. (2008). Urm1 at the crossroad of modifications. "Protein Modifications: Beyond the Usual Suspects" Review Series. *EMBO reports* 9, 1196–1202.
- Perry, R. P., and Kelley, D. E. (1970). Inhibition of RNA synthesis by actinomycin D: Characteristic dose-response of different RNA species. *J. Cell. Physiol.* 76, 127–139.
- Pesin, J. A., and Orr-Weaver, T. L. (2008). Regulation of APC/C activators in mitosis and meiosis. *Annu. Rev. Cell Dev. Biol.* 24, 475–499.
- Peters, J. M. (1994). Proteasomes: protein degradation machines of the cell. *Trends in Biochemical Sciences* 19, 377–382.
- Petroski, M. D., Salvesen, G. S., and Wolf, D. A. (2011). Urm1 couples sulfur transfer to ubiquitin-like protein function in oxidative stress. *PNAS* 108, 1749–1750.
- Philipps, D., Celotto, A. M., Wang, Q. Q., Tarnag, R. S., and Graveley, B. R. (2003). Arginine/serine repeats are sufficient to constitute a splicing activation domain. *Nucleic Acids Research* 31, 6502–6508.
- Pickart, C. M., and Rose, I. A. (1985). Ubiquitin carboxyl-terminal hydrolase acts on ubiquitin carboxyl-terminal amides. *J. Biol. Chem.* 260, 7903–7910.
- Polo, S. E., Blackford, A. N., Chapman, J. R., Baskcomb, L., Gravel, S., Rusch, A., Thomas, A., Blundred, R., Smith, P., Kzhyshkowska, J., et al. (2012). Regulation of DNA-End Resection by hnRNPU-like Proteins Promotes DNA Double-Strand Break Signaling and Repair. *Molecular Cell* 45, 505–516.
- Pont, A. R., Sadri, N., Hsiao, S. J., Smith, S., and Schneider, R. J. (2012). mRNA Decay Factor AUF1 Maintains Normal Aging, Telomere Maintenance, and Suppression of Senescence by Activation of Telomerase Transcription. *Molecular Cell*.
- Porter, A. C. (2008). Preventing DNA over-replication: a Cdk perspective. *Cell Div* 3, 3.

- Price, D. H. (2000). P-TEFb, a Cyclin-Dependent Kinase Controlling Elongation by RNA Polymerase II. *Molecular and Cellular Biology* 20, 2629–2634.
- Proudfoot, N. J. (2011). Ending the message: poly(A) signals then and now. *Genes & Development* 25, 1770–1782.
- Rabut, G., and Peter, M. (2008). Function and regulation of protein neddylation. “Protein modifications: beyond the usual suspects” review series. *EMBO reports* 9, 969–976.
- Ram, O., and Ast, G. (2007). SR proteins: a foot on the exon before the transition from intron to exon definition. *Trends Genet.* 23, 5–7.
- Ramelot, T. A., Cort, J. R., Yee, A. A., Semesi, A., Edwards, A. M., Arrowsmith, C. H., and Kennedy, M. A. (2003). Solution structure of the yeast ubiquitin-like modifier protein Hub1. *J. Struct. Funct. Genomics* 4, 25–30.
- Rasche, A., and Herwig, R. (2010). ARH: predicting splice variants from genome-wide data with modified entropy. *Bioinformatics* 26, 84–90.
- Reed, R., and Hurt, E. (2002). A conserved mRNA export machinery coupled to pre-mRNA splicing. *Cell* 108, 523–531.
- Reinhardt, H. C., and Schumacher, B. (2012). The p53 network: cellular and systemic DNA damage responses in aging and cancer. *Trends Genet.* 28, 128–136.
- Renton, A., Llanos, S., and Lu, X. (2003). Hypoxia induces p53 through a pathway distinct from most DNA-damaging and stress-inducing agents. *Carcinogenesis* 24, 1177–1182.
- Reynolds, A., Leake, D., Boese, Q., Scaringe, S., Marshall, W. S., and Khvorova, A. (2004). Rational siRNA design for RNA interference. *Nat Biotechnol* 22, 326–330.
- Riedl, S. J., and Shi, Y. (2004). Molecular mechanisms of caspase regulation during apoptosis. *Nat. Rev. Mol. Cell Biol.* 5, 897–907.
- Riffell, J. L., Zimmerman, C., Khong, A., McHardy, L. M., and Roberge, M. (2009). Effects of chemical manipulation of mitotic arrest and slippage on cancer cell survival and proliferation. *Cell Cycle* 8, 3025–3038.
- Robberson, B. L., Cote, G. J., and Berget, S. M. (1990). Exon definition may facilitate splice site selection in RNAs with multiple exons. *Molecular and Cellular Biology* 10, 84–94.
- Roca, X., Sachidanandam, R., and Krainer, A. R. (2005). Determinants of the inherent strength of human 5' splice sites. *RNA* 11, 683–698.
- Rudner, D. Z., Breger, K. S., Kanaar, R., Adams, M. D., and Rio, D. C. (1998). RNA binding activity of heterodimeric splicing factor U2AF: at least one RS domain is required for high-affinity binding. *Molecular and Cellular Biology* 18, 4004–4011.
- Ruggero, D. D., Wang, Z. G. Z., and Pandolfi, P. P. P. (2000). The puzzling multiple lives of PML and its role in the genesis of cancer. *Bioessays* 22, 827–835.
- Ruskin, B., Krainer, A. R., Maniatis, T., and Green, M. R. (1984). Excision of an intact intron as a novel lariat structure during pre-mRNA splicing in vitro. *Cell* 38, 317–331.
- Sahi, C., Lee, T., Inada, M., Pleiss, J. A., and Craig, E. A. (2010). Cwc23, an essential J protein critical for pre-mRNA splicing with a dispensable J domain. *Molecular and Cellular Biology* 30, 33–42.
- Saitoh, N., Spahr, C. S., Patterson, S. D., Bubulya, P., Neuwald, A. F., and Spector, D. L. (2004). Proteomic analysis of interchromatin granule clusters. *Mol. Biol. Cell* 15, 3876–3890.
- Sakharkar, M. K., Chow, V. T. K., and Kanguane, P. (2004). Distributions of exons and introns in the human genome. *In Silico Biol* 4, 387–393.

- Sanford, J., Gray, N., Beckmann, K., and Caceres, J. (2004). A novel role for shuttling SR proteins in mRNA translation. *Genes & Development* 18, 755–768.
- Schellenberg, M. J., Ritchie, D. B., and MacMillan, A. M. (2008). Pre-mRNA splicing: a complex picture in higher definition. *Trends in Biochemical Sciences* 33, 243–246.
- Schmidt-Kastner, R., Yamamoto, H., Hamasaki, D., Yamamoto, H., Parel, J.-M., Schmitz, C., Dorey, C. K., Blanks, J. C., and Preising, M. N. (2008). Hypoxia-regulated components of the U4/U6.U5 tri-small nuclear riboprotein complex: possible role in autosomal dominant retinitis pigmentosa. *Mol. Vis.* 14, 125–135.
- Schneider, C., Will, C. L., Makarova, O. V., Makarov, E. M., and Lührmann, R. (2002). Human U4/U6.U5 and U4atac/U6atac.U5 tri-snRNPs exhibit similar protein compositions. *Molecular and Cellular Biology* 22, 3219–3229.
- Schneider, M., Will, C. L., Anokhina, M., Tazi, J., Urlaub, H., and Lührmann, R. (2010). Exon Definition Complexes Contain the Tri-snRNP and Can Be Directly Converted into B-like Precatalytic Splicing Complexes. *Molecular Cell* 38, 223–235.
- Schulz, S., Chachami, G., Kozackiewicz, L., Winter, U., Stankovic-Valentin, N., Haas, P., Hofmann, K., Urlaub, H., Ovaa, H., Wittbrodt, J., et al. (2012). Ubiquitin-specific protease-like 1 (USPL1) is a SUMO isopeptidase with essential, non-catalytic functions. *EMBO reports* 13, 930–938.
- Semlow, D. R., and Staley, J. P. (2012). Staying on message: ensuring fidelity in pre-mRNA splicing. *Trends in Biochemical Sciences* 37, 263–273.
- Seraphin, B. (1995). Sm and Sm-like proteins belong to a large family: identification of proteins of the U6 as well as the U1, U2, U4 and U5 snRNPs. *EMBO J.* 14, 2089–2098.
- Sgorbissa, A., and Brancolini, C. (2012). Cytokine & Growth Factor Reviews. *Cytokine and Growth Factor Reviews* 23, 307–314.
- Shapiro, M. B., and Senapathy, P. (1987). RNA splice junctions of different classes of eukaryotes: sequence statistics and functional implications in gene expression. *Nucleic Acids Research* 15, 7155–7174.
- Sharma, A., Markey, M., Torres-Muñoz, K., Varia, S., Kadakia, M., Bubulya, A., and Bubulya, P. A. (2011). Son maintains accurate splicing for a subset of human pre-mRNAs. *Journal of Cell Science* 124, 4286–4298.
- Sharma, S., Falick, A. M., and Black, D. L. (2005). Polypyrimidine tract binding protein blocks the 5' splice site-dependent assembly of U2AF and the prespliceosomal E complex. *Molecular Cell* 19, 485–496.
- Shen, H., and Green, M. R. (2006). RS domains contact splicing signals and promote splicing by a common mechanism in yeast through humans. *Genes & Development* 20, 1755–1765.
- Shen, H., Kan, J. L. C., and Green, M. R. (2004). Arginine-serine-rich domains bound at splicing enhancers contact the branchpoint to promote prespliceosome assembly. *Molecular Cell* 13, 367–376.
- Shepard, P. J., and Hertel, K. J. (2009). The SR protein family. *Genome Biol.* 10, 242.
- Shkreta, L., Michelle, L., Toutant, J., Tremblay, M. L., and Chabot, B. (2011). The DNA damage response pathway regulates the alternative splicing of the apoptotic mediator Bcl-x. *J. Biol. Chem.* 286, 331–340.
- Shpilka, T., Weidberg, H., Pietrokovski, S., and Elazar, Z. (2011). Atg8: an autophagy-related ubiquitin-like protein family. *Genome Biol.* 12, 226.
- Singh, G., and Cooper, T. (2006). Minigene reporter for identification and analysis of cis elements and trans factors affecting pre-mRNA splicing. *Biotech.* 41, 177–181.

References

- Sleeman, J. E., and Lamond, A. I. (1999). Newly assembled snRNPs associate with coiled bodies before speckles, suggesting a nuclear snRNP maturation pathway. *Curr. Biol.* 9, 1065–1074.
- Sleeman, J., Ajuh, P., and Lamond, A. (2001). snRNP protein expression enhances the formation of Cajal bodies containing p80-coilin and SMN. *Journal of Cell Science* 114, 4407–4419.
- Sobell, H. M. (1985). Actinomycin and DNA transcription. *Proc. Natl. Acad. Sci. U.S.A.* 82, 5328–5331.
- Song, E. J., Werner, S. L., Neubauer, J., Stegmeier, F., Aspden, J., Rio, D., Harper, J. W., Elledge, S. J., Kirschner, M. W., and Rape, M. (2010). The Prp19 complex and the Usp4Sart3 deubiquitinating enzyme control reversible ubiquitination at the spliceosome. *Genes & Development* 24, 1434–1447.
- Song, J., Zhang, Z. M., Hu, W. D., and Chen, Y. (2005). Small ubiquitin-like modifier (SUMO) recognition of a SUMO binding motif - A reversal of the bound orientation. *J. Biol. Chem.* 280, 40122–40129.
- Spector, D. L. (2003). The dynamics of chromosome organization and gene regulation. *Annu. Rev. Biochem.* 72, 573–608.
- Spector, D. L., and Lamond, A. I. (2011). Nuclear Speckles. *Cold Spring Harbor Perspectives in Biology* 3, a000646–a000646.
- Spector, D. L., Fu, X. D., and Maniatis, T. (1991). Associations between distinct pre-mRNA splicing components and the cell nucleus. *EMBO J.* 10, 3467–3481.
- Spénlé, C., Simon-Assmann, P., Orend, G., and Miner, J. H. (2013). Laminin $\alpha 5$ guides tissue patterning and organogenesis. *Cell Adh Migr* 7, 90–100.
- Stark, J., Bazett-Jones, D., Herfort, M., and Roth, M. (1998). SR proteins are sufficient for exon bridging across an intron. *Proc. Natl. Acad. Sci. U.S.A.* 95, 2163–2168.
- Stirling, P. C., Chan, Y. A., Minaker, S. W., Aristizabal, M. J., Barrett, I., Sipahimalani, P., Kobor, M. S., and Hieter, P. (2012). R-loop-mediated genome instability in mRNA cleavage and polyadenylation mutants. *Genes & Development* 26, 163–175.
- Stojdl, D. F., and Bell, J. C. (1999). SR protein kinases: the splice of life. *Biochem. Cell Biol.* 77, 293–298.
- Stoss, O., Stoilov, P., Hartmann, A. M., Nayler, O., and Stamm, S. (1999). The in vivo minigene approach to analyze tissue-specific splicing. *Brain Res. Brain Res. Protoc.* 4, 383–394.
- Strasser, K., Masuda, S., Mason, P., Pfannstiel, J., Oppizzi, M., Rodriguez-Navarro, S., Rondon, A., Aguilera, A., Struhl, K., Reed, R., et al. (2002). TREX is a conserved complex coupling transcription with messenger RNA export. *Nature* 417, 304–308.
- Strous, G. J., van Kerkhof, P., Govers, R., Ciechanover, A., and Schwartz, A. L. (1996). The ubiquitin conjugation system is required for ligand-induced endocytosis and degradation of the growth hormone receptor. *EMBO J.* 15, 3806–3812.
- Struhl, K. (1989). Helix-turn-helix, zinc-finger, and leucine-zipper motifs for eukaryotic transcriptional regulatory proteins. *Trends in Biochemical Sciences* 14, 137–140.
- Stutz, F., Bachi, A., Doerks, T., Braun, I. C., Seraphin, B., Wilm, M., Bork, P., and Izaurralde, E. (2000). REF, an evolutionary conserved family of hnRNP-like proteins, interacts with TAP/Mex67p and participates in mRNA nuclear export. *RNA* 6, 638–650.
- Sugasawa, K., Akagi, J.-I., Nishi, R., Iwai, S., and Hanaoka, F. (2009). Two-Step Recognition of DNA Damage for Mammalian Nucleotide Excision Repair: Directional Binding of the XPC Complex and DNA Strand Scanning. *Molecular Cell* 36, 642–653.

- Sugasawa, K., Okuda, Y., Saijo, M., Nishi, R., Matsuda, N., Chu, G., Mori, T., Iwai, S., Tanaka, K., Tanaka, K., et al. (2005). UV-Induced Ubiquitylation of XPC Protein Mediated by UV-DDB-Ubiquitin Ligase Complex. *Cell* 121, 387–400.
- Švéda, M., Častorálová, M., Lipov, J., Ruml, T., and Knejzlík, Z. (2013). Human UBL5 protein interacts with coilin and meets the Cajal bodies. *Biochemical and Biophysical Research Communications* 436, 240–245.
- Takaishi, Y. Y., Yoshida, Y. Y., Orima, H. H., 6 (2008). Expression of SART-1 mRNA in canine squamous cell carcinomas. *J Vet Med Sci* 70, 1333–1335.
- Tanackovic, G., and Krämer, A. (2005). Human splicing factor SF3a, but not SF1, is essential for pre-mRNA splicing in vivo. *Mol. Biol. Cell* 16, 1366–1377.
- Tang, Z., Mandel, L., Yean, S., Lin, C., Chen, T., Yanagida, M., and Lin, R. (2003). The Kic1 kinase of *Schizosaccharomyces pombe* is a CLK/STY orthologue that regulates cell-cell separation. *Experimental Cell Research* 283, 101–115.
- Tang, Z., Yanagida, M., and Lin, R. J. (1998). Fission yeast mitotic regulator Dsk1 is an SR protein-specific kinase. *J. Biol. Chem.* 273, 5963–5969.
- Tarn, W. Y., and Steitz, J. A. (1994). SR proteins can compensate for the loss of U1 snRNP functions in vitro. *Genes & Development* 8, 2704–2717.
- Tatham, M. H. M., Geoffroy, M.-C. M., Shen, L. L., Plechanovova, A. A., Hattersley, N. N., Jaffray, E. G. E., Palvimo, J. J. J., and Hay, R. T. R. (2008). RNF4 is a poly-SUMO-specific E3 ubiquitin ligase required for arsenic-induced PML degradation. *Nat Cell Biol* 10, 538–546.
- Taylor, W. R., and Stark, G. R. (2001). Regulation of the G2/M transition by p53. *Oncogene* 20, 1803–1815.
- Tokunaga, K., and Tani, T. (2008). Monitoring mRNA export. *Curr Protoc Cell Biol* Chapter 22, Unit 22.13.
- Tokunaga, K., Shibuya, T., Ishihama, Y., Tadakuma, H., Ide, M., Yoshida, M., Funatsu, T., Ohshima, Y., and Tani, T. (2006). Nucleocytoplasmic transport of fluorescent mRNA in living mammalian cells: nuclear mRNA export is coupled to ongoing gene transcription. *Genes Cells* 11, 305–317.
- Tripathi, V., Ellis, J. D., Shen, Z., Song, D. Y., Pan, Q., Watt, A. T., Freier, S. M., Bennett, C. F., Sharma, A., Bubulya, P. A., et al. (2010). The Nuclear-Retained Noncoding RNA MALAT1 Regulates Alternative Splicing by Modulating SR Splicing Factor Phosphorylation. *Molecular Cell* 39, 925–938.
- Tripathi, V., Song, D. Y., Zong, X., Shevtsov, S. P., Hearn, S., Fu, X.-D., Dundr, M., and Prasanth, K. V. (2012). SRSF1 regulates the assembly of pre-mRNA processing factors in nuclear speckles. *Mol. Biol. Cell* 23, 3694–3706.
- Urlaub, H., Raker, V. A., Kostka, S., and Lührmann, R. (2001). Sm protein-Sm site RNA interactions within the inner ring of the spliceosomal snRNP core structure. *EMBO J.* 20, 187–196.
- van der Veen, A. G., and Ploegh, H. L. (2012). Ubiquitin-like proteins. *Annu. Rev. Biochem.* 81, 323–357.
- van der Veen, A. G., Schorpp, K., Schlieker, C., Buti, L., Damon, J. R., Spooner, E., Ploegh, H. L., and Jentsch, S. (2011). Role of the ubiquitin-like protein Urm1 as a noncanonical lysine-directed protein modifier. *PNAS* 108, 1763–1770.
- Van Koningsbruggen, S., Dirks, R. W., Mommaas, A. M., Onderwater, J. J., Deidda, G., Padberg, G. W., Frants, R. R., and van der Maarel, S. M. (2004). FRG1P is localised in the nucleolus, Cajal bodies, and speckles. *Journal of medical genetics* 41, e46–e46.

- Vander Kooij, C. W., Ren, L., Xu, P., Ohi, M. D., Gould, K. L., and Chazin, W. J. (2010). The Prp19 WD40 Domain Contains a Conserved Protein Interaction Region Essential for Its Function. *Structure* 18, 584–593.
- Venables, J. P. (2004). Aberrant and alternative splicing in cancer. *Cancer Research* 64, 7647–7654.
- Vertegaal, A. C. O., Andersen, J. S., Ogg, S. C., Hay, R. T., Mann, M., and Lamond, A. I. (2006). Distinct and overlapping sets of SUMO-1 and SUMO-2 target proteins revealed by quantitative proteomics. *Mol. Cell Proteomics* 5, 2298–2310.
- Visintin, R., and Amon, A. (2000). The nucleolus: the magician's hat for cell cycle tricks. *Curr. Opin. Cell Biol.* 12, 372–377.
- Vogelstein, B., Lane, D., and Levine, A. J. (2000). Surfing the p53 network. *Nature* 408, 307–310.
- Wahl, M. C., Will, C. L., and Lührmann, R. (2009). The Spliceosome: Design Principles of a Dynamic RNP Machine. *Cell* 136, 701–718.
- Wang, F., Liu, M., Qiu, R., and Ji, C. (2011). The dual role of ubiquitin-like protein Urm1 as a protein modifier and sulfur carrier. *Protein Cell* 2, 612–619.
- Wang, Q. E. (2005). DNA repair factor XPC is modified by SUMO-1 and ubiquitin following UV irradiation. *Nucleic Acids Research* 33, 4023–4034.
- Wang, Z., and Burge, C. B. (2008). Splicing regulation: from a parts list of regulatory elements to an integrated splicing code. *RNA* 14, 802–813.
- Waters, S., Marchbank, K., Solomon, E., Whitehouse, C., and Gautel, M. (2009). Interactions with LC3 and polyubiquitin chains link nbr1 to autophagic protein turnover. *FEBS Lett.* 583, 1846–1852.
- Webb, C. J., Romfo, C. M., van Heeckeren, W. J., and Wise, J. A. (2005). Exonic splicing enhancers in fission yeast: functional conservation demonstrates an early evolutionary origin. *Genes & Development* 19, 242–254.
- Weber, G., Cristão, V. F., de L Alves, F., Santos, K. F., Holton, N., Rappsilber, J., Beggs, J. D., and Wahl, M. C. (2011). Mechanism for Aar2p function as a U5 snRNP assembly factor. *Genes & Development* 25, 1601–1612.
- Wei, X., Somanathan, S., Samarabandu, J., and Berezney, R. (1999). Three-dimensional visualization of transcription sites and their association with splicing factor-rich nuclear speckles. *J Cell Biol* 146, 543–558.
- Welchman, R. L., Gordon, C., and Mayer, R. J. (2005). Ubiquitin and ubiquitin-like proteins as multifunctional signals. *Nat. Rev. Mol. Cell Biol.* 6, 599–609.
- White, E. S., and Muro, A. F. (2011). Fibronectin splice variants: understanding their multiple roles in health and disease using engineered mouse models. *IUBMB Life (International Union of Biochemistry and Molecular Biology: Life)* 63, 538–546.
- Wilkinson, C., Dittmar, G., Ohi, M., Uetz, P., Jones, N., and Finley, D. (2004). Ubiquitin-like protein hub1 is required for pre-mRNA splicing and localization of an essential splicing factor in fission yeast. *Curr. Biol.* 14, 2283–2288.
- Wilkinson, K. D., Urban, M. K., and Haas, A. L. (1980). Ubiquitin is the ATP-dependent proteolysis factor I of rabbit reticulocytes. *Journal of Biological Chemistry* 255, 7529–7532.
- Will, C. L., and Lührmann, R. (2001). Spliceosomal UsnRNP biogenesis, structure and function. *Curr. Opin. Cell Biol.* 13, 290–301.
- Will, C. L., and Lührmann, R. (2005). Splicing of a rare class of introns by the U12-dependent spliceosome. *Biological Chemistry* 386, 713–724.

- Witkowski, J. A. (1988). The discovery of “split” genes: a scientific revolution. *Trends in Biochemical Sciences* 13, 110–113.
- Wittschieben, B. Ø., Iwai, S., and Wood, R. D. (2005). DDB1-DDB2 (xeroderma pigmentosum group E) protein complex recognizes a cyclobutane pyrimidine dimer, mismatches, apurinic/apyrimidinic sites, and compound lesions in DNA. *J. Biol. Chem.* 280, 39982–39989.
- Wlodarski, T., and Zagrovic, B. (2009). Conformational selection and induced fit mechanism underlie specificity in noncovalent interactions with ubiquitin. *Proceedings of the National Academy of Sciences* 106, 19346–19351.
- Wood, L. W., and Shillitoe, E. J. (2011). Effect of a caspase inhibitor, zVADfmk, on the inhibition of breast cancer cells by herpes simplex virus type 1. *Cancer Gene Ther.* 18, 685–694.
- Wood, V. V., Gwilliam, R. R., Rajandream, M.-A. M., Lyne, M. M., Lyne, R. R., Stewart, A. A., Sgouros, J. J., Peat, N. N., Hayles, J. J., Baker, S. S., et al. (2002). The genome sequence of *Schizosaccharomyces pombe*. *Nature* 415, 871–880.
- Wu, J. Y., and Maniatis, T. (1993). Specific interactions between proteins implicated in splice site selection and regulated alternative splicing. *Cell* 75, 1061–1070.
- Xiao, R., Sun, Y., Ding, J.-H., Lin, S., Rose, D. W., Rosenfeld, M. G., Fu, X.-D., and Li, X. (2007). Splicing regulator SC35 is essential for genomic stability and cell proliferation during mammalian organogenesis. *Molecular and Cellular Biology* 27, 5393–5402.
- Xie, S. Q., Martin, S., Guillot, P. V., Bentley, D. L., and Pombo, A. (2006). Splicing speckles are not reservoirs of RNA polymerase II, but contain an inactive form, phosphorylated on serine2 residues of the C-terminal domain. *Mol. Biol. Cell* 17, 1723–1733.
- Xing, Y., and Lee, C. (2006). Alternative splicing and RNA selection pressure--evolutionary consequences for eukaryotic genomes. *Nat. Rev. Genet.* 7, 499–509.
- Xu, P., and Peng, J. (2006). Dissecting the ubiquitin pathway by mass spectrometry. *Biochim. Biophys. Acta* 1764, 1940–1947.
- Xu, Y.-Z., and Query, C. C. (2007). Competition between the ATPase Prp5 and branch region-U2 snRNA pairing modulates the fidelity of spliceosome assembly. *Molecular Cell* 28, 838–849.
- Yamazaki, T., Fujiwara, N., Yukinaga, H., Ebisuya, M., Shiki, T., Kurihara, T., Kioka, N., Kambe, T., Nagao, M., Nishida, E., et al. (2010). The closely related RNA helicases, UAP56 and URH49, preferentially form distinct mRNA export machineries and coordinately regulate mitotic progression. *Mol. Biol. Cell* 21, 2953–2965.
- Yang, W., Guastella, J., Huang, J.-C., Wang, Y., Zhang, L., Xue, D., Tran, M., Woodward, R., Kasibhatla, S., Tseng, B., et al. (2003). MX1013, a dipeptide caspase inhibitor with potent in vivo antiapoptotic activity. *Br. J. Pharmacol.* 140, 402–412.
- Yankulov, K., Yamashita, K., Roy, R., Egly, J. M., and Bentley, D. L. (1995). The transcriptional elongation inhibitor 5,6-dichloro-1-beta-D-ribofuranosylbenzimidazole inhibits transcription factor IIH-associated protein kinase. *J. Biol. Chem.* 270, 23922–23925.
- Yashiroda, H., and Tanaka, K. (2004). Hub1 is an essential ubiquitin-like protein without functioning as a typical modifier in fission yeast. *Genes Cells* 9, 1189–1197.
- Yi, C., and He, C. (2013). DNA repair by reversal of DNA damage. *Cold Spring Harbor Perspectives in Biology* 5, a012575.
- Yoshida, S., and Tanaka, R. (2004). Generation of a human leukocyte antigen-A24 restricted antitumor cell with the use of SART-1 peptide and dendritic cells in patients with malignant brain tumors. *Journal of Laboratory and Clinical Medicine* 144, 201–207.

References

- Zandomeni, R., Mittleman, B., Bunick, D., Ackerman, S., and Weinmann, R. (1982). Mechanism of action of dichloro-beta-D-ribofuranosylbenzimidazole: effect on in vitro transcription. *Proc. Natl. Acad. Sci. U.S.A.* 79, 3167–3170.
- Zhang, D., and Zhang, D.-E. (2011). Interferon-Stimulated Gene 15 and the Protein ISGylation System. *Journal of Interferon & Cytokine Research* 31, 119–130.
- Zhou, Z., and Fu, X.-D. (2013). Regulation of splicing by SR proteins and SR protein-specific kinases. *Chromosoma* 122, 191–207.
- Zhu, Q., Wani, G., Yao, J., Patnaik, S., Wang, Q. E., El-Mahdy, M. A., Praetorius-Ibba, M., and Wani, A. A. (2007). The ubiquitin-proteasome system regulates p53-mediated transcription at p21waf1 promoter. *Oncogene* 26, 4199–4208.
- Ziolkowska, A., Carraro, G., Rebuffat, P., Spinazzi, R., Nussdorfer, G. G., Rucinski, M., and Malendowicz, L. K. (2004). Beacon[47-73] inhibits glucocorticoid secretion and growth of cultured rat and human adrenocortical cells. *Int. J. Mol. Med.* 14, 457–461.

9 Abbreviations

APS	ammonium peroxodisulphate	3mG	2,2,7-trimethylguanosine
ATP	adenosine triphosphate	N-	amino-
BES	N,N-Bis(2-hydroxyethyl)-2-aminoethansulfonate	NF κ B	nuclear factor κ B
bp	base pairs	Ni-NTA	nickel-nitrilo triacetate
BSA	bovine serum albumin	NLS	nuclear-localization sequence
BPS	branch point sequence	NP-40	Nonidet P-40
C-	carboxy-	nt	nucleotides
Cdc	cell division cycle	NTP	nucleoside triphosphate
CDK	cell cycle dependent kinase	OD	optical density
cDNA	complementary DNA	Oligo	oligonucleotide
Cy3	carbocyanin 3	ORF	open reading frame
Da	Dalton	pAb	polyclonal antibody
DAPI	4',6-diamidino-2-phenylindole	PAGE	Polyacrylamide gel electrophoresis
DExH	RNA helicase consensus motif	PBS	phosphate buffered saline
DMEM	Dulbecco modified Eagle's minimal essential medium	PCR	polymerase chain reaction
DMSO	dimethylsulfoxide	PEG	polyethylene glycol
DNA	deoxyribonucleic acid	PIPES	piperazin-N,N'-bis(2-ethansulfonsäure)
DNase	deoxyribonuclease	Plk	Polo-like kinase
dNTPs	deoxyribonucleotides	PMSF	phenylmethyl-sulphonylfluoride
ds	double-stranded	PPT	polypyrimidine track
DTT	dithiothreitol	PRP	pre-mRNA processing
ECL	enhanced chemiluminescence	R	Purine base
EDTA	ethylenediaminetetraacetat	RNA	ribonucleic acid
EGFP	enhanced GFP	RNase	ribonuclease
FACS	fluorescence activated cell sorter	RNAi	RNA-Interference
FCS	fetal calf serum	RRM	RNA recognition motif
FITC	fluorescein isothiocyanate	RT	room temperature
FPLC	fast protein liquid chromatography	RT-PCR	reverse transcription PCR
GFP	green fluorescent protein	shRNA	short hairpin RNA
GST	glutathione S-transferase	s.d.	standard deviation
GTP	guanosine triphosphate	SDS	sodium dodecylsulfate
h	hour	siRNA	small interfering RNA
H	histone	SR	serine-arginine rich
HBS	HEPES buffered saline	ss	splice site
HEPES	N-(2-hydroxyethyl)-piperazin-N'-(2-ethansulfonate)	TBS	Tris-buffered saline
Hn	heterogenous nuclear	TCA	trichloroacetic acid
IAP	inhibitor of apoptosis protein	TE	Tris-EDTA buffer
IgG	immunoglobulin G	Tris	Tris-(hydroxymethyl)-aminomethan
I κ B	inhibitor of nuclear factor κ B	TRITC	tetramethylrhodamine isothiocyanate
IP	immunoprecipitation	U snRNA	uridine-rich small nuclear RNA
IPTG	isopropyl- β -D-thiogalactopyranoside	U snRNP	uridine-rich small nuclear ribonucleoprotein
kb	kilobases	V	Volts
kDa	kilo Dalton	W	Watts
M	molar	WB	Western blot/Immunoblot
mAb	monoclonal antibody	WT	wild type
min	minute	W/v	weight per volume
MOPS	3-(N-morpholino)-propane sulfonate	Y	Pyrimidine base
mRNA	messenger RNA		
MT	microtubule		

10 Acknowledgement

Firstly, I would like to sincerely thank my PhD supervisor, Stefan Jentsch, for advising my thesis, his continuous support, and openness to new ideas and approaches. Working in the creative and stimulating atmosphere of his lab allowed me to explore various intriguing fields of molecular cell biology. In insightful discussions I've learned a lot about how science works inside and outside the lab, and I am grateful for these experiences.

Furthermore, I thank the members of the committee for reading and discussing my PhD project and, in particular, Prof. Dr. Angelika Böttger for evaluating this thesis as my co-referee.

I would like to express my sincere gratitude to the many members of the Jentsch department, past and present, who made my time in the lab unforgettable. I am especially grateful to my former lab colleagues Shравan Kumar Mishra and Christian Pohl, who introduced me into the intricate world of Hub1 and sophisticated mammalian tissue culture. We had a great time together, discussing science in the Hub1 club, philosophizing in the cell culture and solving daily lab mysteries. As both have established their own labs I wish them good luck and success for the future.

In addition, I owe many thanks to former lab members, in particular, Steven, Kenji, Dirk, Marian, Michi, Haindl, Per, Elisabeth, Rebecca and Silvia for creating a great working atmosphere and many cheerful times.

I also thank the current people in the lab, especially Max, Jörg, Irina, Sean, Sven, Claudio, Julian, and Ivan for the pleasant and scientifically stimulating environment. Here, I would like to particularly mention Ramazan and Sittinan, the future "Hubbers", whom I wish all the best and good luck with disclosing the remaining Hub1 secrets.

Importantly, I wish to express my heartfelt thanks to Jochen and Ulla, my awesome bench mates, for their care, openness and helpfulness and great technical assistance. Moreover, I also thank Dirk and Alex for their humor, support and assistance.

Furthermore, I owe many deeply-felt thanks to my parents, my sister and my best friends Marcel and Malte, who continuously supported me and believed in me the whole time. I greatly appreciate your understanding, forbearance and helping me not to lose track of life outside the lab. Finally, from the bottom of my heart, I ineffably thank my girlfriend Anca for your love, patience, sympathy and big-hearted support, without whom all this would not have been possible.

11 Curriculum Vitae

I. Personal Data

Name/Address: Tim Dieter Ammon
Adlzreiterstr.32
80337 Munich, Germany

Date of birth: March 4th, 1980

Place of birth: Nordenham, Germany

Nationality: German

II. Educational Background

Since Oct 2005 PhD thesis entitled "*Characterization of the ubiquitin-like protein Hub1 in human cells*" in the lab of Prof. S. Jentsch, Molecular Cell Biology, Max-Planck-Institute of Biochemistry

Oct 2005 Graduation from University of Marburg with Diplom

Oct 2004 - Sep 2005 Diploma thesis entitled "*Characterization of the nucleomorph-encoded ORF 234 and ORF 228 of the Cyptomonad *Guillardia theta**" in the lab of Prof. U.-G. Maier, Applied Botany and Cell Biology, University of Marburg

Oct 2004 Diploma examinations in cell biology (major), infection biology and microbiology

Sep 2002 Intermediate exam in biology (Vordiplom), examinations in physics, chemistry, zoology, botany, microbiology, genetics

Oct 2000 - Sep 2005 Studies of biology at the University of Marburg

Jul 1999 - Aug 2000 Military service at JaBoG 38 (medical unit), Jever

Jun 1999 Graduation with Abitur

1992 - 1999 Gymnasium Nordenham, Germany

1990 - 1992 Orientierungsstufe Mitte Nordenham, Germany

1986 - 1990 Elementary School Atens, Nordenham, Germany

12 Appendix

12.1 Affymetrix Human Exon 1.0 ST microarray data

Summary of exon-specific microarray data after CEL expression profile analysis via Affymetrix PowerTools. Relative and absolute expression profiles of individual probes after Hub1 or control knockdown in U2OS cells were processed using the ARH method (Rasche and Herwig, 2010), resulting in metascors based on Splice index (SI), p-value (P, log10) and arh-value (arh, > 0.03 significant). The metascors are ranked according to unfiltered (0), filtered for cross-hybridization and expression constraints (1) and intensity > mean intensity filter (2).

TR_ID	ARH.SI0	ARH.SI1	ARH.SI2	ARH.PO	ARH.P1	ARH.P2	ARH.arh0	ARH.arh1	ARH.arh2	rank	gene	chr	strand	min_beg	max_end
2501835	10.7232	10.5818	2.1207	8.6526	8.6079	4.0511	12.5587	12.1359	0.3590	1	DPP10	chr2	+	114916411	116318091
3893910	11.7130	11.9898	2.3506	8.3339	8.1401	4.8134	9.8347	8.4750	0.6522	2	TCEA2	chr20	+	62159056	62174079
3185643	11.9818	12.0725	2.3573	8.0817	8.1651	3.6757	8.1038	8.6391	0.2667	3	RGS3	chr9	+	115264200	115399643
3551485	10.3275	10.3373	2.0180	8.1754	8.1600	3.6477	8.7081	8.6057	0.2608	4	EM11	chr14	+	99329506	99477554
3913018	8.0672	8.0206	2.3835	8.1849	8.2097	4.0873	8.7715	8.9405	0.3694	5	LAMA5	chr20	+	60317536	60375742
2519577	10.8528	3.9963	3.8492	8.3306	5.4937	5.5877	9.8097	1.1056	1.1890	6	COL3A1	chr2	+	189547347	189585676
2463227	8.3698	5.0320	1.7725	8.1301	6.6762	3.7799	8.4102	2.7522	0.2897	7	RGS7	chr1	-	239005588	239587058
3917938	10.6510	10.7165	2.0190	7.7170	7.7153	3.6704	6.1248	6.1167	0.2656	8	HUNK	chr21	+	32167531	32297463
3354879	10.0105	10.1720	1.8415	7.4196	7.4813	4.0863	4.8741	5.1106	0.3691	9	HYS1	chr11	+	125258999	125275737
3634852	0.0000	2.8049	2.9118	9.3435	5.1231	5.2924	21.3363	0.8297	0.9460	10	RASGRF1	chr15	-	77041549	77170139
2461473	3.1209	3.0780	2.4325	8.0994	4.3866	4.1163	8.2144	0.4673	0.3779	11	TARBP1	chr1	-	232593783	232681450
2566586	8.6189	2.0496	1.8327	8.9850	4.1014	4.4709	16.2070	0.3735	0.4992	12	TSGA10	chr2	-	98980254	99124404
2582701	9.0205	2.0894	2.4999	8.7200	4.8307	4.6743	13.2259	0.6610	0.5852	13	CCDC148	chr2	-	158736743	159021459
3302805	11.4921	2.5466	2.6899	8.3288	3.9096	4.5182	9.7959	0.3211	0.5180	14	HPS1	chr10	-	100165998	100196611
3422144	5.8660	5.8545	1.9017	7.2973	7.3736	3.5778	4.4370	4.7049	0.2467	15	LGR5	chr12	+	70120128	70264733
3273251	4.5193	4.7429	4.7934	6.1047	6.1916	6.7340	1.7722	1.8951	2.8773	16	DIP2C	chr10	-	312652	725603
2585400	5.8321	3.4654	3.4399	7.1515	5.5810	5.5751	3.9666	1.8239	1.1775	17	SC9A	chr2	-	166763252	166876485
3657041	0.0000	3.5758	3.7868	7.8410	5.3128	5.7194	7.7365	0.9611	1.3164	18	ITGAX	chr16	+	31274023	31301804
2475116	5.9242	2.2894	2.7011	7.5875	4.4993	5.0240	5.5448	0.5104	0.7682	19	PL1	chr2	+	28678289	28719575
2755053	3.4152	3.5060	3.5870	5.9972	5.9790	6.2612	1.6312	1.6085	1.9994	20	CYP4V2	chr4	+	187350017	187371582
3435515	3.5458	3.7908	3.1583	5.9692	6.3098	5.9488	1.5964	2.0757	1.5714	21	CCDC62	chr12	+	121825090	121877866
3758317	4.1652	4.1652	4.3711	5.6489	5.6489	5.8766	1.2466	1.2466	1.4862	22	BRCA1	chr17	-	38450837	38530785
2960955	4.0465	3.8563	3.6846	5.7923	6.0158	5.8100	1.3926	1.6548	1.4118	23	SLC17A5	chr6	-	74359988	74420654
3898355	2.6014	2.4800	2.4617	5.9033	6.5058	6.5392	1.5172	2.4139	2.4768	24	FLRT3	chr20	-	14252688	14266267
2759654	3.7338	3.7636	3.7213	5.6140	5.6664	5.8899	1.2134	1.2636	1.5016	25	ABLIM2	chr4	-	8018189	8211389
2876608	1.4945	3.5034	2.5096	3.9892	6.7241	6.9134	0.3419	2.8556	3.3031	26	XCCL14	chr5	-	134943463	134942679
3898796	4.3113	4.4992	2.2144	6.0672	6.1291	3.4448	1.7217	1.8059	2.2128	27	KIF16B	chr20	-	16201510	16502068
3820161	3.0158	3.0158	2.3957	5.3909	5.3909	6.3941	1.0211	1.0211	2.2510	28	UBL5	chr19	+	9799673	9801762
3108526	3.2844	3.2230	3.0333	5.3943	5.4108	5.6782	1.0237	1.0569	1.2751	29	MATN2	chr8	+	98950579	99117487
2536277	3.5387	3.5547	3.4629	6.1171	5.8562	4.1702	1.7892	1.4631	0.3943	30	BBS1	chr11	+	166734707	166877195
3632801	3.9103	3.5802	3.3795	5.7133	5.6788	4.7002	1.3102	1.1709	0.5971	31	STRAG	chr15	+	72258934	72282168
3946380	3.2571	3.2241	3.4611	5.1377	5.0269	5.7967	0.8391	0.7699	1.3974	32	SGSM3	chr22	+	39126663	39136036
2494064	3.4710	3.4710	1.9207	6.0929	6.0929	3.8798	1.7562	1.7562	0.3136	33	FAHD2A FAHD2B	chr2	+	95432175	95442597
2404693	4.1093	4.0701	1.8296	5.8415	5.8956	3.4083	1.4466	1.5083	0.2154	34	BAI2	chr1	-	31965309	32002184
3430959	3.5710	3.0766	3.1171	5.3857	5.5327	4.7779	1.0170	1.1395	0.6344	35	ACACB	chr12	+	108038798	108188532
3669560	3.2094	3.2063	1.7541	6.1361	5.8802	3.7750	1.8157	1.4904	0.2886	36	WVVOX	chr16	+	76691181	77804044
3463056	2.2037	2.7694	2.4605	5.1986	5.2982	6.0346	0.8797	0.9503	1.6790	37	CSR2	chr12	-	75776692	75796930
2388525	3.2928	3.2559	3.3975	4.9336	4.9498	5.0875	0.7161	0.7252	0.8071	38	SDCCAG8	chr1	+	241486135	241729709
3192580	3.1523	2.5144	2.1787	5.1104	5.8326	5.2077	0.8215	1.4366	0.8859	39	C9orf9	chr9	+	134743578	134755237
2566848	2.6294	2.6665	2.5449	4.9277	5.1105	5.9985	0.7128	0.8216	1.6329	40	AFF3	chr2	-	100087296	99991815
3278198	3.3523	3.3523	3.2111	5.2160	5.2160	4.9534	0.8917	0.8917	0.7272	41	PHYH	chr10	-	13359882	13382033
3174121	3.0524	3.0524	3.2578	4.8504	4.8504	5.1957	0.6712	0.6712	0.8777	42	MAMDC2	chr9	+	71848392	72031670
3798829	1.1461	1.1461	1.0532	4.6632	4.6632	5.0531	0.7395	0.7395	0.7732	43	KALH2	chr22	+	10747970	10747788
3696524	3.6036	3.3586	1.7437	5.3217	5.4005	4.3751	0.9677	1.0287	0.4631	44	PDF COG8	chr16	-	67920122	67931014
3545634	3.2057	2.8195	2.6811	4.5510	4.4351	6.2911	0.5315	0.4854	0.2060	45	NRXN3	chr14	+	78181216	79400194
2837232	3.0431	2.9449	2.9278	5.0602	4.8712	4.9366	0.7901	0.6822	0.7178	46	ITK	chr5	+	156540499	156614549
3059464	2.9207	2.8936	3.0355	4.6150	4.7423	5.4005	0.5587	0.6170	1.0287	47	SEMA3A	chr7	-	83428631	83661808
3150844	2.5644	2.7933	3.0425	4.9652	4.9386	5.1442	0.7339	0.7189	0.8433	48	SNTB1	chr8	-	121619523	121893910
2890660	3.0300	3.0518	3.5434	4.8154	4.5127	4.8542	0.6532	0.5158	0.6732	49	GFPT2	chr15	-	179660336	179712888
3770052	3.1013	3.2211	3.2152	4.5821	4.7389	4.8645	0.5445	0.6154	0.6786	50	SKD2	chr17	-	68846024	68945556
3011911	0.0000	2.3591	1.9913	7.5498	4.0456	3.4994	5.3865	0.3575	0.2317	51	C7orf63	chr7	+	89712489	89777485
3484497	3.2593	3.1552	3.3323	4.7475	4.2743	4.9034	0.6195	0.4279	0.6995	52	FRY	chr13	+	31503993	31768116
2584258	2.8745	2.8566	2.3758	5.0858	5.1568	4.7302	0.8060	0.8517	0.6112	53	KCNH7	chr2	-	162936266	163403440
3637818	2.6413	2.6413	1.8003	5.7206	5.7206	3.7281	1.3176	1.3176	0.2780	54	NTRK3	chr15	-	86221226	86600371
2358393	2.7300	2.8454	2.4733	4.7913	5.0686	4.9376	0.6410	0.7953	0.7183	55	ADAMTS4	chr1	+	148788322	148799763
3953556	1.1449	3.1079	3.1508	4.0427	4.4692	4.0323	0.3567	1.0849	0.7732	56	KALH2	chr22	+	10747970	10747788
3349455	3.0603	3.3694	2.5628	5.0659	5.1503	6.3392	0.7936	0.8473	0.2590	57	TTCL1	chr11	+	112692202	112744393
2745899	2.8074	2.8761	3.2502	4.6437	4.6546	4.6817	0.5713	0.5763	0.5885	58	HHIP	chr4	+	145786667	145879292
2531377	2.7912	2.9716	2.7196	4.7433	5.1244	4.3036	0.6175	0.8305	0.4379	59	SP100	chr2	+	230989257	231115964
3649811	2.7538	2.7538	2.5576	4.4654	4.4654	5.3696	0.4971	0.4971	1.0044	60	NDE1 MYH11	chr16	+	15651623	15725602
2743085	3.5190	3.5760	2.1405	4.6950	5.0641	6.2977	0.5947	0.7925	0.2571	61	LARP2	chr4	+	129215081	129363496
3538789	2.7536	2.7518	3.2691	4.3013	4.3985	4.9657	0.4371	0.4717	0.7342	62	SLC38A6	chr14	+	60517646	60588880
4008855	2.4516	2.9154	3.1464	4.6080	4.4618	4.6813	0.5557	0.4957	0.5884	63	SSX7/19/10/6/3	chrX	-	52689865	52700622
2394478	3.0352	3.2474	2.4478	4.8604	4.8896	3.6571	0.6765	0.6920	0.2628	64	CHD5	chr1	-	6084494	6162755
2607055	2.4796	2.4743	2.6786	4.4908	4.5320	4.8435	0.5070	0.5236	0.6676	65	PASK	chr2	-	241694411	241731162
3986230	1.6424	3.3150	2.584	2.6986	5.1761	5.2161	0.1207	0.8665	0.8917	66	Cxor157	chrX	+	105741977	105809292
3107242	3.1207	3.2183	2.1595	4.7597	4.8534	3.5297	0.6254	0.6728	0.2374	67	TMEM67	chr8	+	94836349	94900556
3374517	2.4060	2.4610	2.4610	4.7623	4.6039	4.6039	0.6367	0.5339	0.5539	68	GLYATL2	chr11	-	58338275	58368706
3301218	2.7627	2.7627	2.2156	4.4235	4.4235	4.8101	0.4810	0.4810	0.6505	69	PDILM1	chr10	-	96987333	97040767
2790486	2.6780	2.7135	1.9307	5.1497	5.1072	3.4579	0.8470	0.8195</							

12.2 Microarray mRNA expression analysis

The table summarizes the 100 most strongly affected transcripts upon Hub1 knockdown in U2OS cells compared to control RNAi treated cells (performed in biological triplicates). The absolute fold change of gene expression is shown for 31 up (green) and 69 down-regulated mRNAs.

Probe Id	p-Value	log (fold_change)	fold_change
2731332	0.0163	3.4167	10.6787
3143112	0.0029	2.9533	7.7454
2582124	0.0089	2.8400	7.1602
2530713	0.0060	2.7533	6.7427
2844293	0.0497	2.5000	5.6569
3740628	0.0223	2.4700	5.5404
3959688	0.0033	2.3900	5.2416
2565349	0.0234	2.3267	5.0164
3740574	0.0072	2.2367	4.7131
3470340	0.0115	2.2167	4.6482
3959700	0.0261	2.1700	4.5002
3740610	0.0021	2.1567	4.4588
3959684	0.0099	2.1333	4.3873
3958389	0.0084	2.1267	4.3671
3551788	0.0389	2.0900	4.2575
3740576	0.0174	2.0700	4.1989
3740548	0.0124	2.0467	4.1315
3958393	0.0008	1.9967	3.9908
3275506	0.0097	1.9700	3.9177
7385547	0.0080	1.9467	3.8548
2406293	0.0026	1.9400	3.8371
3181976	0.0123	1.9067	3.7494
2565203	0.0289	1.8467	3.5967
3740550	0.0142	1.8333	3.5636
2700365	0.0324	1.8167	3.5227
2949093	0.0387	1.8100	3.5064
3740580	0.0181	1.8067	3.4983
3275504	0.0290	1.8000	3.4822
3212366	0.0007	1.7867	3.4502
2844309	0.0453	1.7767	3.4263
3095313	0.0117	1.7700	3.4105

Probe Id	p-Value	log (fold_change)	fold_change
2502842	0.0327	-1.7533	-3.3714
3375999	0.0097	-1.7567	-3.3792
3571667	0.0020	-1.7633	-3.3948
3126368	0.0039	-1.7633	-3.3948
2333136	0.0185	-1.7667	-3.4027
3758928	0.0032	-1.7767	-3.4263
2604998	0.0087	-1.7767	-3.4263
3629103	0.0015	-1.7867	-3.4502
3749528	0.0010	-1.7900	-3.4581
3573933	0.0011	-1.7933	-3.4661
3900091	0.0154	-1.7933	-3.4661
3376556	0.0035	-1.8000	-3.4822
2360700	0.0070	-1.8033	-3.4903
3703112	0.0111	-1.8033	-3.4903
3281703	0.0156	-1.8100	-3.5064
3933923	0.0232	-1.8133	-3.5145
2409069	0.0000	-1.8167	-3.5227
2413153	0.0019	-1.8200	-3.5308
3995392	0.0009	-1.8300	-3.5554
3175971	0.0137	-1.8367	-3.5718
4022370	0.0052	-1.8367	-3.5718
3649811	0.0131	-1.8400	-3.5801
3861786	0.0154	-1.8400	-3.5801
3959613	0.0161	-1.8400	-3.5801
3445123	0.0007	-1.8433	-3.5884
3551728	0.0088	-1.8433	-3.5884
2796066	0.0198	-1.8533	-3.6133
3936913	0.0007	-1.8567	-3.6217
3607510	0.0467	-1.8700	-3.6553
3706219	0.0281	-1.8700	-3.6553
2474240	0.0081	-1.8733	-3.6638
3850660	0.0025	-1.8800	-3.6808
3873115	0.0272	-1.8933	-3.7149
2790486	0.0169	-1.8933	-3.7149
3601955	0.0011	-1.9000	-3.7321
2427007	0.0026	-1.9267	-3.8018
3947227	0.0171	-1.9300	-3.8106
3331903	0.0160	-1.9300	-3.8106
2536303	0.0008	-1.9367	-3.8282
3619945	0.0004	-1.9400	-3.8371
2776088	0.0100	-1.9400	-3.8371
2939232	0.0163	-1.9400	-3.8371
3435362	0.0224	-1.9467	-3.8548
3944922	0.0004	-1.9567	-3.8816
2884623	0.0106	-1.9667	-3.9086
3108526	0.0002	-1.9967	-3.9908
2873785	0.0322	-2.0400	-4.1125
3719210	0.0003	-2.0433	-4.1220
3798829	0.0048	-2.0633	-4.1795
2485636	0.0108	-2.0700	-4.1989
3407849	0.0036	-2.0733	-4.2086
3439178	0.0392	-2.0933	-4.2673
3984655	0.0385	-2.0967	-4.2772
3708245	0.0214	-2.1033	-4.2970
3886223	0.0149	-2.1567	-4.4588
2659560	0.0285	-2.1667	-4.4898
2900051	0.0076	-2.1733	-4.5106
2876608	0.0117	-2.1867	-4.5525
2564520	0.0293	-2.1900	-4.5631
3349293	0.0000	-2.1900	-4.5631
3351841	0.0274	-2.2267	-4.6805
3591365	0.0040	-2.2367	-4.7131
2469252	0.0090	-2.2467	-4.7459
2352804	0.0233	-2.2600	-4.7899
3279058	0.0090	-2.2667	-4.8121
2947063	0.0120	-2.2733	-4.8344
3445028	0.0199	-2.3200	-4.9933
3772158	0.0466	-2.3467	-5.0865
3852565	0.0055	-2.3700	-5.1694

12.3 Data collection and refinement statistics

Data collection and refinement statistics for the human Hub1-HIND complex.

Space group	P 2 ₁ 2 ₁ 2
Cell dimensions	
<i>a</i> , <i>b</i> , <i>c</i> (Å)	87.51, 103.63, 67
<i>α</i> , <i>β</i> , <i>γ</i> (°)	90, 90, 90
Resolution (Å)	50 - 2.0 (2.1 - 2.0)*
Completeness (%)	99.7 (99.8)
R _{merge}	6.4 (34.8)
I/σ(I)	21.9 (4.48)
Redundancy	7.32 (7.2)
Refinement	
No. of reflections	35644
Resolution (Å)	20 - 2.0
R _{work} / R _{free} (%)	21.5 / 26.6
No. atoms	
Protein	5376
Water	206
Overall B (Å ²)	30.6
r. m. s. deviations	
Bond length (Å)	0.01
Bond angles (°)	1.43

*Values in parentheses are for highest-resolution shell.